Date: February 3, 2017

Workshop on Excited Hyperons in QCD Thermodynamics at Freeze-Out (YSTAR2016) Mini-Proceedings

16th - 17th November, 2016 Thomas Jefferson National Accelerator Facility, Newport News, VA, U.S.A.

P. Alba, M. Amaryan, V. Begun, R. Bellwied, S. Borsanyi, W. Broniowski, S. Capstick, E. Chudakov, V. Crede, B. Dönigus, R. G. Edwards, Z. Fodor, H. Garcilazo, J. L. Goity, M. I. Gorenstein, J. Günther, L. Guo, P. Huovinen, S. Katz, M. Mai, D. M. Manley, V. Mantovani Sarti, E. Megías, F. Myhrer, J. Noronha-Hostler, H. Noumi, P. Parotto, A. Pasztor, I. Portillo Vazquez, K. Rajagopal, C. Ratti, J. Ritman, E. Ruiz Arriola, L. L. Salcedo, I. Strakovsky, J. Stroth, A. H. Tang, Y. Tsuchikawa, A. Valcarce, J. Vijande, and V. Yu. Vovchenko

Editors: M. Amaryan, E. Chudakov, K. Rajagopal, C. Ratti, J. Ritman, and I. Strakovsky

Abstract

This Workshop brought top experts, researchers, postdocs, and students from high-energy heavy-ion interactions, lattice QCD and hadronic physics communities together. YSTAR2016 discussed the impact of "missing" hyperon resonances on QCD thermodynamics, on freeze-out in heavy ion collisions, on the evolution of early universe, and on the spectroscopy of strange particles. Recent studies that compared lattice QCD predictions of thermodynamic properties of quark-gluon plasma at freeze-out with calculations based on statistical hadron resonance gas models as well as experimentally measured ratios between yields of different hadron species in heavy ion collisions provide indirect evidence for the presence of "missing" resonances in all of these contexts. The aim of the YSTAR2016 Workshop was to sharpen these comparisons and advance our understanding of the formation of strange hadrons from quarks and gluons microseconds after the Big Bang and in todays experiments at LHC and RHIC as well as at future facilities like FAIR, J-PARC and KL at JLab.

It was concluded that the new initiative to create a secondary beam of neutral kaons at JLab will make a bridge between the hardron spectroscopy, heavy-ion experiments and lattice QCD studies addressing some major issues related to thermodynamics of the early universe and cosmology in general.

PACS numbers: 13.75.Jz, 13.60.Rj, 14.20.Jn, 25.80.Nv.

Contents

1 Preface

1. Preface

This volume presents the mini-proceedings of the workshop on "Excited Hyperons in QCD Thermodynamics at Freeze-Out" which was held at the Jefferson Laboratory (JLab) in Newport News, Virginia, USA, November 16-17, 2016. This workshop is a successor of the workshop "Physics with Neutral Kaon Beam at JLab" [1] held at JLab, February 1-3, 2016. Both workshops were organized as a followup on the letter of intent, "Physics Opportunities with Secondary KL beam at JLab," (LOI-12-15-001), which was presented to PAC 43 at JLab in 2015. The aim of the current workshop was to discuss kaon-nucleon scattering on unpolarized and polarized targets with GlueX setup in Hall D with the emphasis on hyperon spectroscopy and its connection to heavy-ion interactions. The physics impact of the measurement of all missing hyperon states on hadron spectroscopy and thermodynamics of the early universe at freeze-out was the main focus of the workshop.

The unique feature of this series of workshops is a mixture of theory and experiment. Significant progress made by lattice QCD calculations and heavy-ion interactions over the last decade made a quest to unravel missing baryon resonances even stronger due to their great impact on the understanding of thermodynamic properties of the early universe around a microsecond after the Big Bang.

The workshop consisted of 25 talks and summary session. We had about 71 paricipants from 11 different countries with a large amount of younger people showing that this field is interesting and has growing importance. A prominent representatives from different experimental collaborations from different laboratories including JLab, RHIC, LHC, J-PARC, and GSI presented current results and future plans related to hadron spectroscopy with experimental data strongly supporting evidence for a transition from Quark-Gluon Plasma (QGP) to Hadron Resonance Gas (HRG) at critical temperature. The opening talks given by M. Amaryan and E. Chudakov about the proposed facility of neutral long lived kaon (KL) beam at JLab and GlueX setup laid out a ground for further discussions.

Although this mini-proceedings summarizes all talks presented to the workshop, the actual talks in pdf format may be found on the web page of the workshop:
https://www.jlab.org/conferences/YSTAR2016/ .

Finally we would like to take this opportunity to thank all speakers, session chairs, secretaries, and all participants for making this workshop a real success.

2. **Acknowledgments**

The workshop could't have been done without dedicated work of many people. First, we would like to thank service group and the staff of JLab for all their efforts. We would like to thank JLab management, especially Robert McKeown for their help and encouragement to organize this workshop. Financial support was provided by the JLab, Jülich Forschungszentrum, The George Washington and Old Dominion universities.

Newport News, November 2016.

M. Amaryan
E. Chudakov
K. Rajagopal
C. Ratti
J. Ritman
I. Strakovsky

References

[1] M. Amaryan, E. Chudakov, C. Meyer, M. Pennington, J. Ritman, and I. Strakovsky, eds., Mini-Proceedings, *Workshop on Physics with Neutral Kaon Beam at JLab* (KL2016) (2016); arXiv:1604.02141 [hep–ph] .

2 Summaries of Talks

2.1 The K_L^0 Beam Facility at JLab

Moskov Amaryan
Department of Physics
Old Dominion University
Norfolk, VA 23529, U.S.A.

Abstract

In this talk we discuss the possibility to create a secondary K_L^0 beam to be used with GlueX detector in Hall-D at JLab for spectroscopy of excited hyperons.

Nel mezzo del cammin di nostra vita
mi ritrovai per una selva oscura,
che la diritta via era smarrita.

Dante Alighieri

1. **Introduction**

The constituent quark model was astonishingly effective in describing all observed hadrons at a time and even made a predictions that were experimentally confirmed, however even after 50 years hundreds of regular hadronic states made of $q\bar{q}$ and qqq predicted by quark models are still missing. Moreover it is fair to say that the very existence of exotic multi-quark states and QCD inspired hybrids and glueballs is questionable and lucks solid experimental proof.

The reason for this is twofold: on one hand there were not enough dedicated efforts, on the other hand until recently there were not adequate high quality experimental facilities to carry out such studies.

Among predicted regular baryon states, hundreds of missing hyperons attracted much interest due to the presence of heavy strange quark in their wave functions, which makes their widths much smaller compared to solely light-quark made baryons and therefore experimentally easier to be measured. There is a wide experimental program to study hyperons at JLab, but as we understand not everything can be done with electromagnetic probe.

The best way to map out strange baryons and mesons is to use a secondary beam of strange mesons, as it provides one of $s(\bar{s})$-quark, which otherwise is absent in the initial state and will require production of $s\bar{s}$ when hyperons are produced by other incoming particles.

The physics impact and necessity of data obtained by a secondary beam of K_L mesons created by high intensity electron beam of CEBAF at JLab was extensively discussed during KL2016 workshop [1] held in February 2016. The current YSTAR2016 Workshop is organized to explore wider impact of hyperon spectroscopy on problems, which are in the main focus of heavy-ion ineractions and their connections to thermodynamics of the early universe at freeze-out, microseconds after the Big Bang.

In this talk, we describe conceptually the main steps needed to produce intensive K_L beam. We discuss momentum resolution of the beam using time-of-flight technique, as well as the ratio of K_L over neutrons as a function of their momenta simulated based on well known production processes. In some examples the quality of expected experimental data obtained by using GlueX setup in Hall-D will be demonstrated using results of Monte Carlo studies.

The experimental program to search for hybrid mesons in the GlueX experiment at JLab is underway. Over the last decade, significant progress in our understanding of baryons made of light (u, d) quarks have been made in CLAS at JLab. However, systematic studies of excited hyperons are very much lacking with only decades old very scarce data filling the world database in different channels. In this experiment, we propose to fill this gap and study spectra of excited hyperons using the modern CEBAF facility with the aim to impinge produced K_L^0 beam on physics target of GlueX experiment in Hall D. The goal is to study $K_L - p$ and $K_L - d$ interactions and do the hyperon and possibly strange meson spectroscopy.

Unlike to cases with pion or photon beams, kaon beams are crucial to provide the data needed to identify and characterize the properties of hyperon resonances.

Our current experimental knowledge of strange resonances is far worse than our knowledge of N and Δ resonances; however, within the quark model, they are no less fundamental. Clearly there is a need to learn about baryon resonances in the "strange sector" to have a complete understanding of three-quark bound states.

The masses and widths of the lowest mass baryons were determined with kaon-beam experiments in the 1970s [2]. First determination of the pole positions, for instance for $\Lambda(1520)$, were obtained only recently from analysis of Hall A measurement at JLab [3]. An intense kaon beam would open up a new window of opportunity not only to locate missing resonances, but also to establish their properties including their quantum numbers and branching ratios to different decay modes.

A comprehensive review of physics opportunities with meson beams is presented in a recent paper [4]. Importance of baryon spectroscopy in strangeness sector was discussed in [5].

2. **Reactions that Could be Studied with K_L^0 Beam**

   (a) **Two-body Reactions Producing $S = -1$ Hyperons**

$$K_L^0 p \to \pi^+ \Lambda \tag{1}$$
$$K_L^0 p \to \pi^+ \Sigma^0 \tag{2}$$

   (b) **Three-body Reactions Producing $S = -1$ Hyperons**

$$K_L^0 p \to \pi^+ \pi^0 \Lambda \tag{3}$$
$$K_L^0 p \to \pi^+ \pi^0 \Sigma^0 \tag{4}$$
$$K_L^0 p \to \pi^0 \pi^0 \Sigma^+ \tag{5}$$
$$K_L^0 p \to \pi^+ \pi^- \Sigma^+ \tag{6}$$
$$K_L^0 p \to \pi^+ \pi^- \Sigma^- \tag{7}$$

(c) **Two- and Three-body Reactions Producing $S = -2$ Hyperons**

$$K_L^0 p \to K^+ \Xi^0 \tag{8}$$
$$K_L^0 p \to \pi^+ K^+ \Xi^- \tag{9}$$
$$K_L^0 p \to K^+ \Xi^{0*} \tag{10}$$
$$K_L^0 p \to \pi^+ K^+ \Xi^{-*} \tag{11}$$

(d) **Three-body Reactions Producing $S = -3$ Hyperons**

$$K_L^0 p \to K^+ K^+ \Omega^- \tag{12}$$
$$K_L^0 p \to K^+ K^+ \Omega^{-*} \tag{13}$$

3. The K_L^0 Beam in HALL D

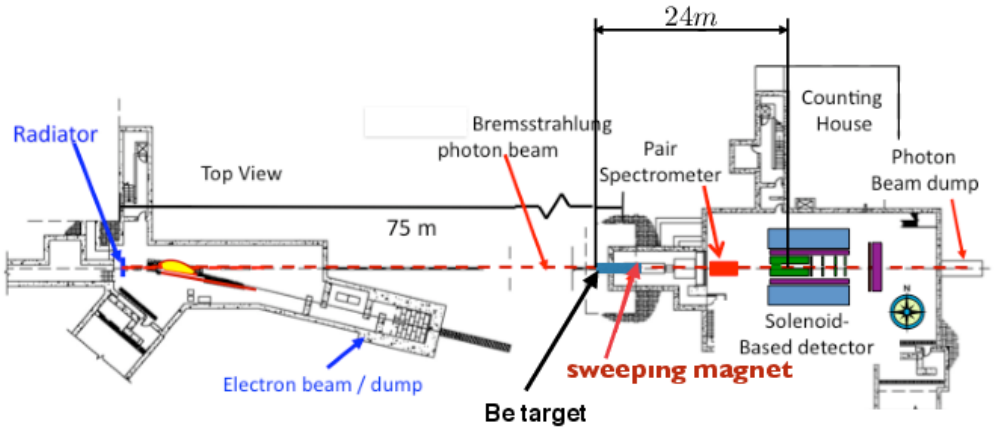

Figure 1: Schematic view of Hall D beamline. See a text for explanation.

In this chapter, we describe photo-production of secondary K_L^0 beam in Hall D. There are few points that need to be decided. To produce intensive photon beam, one needs to increase

radiation length of the radiator up to 10% radiation length. In a first scenario, $E_e = 12$ GeV electrons produced at CEBAF will scatter in a radiator in the tagger vault, generating intensive beam of bremsstrahlung photons. This may will then require removal of all tagger counters and electronics and very careful design of radiation shielding, which is very hard to optimize and design. In a second scenario one may use Compact Photon Source design (for more details see a talk by Pavel Degtiarenko in [1]) installed after the tagger magnet, which will produce bremsstrahlung photons and dump electron beam inside the source shielding the radiation inside. At the second stage, bremsstrahlung photons interact with Be target placed on a distance 16 m upstream of liquid hydrogen (LH_2) target of GlueX experiment in Hall D producing K_L^0 beam. To stop photons a 30 radiation length lead absorber will be installed in the beamline followed by a sweeping magnet to deflect the flow of charged particles. The flux of K_L on (LH_2) target of GlueX experiment in Hall D will be measured with pair spectrometer upstream the target. Details of this part of the beamline (for a details see a talk by Ilya Larin in [1]). Momenta of K_L particles will be measured using the time-of-flight between RF signal of CEBAF and start counters surrounding LH_2 target. Schematic view of beamline is presented in Fig. 1. The bremsstrahlung photons, created by electrons at a distance about 75 m upstream, hit the Be target and produce K_L^0 mesons along with neutrons and charged particles. The lead absorber of $\sim$30 radiation length is installed to absorb photons exiting Be target. The sweeping magnet deflects any remaining charged particles (leptons or hadrons) remaining after the absorber. The pair spectrometer will monitor the flux of K_L^0 through the decay rate of kaons at given distance about 10 m from Be target. The beam flux could also be monitored by installing nuclear foil in front of pair spectrometer to measure a rate of K_S^0 due to regeneration process $K_L + p \to K_S + p$ as it was done at NINA (for a details see a talk my Mike Albrow at this workshop).

Here we outline experimental conditions and simulated flux of K_L^0 based on GEANT4 and known cross sections of underlying subprocesses [6–8].

The expected flux of K_L^0 mesons integrated in the range of momenta $P = 0.3 - 10\ GeV/c$ will be few times $10^4\ K_L^0/s$ on the physics target of the GlueX setup under the following conditions:

- A thickness of the radiator 10%.
- The distance between Be and LH_2 targets in the range of $(20 - 24)$ m.
- The Be target with a length $L = 40$ cm.
- LH_2 target with $R = 3$ cm and $L = 30$ cm.

In addition, the lower repetition rate of electron beam with 64 ns spacing between bunches will be required to have enough time to measure time-of-flight of the beam momenta and to avoid an overlap of events produced from alternating pulses. Low repetition rate was already successfully used by G0 experiment in Hall C at JLab [9].

The radiation length of the radiator needs further studies in order to estimate the level of radiation and required shielding in the tagger region. During this experiment all photon beam tagging detector systems and electronics will be removed.

The final flux of K_L^0 is presented with 10% radiator, corresponding to maximal rate .

In the production of a beam of neutral kaons, an important factor is the rate of neutrons as background. As it is well known, the ratio $R = N_n/N_{K_L^0}$ is on the order 10^3 from primary proton beams [10], the same ratio with primary electromagnetic interactions is much lower. This is illustrated in Fig. 2, which presents the rate of kaons and neutrons as a function of the momentum, which resembles similar behavior as it was measured at SLAC [11].

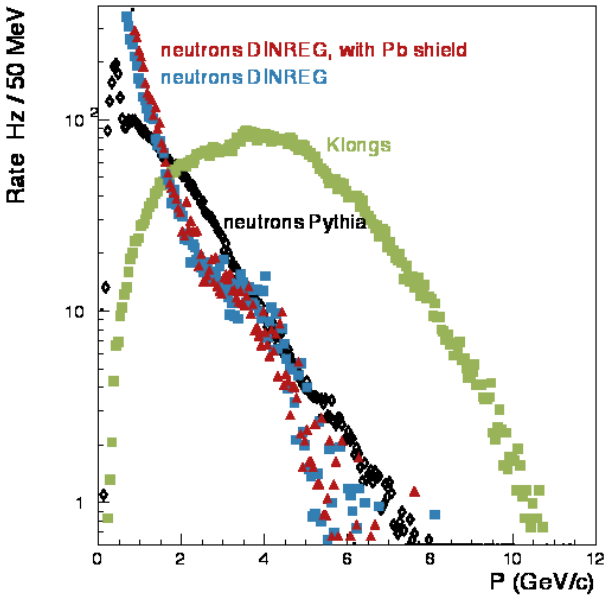

Figure 2: The rate of neutrons (open symbols) and K_L^0 (full squares) on LH_2 target of Hall D as a function of their momenta simulated with different MC generators with $10^4 K_L^0$/sec.

Shielding of the low energy neutrons in the collimator cave and flux of neutrons has been estimated to be affordable, however detailed simulations are under way to show the level of radiation along the beamline.

The response of GlueX setup, reconstruction efficiency and resolution are presented in a talk by Simon Taylor in [1].

4. Expected Rates

In this section, we discuss expected rates of events for some selected reactions. The production of Ξ hyperons has been measured only with charged kaons with very low statistical precision and never with primary K_L^0 beam. In Fig. 3 panel a) shows existing data for the octet ground state Ξ's with theoretical model predictions for W (the reaction center of mass energy) distribution, panel b) shows the same model prediction [12] presented with expected experimental points and statistical error for 10 days of running with our proposed setup with a beam intensity $2 \times 10^3 K_L$/sec using missing mass of K^+ in the reaction $K_L^0 + p \to K^+ \Xi^0$ without detection of any of decay products of Ξ^0 (for more details on this topic see a talk by Kanzo Nakayama in [1]).

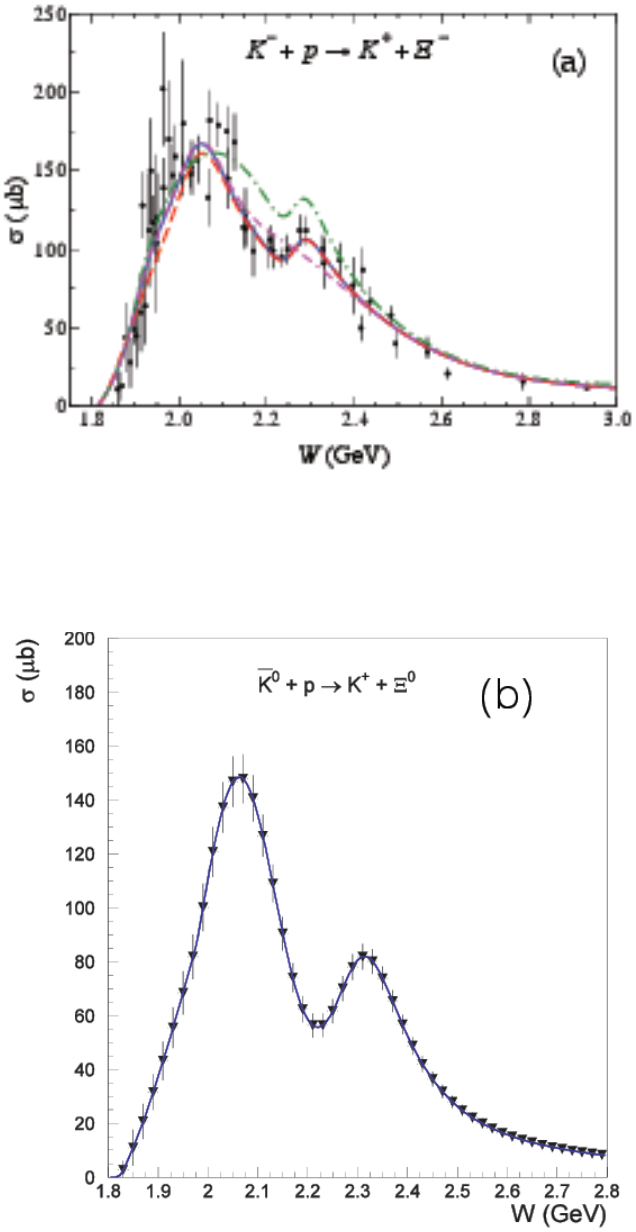

Figure 3: a) Cross section for existing world data on $K^- + p \to K^+\Xi^-$ reaction with model predictions from [12]; b) expected statistical precision for the reaction $K_L^0 + p \to K^+\Xi^0$ in 10 days of running with a beam intensity $2 \times 10^3 K_L$/sec overlaid on theoretical prediction [12].

The physics of excited hyperons is not well explored, remaining essentially at the pioneering stages of '70s-'80s. This is especially true for $\Xi^*(S = -2)$ and $\Omega^*(S = -3)$ hyperons. For example, the $SU(3)$ flavor symmetry allows as many $S = -2$ baryon resonances, as

there are N and Δ resonances combined (≈ 27); however, until now only three [ground state $\Xi(1382)1/2^+$, $\Xi(1538)3/2^+$, and $\Xi(1820)3/2^-$] have their quantum numbers assigned and few more states have been observed [2]. The status of Ξ baryons is summarized in a table presented in Fig. 4 together with the quark model predicted states [13].

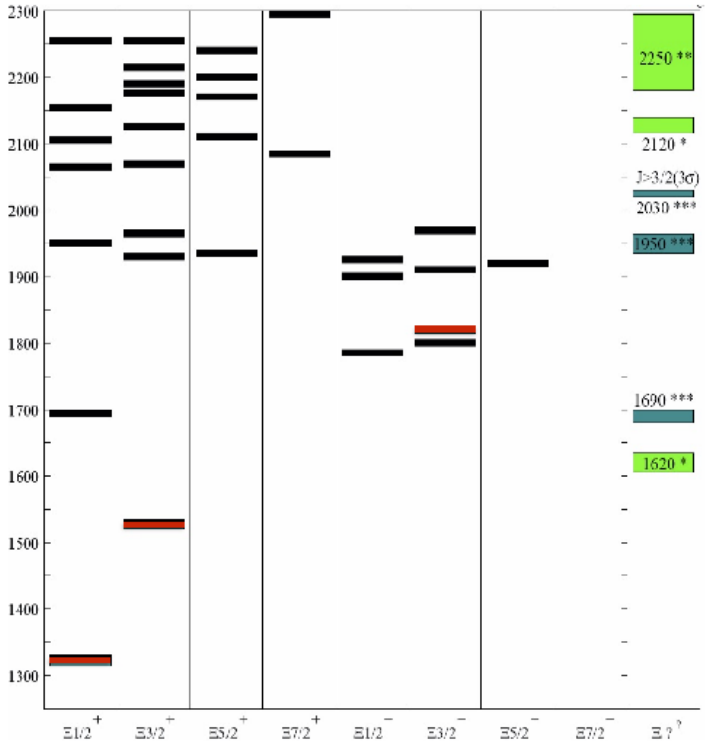

Figure 4: Black bars: Predicted Ξ spectrum based on the quark model calculation [13]. Colored bars: Observed states. The two ground octet and decuplet states together with $\Xi(1820)$ in the column $J^P = 3/2^-$ are shown in red color. Other observed states with unidentified spin-parity are plotted in the rightest column.

Historically the Ξ^* states were intensively searched for mainly in bubble chamber experiments using the K^-p reaction in '60s-'70s. The cross section was estimated to be on the order of 1-10 μb at the beam momenta up to $\sim$10 GeV/c. In '80s-'90s, the mass or width of ground and some of excited states were measured with a spectrometer in the CERN hyperon beam experiment. Few experiments have studied cascade baryons with the missing mass technique. In 1983, the production of Ξ^* resonances up to 2.5 GeV were reported from $p(K^-, K^+)$ reaction from the measurement of the missing mass of K^+ [14]. The experimental situation with Ω^{-*}'s is even worse than the Ξ^* case, there are very few data for excited states. The main reason for such a scarce dataset in multi strange hyperon domain is mainly due to very low cross section in indirect production with pion or in particular-

photon beams. Currently only ground state Ω^- quantum numbers are identified. Recently significant progress is made in lattice QCD calculations of excited baryon states [15, 16] which poses a challenge to experiments to map out all predicted states (for more details see a talk by Robert Edwards at this workshop). The advantage of baryons containing one or more strange quarks for lattice calculations is that then number of open decay channels is in general smaller than for baryons comprising only the light u and d quarks. Moreover, lattice calculations show that there are many states with strong gluonic content in positive parity sector for all baryons. The reason why hybrid baryons have not attracted the same attention as hybrid mesons is mainly due to the fact that they lack manifest "exotic" character. Although it is difficult to distinguish hybrid baryon states, there is significant theoretical insight to be gained from studying spectra of excited baryons, particularly in a framework that can simultaneously calculate properties of hybrid mesons. Therefore this program will be very much complementary to the GlueX physics program of hybrid mesons.

The proposed experiment with a beam intensity $10^4 K_L$/sec will result in about 2×10^5 Ξ^*'s and 4×10^3 Ω^*'s per month.

A similar program for KN scattering is under development at J-PARC with charged kaon beams [17]. The current maximum momentum of secondary beamline of 2 GeV/c is available at the K1.8 beamline. The beam momentum of 2 GeV/c corresponds to $\sqrt{s}$ =2.2 GeV in the $K^- p$ reaction which is not enough to generate even the first excited Ξ^* state predicted in the quark model. However, there are plans to create high energy beamline in the momentum range 5-15 GeV/c to be used with the spectrometer commonly used with the J-PARC P50 experiment which will lead to expected yield of $(3-4) \times 10^5$ Ξ^*'s and 10^3 Ω^*'s per month.

Statistical power of proposed experiment with K_L beam at JLab will be of the same order as that in J-PARC with charged kaon beam.

An experimental program with kaon beams will be much richer and allows to perform a complete experiment using polarized target and measuring recoil polarization of hyperons. This studies are under way to find an optimal solution for the GlueX setup.

5. Summary

In summary we intend to propose production of high intensity K_L beam using photoproduction processes from a secondary Be target. A flux as high as $\sim$ $10^4 K_L$/sec could be achieved. Momenta of K_L beam particles will be measured with time-of-flight. The flux of kaon beam will be measured through partial detection of $\pi^+\pi^-$ decay products from their decay to $\pi^+\pi^-\pi^0$ by exploiting similar procedure used by LASS experiment at SLAC [11]. Besides using unpolarized liquid hydrogen target currently installed in GlueX experiment the unpolarized deuteron target may be installed. Additional studies are needed to find an optimal choice of polarized targets. This proposal will allow to measure KN scattering with different final states including production of strange and multi strange baryons with unprecedented statistical precision to test QCD in non perturbative domain. It has a potential to distinguish between different quark models and test lattice QCD predictions for excited baryon states with strong hybrid content.

6. **Acknowledgments**

This work is supported, in part, by the U.S. Department of Energy, Office of Science, Office of Nuclear Physics, under Award Number DE–FG02–96ER40960.

References

[1] M. Amaryan, E. Chudakov, C. Meyer, M. Pennington, J. Ritman, and I. Strakovsky, eds., Mini-Proceedings, *Workshop on Physics with Neutral Kaon Beam at JLab* (KL2016) (2016); arXiv:1604.02141 [hep–ph] .

[2] C. Patrignani *et al.* (Particle Data Group), Chin. Phys. C **40**, 100001 (2016).

[3] Y. Qiang, Ya. I. Azimov, I. I. Strakovsky, W. J. Briscoe, H. Gao, D. W. Higinbotham, and V. V. Nelyubin, Phys. Lett. B **694**, 123 (2011).

[4] W. J. Briscoe, M. Döring, H. Haberzettl, D. M. Manley, M. Naruki, I. I. Strakovsky, and E. S. Swanson, Eur. Phys. J. A **51**, 129 (2015); arXiv:1503.07763 [hep–ph].

[5] U. Al-Binni *et al.*, *Project X: Physics Opportunities*, in Proceedings, *Community Summer Study 2013: Snowmass on the Mississippi* (CSS2013), Minneapolis, MN, USA, July 29-August 6, 2013, edited by A. S. Kronfeld and R. S. Tschirhart (2013); arXiv:1306.5009 [hep-ex].

[6] H. Seraydaryan *et al.* (CLAS Collaboration), Phys. Rev. C **89**, 055206 (2014); arXiv:1308.1363 [hep–ex].

[7] A. I. Titov and T. S. H. Lee, Phys. Rev. C **67**, 065205 (2003); arXiv:nuclth/0305002 [nucl–th].

[8] G. McClellan, N. B. Mistry, P. Mostek, H. Ogren, A. Osborne, J. Swartz, R. Talman, and G. Diambrini-Palazzi, Phys. Rev. Lett. **26**, 1593 (1971).

[9] D. Androic *et al.* (G0 Collaboration), Nucl. Instrum. Meth. A **646**, 59 (2011); arXiv:1103.0761 [nucl–ex].

[10] W. E. Cleland, B. Goz, D. Freytag, T. J. Devlin, R. J. Esterling, and K. G. Vosburgh, Phys. Rev. D **12**, 1247 (1975).

[11] G. W. Brandenburg *et al.*, Phys. Rev. D **7**, 708 (1973).

[12] B. C. Jackson, Y. Oh, H. Haberzettl, and K. Nakayama, Phys. Rev. C *91*, 065208 (2015); arXiv:1503.00845 [nucl–th].

[13] K.-T. Chao, N. Isgur, and G. Karl, Phys. Rev. D **23**, 155 (1981).

[14] C. M. Jenkins *et al.*, Phys. Rev. Lett. **51**, 951 (1983).

[15] G. P. Engel, C. B. Lang, D. Mohler, and A. Schäfer (BGR Collaboration), Phys. Rev. D **87**, 074504 (2013); arXiv:1301.4318 [hep–lat].

[16] R. G. Edwards, N. Mathur, D. G. Richards, and S. J. Wallace (for Hadron Spectrum Collaboration), Phys. Rev. D **87**, 054506 (2013); arXiv:1212.5236 [hep–ph].

[17] H. Takahashi, Proceedings, *11th International Conference on Hypernuclear and Strange Particle Physics* (HYP 2012), Nucl. Phys. A **914**, 553 (2013).

2.2 Overview of Hall D

Eugene Chudakov
Thomas Jefferson National Accelerator Facility
Newport News, VA 23606, U.S.A.

1. Hall D is a new experimental hall at Jefferson Lab, designed for experiments with a photon beam. The primary motivation for Hall D is the GlueX experiment [1,2], dedicated to meson spectroscopy. The Hall D complex consists of:

   - An electron beam line used to extract the 5.5-pass electrons from the accelerator into the Tagger Hall. The designed beam energy is $E_\circ$ =12 GeV.
   - The Tagger Hall, where the electron beam passes through a thin radiator ($\sim$ 0.01% R.L.) and is deflected into the beam dump. The electrons that lost >30% of their energy in the radiator are detected with scintillator hodoscopes providing a $\sim$0.1% energy resolution for the tagged photons. Aligned diamond radiators allow to produce linearly polarized photons via the Coherent Bremsstrahlung. The beam dump is limited to 60 kW (5 μA at 12 GeV).
   - The Collimator Cave contains a collimator for the photon beam and dipole magnets downstream in order to remove charged particles. The 3.4 mm diameter collimator, located about 75 m downstream of the radiator, selects the central cone of the photon beam increasing its average linear polarization, up to $\sim$40% in the coherent peak at 9 GeV.
   - Hall D contains several elements of the photon beam line, and the main spectrometer. A Pair Spectrometer consists of a thin converter, a dipole magnet, and a two-arm detector used to measure the energy spectrum of the photon beam. The main spectrometer is based on a 2-T superconducting solenoid, 4 m long and 1.85 m bore diameter. The liquid hydrogen target is located in the front part the solenoid. The charged tracks are detected with a set of drift chambers; photons are detected with two electromagnetic calorimeters. There are also scintillator hodoscopes for triggering and time-of-flight measurements. The spectrometer is nearly hermetic in an angular range of $1^\circ < \theta < 120^\circ$. The momentum resolution is $\sigma_P/p \sim 1-3\%$ depending on the polar angle θ. The energy resolution of the electromagnetic calorimeters is about 7% at 1 GeV.

   The main spectrometer is designed for photon beam rates below 100 MHz in the coherent peak. Such a rate can be provided by a 2.2 μA beam on a 0.02 mm = 0.0125% R.L. diamond crystal. The 1-st stage of GlueX is planned to run at a lower rate of 10 MHz.

   Hall D and the GlueX experiment had 3 commissioning runs in 2014-2016. By April 2016 all the systems have been commissioned at some level and most of them have reached the specifications. Preliminary results of the 2014-2015 commissioning have been reported [3].

   In addition to the GlueX experiment, two other experiments (both using Primakoff-type reactions) have been approved by the Program Advisory Committee (PAC). In total, about 500 days of effective running have been approved by the PAC.

2. **Acknowledgments**

This material is based upon work supported by the U.S. Department of Energy, Office of Science, Office of Nuclear Physics under contract DE–AC05–06OR23177.

References

[1] M. Dugger *et al.* (GlueX Collaboration), arXiv:1210.4508.

[2] A. AlekSejevs *et al.* (GlueX Collaboration), arXiv:1305.1523.

[3] H. A. Ghoul *et al.* (GlueX Collaboration), in *16th International Conference on Hadron Spectroscopy* (Hadron 2015) Newport News, Virginia, USA, September, 2015; arXiv:1512.03699.

2.3 Can K-Long Beams Find Missing Hyperon Resonances ?

D. Mark Manley
Department of Physics
Kent State University
Kent, OH 44242 U.S.A.

Abstract

The problem of "missing resonances" is discussed with particular emphasis on missing hyperon resonances. It is shown that $K_L^0 p$ reactions would be an ideal means to search for Σ^* resonances due to their isospin-1 selectivity. Production reactions will likely be needed in order to search for missing Λ^* and Σ^* resonances that couple weakly to $K_L^0 p$. Suggestions are given for specific production reactions that would allow searches for missing Λ^*, Σ^*, Ξ^*, and Ω^* resonances.

1. Introduction

It is convenient to describe baryons with a "quark shell model" in which each quark moves in a mean field generated mainly by the gluons in the hadron. Lattice gauge calculations have shown that the predicted spectrum of excited states is more-or-less consistent with what is expected from SU(6) symmetry. In such models, baryons are grouped into three possible SU(6) multiplets consisting of flavor octets, decuplets, or singlets with total quark intrinsic spin of either 1/2 (spin doublets) or 3/2 (spin quartets):

$$\begin{aligned} \mathbf{56}_S &= {}^2 8 + {}^4 10, \\ \mathbf{70}_M &= {}^2 8 + {}^4 8 + {}^2 10 + {}^2 1, \\ \mathbf{20}_A &= {}^2 8 + {}^4 1. \end{aligned}$$

The uds basis, which takes into account the heavier mass of the strange quark, provides a better physical description of the hyperon resonances, but the SU(6) basis is simpler for counting the number of states. In a harmonic-oscillator shell-model description, the SU(6) multiplets contained in the first three oscillator bands have the following structure [1]:

$$\begin{aligned} N=0 \qquad \psi(\mathbf{56},0^+) &= (1s)^3, \\ N=1 \qquad \psi(\mathbf{70},1^-) &= (1s)^2(1p), \\ N=2 \qquad \psi(\mathbf{56},0^+) &= \sqrt{\frac{2}{3}}(1s)^2(2s) + \sqrt{\frac{1}{3}}(1s)(1p)^2, \\ \psi(\mathbf{70},0^+) &= \sqrt{\frac{1}{3}}(1s)^2(2s) + \sqrt{\frac{2}{3}}(1s)(1p)^2, \\ \psi(\mathbf{56},2^+) &= \sqrt{\frac{2}{3}}(1s)^2(1d) - \sqrt{\frac{1}{3}}(1s)(1p)^2, \\ \psi(\mathbf{70},2^+) &= \sqrt{\frac{1}{3}}(1s)^2(1d) - \sqrt{\frac{2}{3}}(1s)(1p)^2, \end{aligned}$$

$$\psi(\mathbf{20}, 1^+) \;=\; (1s)(1p)^2.$$

The eight SU(6) multiplets that are allowed in the $N = 3$ band are: $(\mathbf{56}, 1^-)$, $(\mathbf{70}, 1^-)$, $(\mathbf{70}, 1^-)$, $(\mathbf{20}, 1^-)$, $(\mathbf{70}, 2^-)$, $(\mathbf{56}, 3^-)$, $(\mathbf{70}, 3^-)$, and $(\mathbf{20}, 3^-)$ and the allowed shell-model configurations are listed in Table 1. Here L is the total orbital angular momentum of the constituent quarks and the total parity is shown as a superscript.

$(1s)^2(2p)$	$L = 1$
$(1s)^2(1f)$	$L = 3$
$(1s)(1p)(2s)$	$L = 1$
$(1s)(1p)(1d)$	$L = 1, 2, 3$
$(1p)^3$	$L = 1, 3$

Table 1: Shell-model configurations allowed for baryons in the $N = 3$ oscillator band.

Pure hyperon states in the $N = 2$ ($\mathbf{20}$,1^+) multiplet cannot couple to $\overline{K}N$ via a single-quark transition operator. They will not be considered further. Similarly, pure hyperon states in the $N = 3$ ($\mathbf{20}$,1^-), ($\mathbf{70}$,2^-), and ($\mathbf{20}$,3^-) multiplets cannot couple to $\overline{K}N$ via a single-quark transition operator. They will also not be considered further. All baryons predicted to belong to these multiplets are "missing" and likely to stay that way.

2. **Missing Resonances**

^{2}8	N(939)	****	^{4}10	Δ(1232)	****
1/2$^+$	Λ(1116)	****	3/2$^+$	Σ(1385)	****
	Σ(1193)	****		Ξ(1530)	****
	Ξ(1322)	****		Ω(1672)	****

Table 2: The $N = 0$ ($\mathbf{56}$,0^+) ground-state baryons. All are well-established 4-star states and none are missing.

Tables 2 to 7 compare experimental observations with predictions for low-lying states in the first three harmonic-oscillator bands. Assignments for some states are educated guesses. Star ratings are from the *Review of Particle Physics* [2]. Table 8 gives a summary of the number of missing states for each oscillator band. For counting purposes, 1-star states are included in the count for missing states, but 2-star states are not. As one might expect, most predicted Ξ^* and Ω^* resonances are missing. Candidate states have been found for most of the predicted N^* and Δ^* resonances, if one ignores states in the ($\mathbf{20}$,1^+) multiplet. However, a large number of predicted Σ^* resonances are also missing. Many or most of these states might be found using measurements of $K^0_L p$ scattering, which is isospin-1 selective and would therefore be an ideal means to study Σ^* resonances. Further details are provided in the next section.

^{2}8	N(1535)	****	^{2}8	N(1520)	****						
1/2$^-$	Λ(1670)	****	3/2$^-$	Λ(1690)	****						
	Σ(1620)	*		Σ(1670)	****						
	Ξ(1690)	***		Ξ(1820)	***						
^{4}8	N(1650)	****	^{4}8	N(1700)	***	^{4}8	N(1675)	****			
1/2$^-$	Λ(1800)	***	3/2$^-$	Λ		5/2$^-$	Λ(1830)	****			
	Σ(1750)	***		Σ			Σ(1775)	****			
	Ξ(1950)	***		Ξ			Ξ(2030)	***			
^{2}10	Δ(1620)	****	^{2}10	Δ(1700)	****	^{2}1	Λ(1405)	****	^{2}1	Λ(1520)	****
1/2$^-$	Σ		3/2$^-$	Σ(1940)	***	1/2$^-$			3/2$^-$		
	Ξ			Ξ							
	Ω			Ω							

Table 3: The $N = 1$ ($\mathbf{70}$,1$^-$) negative-parity excited states. The spin-parity quantum numbers of Ξ(1690), Ξ(1950), and Ξ(2030) are unmeasured.

^{2}8	N(1440)	****	^{4}10	Δ(1600)	***
1/2$^+$	Λ(1600)	***	3/2$^+$	Σ	
	Σ(1660)	***		Ξ	
	Ξ			Ω	

Table 4: The $N = 2$ ($\mathbf{56}$,0$^+$) positive-parity excited states.

^{2}8	N(1720)	****	^{2}8	N(1680)	****						
3/2$^+$	Λ(1890)	****	5/2$^+$	Λ(1820)	****						
	Σ			Σ(1915)	****						
	Ξ			Ξ							
^{4}10	Δ(1910)	****	^{4}10	Δ(1920)	***	^{4}10	Δ(1905)	***	^{4}10	Δ(1905)	***
1/2$^+$	Σ		3/2$^+$	Σ		5/2$^+$	Σ		7/2$^+$	Σ(2030)	****
	Ξ			Ξ			Ξ			Ξ	
	Ω			Ω			Ω			Ω	

Table 5: The $N = 2$ ($\mathbf{56}$,2$^+$) positive-parity excited states.

^{2}8	N(1710)	***	^{4}8	N		^{2}10	Δ(1750)	*	^{2}1	Λ(1710)	*
1/2$^+$	Λ(1810)	***	3/2$^+$	Λ		1/2$^+$	Σ		1/2$^+$		
	Σ(1880)	**		Σ			Ξ				
	Ξ			Ξ			Ω				

Table 6: The $N = 2$ ($\mathbf{70}$,0$^+$) positive-parity excited states.

^{2}8	N		^{2}8	$N(1860)$	*						
3/2$^+$	Λ		5/2$^+$	Λ							
	Σ			Σ							
	Ξ			Ξ							
^{4}8	$N(1880)$	**	^{4}8	$N(1900)$	***	^{4}8	$N(2000)$	**	^{4}8	$N(1990)$	**
1/2$^+$	Λ		3/2$^+$	Λ		5/2$^+$	Λ		7/2$^+$	$\Lambda(2020)$	*
	Σ			Σ			Σ			Σ	
	Ξ			Ξ			Ξ			Ξ	
^{2}10	Δ		^{2}10	$\Delta(2000)$	**	^{2}1	Λ		^{2}1	$\Lambda(2110)$	***
3/2$^+$	Σ		5/2$^+$	Σ		3/2$^+$			5/2$^+$		
	Ξ			Ξ							
	Ω			Ω							

Table 7: The $N = 2$ ($\mathbf{70}$,2^+) positive-parity excited states.

Baryon	$N = 0$	$N = 1$	$N = 2$
N	0	0	2
Δ	0	0	2
Λ	0	1	9
Σ	0	3	15
Ξ	0	3	19
Ω	0	2	8

Table 8: Summary of numbers of low-lying missing baryon resonances. For counting purposes, 1-star states are included as "missing" but 2-star states are not. All predicted states in the $N = 2$ ($\mathbf{20}$,1^+) multiplet are missing but are not included in these totals.

3. PWA Formalism

Here, we summarize some of the physics issues involved with $K^0_L p$ scattering. The differential cross section and polarization for $K^0_L p$ scattering are given by

$$\frac{d\sigma}{d\Omega} = \lambda\!\!\!^{-2}(|f|^2 + |g|^2),$$

$$P\frac{d\sigma}{d\Omega} = 2\lambda\!\!\!^{-2}\mathrm{Im}(fg^*),$$

where $\lambda\!\!\!^{-} = \hbar/k$, with k the magnitude of c.m. momentum for the incoming meson. Here $f = f(W, \theta)$ and $g = g(W, \theta)$ are the usual spin-nonflip and spin-flip amplitudes at c.m. energy W and meson c.m. scattering angle θ.

In terms of partial waves, f and g can be expanded as

$$f(W, \theta) = \sum_{l=0}^{\infty}[(l + 1)T_{l+} + lT_{l-}]P_l(\cos\theta),$$

$$g(W,\theta) = \sum_{l=1}^{\infty}[T_{l+} - T_{l-}]P_l^1(\cos\theta).$$

Here l is the initial orbital angular momentum, $P_l(\cos\theta)$ is a Legendre polynomial, and $P_l^1(\cos\theta) = \sin\theta \times dP_l(\cos\theta)/d(\cos\theta)$ is an associated Legendre function. The total angular momentum for T_{l+} is $J = l + \frac{1}{2}$, while that for T_{l-} is $J = l - \frac{1}{2}$.

We may ignore small CP-violating terms and write

$$K_L^0 = \frac{1}{\sqrt{2}}(K^0 - \overline{K^0}) \qquad \text{and} \qquad K_S^0 = \frac{1}{\sqrt{2}}(K^0 + \overline{K^0}).$$

We have both $I = 0$ and $I = 1$ amplitudes for KN and $\overline{K}N$ scattering, so that amplitudes $T_{l\pm}$ can be expanded in isospin amplitudes as

$$T_{l\pm} = C_0 T_{l\pm}^0 + C_1 T_{l\pm}^1,$$

where $T_{l\pm}^I$ are partial-wave amplitudes with isospin I and total angular momentum $J = l \pm \frac{1}{2}$, with C_I the appropriate isospin Clebsch-Gordon coefficients. The amplitudes for $K_L^0 p$ reactions leading to two-body final states are:

$$\begin{aligned}
T(K_L^0 p \to K_S^0 p) &= \frac{1}{2}\left(\frac{1}{2}T^1(KN \to KN) + \frac{1}{2}T^0(KN \to KN)\right) \\
&- \frac{1}{2}T^1(\overline{K}N \to \overline{K}N), \\
T(K_L^0 p \to \pi^+\Lambda) &= -\frac{1}{\sqrt{2}}T^1(\overline{K}N \to \pi\Lambda), \\
T(K_L^0 p \to \pi^+\Sigma^0) &= -\frac{1}{2}T^1(\overline{K}N \to \pi\Sigma), \\
T(K_L^0 p \to \pi^0\Sigma^+) &= \frac{1}{2}T^1(\overline{K}N \to \pi\Sigma), \\
T(K_L^0 p \to K^+\Xi^0) &= -\frac{1}{\sqrt{2}}T^1(\overline{K}N \to K\Xi).
\end{aligned}$$

These amplitudes show that only Σ^* resonances are formed as s-channel intermediate states in $K_L^0 p$ reactions. The reaction $K_L^0 p \to K_S^0 p$ is not ideal for finding missing Σ^* states that couple weakly to $\overline{K}N$ because of nonresonant KN background and because the amplitude involves $\overline{K}N$ in both initial and final states. The inelastic two-body reactions listed above would be better probes for finding missing Σ^* states due to isospin selectivity, absence of nonresonant KN background, and the fact that their amplitudes only involve $\overline{K}N$ coupling in the initial state.

To search for missing Σ^* states that couple weakly to $\overline{K}N$, one should also use production reactions such as $K_L^0 p \to \pi^+\Sigma^{0*}$, with $\Sigma^{0*} \to \pi^0\Lambda$, or use $K_L^0 p \to \pi^0\Sigma^{+*}$, with $\Sigma^{+*} \to \pi^+\Lambda$. Note that the $\pi\Lambda$ decays establish Σ^* states ($I = 1$) uniquely. In principle, one could search for Λ^* resonances using $K_L^0 n$ reactions, but doing so presents additional problems such as Fermi motion smearing and the need to identify quasi-free $K_L^0 n$ reactions from

measurements on a deuterium target. To search for missing Λ^* states that couple weakly to $\overline{K}N$, one should instead use production reactions such as $K^0_L p \to \pi^+\Lambda^*$, with $\Lambda^* \to \pi^+\Sigma^-$, $\Lambda^* \to \pi^-\Sigma^+$, or $\Lambda^* \to \pi^0\Sigma^0$. Note that the $\pi^0\Sigma^0$ decays establish Λ^* states ($I = 0$) uniquely. Narrow states could be identified using missing-mass techniques, but the determination of spin-parity quantum numbers would need a partial-wave analysis analogous to those used in meson spectroscopy studies. To search for missing Ξ^* or Ω^* states, one needs production reactions such as $K^0_L p \to K^+\Xi^{0*}$, $K^0_L p \to \pi^+K^+\Xi^{-*}$, and $K^0_L p \to K^+K^+\Omega^{-*}$.

4. **Summary and Conclusions**

New data for inelastic $K^0_L p$ scattering would significantly improve our knowledge of Σ^* resonances. To search for missing hyperon resonances, we need measurements of production reactions:

Σ^*: $K^0_L p \to \pi\Sigma^* \to \pi\pi\Lambda$,
Λ^*: $K^0_L p \to \pi\Lambda^* \to \pi\pi\Sigma$,
Ξ^*: $K^0_L p \to K\Xi^*, \pi K\Xi^*$,
Ω^*: $K^0_L p \to K^+K^+\Omega^*$.

If such measurements can be performed with good energy and angle coverage and good statistics, then it is very likely that measurements with K^0_L beams would find several missing hyperon resonances.

5. **Acknowledgments**

The author thanks Dr. Igor Strakovsky and the other organizers for inviting him to speak at the workshop. This material is based upon work supported by the U.S. Department of Energy, Office of Science, Office of Medium Energy Nuclear Physics, under Award No. DE–SC0014323.

References

[1] D. Faiman and A. W. Hendry, Phys. Rev. D **173**, 1720 (1968).

[2] K. A. Olive *et al.* (Particle Data Group), Chin. Phys. C **38**, 090001 (2014).

2.4 The Quark Model and the Missing Hyperons

Fred Myhrer
Department of Physics and Astronomy
University of South Carolina
Columbia, SC 29208, U.S.A.

Abstract

The mass spectrum of the first excited negative parity Y^* states is presently not well established. The missing hyperon states will provide important clues about the dominant dynamics among the light quarks (u, d, and s) including their confinement properties. Accurate information of the partial decays of the first excited negative parity Λ^* and Σ^* states is extremely valuable in determining the main features of the interactions among the quarks. These quark-model interactions are due to gluon- and pseudo-meson exchanges. The latter is required by chiral symmetry. As will be presented, these interactions will strongly affect the partial decay widths of these hyperons.

1. The Quark Models

The interactions among the quarks are guided by the dynamics and symmetry properties of QCD. For high four-momentum hadronic processes where the strong coupling, α_s, is small, perturbative QCD is applicable and has been successful in describing these processes. However, at low energy α_s is not small and a model approach is necessary in order to study the ground- and excited states of baryons. In order to build a reasonable model we need to investigate which dynamical forces dominate among the "light" quarks, u, d and s. The Λ^* and Σ^* states have one s quark and two almost massless u and d quarks. Could this extra feature of having one quark with mass $m_s \gg m_u, m_d$ give us some extra insight into QCD beyond what the N^* and Δ^* states can provide? These quarks have current masses smaller than the QCD scale Λ_{QCD}, and it appears reasonable to assume that chiral symmetry considerations will be of importance for baryons involving these three light quarks. As we will discuss, chiral symmetry requirements introduce quark-interactions which affect the structure and the decays of the excited baryons.

A quark model for the hyperons includes quark confinements and effective quark-quark interactions. One presumes that the exchange of multiple soft gluons including self-interactions among the gluons will give raise to quark confinement. However, quark confinement is not really understood at present. The non-relativistic quark model (NRQM) of Isgur and Karl and their coworkers [1] uses the harmonic oscillator potential to simulate confinement and the effective one-gluon exchange (OGE) to describe the spin-dependent quark interactions. This NRQM is reasonably successful in reproducing the measured baryon mass-spectrum and the decays of the excited baryons, see also the presentation by Capstick [2]. The NRQM of Isgur and Karl was the main focus of an earlier conference presentation [3].

In this talk, I will concentrate on the MIT bag model where a confinement condition is imposed on the relativistic u, d and s quarks. In the bag model chiral symmetry is implemented phenomenologically by requiring the axial current to be continuous. This means that outside the confinement region the axial current is carried by a pseudo-scalar meson cloud

surrounding the three-quark bag (the "bare" baryon). In the chiral (cloudy) bag model these pseudo-scalar mesons mimic $\bar{q}q$ 0^- excitations, and effectively introduces spin-dependent interactions among the quarks with a coupling strength determined by the axial current. In addition, an effective interaction due to one-gluon exchange among the confined, relativistic quarks is included. This chiral (cloudy) bag model will predict the decay channel widths of excited baryons to ground state baryons plus a meson (π, K and/or η) or their electromagnetic transition to a lower baryon state. In this paper, I will concentrate only on the first excited hyperons, the negative parity Λ^* and Σ^* states, and make some observation on what we could learn about the effective quark dynamics in a quark model. We will assume that these hyperons are mainly composed of three valence quarks and present how the quark interactions will change the hyperon states' compositions and their partial decays. Some comments regarding the $\Lambda(1405)$ will be made.

According to the quark model there are several states among the first excited hyperon states which are missing or are not established. A natural question is: Do QCD require that these missing states should exist, or does QCD require further model restrictions not implemented in todays quark models? At this conference, we learned that in order to understand measurements in heavy-ion collisions, the number of hyperon states with masses below about 2.5 GeV is very important, e.g., see talk by Rene Bellwied [4]. As presented, it appears that the heavy-ion data require more hyperon states than what have been listed by PDG [5].

The generic non-relativistic baryon wave function has the following structure

$$\Psi = \Psi_{color}\ \Psi_{flavor}\ \Psi_{spin}\ \Psi_{space}\ . \tag{1}$$

We assume that isospin is a good symmetry, *i.e.*, in the bag model the u and d quarks are massless, *i.e.,* m_u = m_d = m_q =0. Since the s quark has a mass $m_s > m_q$, SU$_F$(3) is a broken symmetry and we therefore adopt the uds basis when the baryon wave functions are determined. Other quark model assumptions are:

- All hadrons are $SU(3)$-color singlets, *i.e.*, Ψ_{color} is a totally anti-symmetric wave function under the interchange of any two quarks.
- Confinement of quarks is universal condition, the same for all quark flavors.
- The Pauli principle requires that two identical quarks must have a totally anti-symmetric wave function. Since Ψ_{color} is anti-symmetric the product of the other components in Eq.(1) must be symmetric under the interchange of any two quarks.
- Non-relativistic quarks interact via an effective one-gluon-exchange a la De Rujula *et al.* [6]. This effective gluon exchange generates a spin-dependent interaction among the quarks and makes the *decuplet* baryons heavier than the *octet* baryons.

The non-relativistic effective OGE between quarks i and j is:

$$H^{ij}_{hyp} \ = \ A_{ij}\left\{\frac{8\pi}{3}\vec{S}_i\cdot\vec{S}_j\delta^3(\vec{r}_{ij}) + \frac{1}{r^3_{ij}}\left(\frac{3(\vec{S}_i\cdot\vec{r}_{ij})(\vec{S}_j\cdot\vec{r}_{ij})}{r^2_{ij}} - \vec{S}_i\cdot\vec{S}_j\right)\right\}\ , \tag{2}$$

where A_{ij} is a constant which depends on the constituent quark masses [6]. Note that this non-relativistic reduction of the effective OGE quark-quark interaction neglects the spin-orbit force. Isgur and Karl argue that the spin-orbit force should be small. This argument

is confirmed in the cloudy bag model evaluation where the relativistic quark P-state with j=3/2 has a lower energy than j=1/2, *i.e.*, the bag model's confinement condition introduces an effective spin-orbit splitting of quark states. Fortunately, in the chiral bag the relativistic OGE introduces a spin-orbit force of opposite sign and basically cancel the one from confinement. *Effectively what remains are the spin-spin and tensor interactions due to OGE and the pseudo-scalar meson (e.g., pion, K) cloud surrounding the quark core*, see for example Refs. [7, 8].

The spin-spin and the tensor quark-quark interactions in Eq.(2) are closely related, and the tensor component will produce a spatial D-state quark wave function. These interactions are similar to the meson exchange forces between nucleons in ^3H and ^3He, and analogously we expect the three valence quark baryon ground states to have similarly mixed three-quark spatial wave functions, *i.e.,* a mixture of S, S′ and D quark states. For example, due to H^{ij}_{hyp} Isgur and Karl [1] find that the nucleon has the structure:

$$|N\rangle \;\simeq\; 0.90|^2S_S\rangle - 0.34|^2S'_S\rangle - 0.27|^2S_M\rangle - 0.06|^2D_M\rangle\,, \tag{3}$$

where $|S'\rangle$ and $|D\rangle$ are the excited S- and D- quark states of the harmonic oscillator. The subscripts S and M denote symmetric and mixed symmetry spatial states, respectively. Similarly, Isgur and Karl find the $\Lambda(1116)$ state to be:

$$|\Lambda\rangle \;\simeq\; 0.93|^2S_S\rangle - 0.30|^2S'_S\rangle - 0.20|^2S_M\rangle - 0.03|^4D_M\rangle - 0.05|\mathbf{1},^2S_M\rangle. \tag{4}$$

The effective pseudo-scalar meson cloud of the chiral bag model surrounding the quark core of the baryons will also contribute to the spatial mixture of states. The spatial admixtures in the baryon ground states beyond the completely symmetric $|^2S_S\rangle$ state strongly affect some excited hyperon partial decay widths. In the next section, we will focus on the cloudy bag model evaluation of the spin-flavor admixture of the excited hyperon states.

2. Some Excited Hyperon states and Their Decays

The main decay channels of the some of the negative parity Λ^* and the $\Sigma(1775)$ states are tabulated in Table 1. The partial widths of the Λ^* states to the open meson baryon ground states and the $\Sigma(1775)$ decay to $\bar{K}N$ are from Ref. [5]. Except for the two lowest Λ^* mass states, the table makes clear that most of the partial widths are not well determined. The masses of these first excited hyperon states are shown in Fig. 1 where the uncertainties in the masses are indicated by the heights of the boxes. Also included are the two states given three stars in the PDG classification. In Fig. 1 the boxes with the question marks have two or one star PDG classification [5]. Two states "predicted" by the quark model, one Λ^* and one Σ^*, are completely missing in Ref. [5], *i.e.,* they have not been observed. The mass spectrum and the decay widths into specific final states can be strongly influenced by the spin-flavor admixtures as well as the spatial admixtures of the ground state baryons illustrated in Eqs. (3) and (4).

Table 1 : Ref. [5] gives the hadronic decay branching ratios for some Λ^* states and $\Sigma(1775)$.

$\Lambda^* - j^P$	Decay Product	%	Comment
$\Lambda(1405) - \frac{1}{2}^-$	$\pi\Sigma$	100	K^-p bound state?
$\Lambda(1520) - \frac{3}{2}^-$	$\bar{K}N$	45 ± 1	–
	$\pi\Sigma$	42 ± 1	–
	$\pi\pi\Lambda$	10 ± 1	via $\pi\Sigma(1385)$ mainly?
	$\pi\pi\Sigma$	0.9 ± 0.1	$\gamma\Lambda \sim 0.85\%$
$\Lambda(1670) - \frac{1}{2}^-$	$\bar{K}N$	$20 - 30$	–
	$\pi\Sigma$	$25 - 55$	–
	$\eta\Lambda$	$10 - 25$	–
$\Lambda(1690) - \frac{3}{2}^-$	$\bar{K}N$	$20 - 30$	–
	$\pi\Sigma$	$20 - 40$	–
	$\pi\pi\Lambda$	~ 25	–
	$\pi\pi\Sigma$	~ 20	–
	$\eta\Lambda$	?	–
$\mathbf{\Lambda(1850) - \frac{5}{2}^-}$	$\mathbf{\bar{K}N}$	$3 - 10$	–
	$\pi\Sigma$	$35 - 75$	–
	$\eta\Lambda$	?	–
$\mathbf{\Sigma(1775) - \frac{5}{2}^-}$	$\mathbf{\bar{K}N}$	$10 - 40$	–

This section will highlight results obtained in the chiral (cloudy) bag model. In a bag model evaluation the three valence quarks move relativistically. We assume that one valence quark is in one of the two possible P-states ($P_{1/2}$ or $P_{3/2}$). The two others are in the S state. We further assume that since the three-quark center-of-mass (c.m.) operator is a symmetric operator acting on the dominant symmetric three-quark ground state, the symmetric spatial wave function of the excited hyperons will describe their c.m. motion. The first excited negative parity Λ^* and Σ^* states therefore have a wave function, Ψ_{space}, which has mixed spatially symmetry. This will place restrictions on the possible flavor and spin wave function given in Eq. (1). Note, for example, that the $\Lambda(1850)$ or the $\Sigma(1775)$ $\frac{5}{2}^-$- states are pure $|^4 8\rangle$ states, *i.e.*, their spin wave function, Ψ_{spin}, is completely symmetric.

In this bag model it is the P-state quark which couples to the outgoing meson (π, K, or η) or the emitted photon in the decay of this excited state. The quark model predicts three possible Λ^* $\frac{3}{2}^-$-states and three possible Λ^* $\frac{1}{2}^-$-states, and gives the following general decomposition in terms of spin and $SU_F(3)$ multiplets:

$$|\Lambda^*\rangle \;=\; a|^2\mathbf{1}\rangle + b|^4\mathbf{8}\rangle + c|^2\mathbf{8}\rangle \; . \tag{5}$$

The corresponding Σ^*-states have the general structure:

$$|\Sigma^*\rangle \;\simeq\; \tilde{a}|^2\mathbf{10}\rangle + \tilde{b}|^4\mathbf{8}\rangle + \tilde{c}|^2\mathbf{8}\rangle. \tag{6}$$

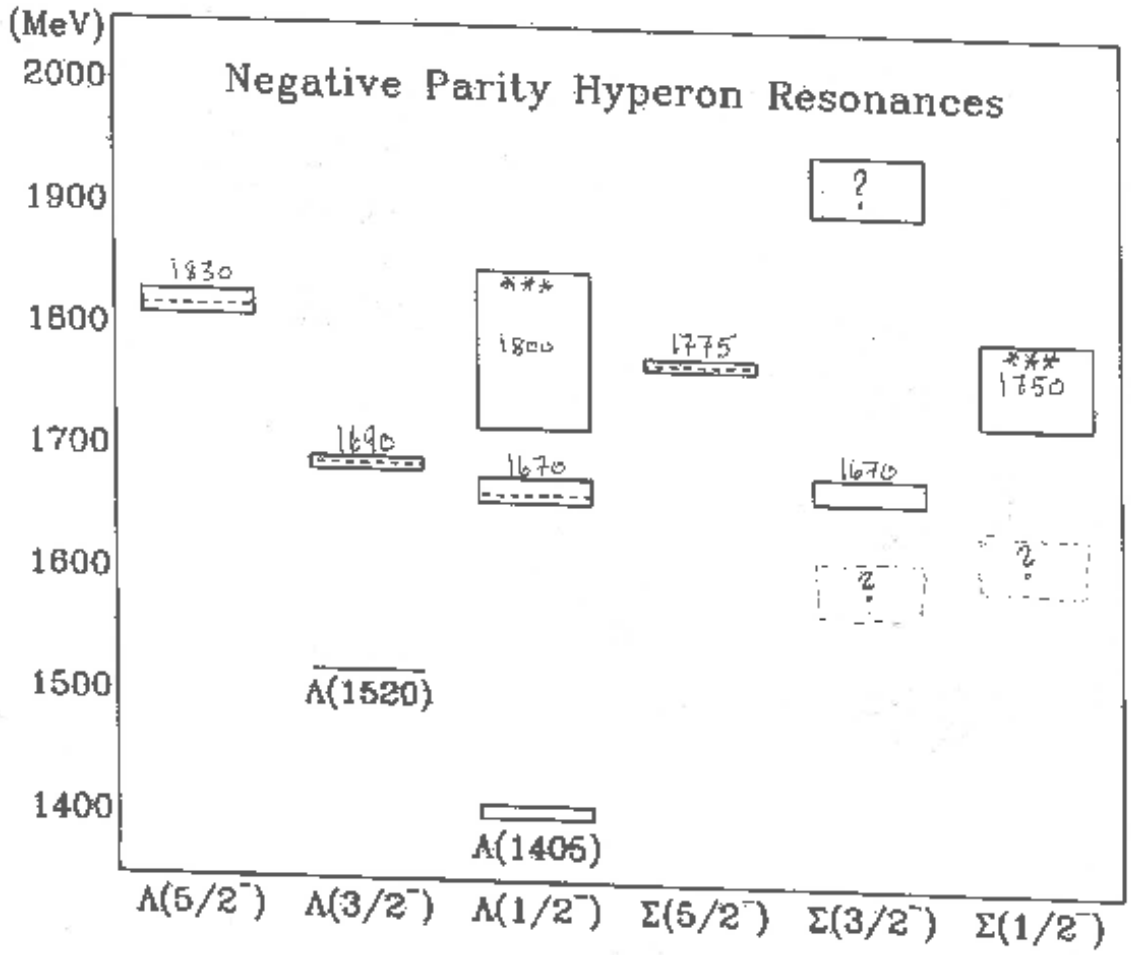

Figure 1: The confirmed mass spectrum of the first excited negative parity Λ^* and Σ^* states where we have included three-star states in Ref. [5]. The height of the boxes illustrate the mass uncertainties of the "established" states. The boxes with the question marks are states which are controversial. According to quark models there are two completely missing three-quark states in this figure.

Different quark models give different values for the sets of the three coefficients. Using the harmonic oscillator of the NRQM of Isgur and Karl find $a = 0.92$, $b = -0.04$ and $c = 0.39$ [1], which result in the following values for the two electromagnetic widths: $\Gamma[\Lambda(1520) \to \Lambda\gamma] = 96$ keV and $\Gamma[\Lambda(1520) \to \Sigma^0\gamma] = 74$ keV [9]. The cloudy bag model calculation produces the set of values $a = 0.95$, $b = -0.09$ and $c = 0.30$, which gives for the same photon decay widths: $\Gamma[\Lambda(1520) \to \Lambda\gamma] = 32$ keV, $\Gamma[\Lambda(1520) \to \Sigma^0\gamma] = 49$ keV [8]. In other words, a small change in the spin-flavor mixture of the Λ^* states will strongly influence the decay widths of these states.

In order to further dissect these results, we list in Table 2 the cloudy bag model intermediate results of Ref. [8] for the electromagnetic decay widths from each of the spin-flavor components of two excited Λ^* states. Further it is assumed that both $\Lambda(1116)$ and Σ^0 ground states have a totally symmetric spatial $|^2S_S\rangle$ state[1]. (Note that in the cloudy bag model the photon is also emitted from the virtual meson cloud.) Comparing these results one infers that these decay rates are very sensitive to the coefficients a, b, and c in Eq.(5).

Table 2 : The pure spin-flavor radiative decay widths of $\Lambda(1520)$ and $\Lambda(1405)$ in keV to ground state hyperons are extracted from evaluation-notes of Ref. [8]. Each column assumes the excited Λ^* is only in the indicated pure spin-flavor state.

Transition	$\|^2 1\rangle$	$\|^4 8\rangle$	$\|^2 8\rangle$
$\Lambda(1520) \to \gamma\Lambda$	24	21	23
$\Lambda(1520) \to \gamma\Sigma^0$	91	58	93
$\Lambda(1405) \to \gamma\Lambda$	42	0.2	33
$\Lambda(1405) \to \gamma\Sigma^0$	98	0.03	91

The admixture of the spin-flavor multiplets in excited hyperon states changes with the interactions among quarks. This is illustrated in Fig. 2 where we plot and list the masses of the three Σ^* $\frac{1}{2}^-$ states versus the strength α_s of the effective OGE interaction taken from the intermediate evaluations of Ref. [8]. As a function of the strength of the meson-cloud interaction one observes similar behaviors. (As stated earlier, the coupling of the meson cloud is fixed by the continuity requirement of the axial current.) The graphs in Fig. 2 give the intermediate hyperon masses for bag model parameters, $B^{1/4} = 145$ MeV, "zero-point" energy parameter $Z_0 = 0.45$ and strange quark mass $m_s = 250$ MeV, see Ref. [8]. Listed are the spin flavor compositions of the three states for $\alpha_s = 0$ and $\alpha_s = 2$. The figure shows how rapidly the spin flavor composition can change with increasing strength of the OGE interaction, α_s. Ref. [8] found a reasonable hyperon mass spectrum (apart from the lowest Λ^* $\frac{1}{2}^-$ state mass) for $\alpha_s = 1.5$.

[1] Including the configuration mixing in, e.g., $\Lambda(1116)$, Eq. (4) may change Γ_γ by 50% or more, see, e.g., the discussion in Ref. [3].

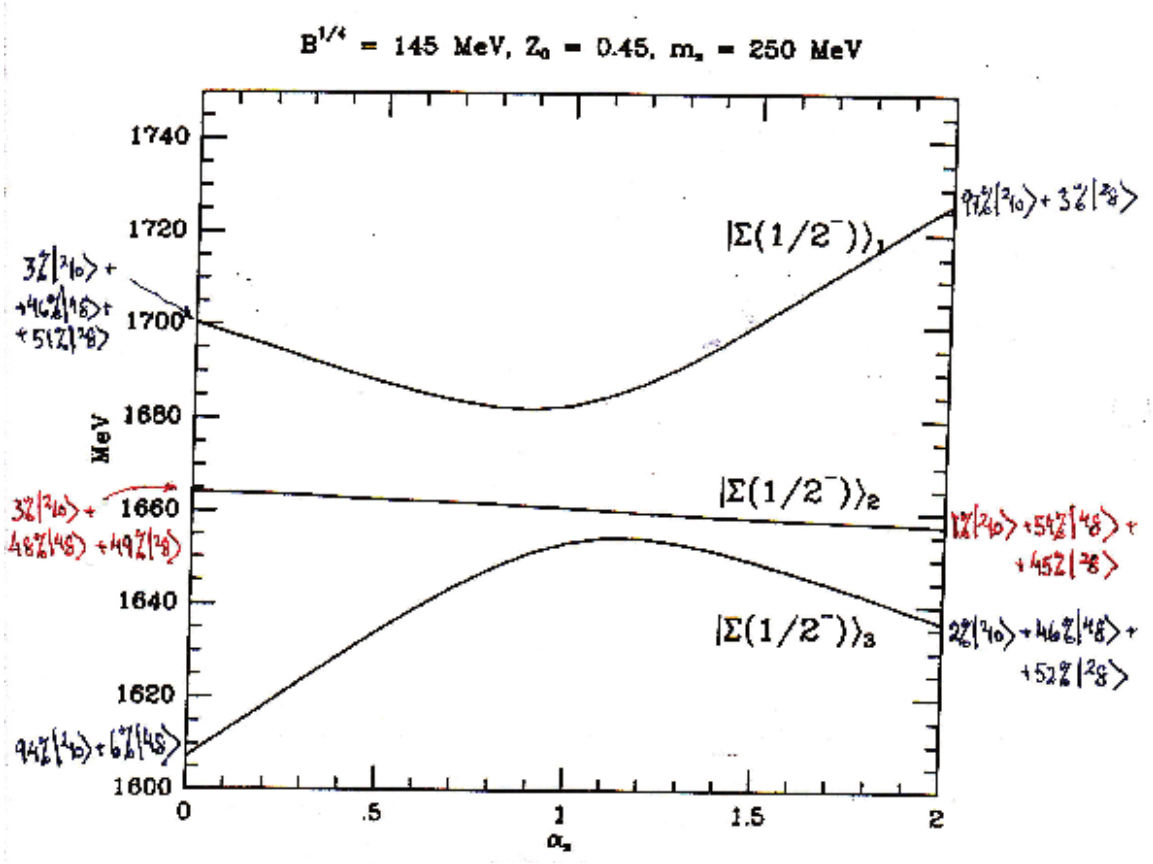

Figure 2: The intermediate evaluated masses of the three $\Sigma^* \frac{1}{2}^-$ states as a function of the strength α_s of the effective OGE. The spin-flavor multiplet contents of the states are listed for $\alpha_s = 0$ and $\alpha_s = 2.0$ and indicate how the spin-flavor of the states changes with α_s. The pseudo-scalar cloud interaction with the quarks also affects the flavor-spin multiplet content of the states.

3. An Illuminating Hadronic Decay Rate Argument

Following Ref. [1], the spatial wave function of three quarks is given by the two relative coordinates between the three quarks

$$\vec{\rho} \;=\; (\vec{r}_1 - \vec{r}_2)/\sqrt{2} \;\text{ and }\; \vec{\lambda} = (\vec{r}_1 + \vec{r}_2 - 2\vec{r}_3)/\sqrt{6}. \tag{7}$$

Here quarks 1 and 2 are the u and d quarks, and quark 3 is the s-quark. In the NRQM, the corresponding reduced constituent quark masses are $m_\rho = m_q^{con}$ and $m_\lambda = 3m_q^{con}m_s^{con}/(2m_q^{con} + m_s^{con})$. As presented by Capstick [2], the harmonic oscillator potential gives a difference in ρ and λ oscillator frequencies, ω_ρ and ω_λ due to the difference in the two reduced quark masses [1] resulting in a hyperon mass difference of,

$$\hbar(\omega_\rho - \omega_\lambda) = \hbar\omega_\rho \left[1 - \left(\frac{2(m_q^{con}/m_s^{con}) + 1}{3}\right)^{1/2}\right] \simeq 75 \text{ MeV}\,. \tag{8}$$

As shown by Capstick [2] and also in a talk at the KL2016 Workshop [3], the mass splitting between the $\Lambda^*(5/2^-)$ and the $\Sigma^*(5/2^-)$ states, shown in Fig. 1, can easily be understood by this difference in frequencies. (H_{hyp} will modify the mass difference between the two $(5/2)^-$ states [1].)

The difference in the spatial decomposition of the two $J^P = 5/2^-$ states' wave functions has the following decay implications: The spin wave function, Ψ_{spin}, of both $J^P = 5/2^-$ states is completely symmetric. The $\Lambda^*(1830)$ is an isospin singlet and therefore Ψ_{space} of Eq. (1) must have the anti-symmetric $\vec{\rho}$-dependence, *i.e.,* it decouples from $\bar{K}N$ since the nucleon spatial wave function is symmetric under the interchange $1 \leftrightarrow 2$. The $\Sigma^*(1775)$ is symmetric in isospin and therefore Ψ_{space} must be symmetric, *i.e.,* it has a symmetric $\vec{\lambda}$-dependence and couples easily to $\bar{K}N$. When modifications due to H_{hyp} is included, the difference in the two observed decays widths are explained [1] as follows.

The expressions in Eqs. (3) and (4) derived using H_{hyp}^{ij} tell us that the ground state baryons are not pure symmetric $|^2S_S\rangle$ states. By including the mixed symmetric component $|^2S_M\rangle$ of the nucleon state, Ref. [1] finds the following ratio of decay amplitudes,

$$\frac{\text{A}(\Lambda^*(1830) \to \bar{K}N)}{\text{A}(\Sigma^*(1775) \to \bar{K}N)} \simeq -0.28\,. \tag{9}$$

This example illustrates the close relations between the internal structure of the initial and final baryon and the magnitude of the corresponding decay width. This ratio should be compared with the ratio of decay widths extracted from the Ref. [5] and listed in Table 1.

The cloudy (chiral) bag model where the coupling to the outgoing meson is fixed by the required continuation of the axial current, the hadronic decay widths are determined. However, as shown, the spin-flavor mixing of the excited states (and the ground states) due to the quark interactions are critical in evaluating the various hadronic (and electromagnetic) partial decay widths. A more precise determination of these partial decay widths will allows us to better describe the effective interactions among the light confined quarks.

4. **Comments Regarding** $\Lambda(1405)$

A common puzzle within quark models, which has not been resolved satisfactory, is: Why is $\Lambda(1405)$ about 100 MeV below $\Lambda(1520)$ in mass? If we assume that the Λ^* states are mainly three-quark states, quark models have serious problems generating this large observed spin-orbit-like mass splitting between these two Λ^* states. At present it is very difficult within quark models to generate a large mass difference between these two states since, as shown, the effective spin-orbit interaction among quarks appears to be negligibly small. In the cloudy bag model, the P-state quark with $j = 3/2$ has a lower energy than the $j = 1/2$ state. This means the bag confinement condition imposes an effective spin-orbit splitting of the quark P-state which is mostly cancelled by the effective OGE interactions. This strengthen the original argument of Isgur and Karl [1] that the effective spin-orbit interaction is negligible in quark models. Effectively what remains are the spin-spin and tensor interactions among the quarks. Could a strong non-linear coupling of the lowest $J^P = \frac{1}{2}^-$ three-quark state to the meson-baryon decay channels (beyond how this is presently treated in cloudy bag models) explain this mass-splitting?

Historically, Dalitz and Tuan [10] proposed that $\Lambda(1405)$ is a K^-p bound state (a "quark molecule"). Could it have a large multi-quark (pentaquark) state component? What are the differences between a pentaquark state and a "quark molecule"? A renewed and better treatment of the meson cloud in the chiral bag model could possibly generate a strong enough meson-baryon interaction in order to generate a K^-p bound state. Apart from recent measurements of the K^-p atom [11], most $\bar{K}p$ scattering data are very old. We urgently need more and better data to settle the numerous theoretical discussions regarding the nature of $\Lambda(1405)$.

5. **Summary**

It is imperative that we can experimentally establish the mass spectrum of the lowest excited negative parity Λ^* and Σ^* states in order to enhance our understanding of how QCD operates among the three confined "light" quarks u, d and s. The forthcoming JLab proposal on a K^0_L beam is promising. K^0_L scattering off a hydrogen target can access Σ^* states and hopefully could firmly establish some of the missing Σ^* states in Fig. 1. The Σ^* states decay to $\bar{K}N$ or $\pi\Sigma$ or possibly both, as well as $\pi\Lambda$ according to theory estimates. However, some Σ^* states might not couple strongly to the $\bar{K}N$. In order to explore the Λ^* states, the reaction $\gamma + p \to K^+\Lambda^*$ appears to be a possible Λ^* direct production channel.

As is evident from Table 1 and this presentation, more precise measurements of the branching ratios of these excited hyperon decays will enhance our understanding of these states, and give better insight of the behavior of the interactions of the confined light quarks.

6. **Acknowledgments**

The author is grateful for generous travel support to the YSTAR conference from Jefferson Lab. and the USC's Physics and Astronomy Department.

References

[1] N. Isgur and G. Karl, Phys. Rev. Lett. **41**, 1269 (1978); Phys. Lett. B **74**, 353 (1978); Phys. Rev. D **18**, 4187 (1978); R. Koniuk and N. Isgur, Phys. Rev. D **21**, 1868 (1980).

[2] S. Captick, talk at this conference.

[3] F. Myhrer, talk at the KL2016 Workshop; arXiv:1604.02141. pp. 49 – 55.

[4] R. Bellwied, talk at this conference.

[5] K. A. Olive *et al.* (Particle Data Group), Chin. Phys. C **38**, 090001 (2014).

[6] A. De Rujula, H. Georgi, and S. L. Glashow, Phys. Rev. D **12**, 147, (1975).

[7] F. Myhrer and J. Wroldsen, Rev. Mod. Phys. **60**, 629 (1988).

[8] Y. Umino and F. Myhrer, Phys. Rev. D **39**, 3391; Nucl. Phys. A **529**, 713 (1991), *ibid.* **554**, 593 (1993).

[9] J. W. Darewych, M. Horbatsch, and R. Koniuk, Phys. Rev. D **28**, 1125 (1983).

[10] R. H. Dalitz and S. F. Tuan, Ann. Phys. **10**, 307 (1960).

[11] M. Bazzi *et al.* (SIDDHARTA Collaboration), Phys. Lett. B **704**, 113 (2011); M. Iwasaki *et al.* (KEK-collaboration), Phys. Rev. Lett. **78**, 3067 (1997).

2.5 Ambiguities of the Antikaon-Nucleon Scattering Amplitude

Maxim Mai
Institute for Nuclear Studies and Department of Physics
The George Washington University
Washington, DC 20052, U.S.A.

Abstract

In this talk we discuss the modern approaches of the theory of antikaon-nucleon scattering based on unitarization of the interaction potential derived from Chiral Perturbation Theory. Such approaches rely on very old experimental data, when fitting their free parameters. Thus, ambiguities arise the description of the data. We demonstrate these ambiguities on the example of one specific framework and discuss several possibilities to overcome these.

1. Introduction

Antikaon-nucleon scattering is one of the most discussed reactions among the meson-baryon interaction channels from the corresponding ground state octets. At energies below the chiral symmetry breaking scale, Chiral Perturbation Theory (ChPT) allows one to investigate the meson-baryon scattering amplitudes systematically, see Ref. [1] for a recent review on baryon ChPT. The full calculation of the scattering length up to next-to-next-to-leading chiral order yields $a_{\bar{K}N}^{I=0} = +0.53 + 0.97 - (0.40 - 0.22i) = +1.11 + 0.22i$ fm, see Ref. [2]. The convergence of the series is rather slow, which is presumably due to the large kaon mass as well as large difference of the coupled channels thresholds. Further, the net result disagrees with the experimental one ($a_{\bar{K}N}^{I=0} \approx -0.53 + 0.77i$ fm) even in the sign. This result is derived from from the measurement of the energy shift and width of kaonic hydrogen in the SIDDHARTA experiment at DAΦNE [3], using the Deser-type formula from Ref. [4]. The main reason for this behavior is the presence of a sub-threshold resonance, the so-called $\Lambda(1405)$ in this channel, which was already indicated in the early studies of total cross section [5]. Therefore, a perturbative treatment inevitably breaks down and non-perturbative techniques are required.

The chiral unitary approach (UChPT) is considered to be the best non-perturbative framework to address the SU(3) dynamics in such a type of systems. Many studies have been performed in the last two decades using different versions of this framework, see, e.g., Refs. [6–13]. Exploring the complex energy plane, it has been observed in Ref. [13] for the first time that the resonant behavior in the $\bar{K}N$ channel is associated with a two-pole structure, see Ref. [9] for a review. However, the available $K^- p \to MB$ total cross section data alone do not allow to pin down the positions of both poles with good precision, see, e.g., Ref. [6, 11]. Further, in a direct comparison [14] of the most recent approaches on antikaon-nucleon scattering [11, 15–17] it was found that the predictions of different approaches disagree strongly on the scattering amplitude in the Isospin $I = 1$ sector already in the close proximity of the $\bar{K}N$ threshold. Further, it was found that in all analyzed models not only the position, but also the origin of the wider pole varies between different approaches and even within different fitting scenarios of each single approach.

The main purpose of this work is to study this ambiguity as well as to suggest ways to reduce it. To perform this study in a systematic manner, we will restrict ourselves here to one single, but the most general framework derived in Refs. [11, 18]. We will show that at least several solutions for the antikaon-nucleon scattering amplitude agree with the experimental scattering data. However, including data, e.g, from photoproduction experiment at CLAS [19], some of these solutions can be disregarded as unphysical. Further, using synthetic data we discuss the possible impact of the new measurements of cross sections, which might become available in the proposed $K_{\rm long}$-beam experiment at Jefferson Lab [20].

2. Chiral Unitary Approach

(a) Model

The present analysis is based on the amplitude constructed and described in detail in Refs. [11, 18, 21], to which we refer the reader for the conceptual details. We start from the chiral Lagrangian of the leading (LO) and next-to-leading (NLO) chiral order, see Refs. [22, 23]. For the reasons presented in Refs. [11, 18, 21], the s- and u-channel one-baryon exchange diagrams are neglected, leaving us with the following chiral potential

$$\begin{aligned} V(\not{q}_2, \not{q}_1; p) =& A_{WT}(\not{q}_1 + \not{q}_2) + A_{14}(q_1 \cdot q_2) + A_{57}[\not{q}_1, \not{q}_2] + A_M \\ &+ A_{811}\Big(\not{q}_2(q_1 \cdot p) + \not{q}_1(q_2 \cdot p)\Big)\,, \end{aligned} \tag{1}$$

where the incoming and outgoing meson four-momenta are denoted by q_1 and q_2, whereas the overall four-momentum of the meson-baryon system is denoted by p. The symbols A_{WT}, A_{14}, A_{57}, A_M and A_{811} denote the 10-dimensional matrices which encode the coupling strengths between all 10 channels of the meson-baryon system for strangeness $S = -1$, i.e., $\{K^- p$, $\bar{K}^0 n$, $\pi^0\Lambda$, $\pi^0\Sigma^0$, $\pi^+\Sigma^-$, $\pi^-\Sigma^+$, $\eta\Lambda$, $\eta\Sigma^0$, $K^+\Xi^-$, $K^0\Xi^0\}$. These matrices depend on the meson decay constants, the baryon mass in the chiral limit, the quark masses as well as 14 low-energy constants (LECs) as specified in the original publication [11].

Due to the appearance of the $\Lambda(1405)$ resonance just below the $\bar{K}N$ threshold and large momentum transfer, the strict chiral expansion is not applicable for the present system. Instead, the above potential is used as a driving term of the coupled-channel Bethe-Salpeter equation (BSE), for NLO approaches see, e.g., Ref. [6, 12, 15, 16, 24–26]. For the meson-baryon scattering amplitude $T(\not{q}_2, \not{q}_1; p)$ the integral equation to be solved reads

$$T(\not{q}_2, \not{q}_1; p) = V(\not{q}_2, \not{q}_1; p) + i \int \frac{d^d l}{(2\pi)^d} V(\not{q}_2, \not{l}; p) S(\not{p} - \not{l}) \Delta(l) T(\not{l}, \not{q}_1; p)\,, \tag{2}$$

where S and Δ represent the baryon (of mass m) and the meson (of mass M) propagator, respectively, and are given by $iS(\not{p}) = i/(\not{p} - m + i\epsilon)$ and $i\Delta(k) = i/(k^2 - M^2 + i\epsilon)$. Moreover, T, V, S, and Δ in the last expression are matrices in the channel space. The loop diagrams appearing above are treated using dimensional regularization and applying the usual $\overline{\rm MS}$ subtraction scheme in the spirit of our previous work [18]. Note that the modified loop integrals are still scale-dependent. This scale μ reflects the influence

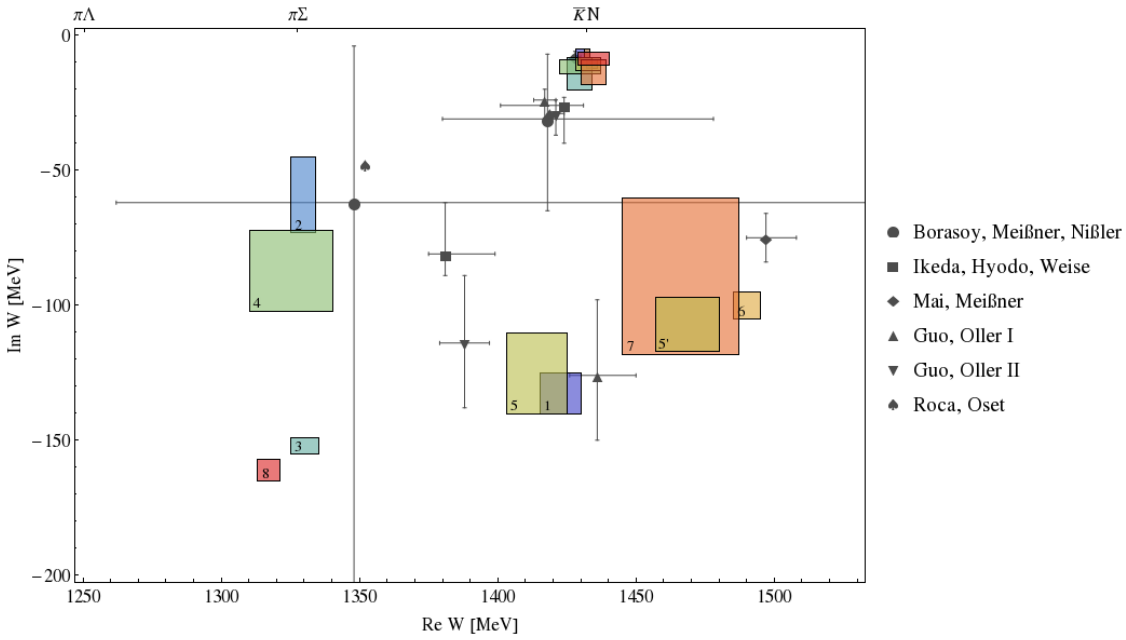

Figure 1: Double pole structure of the $\Lambda(1405)$ in the complex energy plane for the eight solutions that describe the scattering and the SIDDHARTA data. For easier reading, we have labeled the second pole of these solutions by the corresponding fit #, where 5 and $5'$ denote the second pole on the second Riemann sheet, connected to the real axis between the $\pi\Sigma - \bar{K}N$ and $\bar{K}N - \eta\Lambda$ thresholds, respectively. For comparison, various results from the literature are also shown, see Refs. [6, 12, 15, 16, 27].

of the higher-order terms not included in our potential. It is used as a fit parameter of our approach. To be precise, we have 6 such parameters in the isospin basis.

The above equation can be solved analytically, if the kernel contains contact terms only, see Ref. [21] for the corresponding solution. Using this solution for the strangeness $S = -1$ system, we have shown in Ref. [12] that once the full off-shell amplitude is constructed, one can easily reduce it to the on-shell solution, i.e., setting all tadpole integrals to zero. It appears that the double pole structure of the $\Lambda(1405)$ is preserved by this reduction and that the position of the two poles are changing only by about 20 MeV in the imaginary part. On the other hand, the use of the on-shell approximation of the Eq. (2) reduces the computational time roughly by a factor of 30. Therefore, since we wish to explore the parameter space in more detail, it seems to be safe and also quite meaningful to start from the solution of the BSE (2) with the chiral potential (1) on the mass-shell. Once the parameter space is explored well enough we can slowly turn on the tadpole integrals obtaining the full off-shell solution. Such a solution will become a part of a more sophisticated two-meson photoproduction amplitude in a future publication.

(b) **Fit Procedure and Results**

The free parameters of the present model, the low-energy constants as well as the regularization scales μ are adjusted to reproduce all known experimental data in the

meson-baryon sector. The main bulk of this data consists of the cross sections for the processes $K^-p \to K^-p$, $K^-p \to \bar{K}^0 n$, $K^-p \to \pi^0\Lambda$, $K^-p \to \pi^+\Sigma^-$, $K^-p \to \pi^0\Sigma^0$, $K^-p \to \pi^-\Sigma^+$ for laboratory momentum $P_{\rm lab} < 300$ MeV from Refs. [28–31]. Electromagnetic effects are not included in the analysis and assumed to be negligible at the measured values of $P_{\rm lab}$. Additionally, at the antikaon-nucleon threshold, the following decay ratios from Refs. [32, 33] as well as the energy shift and width of kaonic hydrogen in the 1s state, i.e., $\Delta E - i\Gamma/2 = (283 \pm 42) - i(271 \pm 55)$ eV from the SIDDHARTA experiment at DAΦNE [3]. The latter two values are related to the K^-p scattering length via the modified Deser-type formula [4].

The fit procedure was performed as follows: First, for randomly chosen starting values of the free parameters (in a natural range) the fit was performed to all threshold values and cross section data. Repeating this procedure several thousand times, we ended with several dozen of parameter sets that describe the data equally well. For each of these sets the amplitudes were analytically continued to the positive and negative complex energy plane. Thereafter, every unphysical solution, e.g., those with poles on the first Riemann sheet for $\mathrm{Im}(W) < 200$ MeV ($W := \sqrt{p^2}$), was sorted out. Eight best solutions were obtained by this procedure, see Tab. 1, whereas the next best $\chi^2_{\rm d.o.f.}$ are at least one order of magnitude larger. Although the fit results look very promising, we would like to point out that there are quite a few (20) free parameters in the model. The latter are assumed to be of natural size, but not restricted otherwise. Thus, we can not exclude that there might be more solutions which describe the assumed experimental data equally well.

The data are described equally well by all eight solutions, showing, however, different functional behavior of the cross sections as a function of $P_{\rm lab}$. These differences are even more pronounced for the scattering amplitude f_{0+}, which is fixed model independently only in the K^-p channel at the threshold by the scattering length a_{K^-p}. Similar observation was made in the comparison of this approach with other most recently used UChPT models in Ref. [14].

When continued analytically to the complex W plane, all eight solutions confirm the double pole structure of the $\Lambda(1405)$, see Fig. 1. The scattering amplitude is restricted around the $\bar{K}N$ threshold by the SIDDHARTA measurement quite strongly. Therefore, in the complex W plane we observe a very stable behavior of the amplitude at this energy, i.e., the position of the narrow pole agrees among all solutions within the 1σ parameter errors, see Fig. 1. This is in line with the findings of other groups [6, 15, 16], i.e., one observes stability of the position of the narrow pole. Quantitatively, the first pole found in these models is located at somewhat lower energies and is slightly broader than those of our model. In view of the stability of the pole position, we trace this shift to the different treatment of the Born term contributions to the chiral potential utilized in Refs. [6, 15, 16].

The position of the second pole is, on the other hand, less restricted. To be more precise, for the real part we find three clusters of these poles: around the $\pi\Sigma$ threshold, around the $\bar{K}N$ threshold as well as around 1470 MeV. For several solutions there is some agreement in the positions of the second pole between the present analysis and the one of Ref. [16] and of our previous work [12]. However, as the experimental data

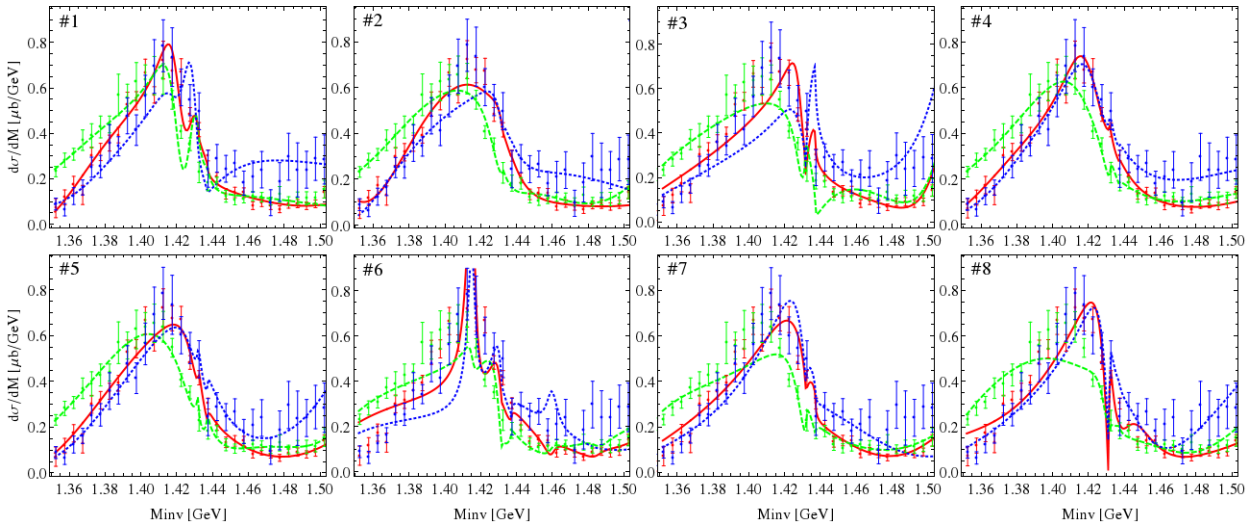

Figure 2: Comparison of all solutions describing the $\pi\Sigma$ mass distribution at $\tilde{W} = 2.5$ GeV in all three channels $\pi^+\Sigma^-$ (green, dashed), $\pi^-\Sigma^+$ (full, red) and $\pi^0\Sigma^0$ (blue, dotted).

Fit #	1	2	3	4	5	6	7	8
$\chi^2_{\rm d.o.f.}$ (hadronic data)	1.35	1.14	0.99	0.96	1.06	1.02	1.15	0.90
$\chi^2_{\rm p.p.}$ (CLAS data)	3.18	1.94	2.56	1.77	1.90	6.11	2.93	3.14

Table 1: Quality of the various fits in the description of the hadronic and the photoproduction data from CLAS. For the definition of $\chi^2_{\rm p.p.}$, see the text.

is described similarly well by all fit solutions, one can not reject any of them. Thus, the distribution of poles represents the systematic uncertainty of the present approach. It appears to be quite large, but is still significantly smaller than in the older analysis of Ref. [6] based on scattering data only.

3. Reduction of the Model Ambiguities

In the previous section we have exemplified that the old scattering data [28–31] together with the recent and very important measurement of the kaonic hydrogen characteristics [3] alone do not fix the antikaon-nucleon scattering amplitude well enough. There are, however, several (proposed) measurements which may lead to a reduction of this ambiguity. In the following we wish to present what is in our view most promising ways to do so.

(a) Photoproduction data

Recently, very sophisticated measurements of the reaction $\gamma p \to K^+\Sigma\pi$ were performed by the CLAS collaboration at JLab, see Ref. [34]. There, the invariant mass distribution of all three $\pi\Sigma$ channels was determined in a broad energy range and with high resolution. Finally, from these data the spin-parity analysis of the $\Lambda(1405)$ was performed in Ref. [19].

First theoretical analyses have been performed on the basis of a chiral unitary approach in Refs. [11, 27, 35, 36]. In the following, we present the results of the analysis of Ref. [11], which relies on the hadronic scattering amplitude described in the previous section. In this study, we assumed the simplest ansatz for the photoproduction amplitude

$$\mathcal{M}^j(\tilde{W}, M_{\rm inv}) = \sum_{i=1}^{10} C^i(\tilde{W})\, G^i(M_{\rm inv})\, f_{0+}^{i,j}(M_{\rm inv})\,, \tag{3}$$

where $\tilde{W}$ and $M_{\rm inv}$ denote the total energy of the system and the invariant mass of the $\pi\Sigma$ sub-system, respectively. For a specific meson-baryon channel i, the Greens function is denoted by $G^i(M_{\rm inv})$, and the energy-dependent (and in general complex valued) constants $C^i(\tilde{W})$ describe the reaction mechanism of $\gamma p \to K^+ M_i B_i$. The hadronic final-state interaction is captured by the standard Höhler partial waves f_{0+}, derived from Eq. (2). For more details, i.e., the explicit form of the Greens function we refer the reader to the original publication [11].

Clearly, a more sophisticated ansatz is required to address scattering and photoproduction data simultaneously, while fulfilling in the same time the gauge invariance. Such an approach can be developed along the techniques used for the analysis of the single meson photoproduction, see Refs. [21, 37]. The question we wish to address here is, however, different. Namely, whether all obtained hadronic solutions allow for a good description of the photoproduction data using such a flexible ansatz. Thus, without altering the parameters of the hadronic part (8 solutions) in the photoproduction amplitude Eq. (3), we fit the unknown constants $C^i(\tilde{W})$ to reproduce the CLAS data in all three measured final states ($\pi^+\Sigma^-$, $\pi^0\Sigma^0$, $\pi^-\Sigma^+$) and for all 9 measured total energy values ($\tilde{W} = 2.0, 2.1, .., 2.8$ GeV).

The resulting values of χ^2 per data point for these fits are collected in the third row of the Table 1, whereas for the further details and error analysis we again refer to the original publication [11]. They show that even within such a flexible ansatz the solutions #1, #3, #6, #7 and #8 of the eight hadronic solutions do not allow for a decent description of the high-quality CLAS data. The failure of these solutions becomes even more evident when comparing the $\pi\Sigma$ mass distribution of all eight solutions at one (typical) energy $\tilde{W} = 2.5$ GeV, see Fig. 2. Consequently, only three of originally eight solutions can be considered as physical with respect to the CLAS data, which indeed reduces the ambiguity of the antikaon-nucleon scattering amplitude substantially.

(b) **Kaonic Deuterium**

The $K^- p$ scattering amplitude at the threshold is fixed very well by the strong energy shift and width of the kaonic hydrogen, measured in the SIDDHARTA experiment [3]. However, this does not fix the full $\bar{K}N$ scattering amplitude at the threshold, which has two complex valued components, i.e., for isospin $I = 0$ and $I = 1$. To fix both components one requires another independent measurement, such as the energy shift and width of the kaonic deuterium. Such a measurement is proposed at LNF [38] and J-PARC [39]. Ultimately, this quantity can be related to the antikaon-deuteron scattering length by the well known Deser-type relations (see, e.g., Refs. [4, 40–42]) and then to the antikaon-nucleon scattering length, using an effective field theory framework, see,

e.g., Ref. [43].

(c) **Additional Scattering Data**

The scattering data [28–31] used to fix the $\bar{K}N$ scattering amplitude as described in the last section stem from very old bubble chamber experiments. From the theoretical point of view, improvement of these data would be the best way to reduce the ambiguity of the theoretical predictions. The proposed measurement of the two-body interaction of $K_{\rm long}$-beam and the proton target at JLab [20] can potentially lead to such an improvement of the data.

In the following, we wish to quantify the above statement, using the already obtained solutions of the hadronic model of the last section. We do so by generating a set of new synthetic data on total cross sections in the same channels as before, using our best solution #4 in the momentum interval $P_{\rm lab} = 100 - 300$ MeV. We assume the energy binning to be fixed, and randomize the synthetic data by Gaussian distribution with a standard deviation of $\Delta\sigma$ for the charged and $2\Delta\sigma$ for the neutral final state channels. The latter is assumed to account for the fact that neutral channels are usually more intricate to measure.

We have tested different scenarios - considering different energy binning (ΔP), measurement accuracy ($\Delta\sigma$) and whether the new synthetic data complements or replaces the old data. Without further fitting, we have compared the new $\chi^2_{\rm d.o.f.}$ of all solutions, obtained in the previous section. We found that at least four of the obtained eight solutions are not compatible with the updated data for $\Delta\sigma \leq 5$ MeV and $\Delta P \sim 10$ MeV. This procedure appears to be more sensitive to the measurement accuracy than on the energy binning - for $\Delta\sigma \geq 10$ MeV none of the solutions could be sorted out for any of chosen values of ΔP. A complete replacement of the old by the new (synthetic) data does not change our findings qualitatively, but increases the differences between new $\chi^2_{\rm d.o.f.}$ values slightly. In summary, this preliminary and simplistic analysis underlines the importance of the re-measurement of the cross section data on $\bar{K}N$ scattering in a modern experimental setup, such as the one proposed in Ref. [20].

4. Acknowledgments

The speaker is grateful to the organizers of the workshop for the invitation. The vast part of the work presented at the YSTAR2016 workshop was performed in the HISKP at the University of Bonn in collaboration with Ulf-G. Meißner, whom he thanks for a careful reading of the manuscript. The speaker is grateful for multiple interesting discussions with M. Döring, A. Cieply, P. Bruns and D. Sadasivan on this matter. Currently, the speaker is supported by the German Research Foundation (DFG) under the fellowship MA 7156/1–1.

References

[1] V. Bernard, Prog. Part. Nucl. Phys. **60**, 82 (2008); [arXiv:0706.0312 [hep–ph]].

[2] M. Mai, P. C. Bruns, B. Kubis, and U.-G. Meißner, Phys. Rev. D **80**, 094006 (2009); [arXiv:0905.2810 [hep–ph]].

[3] M. Bazzi *et al.*, Phys. Lett. B **704** 113 (2011); [arXiv:1105.3090 [nucl–ex]].

[4] U.-G. Meißner, U. Raha, and A. Rusetsky, Eur. Phys. J. C **35**, 349 (2004); [hep–ph/0402261].

[5] R. H. Dalitz and S. F. Tuan, Annals Phys. **8**, 100 (1959).

[6] B. Borasoy, U.-G. Meißner and R. Nißler, Phys. Rev. C **74** (2006) 055201; [hep–ph/0606108].

[7] E. Oset and A. Ramos, Nucl. Phys. A **635**, 99 (1998) [nucl–th/9711022].

[8] D. Jido, J. A. Oller, E. Oset, A. Ramos, and U.-G. Meißner, Nucl. Phys. A **725**, 181 (2003); [arXiv:nucl–th/0303062].

[9] T. Hyodo and D. Jido, Prog. Part. Nucl. Phys. **67**, 55 (2012); [arXiv:1104.4474 [nucl–th]].

[10] N. Kaiser, P. B. Siegel, and W. Weise, Nucl. Phys. A **594**, 325 (1995); [nucl–th/9505043].

[11] M. Mai and U.-G. Meißner, Eur. Phys. J. A **51**, 30 (2015); [arXiv:1411.7884 [hep–ph]].

[12] M. Mai and U.-G. Meißner, Nucl. Phys. A **900**, 51 (2013); [arXiv:1202.2030 [nucl–th]].

[13] J. A. Oller and U.-G. Meißner, Phys. Lett. B **500**, 263 (2001); [arXiv:hep–ph/0011146].

[14] A. Cieplý, M. Mai, U.-G. Meißner, and J. Smejkal, Nucl. Phys. A **954**, 17 (2016); [arXiv:1603.02531 [hep–ph]].

[15] Y. Ikeda, T. Hyodo, and W. Weise, Nucl. Phys. A **881**, 98 (2012); [arXiv:1201.6549 [nucl–th]].

[16] Z. H. Guo and J. A. Oller, Phys. Rev. C **87**, 035202 (2013); [arXiv:1210.3485 [hep–ph]].

[17] A. Cieply and J. Smejkal, Nucl. Phys. A **881**, 115 (2012); [arXiv:1112.0917 [nucl–th]].

[18] P. C. Bruns, M. Mai, and U.-G. Meißner, Phys. Lett. B **697**, 254 (2011); [arXiv:1012.2233 [nucl–th]].

[19] K. Moriya *et al.* [CLAS Collaboration], Phys. Rev. Lett. **112**, 082004 (2014); [arXiv:1402.2296 [hep–ex]].

[20] M. Amaryan, AIP Conf. Proc. **1735**, 040006 (2016); [arXiv:1512.06965 [physics.ins–det]].

[21] M. Mai, P. C. Bruns, and U.-G. Meißner, Phys. Rev. D **86**, 094033 (2012); [arXiv:1207.4923 [nucl–th]].

[22] A. Krause, Helv. Phys. Acta **63**, 3 (1990).

[23] M. Frink and U.-G. Meißner, JHEP **0407**, 028 (2004); [arXiv:hep–lat/0404018].

[24] B. Borasoy, R. Nißler, and W. Weise, Eur. Phys. J. A **25**, 79 (2005) 79; [hep–ph/0505239].

[25] J. A. Oller, Eur. Phys. J. A **28**, 63 (2006); [hep–ph/0603134].

[26] Y. Ikeda, T. Hyodo, and W. Weise, Phys. Lett. B **706**, 63 (2011); [arXiv:1109.3005 [nucl–th]].

[27] L. Roca and E. Oset, Phys. Rev. C **87**, 055201 (2013); [arXiv:1301.5741 [nucl–th]].

[28] J. Ciborowski *et al.*, J. Phys. G **8**, 13 (1982).

[29] W. E. Humphrey and R. R. Ross, Phys. Rev. **127**, 1305 (1962).

[30] M. Sakitt, T. B. Day, R. G. Glasser, N. Seeman, J. H. Friedman, W. E. Humphrey, and R. R. Ross, Phys. Rev. **139**, B719 (1965).

[31] M. B. Watson, M. Ferro-Luzzi, and R. D. Tripp, Phys. Rev. **131**, 2248 (1963).

[32] D. N. Tovee *et al.*, Nucl. Phys. B **33** 493 (1971).

[33] R. J. Nowak *et al.*, Nucl. Phys. B **139**, 61 (1978).

[34] K. Moriya *et al.* [CLAS Collaboration], Phys. Rev. C **87**, 035206 (2013); [arXiv:1301.5000 [nucl–ex]].

[35] L. Roca and E. Oset, Phys. Rev. C **88**, 055206 (2013); [arXiv:1307.5752 [nucl–th]].

[36] S. X. Nakamura and D. Jido, PTEP **2014**, 023D01 (2014); [arXiv:1310.5768 [nucl–th]].

[37] B. Borasoy, P. C. Bruns, U.-G. Meißner, and R. Nißler, Eur. Phys. J. A **34**, 161 (2007); [arXiv:0709.3181 [nucl–th]].

[38] SIDDHARTA-2 Collaboration, Proposal at Laboratori Nazionali di Frascati of INFN, "The upgrade of the SIDDHARTA apparatus for an enriched scientific case," 2010.

[39] C. Berucci *et al.*, Letter of Intent for J-PARC, "Measurement of the strong interaction induced shift and width of the 1s state of kaonic deuterium," 2013.

[40] S. Deser, M. L. Goldberger, K. Baumann and W. E. Thirring, Phys. Rev. **96**, 774 (1954).

[41] U.-G. Meißner, U. Raha, and A. Rusetsky, Eur. Phys. J. C **47**, 473 (2006); [nucl–th/0603029].

[42] J. Gasser, V. E. Lyubovitskij, and A. Rusetsky, Phys. Rept. **456**, 167 (2008); [arXiv:0711.3522 [hep–ph]].

[43] M. Mai, V. Baru, E. Epelbaum, and A. Rusetsky, Phys. Rev. D **91**, 054016 (2015); [arXiv:1411.4881 [nucl–th]].

2.6 Bound States of N's and Ξ's

Volker Crede
Department of Physics
Florida State University
Tallahassee, FL 32306-4350, U.S.A.

Simon Capstick
Department of Physics
Florida State University
Tallahassee, FL 32306-4350, U.S.A.

Abstract

Experimental information on the spectrum, structure, and decays of strangeness -2 Cascade baryons is sparse compared to non-strange and strangeness -1 baryons. It is argued that an experimental program at Jefferson Lab using the photo-production and the GlueX detector to study the physics of Cascades is of considerable interest, since it is likely that the lightest Cascade baryons of a given spin and parity are relatively narrow. If this is verified in an experiment, this would confirm the flavor independence of the confining interaction that is assumed in models. These narrow widths may also make it possible to measure the isospin-symmetry violating mass splittings in a spatially-excited baryon for the first time. Copious data for excited strangeness -1 baryons will be collected along with the data for Cascade baryons in such an experimental program. Photo-production reactions which can be used to study excited Cascade baryons are described, and simulations made to understand the production of a ground-state and an excited-state Cascade baryon in the GlueX experiment are discussed, along with possible sources of background.

1. Introduction

The spectrum of multi-strange hyperons is poorly known, with only a few resonances whose existence is well established. Among the doubly-strange states, the two ground-state Cascades, the octet member Ξ and the decuplet member $\Xi^*(1530)$, have four-star status in the RPP [1], with only four other three-star candidates. On the other hand, more than 20 N^* and Δ^* resonances are rated with at least three stars by the Particle Data Group (PDG). Of the six Ξ states that have at least three-star ratings, only two are listed with weak experimental evidence for their spin-parity (J^P) quantum numbers: $\Xi(1530)\,\frac{3}{2}^+$ [2], $\Xi(1820)\,\frac{3}{2}^-$ [3]. All other J^P assignments are based on quark-model predictions.

Flavor SU(3) symmetry predicts as many Ξ resonances as N^* and Δ^* states combined, suggesting that many more Cascade resonances remain undiscovered. The three lightest quarks, u, d, and s, have 27 possible flavor combinations: $3 \otimes 3 \otimes 3 = 1 \oplus 8 \oplus 8' \oplus 10$ and each multiplet is identified by its spin and parity, J^P. Flavor SU(3) symmetry implies that the members of the multiplets differ only in their quark makeup, and that the basic properties of the baryons should be similar, although the symmetry is known to be broken by the strange-light quark mass difference. The octets consist of N^*, Λ^*, Σ^*, and Ξ^* states. We thus expect that for every N^* state, there should be a corresponding Ξ^* state with similar properties. Additionally, since the decuplets consist of Δ^*, Σ^*, Ξ^*, and Ω^* states, we also expect for every

Δ^* state to find a decuplet Ξ^* with similar properties. In a simple quark model picture, the strange states will fit into multiplets which correspond to those of the $u,\ d$ sector. However, it could be that the dynamics of the excited baryons differ from those of the lower-lying states; for example, the pattern of their decays may be systematically different. Parity doublets may appear in some sectors with increasing mass. Should we expect doubly-strange baryons with properties similar to those of the $\Lambda(1405)$ with $J^P = 1/2^-$ and the Roper N^* with $J^P = 1/2^+$, which do not fit easily the conventional picture of three quarks in the baryon? The dependence of the physics of these unusual states on the number of strange quarks is of crucial importance to our understanding of them, which motivates the collection of a significant database on multi-strange baryons.

2. Ξ **Spectrum and Decays**

The Ξ hyperons have the doubly-strange quark content $|ssu\rangle$ and $|ssd\rangle$. An interesting feature of the Ξ spectrum is that there are fewer degeneracies than in the light-quark baryon spectrum. If the confining potential is independent of quark flavor, the energy of spatial excitations of a given pair of quarks will be inversely proportional to their reduced mass. If all three quark masses are the same, the excitation energy of either of the two relative coordinates will be the same, which will lead to degeneracies in the excitation spectrum. However, with two strange quarks and one light quark, the excitation energy of the relative coordinate of the strange quark pair is smaller. This means that the lightest excitations in each partial wave are between the two strange quarks, and that the degeneracy between excitations of the two relative coordinates is lifted. The spectrum of Ξ baryons calculated using the relativized quark model [4] along with information about Ξ states extracted from experiment is shown in Figure 1. A comparison of results from this model for the masses of non-strange and strangeness -1 baryons with those extracted from experimental data makes it likely that the lowest-mass positive-parity excited Ξ^* states are lower than shown in Fig. 1, and that the spectrum of negative-parity excited states should have larger splittings.

In the absence of configuration mixing and in a spectator decay model, Ξ states with the relative coordinate of the strange-quark pair excited cannot decay to the ground state Ξ and a pion, because of orthogonality of the part of the spatial wave function between the two strange quarks in the initial excited state and in the final ground state. Having instead to decay to final states that include Kaons rules out the decay channel with the largest phase space for the lightest states in each partial wave, substantially reducing their widths [5]. This selection rule is modified by (configuration) mixing in the wave function; however, color-magnetic hyperfine mixing is weaker in Ξ states because this interaction is smaller between quarks of larger masses. The flavor-spin [SU(6)] coupling constants at the decay vertices for $N,\ \Delta \to N\pi,\ \Delta\pi$ are significantly larger than those for $\Xi,\ \Xi^* \to \Xi\pi,\ \Xi^*\pi$ decays [6], which also reduces these widths. The result is that the well known lower-mass resonances have widths Γ_{Ξ^*} of about 10 - 20 MeV, which is 5 - 30 times narrower than is typical for N^*, Δ, Λ, and Σ states.

The first excited state with nucleon quantum numbers, the Roper resonance at 1440 MeV, is interesting because its low mass is hard to explain in models containing only three quarks. It is likely that this is because the pole position of this resonance is shifted because of strong coupling to the $N\pi\pi$ channel, which also contributes to its large width of about 350 MeV. Ex-

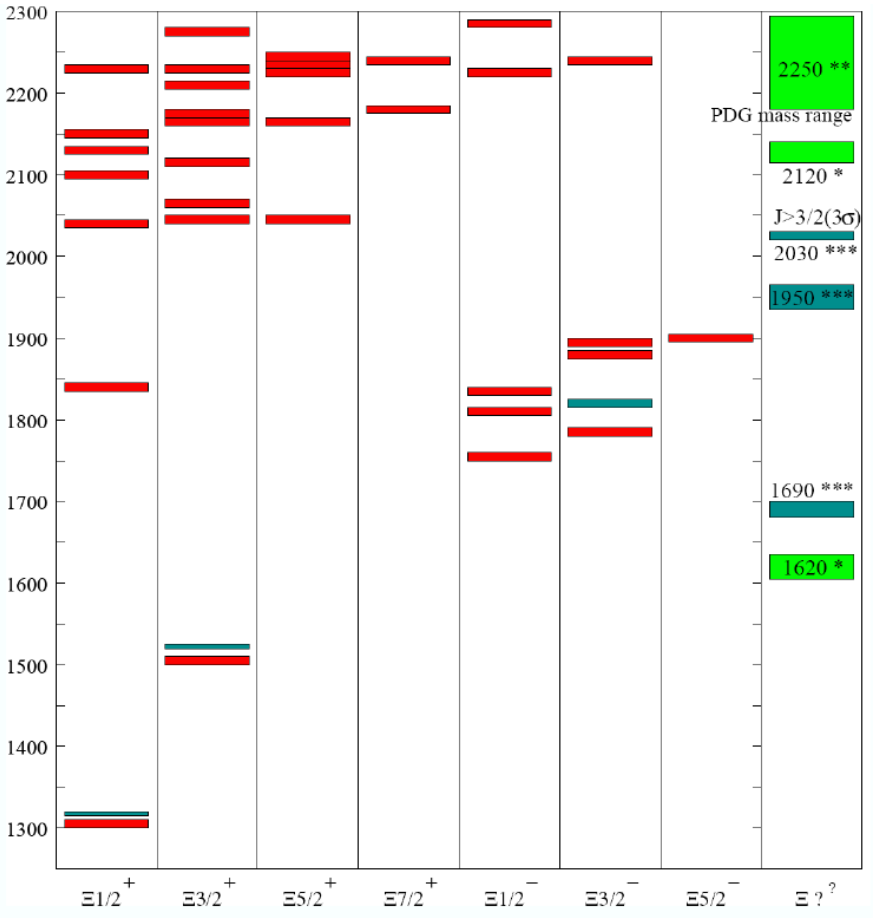

Figure 1: Relativized model spectrum of Ξ baryons [4] below 2300 MeV (red bars) compared to masses extracted from experiment and their uncertainties (dark green bars for well known states, light green bars for tentative states). Experimental states with undetermined spins and/or parities are placed in the last column on the right.

traction of its properties from partial-wave analysis of πN scattering and photo-production data is made difficult by a complicated pole structure and by the presence of a second nucleon resonance with $J^P = \frac{1}{2}^+$ at 1710 MeV with a width of roughly 100 MeV. The equivalent Ξ^* state should be quite narrow and so be relatively easy to separate from the next Ξ^* $\frac{1}{2}^+$, which itself should be relatively narrow, and from the lightest negative-parity excitations, which are also relatively narrow.

These features render possible a wide-ranging program to study the physics of the Cascade hyperon and its excited states. The study of these hyperons has focused until recently on their production in K^-p reactions, although some Ξ^* states were found using high-energy hyperon beams. Photo-production appears to be a very promising alternative. Results from earlier Kaon-beam experiments indicate that it is possible to produce the Ξ ground state through the decay of high-mass Y^* states [7–9]. It is therefore possible to produce Cascade resonances through t-channel photo-production of hyperon resonances using the photo-production re-

action $\gamma p \rightarrow K K \Xi^{(*)}$. The CLAS collaboration investigated this reaction [10], but no signicant signal for an excited Cascade state was observed, other than that of the decuplet ground state $\Xi(1530)$. The absence of higher-mass signals is very likely due to the low photon energies available to these experiments and the limited acceptance of the CLAS detector. Equipped with a Kaon-identification system, the GlueX experiment will be well suited to search for and study excited Ξ resonances.

To summarize, it would be interesting to see in a Cascade physics program at Jefferson Lab the lightest excited Ξ^* states of a given spin and parity J^P decoupling from the $\Xi\pi$ channel, confirming the flavor independence of confinement. Measurements of the isospin-symmetry violating mass splittings ($\Xi^{*-} - \Xi^{*0}$) in spatially excited Cascade states are also possible, for the first time in a spatially-excited hadron. Currently, mass splittings like $n-p$ or $\Delta^0 - \Delta^{++}$ are only available for the octet and decuplet ground states, but are hard to measure in excited $N,\ \Delta$ and $\Sigma,\ \Sigma^*$ states, which are broad. The lightest Cascade baryons are expected to be narrower, and measuring the $\Xi^- - \Xi^0$ splitting of spatially-excited Ξ states remains a strong possibility. Such measurements would allow an interesting probe of excited-hadron structure, and would provide important input for quark models which explain the isospin-symmetry violating mass splittings by the effects of the difference of the u- and d-quark masses and of the electromagnetic interactions between the quarks.

3. Ξ Searches using the GlueX Experiment

The Cascade octet ground states (Ξ^0, Ξ^-) can be studied in the GlueX experiment *via* exclusive t-channel (meson exchange) processes in the reactions

$$\gamma p \rightarrow K\, Y^* \rightarrow K^+ (\, \Xi^- K^+),\ K^+ (\, \Xi^0 K^0),\ K^0 (\, \Xi^0 K^+) . \tag{1}$$

The production of such two-body systems involving a Ξ particle also allows the study of highly-excited Λ^* and Σ^* states. Initially, the Ξ octet ground states (Ξ^0 and Ξ^-) will be challenging to study via exclusive t-channel (meson exchange) production. The typical final states have kinematics for which the baseline GlueX detector has very low acceptance due to the high-momentum forward-going Kaon and the relatively low-momentum pions produced in the Ξ decay. However, the production of the Ξ decuplet ground state, $\Xi(1530)$, and other Ξ^* states decaying to $\Xi\pi$ results in a lower momentum Kaon at the upper vertex, and heavier Ξ states produce higher momentum pions in their decays.

The Cascade decuplet ground state, $\Xi(1530)$, and other excited Cascades can be searched for and studied in the reactions

$$\gamma p \rightarrow K\, Y^* \rightarrow K^+ (\, \Xi\, \pi\,) K^0,\ K^+ (\, \Xi\, \pi\,) K^+,\ K^0 (\, \$ \tag{2}$$

The lightest excited Ξ states of a given spin and parity J^P are expected to decouple from $\Xi\pi$ and can be searched for and studied in the reactions

$$\gamma p \rightarrow K\, Y^* \rightarrow K^+ (\, K\Lambda\,)_{\Xi^{-*}} K^+,\ K^+ (\, K\Lambda\,)_{\Xi^{0*}} K^0,\ K^0 (\, K\Lambda\,)_{\Xi^{0*}} K^+ , \tag{3}$$

$$\gamma p \rightarrow K\, Y^* \rightarrow K^+ (\, K\Sigma\,)_{\Xi^{-*}} K^+,\ K^+ (\, K\Sigma\,)_{\Xi^{0*}} K^0,\ K^0 (\, K\Sigma\,)_{\Xi^{0*}} K^+ . \tag{4}$$

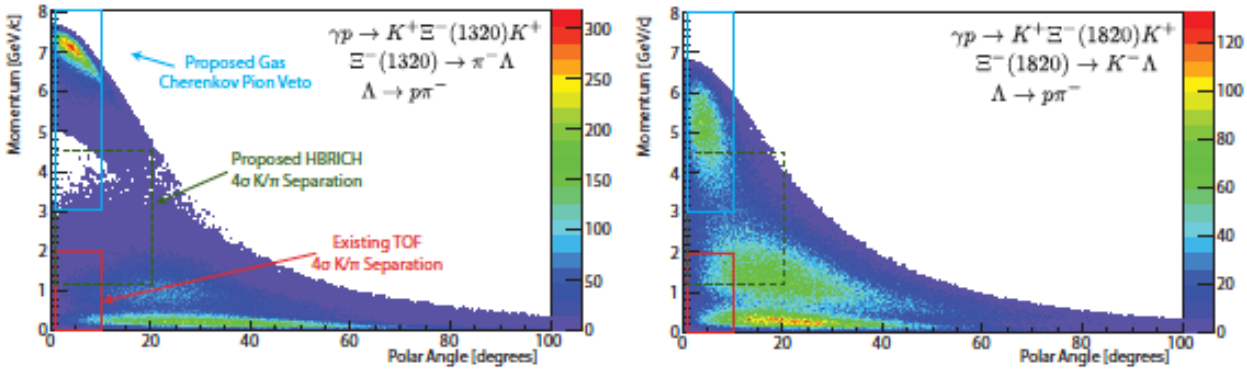

Figure 2: Generated momentum versus polar angle for all tracks in the simulated reactions (a) $\gamma p \to K^+\,\Xi^-(1320)K^+$ and (b) $\gamma p \to K^+\,\Xi^-(1820)K^+$. The decay of the Cascade resonance and assigments of final-state particles to observed high-density regions in phase space are described in the plots.

Our simulations and application of state-of-the-art analysis tools [11] show that background from competing hadronic reactions will be much reduced because of the unique signature provided by the two associated Kaons in photo-production, in combination with the additional information found by analyzing the weak-decay secondary vertices of ground-state strangeness -1 hyperons in the final state.

However, decays such as $Y^* \to \phi\Lambda,\ \phi\Sigma$ might contribute to the background for certain final states. Larger contributions to the background will more likely come from events with pions misidentified as Kaons, as well as other reconstruction and detector inefficiencies. To extract small Cascade signals at masses above the $\Xi(1530)$, it will therefore be important to reduce the background by kinematically reconstructing complete final states. A full exclusive reconstruction also enhances the possibility of being able to measure the J^P of these states.

We have simulated the production of the $\Xi^-(1320)$ and $\Xi^-(1820)$ resonances to better understand the kinematics of these reactions. The photo-production of the $\Xi^-(1320)$ decaying to $\pi^-\Lambda$ and of the $\Xi^-(1820)$ decaying to ΛK^- is shown in Fig. 2. These reactions results in the $K^+K^+\pi^-\pi^-p$ and $K^+K^+K^-\pi^-p$ final states, respectively. Reactions involving excited Cascades have "softer" forward-going Kaons, and there is more energy available on average to the Cascade's decay products. Both plots show three regions of high density. The upper momentum region ($>$ 4 GeV/c) consists of forward-going K^+ tracks from the associated production of an excited hyperon. The middle momentum regions (1-2 GeV/c) are a mixture of K^-, K^+, and proton tracks, while the lower region (below 1 GeV/c) contains mostly π^- tracks. The high-momentum Kaon tracks with momenta larger than about 2.5 GeV/c cannot be identified with the current GlueX PID system. Shown in Fig. 2 in solid (red), dashed (green), and dotted (blue) are the regions of phase space where the existing time-of-flight (TOF) detector, the proposed Hadron Blind RICH (HBRICH) detector, and proposed gas Cherenkov detector provide pion/Kaon discrimination at the four standard deviation level [12].

4. **Acknowledgments**

The authors thank the technical staff at Jefferson Lab and at all the participating institutions for their invaluable contributions to the success of the experiment. This material is based upon work supported by the U.S. Department of Energy, Office of Science, Office of Nuclear Physics, under Contract No. DE–AC05–06OR23177. The GlueX simulations discussed here comprise part of the PhD dissertation work of FSU graduate student Nathan Sparks. Florida State University acknowledges support under grant DE–FG02–92ER40735.

References

[1] K. A. Olive *et al.* [Particle Data Group], Chin. Phys. C **38**, 090001 (2014).

[2] B. Aubert *et al.* [BABAR Collaboration], Phys. Rev. D **78**, 034008 (2008).

[3] S. F. Biagi *et al.*, Z. Phys. C **34**, 175 (1987).

[4] S. Capstick and N. Isgur, Phys. Rev. D **34**, 2809 (1986).

[5] K. T. Chao, N. Isgur, and G. Karl, Phys. Rev. D **23**, 155 (1981).

[6] P. Zenczykowski, Annals Phys. **169**, 453 (1986).

[7] R. D. Tripp, D. W. G. Leith, A. Minten *et. al.*, Nucl. Phys. B **3**, 10 (1967).

[8] G. Burgun *et al.*, Nucl. Phys. B **8**, 447 (1968).

[9] P. J. Litchfield *et al.*, Nucl. Phys. B **30**, 125 (1971).

[10] L. Guo *et al.* [CLAS Collaboration], Phys. Rev. C **76**, 025208 (2007).

[11] A. AlekSejevs *et al.* [GlueX Collaboration], arXiv:1305.1523 [nucl-ex].

[12] M. Dugger *et al.* [GlueX Collaboration], arXiv:1408.0215 [physics.ins-det].

2.7 Hyperon Photoproduction at Jefferson Lab

Lei Guo (for CLAS Collaboration)
Physics Department
Florida International University
Miami, FL 33199, U.S.A

Abstract

Compared to the many recent experimental progress made in the nucleon resonances, the advances in hyperon spectroscopy have been scarce. The large amount of photoproduction data that have been collected in the past decade by the CLAS collaboration, and the next generation of experiments to be erson Lab, will make it possible to investigate the production mechanisms of all three sectors of hyperon states. It could also become possible to discover the missing hyperon states as expected by various quark model predictions and Lattice QCD calculations.

1. Introduction

The strange quark plays an important role in understanding the strong interaction of nucleons. Even though photo- and electroproduction of strangeness has been carried out since the 1950s, there is still no unambiguous and comprehensive model describing the reaction mechanism of baryon and hyperon ($S = -1, -2$ and -3) resonances. This is due, in part, to the difficulties encountered in modeling the strong interaction in the non-perturbative regime. As such, the problem has been approached through the use of effective field theories [1–4], Regge models [5] and hybrid Regge-plus-resonance (RPR) models [6, 7], and more recently, through coupled-channel analyses [8–11]. All of these methods require large and precise data sets in order to constrain fitting parameters. In addition to the crucial study of the strange-quark production mechanism itself, an important part of these efforts is the identification of nucleon and hyperon resonances predicted by various QCD-based models [12–14] but not previously observed. Recent progress in the hyperon sectors in lattice calculations [15] has also made it more urgent to obtain experimental data. Compared with the nucleon resonances sectors, the status of hyperon spectroscopy leaves much to be desired. In the search for missing nucleon resonances, a major difficulty arises from many overlapping broad states. Cascade resonances are typically much narrower and comparatively easier to identify. The status $S = -1$ hyperon states lie somewhere between the nucleon resonances and the cascade sector. In particular, more than 30 excited states are predicted to lie between 2 GeV and 2.3 GeV [13]. Currently, there are only five $S = -1$ states considered to be established, with three or four star rating in the PDG [16] in that region. On the other hand, the $S = -3$ Ω^- state has never been observed in photoproduction. The main issue with the multi-strangeness sector can be attributed to the lack of experimental data as a result of small cross sections. With the existing high statistics data that have been collected in the past decade at Jefferson Lab, and the future experiment at CLAS12 and GlueX, there is a significant opportunity for making progress at all three sectors of the hyperon spectroscopy.

2. Photoproduction Mechanism for Hyperons

With a high energy photon beam, it is generally understood that hyperons can be produced via a series of kaon exchanges. Near threshold, the contributions from intermediate nu-

cleon resonances that decay to strange particles, such as $K\Lambda$ and $K\Sigma$, are expected to be significant. In fact, recent CLAS data [17, 18] on the polarization observables for Λ and Σ photoproduction have played an important role in establishing nucleon resonances. However, the non-resonance contributions of hyperon photoproduction remain not entirely understood. For example, a recent study [19] showed that Λ photoproduction on a proton target, seems to be consistent with only K exchanges. Σ^0 photoproduction on a proton target, on the other hand, has comparable contributions from both K and K^* exchanges. Decay angular distributions for excited hyperons such as $\Lambda(1520)$, have been investigated in the past to probe the exchange mechanism in both photoproduction [20] and electroproduction [21]. However, higher statistics was needed. Recent CLAS data on $\Lambda(1520)$, $\Lambda(1405)$ and $\Sigma(1385)$ photoproduction [22] are also suggestive of the contributions of intermediate nucleon resonances. The non-resonance contributions for these states can be further constrained by investigating these states at higher energies, expected to be feasible at both CLAS12 and GlueX.

3. **Beam Helicity Asymmetry in K^+K^- Photoproduction**

Excited $S = -1$ hyperons could be produced in reactions such as $\gamma p \to pK^+K^-$. However, such a reaction also has significant contribution from intermediate meson resonances that decay to $K\bar{K}$. This would be even more complicated in the analogous reaction in the nucleon sector, $\gamma p \to p\pi^+\pi^-$, where the two pion photoproduction is believed to be important for identifying the missing nucleon states. In that reaction, both pions can also resonance with the nucleons, in addition to them being the decay products of intermediate meson states. The K^+K^- photoproduciton, on the hand, does have the advantage due to the lack of NK resonances. In the end, however, the complete understanding of two pesudoscalar meson photoproduction typically still rely on models using effective lagrangian approach. In particular, it is important to point out that polarization observables such as the beam helicity asymmetry $I^{\odot}$ is expected to be sensitive to the interference of the various competing mechanisms [23], and essential to extract the information of the intermediate resonances.

The beam helicity asymmetry $I^{\odot}(\tau)$, is defined by

$$I^{\odot}(\tau) = \frac{1}{P_{\gamma}(\tau)} \frac{\sigma^+(\tau) - \sigma^-(\tau)}{\sigma^+(\tau) + \sigma^-(\tau)}, \tag{1}$$

where τ is a kinematic bin, and $\sigma^{\pm}$ is cross sections for photons in a $\pm$ helicity state. $I^{\odot}$ is typically measured as a function of the angle ϕ between different planes, such as the K^+K^- plane and the production plane in the center-of-momentum frame. Although the beam helicity asymmetries have been measured in reactions such as $\gamma p \to p\pi^+\pi^-$ [24], no data exist for the two-kaon counterparts. The CLAS experiment E04-005 (g12) [25], using a photon beam with energies up to 5.4 GeV, and circular polarization up to 70%, has made it possible to perform these measurements for the two-kaon photoproduction on a proton target [26]. In Fig. 1, the asymmetries between the K^+K^+ and $\pi^-\pi^+$ are shown together, for events with $E_{\gamma} > 2.8$ GeV, as a function of the angle between the two-meson plane and the production plane. The features of the two reactions are strikingly different, with the two-pion channel showing a dominant $sin(2\phi)$ behavior, while the two-kaon data is mostly changing as a function of $sin(\phi)$. This could be due to the fact of that two-kaon photproduction is not expected to have contributions of pK^+ resonances, while $p\pi^{+/-}$ resonances are certainly

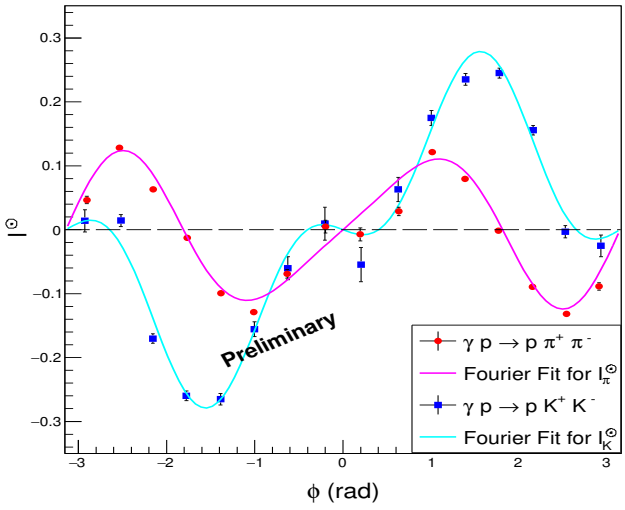

Figure 1: The beam helicity asymmetries, as a function of ϕ, for the reaction of $\gamma p \to p\pi^+\pi^-$(red solid circles), and $\gamma p \to pK^+K^-$ (blue solid squares), from the g12 data set. ϕ is the angle between the production plane and the two-meson plane. The results are integrated over for the E_γ range of $2.8 - 5.4$ GeV and other kinematic variables.

not forbidden. However, in order to further probe the underlying contributions of various intermediate resonances, the beam helicity asymmetry must be measured as a function of various kinematic variables, such as w (Fig. 2) and t.

The angular dependence of the asymmetries, can be fitted to a Fourier series. The sensitivities of these Fourier coefficients to kinematic variables such as pK^- invariant mass (Fig. 3), as well as the definition of the planes, are indicative of the possible contributions of various intermediate hyperon resonances. However, it is important to point out that these results must be combined with cross section measurements, in order to provide meaningful constraints for the production models of two-kaon photoproduction. These efforts are in progress, and could further our understanding of the intermediate $S = -1$ hyperon resonances.

4. **Cascade Polarization in Photoproduction**

Recent CLAS data established that the lowest excited cascades, such as $\Xi(1320)$ and $\Xi(1530)$, can be produced copiously using a photon beam and a thick target for high luminosity [27]. Cascade production is also intimately related to excited hyperons [28, 29]. The $S = -1$ hpyeron states above 2 GeV can be studied in unique channels such as $Y^* \to \Xi^- K^+$, as well as the typical decay mode of $Y^* \to N\bar{K}^{(*)}$. Similar to the important roles of the Λ and Σ polarizations played in extracting the information of the intermediate nucleon resonances, the Ξ^- polarization has also been expected to be essential in constraining the contributions of various intermediate high-mass $S = -1$ hyperons states. Due to the self-analyzing nature of the $\Xi(1320)$ weak decay, its polarization can be measured in various photo-nucleon reactions. In reactions such as $\gamma p \to K^+K^+\Xi^-(1320)$, with two pseudoscalar mesons (K^+) and one $J = \frac{1}{2}$ baryon ($\Xi^-(1320)$) in the final state, the expectation for Ξ^- polarization could be

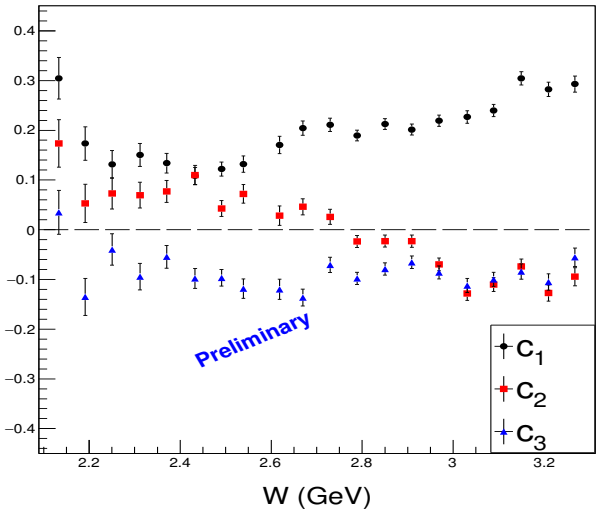

Figure 2: The beam helicity asymmetries as a function of ϕ, are fitted to a Fourier series up to $sin(3\phi)$. The coefficients are plotted as a function of W.

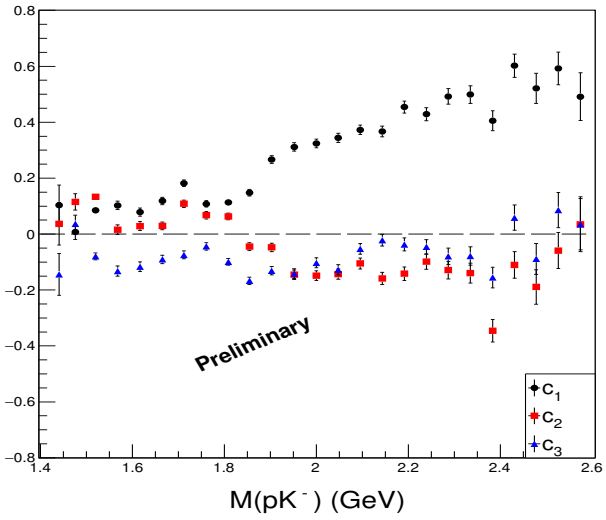

Figure 3: The beam helicity asymmetries as a function of ϕ, are fitted to a Fourier series up to $sin(3\phi)$. The coefficients are plotted as a function of pK^- invariant mass

very different from that of Λ in $\gamma p \to K^+\Lambda$. In fact, recent results on the polarization observables in reactions such as $\gamma p \to \pi\pi N$, using a more realistic three-body framework [30], suggests that the $\Xi^-(1320)$ polarization in all three directions could be non-zero. In addition, quasi-two-body models for Ξ^- photoproduction also suggest non-zero Ξ^- transferred polarization (C_z) [28]. Therefore, the measurement of Ξ^- polarization is an important tool to reveal the production mechanism, for which differential cross section measurements alone

are not sufficient.

Recent CLAS data collected by the experiment E04-005 has made the measurement of Ξ^- polarization in photoproduction possible for the first time [31]. In reaction $\gamma p \rightarrow K^+K^+\pi^-(\Lambda)$, the Ξ^- was constrained from both the K^+K^+ missing mass and $\pi^-\Lambda$ invariant mass. The Λ is identified using the missing mass technique. The Ξ^- decay is then fully reconstructed. The circular polarization of the beam is a function of the beam energy and the electron beam polarization, allowing the determination of the transferred polarizations C_x and C_z as well. The z-axis is along the beam, and the y-axis is along the norm of the production plane, defined by the beam, target and Ξ^- vectors in the center-of-momentum frame. Preliminary results of the measured polarizations are shown as a function of Ξ^- center-of-momenum angle, in Fig. 4. These results are compared with calculations using parameters from Ref. [28], and Ref. [29], which includes contributions from intermediate hyperons with $J > \frac{3}{2}$. It is important to point out that the lack of statistics in the existing data does not provide any differentiating power for distinguish the models. Furture experiments, discussed in the next section, will certainly be able to take these measurements to the necessary levels.

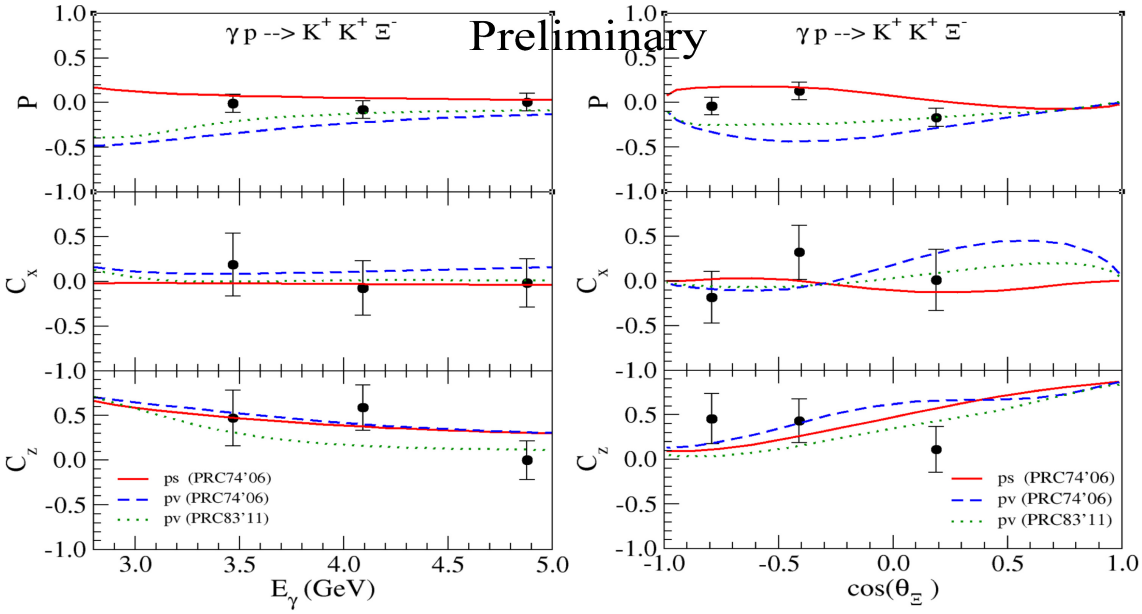

Figure 4: Ξ^- polarization observables (Top: P, Middle: C_x, Bottom: C_z) as a function of E_γ (Left) and Ξ^- angles in the center-of-momentum frame(Right). Only the statistical uncertainties, which are dominant, are shown. The red solid curve is based on the model from Ref. [28], using pseudo-vector coupling. The blue dash-dotted curve uses pseudo-scalar coupling. The green dashed curve includes contributions from intermediate hyperons with $J > \frac{3}{2}$ [29]. The theoretical curves are for $E_\gamma = 4$ GeV.

5. Ω^- Photoproduction and the Very Strange Experiment at CLAS12

The prediction and discovery of the Ω^- baryon certainly was one of the great triumphs of the quark model. However, half a century later, there has been little new information

about the Ω and Ξ baryons. In fact, only two Ω states and six Ξ states are considered to be well-established, with at least three-star ratings in the PDG [16]. Production of doubly- or triply-strange baryons by means of a photon beam (as with CLAS currently and with CLAS12 and GlueX in the future) is expected to shed light on the genesis of these states which involves the production of multiple $s\bar{s}$ pairs from the vacuum. This significant change in baryon strangeness number from initial ($S = 0$) to final state ($S = -3, -2$) could result from direct production via vector-meson dominance or from a sequence of intermediate transitions. Inference on the production mechanisms of these states in γp collisions can be obtained from precision measurements of the cross section and the invariant mass of these states.

The CLAS12 Very Strange Experiment, E12-11-005a [32], is expected to yield valuable data in the physics of Ω and cascade states. This experiment takes advantage of the large luminosity after the 12 GeV upgrade at the Thomas Jefferson Laboratory. Using the CLAS12 spectrometer and the Forward Tagger (FT) for the quasi-real photon beams, E12-11-005a is expected to yield unprecedented statistics in the production of Cascade and Omega baryons. Excited cascades can be investigated in reactions such as $\gamma p \to K^+K^+\Xi^-(1820), \Xi^-(1820) \to K^-\Lambda, \Lambda \to p\pi^-$. This would allow the determination of the spin and parity of the observed excited cascade states [33]. The polarization of ground state Ξ can also be measured with uncertainties sufficiently small to constrain production models that currently can not separate the contributions of various intermediate hyperon resonances. As for the Ω^- photoproduction, detailed differential cross section measurements can be performed, necessary for the understanding the production mechanism, differentiating various models such as vector meson dominance and a sequential decay of intermediate states.

The expected statistics of various reactions for E12-11-005a, is summarized in the Table 1:

	Detected Particles	Measured Decays	Total Detected
Ω^-	$K^+K^+K^0$		$\sim$ 7k
Ω^-	$K^+K^+K^0K^-$	Ω^-	$\sim$ 1k
Ξ^-	$K^+K^+\pi^-$	Ξ^-	$\sim$ 0.9M
$\Xi^-(1530)$	$K^+K^+\pi^-$	$\Xi^-(1530)$	$\sim$ 270k
$\Xi^-(1820)$	$K^+K^+K^-p$	$\Xi^-(1820), \Lambda$	$\sim$ 12k

Table 1: Expected Particle Rate for the CLAS12 Very Strange Experiment (E12-11-005a), based on the simulation including detection efficiency and branching ratios. 80 beam days were assumed.

6. **Summary**

With the effort of the Jefferson Lab 12 GeV upgrade ongoing, and the next generation of high statistics photoproduction experiments expected to yield unprecedented amount of data for hyperon states, it is an exciting time for hyperon spectroscopy. The existing data from the CLAS collaboration have already demonstrated the feasibility and importance of the various polarization observables in hyperon production, and its relation with the intermediate resonances. Future data from both CLAS12 and GlueX will no doubt provide more detailed measurements to understand the production mechanisms of the various hyperon states.

7. **Acknowledgments**

The authors would like to thank the Jefferson Lab Hall B staff, the very strange collaboration, and the CLAS g12 group. This work was supported by DOE award DE-SC0013620.

References

[1] H. Haberzettl *et al.*, Phys. Rev. C **58**, R40 (1998).

[2] T. Mart and C. Bennhold, Phys. Rev. C **69**, 012201 (2000).

[3] A. de la Puente, O. Maxwell, and B. Raue, Phys. Rev. C **80**, 065205 (2009).

[4] O. Maxwell, Phys. Rev. C **85**, 034611 (2012).

[5] M. Guidal, J. M. Laget, and M. Vanderhaegen, Phys. Rev. C **68**, 058201 (2003).

[6] T. Corthals *et al.*, Phys. Lett. B **656**, 186 (2007).

[7] T. Vrancx. L Cruz, J. Ryckebusch, and P. Vancraeyveld, Phys. Rev. C **84**, 045201(2011)

[8] A. V. Anisovich *et al.*, Eur. Phys. J. A **48**, 15 (2012).

[9] G. Penner and U. Mosel, Phys. Rev. C **66**, 055212 (2002).

[10] M. Döring *et al.*, Nucl. Phys. A **851**, 58 (2011).

[11] H. Kamano, S. X. Nakamura, T.-S.H. Lee, and T. Sato, Phys. Rev. C **81**, 065207 (2010).

[12] R. Koniuk and N. Isgur, Phys. Rev. D **21**, 1868 (1980).

[13] S. Capstick and W. Roberts, Phys. Rev. D **58**, 074011 (1998).

[14] S. Capstick and N. Isgur, Phys. Rev. D **34**, 2809 (1986).

[15] R. Edwards, J. Dudek, D. Richards, and S. Wallace, Phys. Rev. D **84**, 074508 (2011).

[16] C. Patrignani *et al.* (Particle Data Group), Chin. Phys. C **40**, 100001 (2016).

[17] R. Bradford *et al.*, Phys. Rev. C **75**, 035205 (2007).

[18] M. E. McCracken *et al.*, Phys. Rev. C **81**, 025201 (2010).

[19] A. Freese *et al.*, arXiv:1609.03879 [hep-ph] (2016).

[20] D. P. Barber *et al.*, Z. Phys. C **7**, 17 (1980).

[21] S. P. Barrow *et al.*, Phys. Rev. C **64**, 044601 (2001).

[22] K. Moriya *et al.*, Phys. Rev. C **88**, 045201 (2013).

[23] W. Roberts, Phys. Rev. C **73**, 035215 (2006).

[24] S. Strauch *et al.*, Phys. Rev. Lett. **95**, 162003 (2005)

[25] P. Eugenio *et al.*, Jefferson Lab Expriment E04-005 (2004).

[26] R. Badui, Ph.D Thesis, Florida International University (2016).

[27] L. Guo *et al.*, Phys. Rev. C **76**, 025208 (2007).

[28] K. Nakayama *et al.*, Phys. Rev. C **74**, 035205 (2006).

[29] J. Man, Y. Oh, and K. Nakayama, Phys. Rev. C **83**, 055201 (2011).

[30] W. Roberts *et al.*, Phys. Rev. C **71**, 055201 (2005).

[31] J. Bono, Ph.D Thesis, Florida International University (2014).

[32] *Photoproduction of the very strangest baryons on the proton target in CLAS12*, Spokespersons: L. Guo, M. Dugger, J. Goetz, E. Pasyuk, I. I. Strakovsky, D. P. Watts, and V. Ziegler (The Very Strange Collaboration), JLab Proposal E12–11–005a, Newport News, VA, USA, 2013.

[33] N. Byers and S. Fenster, Phys. Rev. Lett. **11**, 52 (1963).

2.8 The Role of Hadron Resonances in Hot Hadronic Matter

José L. Goity
Department of Physics
Hampton University
Hampton, VA 23668, U.S.A. &
Thomas Jefferson National Accelerator Facility
Newport News, VA 23606, U.S.A.

Abstract

Hadron resonances can play a significant role in hot hadronic matter. Of particular interest for this workshop are the contributions of hyperon resonances. The question about how to quantify the effects of resonances is here addressed. In the framework of the hadron resonance gas, the chemically equilibrated case, relevant in the context of lattice QCD calculations, and the chemically frozen case relevant in heavy ion collisions are discussed.

1. Introduction

Lattice QCD (LQCD) and high energy heavy collisions (RHICs) give access to QCD thermodynamics in the limit of low or vanishing conserved charges (Baryon number B, strangeness S or electric charge Q). While LQCD addresses the case of chemically equilibrated hot matter, which corresponds ot the early universe, HICs produces a fireball which expands too fast for chemical equilibrium to be maintained giving rise to a hot hadronic system which at kinetic freeze out is well off chemical equilibrium. At temperatures between 0.15 – 0.17 GeV a cross over transition occurs from a quark-gluon to a hadronic phase. The rigorous description of the hadronic phase is in principle possible with a full knowledge of the S-matrix [1]. Absent that knowledge, one needs to consider models. The simplest model, known as the hadron resonance gas (HRG) turns out to provide a remarkably good description of thermodynamic observables. The HRG is to a first approximation an ideal gas of hadrons, consisting of mesons and baryons and their resonances. The HRG gas is then determined simply by the hadron spectrum. The hadron spectrum is however incompletely known, in particular for baryons, and thus one question is how important the role of such "missing" states may be in the HRG; this issue is the main focus of this note. Several indications of missing states exist, namely the known hadron spectrum has very few complete $SU(3)$ multiplets, and recent LQCD calculations show the existence of yet unobserved states, albeit at larger quark masses for baryons [2]. A first estimation of the missing states is based on SU(3) and the PDG listed baryons is given by the number of different strangeness isospin multiplets, namely: $\#\Sigma = \#\Xi = \#N + \#\Delta$ (PDG- 26; 12; 49), $\#\Omega = \#\Delta$ (4; 22), and $\#\Lambda = \#N + \#$ singlets (18; 29). Thus on this count alone we are missing the following isospin multiplets: 23 Σ, 11 Λ, 37 Ξ and 18 Ω. One expects even more missing states according to the quark model, LQCD, and/or the $SU(6) \times O(3)$ organization of multiplets. The question is therefore how sensitive is the HRG to those missing states, which consist in particular of a large number of hyperons.

The HRG is determined by the pressure, where the contribution to the partial pressure by a

given iso-multiplet i is:

$$p_i = T\frac{\partial}{\partial V}\log Z_i = T^2\, m_i^2\, d_i\, \frac{1}{2\pi^2}\sum_{k=1}^{\infty}\frac{(-1)^{(1+k)B_i}}{k^2}\; K_2(k\frac{m_i}{T})\; e^{k\mu_i/T}, \tag{1}$$

where B_i the baryon number, $d_i = (2I_i+1)(2J_i+1)$, and μ_i is a chemical potential, and K_2 is the modified Bessel function. For our purposes where $T < 0.16$ GeV, keeping only the first term in the sum is sufficient for all hadrons except the π, K and η mesons. Here we use the meson resonances listed in the PDG, and for baryons we choose to use $SU(6) \times O(3)$ multiplets with the mass formulas provided in Ref. [3], where we will include the $\mathbf{56}$ and $\mathbf{70}$ multiplets with $\ell = 0, \cdots 4$.

2. HRG in Chemical Equilibrium: LQCD

We use here the results for QCD thermodynamics obtained in LQCD, and the results are those of Ref. [4–6]. Above the cross over transition there is a slow evolution towards the ideal quark-gluon gas. Below the transition the HRG gives a remarkably good description of the thermodynamic observables, as shown in Fig. 1. The figure also shows the effect of excluding baryon resonances; those effects for the pressure p and the entropy s are modest for $T < 0.15$ GeV, and the effects of the hyperon resonances become almost insignificant. Figs. 2 and 3 show the effects of resonances in particle densities. Clearly it is not possible to disentangle the baryon resonance effects through the global thermodynamic observables of the hadron gas vis-à-vis the LQCD results. In chemical equilibrium, resonances rapidly disappear with the falling temperature and so do their effects on total thermodynamic observables. It is therefore necessary to have more sensitive observables in order to find the composition of the hadron gas: for hyperons one needs to filter strangeness. This is achieved via the study of correlations. In particular the susceptibilities (see for instance Refs. [7–9]) provide a useful tool. They are defined by:

$$\chi_2^{QQ'} \equiv \frac{1}{T^2}\frac{\partial^2 p}{\partial\mu_Q \partial\mu_{Q'}}, \tag{2}$$

where Q and Q' are conserved charges. If we consider only baryons, we have that $\chi_2^{BB} \sim (n_B + n_{\overline{B}})/T^3$ and $\chi_2^{BS} \sim (n_Y + n_{\overline{Y}})/T^3$: the HRG gives a very simple relation of the susceptibilities to the particle number densities, which can be tested with the LQCD [**?**], as shown in Fig. 4. The agreement is reasonably good, in particular for χ_2^{BS}, which provides perhaps the best indication of the role of excited hyperons for $T > 0.13$ GeV. For more extensive discussions of fluctuations and LQCD results see [8–10].

Although one expects resonances to have contributions whose magnitude is similar to the ones estimated with the HRG, it is also true that deviations from the approximation of the HRG may be of similar significance, and thus the LQCD results do not seem to permit for a definite estimate of what we are missing in terms of baryon resonance states.

3. HRG off Chemical Equilibrium: RHICS

The hot hadronic system produced in high energy HICs is for most of its brief expansion off chemical equilibrium. In the HRG description, this requires the inclusion of chemical potentials to account for the overabundance of the different hadrons. The presentation

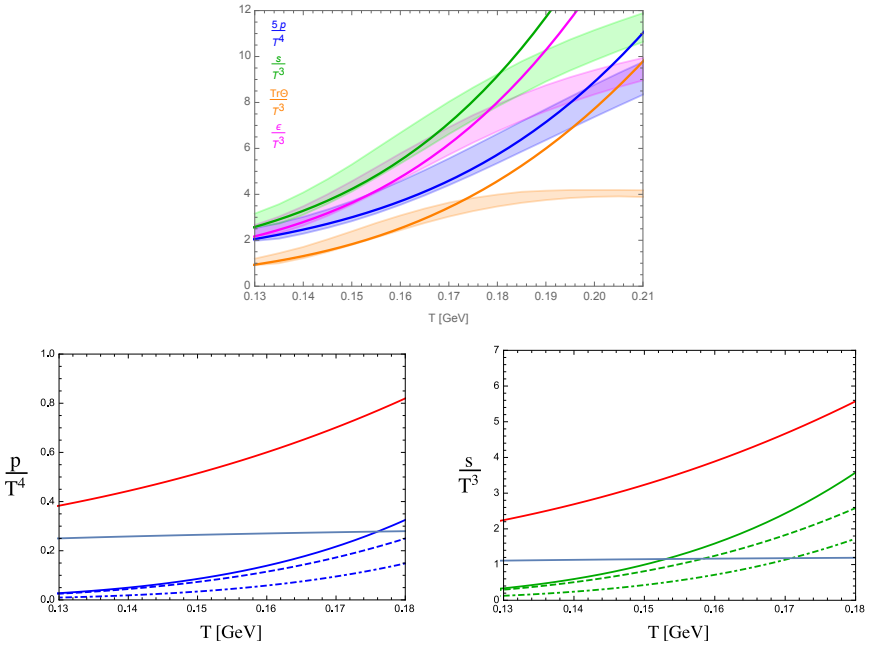

Figure 1: Thermodynamic observables at vanishing chemical potentials. Upper panel: bands from LQCD calculations [4], solid lines from HRG. s is the entropy density, ϵ is the internal energy, and $\mathrm{Tr}\Theta$ is the trace of the energy momentum tensor. Lower panels show meson contributions (red), pion contributions (gray), baryon contributions (solid), baryons with hyperon resonances removed (dashed) and only hyperons (dotdash).

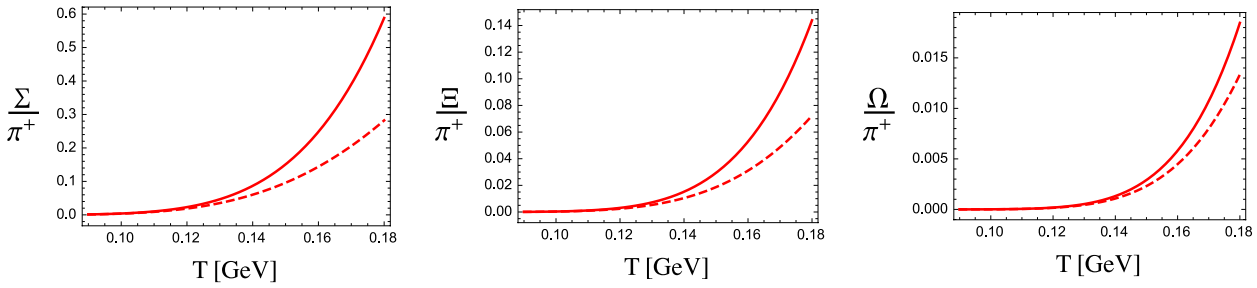

Figure 2: HRG hyperon number ratios with respect to π^+. Solid (dashed) line includes (excludes) baryon resonances.

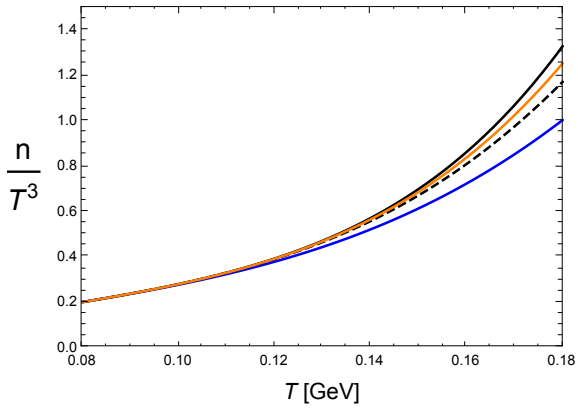

Figure 3: Total particle number density at vanishing chemical potentials. All hadrons (black), all hadrons except hyperon resonances (orange), all hadron except all baryon resonances (dashed), and mesons only (blue).

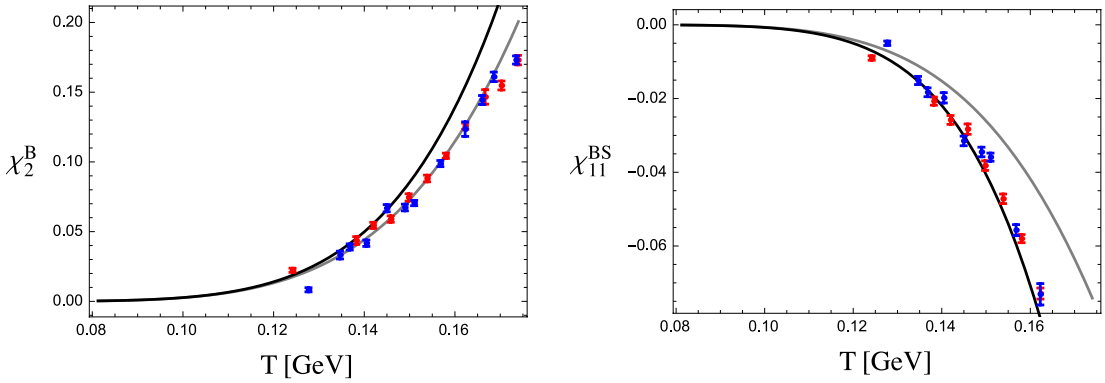

Figure 4: Baryon-Baryon number density susceptibility. In black the HRG, in gray the HRG with hyperon resonances removed, and the LQCD data is from Ref. [5]

here is basic, ignoring possible effects of hydrodynamics, and corresponds to describing the thermodynamics of the HRG in the local co-moving frame; it should be reasonably good for discussing particle yields. In the absence of net B, S and Q, we associate to each isospin multiplet a chemical potential, equal to that of the corresponding antiparticles. Processes which remain in equilibrium give relations between chemical potentials, e.g., if $A + B \leftrightarrow C + D$ is in equilibrium, then $\mu_A + \mu_B = \mu_C + \mu_D$, or $A + B \leftrightarrow C^*$ implies $\mu_{C^*} = \mu_A + \mu_B$. The existence of different reaction channels requires information about partial rates. Such information is extremely poorly known for most resonances, in particular baryons, and therefore one needs to resort to models. For the purpose of our discussion we adopt a very simple model, which assumes: i) resonances are in chemical equilibrium with respect to their decay products, ii) non-strange meson resonances decay only into pions, iii) strange meson resonances decay into one Kaon and pions, iv) all baryon resonances have 2-body decays into the ground state octet and decuplet, v) all non-strange baryon resonances decay only via pion emission, vi) Σ, Λ and Ξ resonances decay with different rates emitting pions and K or $\overline{K}$. Resonance chemical potentials are then given by:

$$\mu_i^{M^*} = \sum_{j=\pi,K} \nu_{ij}^{M^*} \mu_j \ , \qquad \mu_i^{B^*} = \sum_{j=N,\Sigma,\Lambda,\Xi,\Omega} \nu_{ij}^{B^*} (\mu_j + \delta_{S_i\, S_j}\, \mu_\pi + \delta_{S_i\, (S_j \pm 1)}\, \mu_K), \quad (3)$$

where the decay rates are encoded in:

$$\begin{aligned} \nu_{ij}^{M^*} &= \delta_{S_i 0}\, \delta_{j\pi}\, \overline{\eta}_i + \delta_{S_i\, \pm 1}\, (\delta_{jK} + (\overline{\eta}_i - 1)\delta_{j\pi}) \\ \nu_{ij}^{B^*} &= \delta_{S_i 0}\, \delta_{S_j 0} + \delta_{|S_i|3}\, \delta_{|S_j|2} + \sum_{S=1,2} \delta_{S\, |S_i|}\, (r_i\, \delta_{S_i\, S_j} + \frac{1 - r_i}{2}\, \delta_{S_i\, (S_j \pm 1)}) \ , \quad \sum_j \nu_{ij}^{B^*} = 4 \end{aligned} \quad (4)$$

where $\overline{\eta}_i$ is the average particle multiplicity in the decay of the meson resonance i, and r_i is the branching fraction of pion emission in the decay of the baryon resonance i. With this one can define effective particle number densities:

$$\overline{n}_i^M = n_i^M + \sum_j \nu_{ji}^{M^*} n_j^{M^*} \ , \qquad \overline{n}_i^B = n_i^B + \sum_j \nu_{ji}^{B^*} n_j^{B^*}, \quad (5)$$

where i indicates a stable meson or baryon, and n are the number densities obtained with the corresponding chemical potentials. For simplicity we have neglected the baryon resonance decay contribution to $\overline{n}_i^M$. The particle number densities $\overline{n}_i = \partial p / \partial \mu_i$ are the ones observed after kinetic freeze out.

Here the discussion is focused on the possible effects of resonances in the observed particle yields in RHICs. One can consider ratios of yields, and also fluctuations. The ratios remain constant after chemical freeze out. One can consider more detailed chemical freeze out for different hadrons [11], but for brevity we take a simple one, namely freeze out at about $T = 0.15$ GeV for all stable hadrons. Due to our lack of knowledge and for simplicity we take $r_i = r$ for all i, and check the dependencies on r. Using the yield ratios with respect to pions from ALICE [12], Fig. 5, we choose $\mu_\pi = 0$ at $T = 0.15$ GeV (this choice is arbitrary here, and in particular the value of μ_π at kinetic freeze out is sensitive to it); determinations of the initial μ_π can be improved via knowledge of it at kinetic freeze out. Fitting to the ALICE yield ratios one fixes the chemical potentials μ_i at the that initial T. To see how the

HRG evolves one uses the approximation [13] that the ratios of the densities of conserved particle numbers to total entropy remain approximately constant, namely $\overline{n}_i/s \sim$ const. This gives the chemical potentials in Figs. 5 and 6. One notices that, as expected, the baryon resonances play a very marginal a role in the evolution of the meson component of the HRG (mostly because of the assumption in Eqn. (5)); for nucleons the effects are also marginal except at higher T. The main sensitivity to resonances is on the hyperons, and it depends very much on the value of r. The effects of baryon resonances on the effective chemical potentials defined by the relation $n_i(T, \overline{\mu}_i) = \overline{n}_i(T, \{\mu_j\})$ are also relatively small. Clearly the effects of the baryon resonances are below other effects, such as the initial conditions right after hadronization and/or the uncertainties in the resonances' partial decay fractions. Thus, it is necessary to use more sensitive observables to acquire more sensitivity. For that purpose, one can consider susceptibilities such as the ones mentioned earlier, now adapted to a HRG off chemical equilibrium. They are simply defined by:

$$\chi_2^{ij} = \frac{1}{T^2} \frac{\partial^2 p}{\partial \mu_i \partial \mu_j}, \tag{6}$$

where the experimentally accessible quantities are ratios of those susceptibilities, namely:

$$R_{kl}^{ij} = \frac{\chi_2^{ij}}{\chi_2^{kl}}. \tag{7}$$

Using the HRG off chemical equilibrium one easily calculates the ratios. The most relevant ones involving hyperons are shown in Fig. 7. The ratios are sensitive to the value of r: while for the case $r = 1$ one cannot distinguish effects of resonances, those effects are significant for $r = 0.5$. In particular one needs the resonances to have a non-vanishing $R_{NN}^{\Omega\Xi}$. Thus, the analysis of particle number fluctuations and correlations are the most sensitive tool to extract information on resonance effects from RHICs data. Those effects come however modulated by resonance partial decay rates which are little known. For further discussion involving higher order correlations/fluctuations see Ref. [14].

4. Comments

In principle, it is possible to obtain indications of hadron resonance effects, in particular baryons, in the hadronic phase of hot QCD. Studies with LQCD and RHICs are the sources of relevant information. Using the HRG one can then quantify those effects within the model, and draw conclusions as discussed in this note. For the case of LQCD, the main sensitivity to resonances resides in fluctuations/correlations such as susceptibilities, which strongly indicate the importance of hyperon resonances for $T > 0.13$ GeV. In the case of RHICs there is less certainty on the conclusions due to lack of knowledge of the initial thermodynamic state of the hadronic fireball and of the partial decay rates of resonances which affect the expansion off chemical equilibrium. There is however interesting information encoded in ratios of correlations, which may definitely require the effect of resonances to be explained.

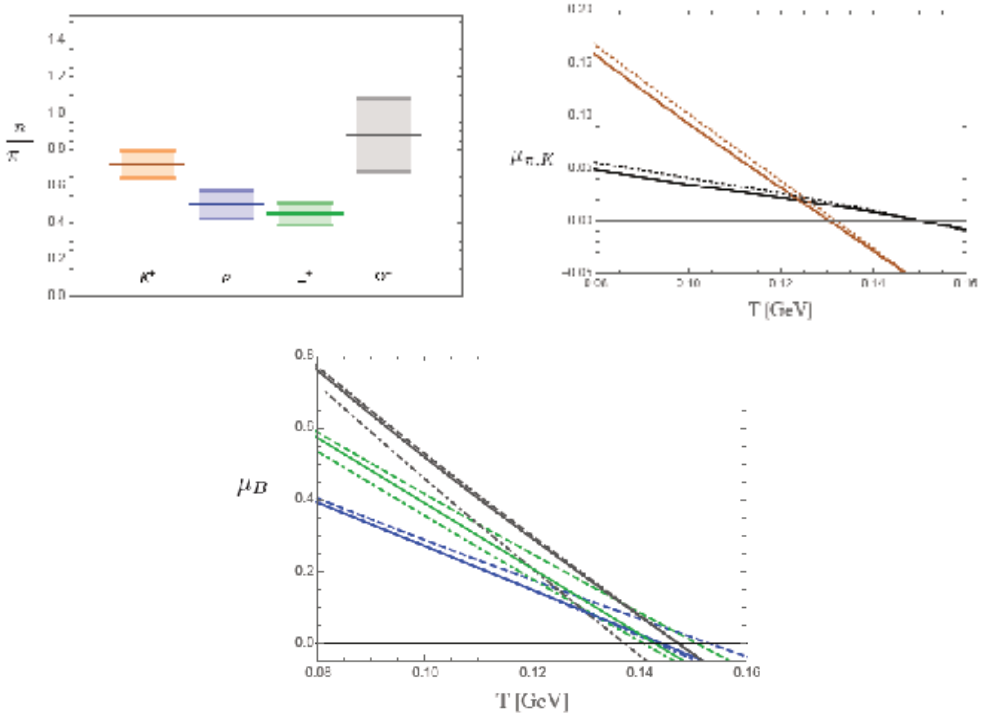

Figure 5: Upper left: particle number density ratios with respect to π^+ from ALICE Pb-Pb collisions at 2.76 TeV [12], scaled according to: $5 \times K^+$, $10 \times p$, $100 \times \Xi^+$ and $10^3 \times \Omega^-$. They are inputs to fit initial values of chemical potentials at $T = 0.15$ GeV. Upper right: evolution of μ_π (black) and μ_K (brown) with T: full HRG (solid) and HRG with no baryon resonances (dotted). Lower panel: baryon chemical potentials, N (blue), Ξ (green) and Ω^- (gray); full HRG with $r = 1$ (solid) and $r = 0.5$ (dotdash), and HRG without resonances (dashed).

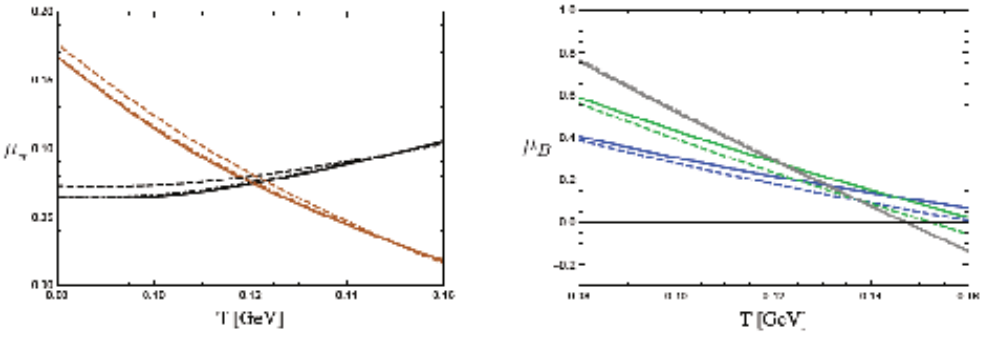

Figure 6: Left: pion effective chemical potential in GeV, and right: baryon effective chemical potentials. Same conditions as in Fig. 5.

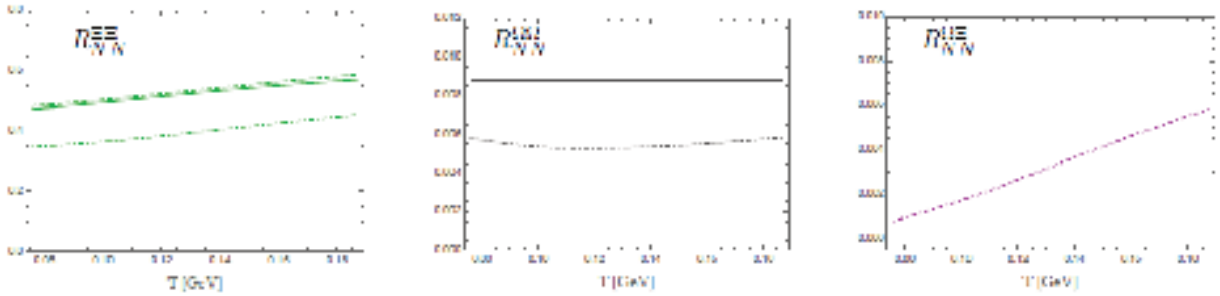

Figure 7: Correlation ratios: HRG with $r = 1$ (solid), with $r = 0.5$ (dotdash) and with no resonances (dashed).

5. **Acknowledgments**

This work was supported in part by DOE Contract No. DE–AC05–06OR23177 under which JSA operates the Thomas Jefferson National Accelerator Facility and by the National Science Foundation through grants PHY–1307413 and PHY–1613951.

References

[1] R. Dashen, S. K. Ma, and H. J. Bernstein, Phys. Rev. **187**, 345 (1969).

[2] R. G. Edwards, N. Mathur, D. G. Richards, and S. J. Wallace (Hadron Spectrum Collaboration), Phys. Rev. D **87**, 054506 (2013).

[3] J. L. Goity and N. Matagne, Phys. Lett. B **655**, 223 (2007).

[4] A. Bazavov *et al.* (HotQCD Collaboration), Phys. Rev. D **90**, 094503 (2014).

[5] A. Bazavov *et al.* (HotQCD Collaboration), Phys. Rev. D **86**, 034509 (2012).

[6] A. Bazavov *et al.*, Phys. Rev. Lett. **109**, 192302 (2012).

[7] R. Bellwied *et al.*, Phys. Rev. D **92**, 114505 (2015).

[8] P. Alba *et al.*, these proceedings.

[9] E. Ruiz Arriola *et al.*, these proceedings.

[10] R. Bellwied *et al.*, Phys. Rev. Lett. **111**, 202302 (2013).

[11] R. Bellwied, J. Phys. Conf. Ser. **736**, 012018 (2016), and references therein.

[12] B. Abelev *et al.* (ALICE Collaboration), Phys. Rev. Lett. **109**, 252301 (2012).
D. Alexandre *et al.* (ALICE Collaboration), Nucl. Phys. A **931**, 1093 (2014).

[13] H. Bebie, P. Gerber, J. L. Goity, and H. Leutwyler, Nucl. Phys. B **378**, 95 (1992).

[14] R. Bellwied, these proceedings and references therein.

2.9 Bound States of N's and Ξ's

Humberto Garcilazo
Escuela Superior de Física y Matemáticas
Instituto Politécnico Nacional
07738 México D.F., Mexico

Alfredo Valcarce
Departamento de Física Fundamental and IUFFyM
Universidad de Salamanca
E-37008 Salamanca, Spain

Javier Vijande
Departamento de Física Atómica, Molecular y Nuclear
Universidad de Valencia &
IFIC (UV-CSIC)
E-46100 Valencia, Spain

Abstract

Using local central Yukawa-type Malfliet-Tjon interactions reproducing the low-energy parameters and phase shifs of the NN system and the latest updates of the $N\Xi$ and $\Xi\Xi$ Nijmegen ESC08c potentials, we point out that these interactions predict bound states of 2, 3, and 4 particles consisting of nucleons and cascades so that very likely there will be a full periodic table of Ξ hypernuclei. We also discuss a resonant solution of the coupled ΞNN-$\Lambda\Lambda N$ system.

1. S-wave Two-body Interactions

We have studied the bound-state problem of few-body systems composed of N's and Ξ's using two-body interactions of Malfliet-Tjon type [1] that fit the low-energy data and the phase shift of a given two-body channel. These interactions are of the form

$$V^{ij}(r) = -A\frac{e^{-\mu_A r}}{r} + B\frac{e^{-\mu_B r}}{r}\,, \tag{1}$$

that is, an attractive and a repulsive Yukawa terms. We give in Table 1 the parameters of these interactions for the NN, $N\Lambda$, $N\Xi$, and $\Xi\Xi$ systems. As shown in Ref. [1], the NN interactions given in Table 1 predict a tritium binding energy of 8.3 MeV which is not far from the experimental value of 8.48 MeV. Also, if we use those NN interactions together witn the $N\Lambda$ interactions given in Table 1, we obtain a Λ-hypertriton separation energy of 144 keV which is quite consistent with the experimental value of 130 $\pm$ 50 keV. Thus, our approach appears to be reasonable. The interactions of the $N\Xi$ and $\Xi\Xi$ subsystems are based in the latest updates of the Nijmegen ESC08c potentials [2, 3]. In the $N\Xi$ case the singlet interactions are repulsive and the triplet ones are attractive, in particular the (1,1) interaction has a bound state of about 1.6 MeV the so-called D^* [2]. For the $\Xi\Xi$ subsystem, on the other hand, the singlet channel is attractive and the triplet is repulsive.

Table 1: Parameters of the local potentials given by Eq. (2) for the NN, $N\Lambda$, $N\Xi$, and $\Xi\Xi$ subsystems.

	(i,j)	A(MeV fm)	$\mu_A(\mathrm{fm}^{-1})$	B(MeV fm)	$\mu_B(\mathrm{fm}^{-1})$
NN	$(0,1)$	626.885	1.55	1438.72	3.11
	$(1,0)$	513.968	1.55	1438.72	3.11
ΛN	$(1/2,0)$	280	2.00	655	3.55
	$(1/2,1)$	170	1.95	670	4.60
ΞN	$(0,0)$	120	1.30	510	2.30
	$(0,1)$	434	2.68	980	6.61
	$(1,0)$	290	3.05	155	1.60
	$(1,1)$	568	4.56	425	6.73
$\Xi\Xi$	$(0,1)$	210	1.60	560	2.05
	$(1,0)$	155	1.75	490	5.60

2. Three-body Equations

Restricting ourselves to configurations where all three particles are in S-wave states the Faddeev equations for the bound-state problem in the case of three baryons with total isospin I and total spin J are

$$T^{i_ij_i}_{i;IJ}(p_iq_i) = \sum_{j\neq i}\sum_{i_jj_j} h^{i_ij_i;i_jj_j}_{ij;IJ}\frac{1}{2}\int_0^\infty q_j^2 dq_j \int_{-1}^{1} d\cos\theta\, t_{i;i_ij_i}(p_i,p_i';E-q_i^2/2\nu_i) \times\frac{1}{E-p_j^2/2\mu_j-q_j^2/2\nu_j}\, T^{i_jj_j}_{j;IJ}(p_jq_j), \tag{2}$$

$t_{i;i_ij_i}$ is the amplitude of the pair jk with isospin i_i and spin j_i while $h^{i_ij_i;i_jj_j}_{ij;IJ}$ are the spin-isospin recoupling coefficients. p_i is the momentum of the pair jk (with ijk an even permutation of 123) and q_i the momentum of particle i with respect to the pair jk while μ_i and ν_i are the corresponding reduced masses.

3. The Four-body Problem

The four-body problem has been addressed by means of a generalized variational method. The nonrelativistic hamiltonian will be given by,

$$H = \sum_{i=1}^{4}\frac{\vec{p}_i^{\,2}}{2m_i} + \sum_{i<j=1}^{4} V(\vec{r}_{ij})\,, \tag{3}$$

where the potentials $V(\vec{r}_{ij})$ have been discussed in the previous section. For each channel s, the variational wave function will be the tensor product of a spin ($|S_{s_1}\rangle$), isospin ($|I_{s_2}\rangle$), and radial ($|R_{s_3}\rangle$) component. Once the spin and isospin parts are integrated out, the coefficients of the radial wave function are obtained by solving the system of linear equations,

$$\sum_{s'\,s}\sum_{i}\beta^{(i)}_{s_3}\left[\langle R^{(j)}_{s'_3}|\,H\,|R^{(i)}_{s_3}\rangle - E\,\langle R^{(j)}_{s'_3}|R^{(i)}_{s_3}\rangle\delta_{s,s'}\right] = 0 \qquad \forall\, j\,, \tag{4}$$

where the eigenvalues are obtained by a minimization procedure.

4. **Strong Decay of Ξ-Hypernuclei**

   Ξ-hypernuclei can undergo a strong decay due to the process

$$N + \Xi \to \Lambda + \Lambda, \tag{5}$$

   which takes place in the $(i, j) = (0, 0)$ two-body channel when only S-wave configurations are taken into account. Thus, in that case a Ξ-hypernucleus will be stable if the ΞN two-body channels do not include the (0,0) channel. More generally, since the strong decay process (5) can only take place in isospin 0 two-body channels, a Ξ-hypernucleus where all the two-body channels are in isospin 1 states will be stable under the strong interaction. We will consider examples of these two cases in the next sections.

5. **The $NN\Xi$ $(I, J^P) = (\frac{1}{2}, \frac{3}{2}^+)$ State**

   In this three-body state the spins of the three baryons are parallel so that the two-body subsystems must all be in spin-triplet channels. They are the $NN\ ^3S_1(I = 0)$ channel which contains the deuteron and the $N\Xi\ ^3S_1(I = 0)$ and $^3S_1(I = 1)$ channels. As we have mentioned before, these two $N\Xi$ channels are attractive and moreover the last one contains the D^* bound state. Therefore, one expects that the three-body state will be bound with a large binding energy and indeed that is the case since we obtain for the binding energy

$$B = 17.2\ \text{MeV}. \tag{6}$$

   Notice that the $\Xi N\ ^1S_0(I = 0)$ (0,0) channel does not contributes so that in this pure S-wave configuration the bound state is stable. Of course there will be a contribution to the width by the decay $N + \Xi \to \Lambda + \Lambda$ when $N\Xi$ is in a P-wave and the spectator nucleon is also in a P-wave but due to the angular momentum barriers one expects that this width will be very small. In our previous works [4,5] we have reported a smaller value for this energy since we erroneously quoted the separation energy instead of the binding energy as well as the effect of a small numerical error.

6. **Maximal Isospin States**

   The decay process $N + \Xi \to \Lambda + \Lambda$ can not take place if the Ξ-hypernucleus is in a state of maximal isospin since in that case all the ΞN and $\Xi\Xi$ two-body subsystems must necessarily be in an isospin 1 state [6]. This will be the case for systems consisting only of neutrons and negative Ξ's or composed only of protons and neutral Ξ's.

   We show in Table 2 the first four maximal-isospin Ξ-hypernuclei. Since both N and Ξ have isospin 1/2 the total isospin of these hypernuclei is equal to the number of baryons divided by two. Since the space and spin parts of these Ξ-hypernuclei is the same as those of the corresponding ordinary nuclei they could be formed by simply replacing the protons of the ordinary nuclei by negative Ξ's or the neutrons by neutral Ξ's. Very likely there will be a full periodic table of stable maximal-isospin Ξ-hypernuclei.

Table 2: Binding energies of the first four Ξ-hypernuclei.

hypernucleus	(I, J^P)	B (MeV)
${}^{2}_{\Xi}H$	$(1, 1^+)$	1.6
${}^{3}_{\Xi}H$	$(\frac{3}{2}, \frac{1}{2}^+)$	2.9
${}^{3}_{\Xi\Xi}He$	$(\frac{3}{2}, \frac{1}{2}^+)$	4.5
${}^{4}_{\Xi\Xi}He$	$(2, 0^+)$	7.4

7. **The KISO Event**

The only Ξ-hypernucleus observed up to now, the so-called KISO event [7], takes place through the process

$$\Xi^- + {}^{14}\,N \rightarrow {}^{10}_{\Lambda}\,Be + {}^{5}_{\Lambda}\,He, \tag{7}$$

where the bound state, once formed, immediately decays due to the strong process $N + \Xi \rightarrow \Lambda + \Lambda$ giving rise to the two fragments observed, each one being a Λ-hypernucleus. The separation energy of the Ξ-hypernucleus is 4.4 MeV which is of the same order of magnitude as the binding energies of Table 2.

8. **The ΞNN—$\Lambda\Lambda N$ $(I, J^P) = (\frac{1}{2}, \frac{1}{2}^+)$ Resonance**

The ΞNN system is coupled to the $\Lambda\Lambda N$ system in the $(I, J^P) = (\frac{1}{2}, \frac{1}{2}^+)$ state since the $N\Xi$ (0,0) channel which is responsible for the strong decay is allowed to participate. Thus, in order to look for three-body resonances in this system one has to solve the integral equations of the coupled three-body system in the complex plane. This has been done using separable potentials [8] taking the Ξ mass as the average of the Ξ^0 and Ξ^- and the nucleon mass as the average of the proton and neutron. We used the low-energy parameters of the Nigmegen ESC08 baryon-baryon interactions for the systems with strangeness 0, -1, and -2 to construct a separable potential model of the coupled $\Lambda\Lambda N$—ΞNN system in order to study the position and width of the three-body $(I, J^P) = (\frac{1}{2}, \frac{1}{2}^+)$ resonance.

We found that the three-body resonance lies at [8]

$$E_0 = 23.408 - i0.045 \;\; \text{MeV} \tag{8}$$

measured with respect to the $\Lambda\Lambda N$ threshold, *i.e.*, just 0.012 MeV below the Ξd threshold. Thus, this is a loosely bound state of a Ξ and a deuteron with a small decay width into $\Lambda\Lambda N$.

The result (8) is somewhat intriguing, in particular the very small width, since the $\Lambda\Lambda N$ threshold is open. In order to understand that result we disconected the $N\Xi$ (0,0) channel and got an eigenvalue of $E_0 = 23.386$ MeV. Thus, the effect of the $\Lambda\Lambda - N\Xi$ (0,0) channel in the energy eigenvalue is negligible near the Ξd threshold. Adding the rest masses to the result (8) we get that the three-body $(\frac{1}{2}, \frac{1}{2})$ resonance lies at $W_0 = 3194$ MeV and has a very small width of $\Gamma = 0.09$ MeV.

The negligible effect of the absorption channel is a consequence of the very small binding energy which implies that the main component of the wave function is a Ξ orbiting

around the deuteron at a very long distance. Using first order perturbation theory one can estimate the effect of the absorptive channel as $\delta E = \langle \Psi \mid H_{ABS} \mid \Psi \rangle$, where $H_{ABS} = V_{N\Xi\to\Lambda\Lambda} G_0 V_{\Lambda\Lambda\to N\Xi}$. So that H_{ABS} is a short-range operator while Ψ is long ranged so that the overlap between Ψ and H_{ABS} is very small and consequently δE is negligible.

Finally, since the effect of the absorptive channel is negligible, we calculated the ΞNN bound state using the NN and $N\Xi$ Malfliet-Tjon potentials of Table 1 without the $N\Xi$ (0,0) channel and found that the system is unbound by about 0.01 MeV which means that in this case the state will appear as a very sharp resonance just above the Ξd threshold.

Thus, the $(I, J^P) = (\frac{1}{2}, \frac{1}{2}^+)$ state will appear as a very sharp resonance either just above or just below the Ξd threshold.

9. **Acknowledgments**

This work has been partially funded by COFAA-IPN (México), by Ministerio de Educación y Ciencia and EU FEDER under Contracts No. FPA2013-47443 and FPA2015-69714-REDT, by Junta de Castilla y León under Contract No. SA041U16, and by Generalitat Valenciana PrometeoII/2014/066. H. G. wishes to thank the organizers of YSTAR2016 for some finantial support during the workshop. A. V. is thankful for financial support from the Programa Propio XIII of the University of Salamanca.

References

[1] R. A. Malfliet and J. A. Tjon, Nucl. Phys. A **127**, 161 (1969).

[2] M. M. Nagels, Th. A. Rijken, and Y. Yamamoto, arXiv:1504.02634.

[3] Th. A. Rijken, M. M. Nagels, and Y. Yamamoto, Few-Body Syst. **54**, 801 (2013).

[4] H. Garcilazo and A. Valcarce, Phys. Rev. C **93**, 034001 (2016).

[5] H. Garcilazo and A. Valcarce, Phys. Rev. C **93**, 064003 (2016).

[6] H. Garcilazo, A. Valcarce, and J. Vijande, Phys. Rev. C **94**, 024002 (2016).

[7] K. Nakazawa *et al.*, Prog. Theor. Exp. Phys. (2015) 033D02.

[8] H. Garcilazo, Phys. Rev. C **93**, 024001 (2016).

2.10 Status and Plans of HADES

Joachim Stroth (for HADES Collaboration)
Institut für Kernphysik
Goethe-Universität Frankfurt
D-60438 Frankfurt am Main, Germany

Abstract

HADES is operated at the SIS18 and investigates the microscopic properties of resonance matter formed in heavy-ion collision in the 1 A GeV energy regime. Important topics of the research program are the mechanisms of strangeness production, the emissivity of resonance matter and the role of baryonic resonances herein. The latter topic is addressed also by investigation of exclusive channels in proton and pion beam induced reaction, both for hadronic and semi-leptonic final states. To optimize the performance of the spectrometer for the FAIR Phase-0 campaign, several upgrade project are underway.

1. **Properties of Hadron Resonances and Resonance Matter**

In central collisions of heavy ions at energies around a few A GeV , strongly interacting matter is substantially compressed and collective kinetic energy dissipated into intrinsic degrees of freedom. As a result, baryonic resonances are formed and in the final state of the reaction increasing abundances of mesonic states are observed as the beam energy rises. A scientific challenge is to understand the microscopic properties of the matter formed in the early stages of such collisions. Indeed, from studies using microscopic transport models, it is observed that the density in the interior of the collision zone may reach up to three times nuclear ground state density already at a beam energy of 1 A GeV. In such an environment hadronic states will likely change their properties compared to those observed in vacuum. Several experiments have tried to search for modifications of vector mesons states using their decay into lepton pairs. Although the results are not conclusive yet, a general trend examined is a strong broadening of vector meson states in the medium already for cold nuclear matter. A crucial question of QCD is under which conditions of density and temperature hadrons will ultimately lose their hadronic character and the system in such collisions will change from hadron gas into exotic states of strongly interacting matter? The situation at colliders (RHIC, LHC) is qualitatively very different. Due to the high gamma factors, the initial state at mid-rapidity is characterized by nearly instantaneous parton parton interactions which create a state of extreme energy density. The system then evolves through

Figure 1 depicts a sketch of the phase diagram of strongly interacting matter. The experimental information is depicted by symbols localizing the chemical freeze-out region which depend on system size and on beam energy. They remarkably line up along a narrow corridor spanning from LHC ($T \simeq 160$ MeV, $\mu_B \simeq 0$ MeV) down to SIS18 energies ($T \simeq 50$ MeV, $\mu_B \simeq 800$ MeV) and are determined with the help of statistical hadronization models from final state particle abundances measured in these collisions. Also shown is the expectation value of the chiral condensate calculated in a Polyakov–Quark–Meson Model approach as a function of baryo-chemical potential (μb) and temperature [1]. The systematics of these freeze-out points suggests that a thermal spectrum of hadrons is observed even at low energies, where a quark gluon plasma is not formed.

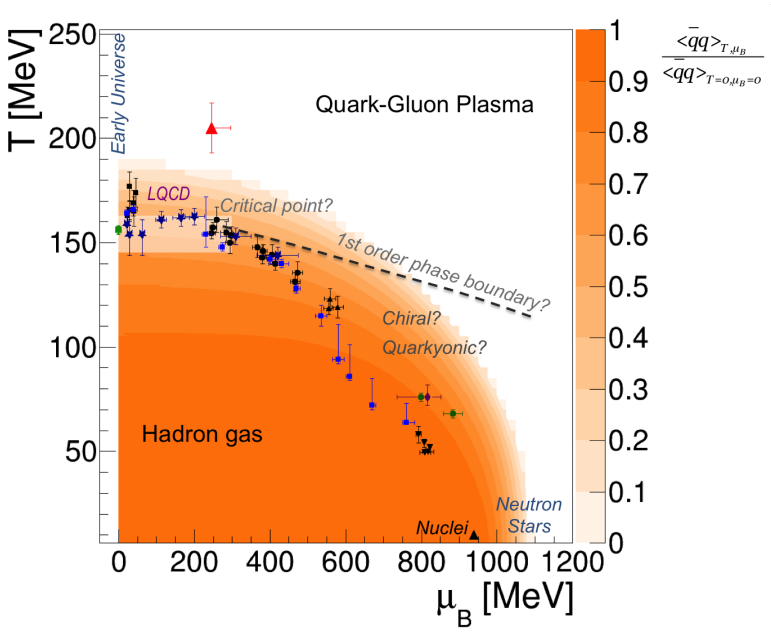

Figure 1: Sketch of the phase diagram of strongly interacting matter. The shaded area reflects the expectation value of the chiral condensate relative to its vacuum value. The data points are freeze-out configurations obtained by analyzing hadron final states in the framework of statistical hadronization models.

To learn more about the microscopic structure of matter in the region of high baryo-chemical potential HADES pursues a strategy, which relies on systematic measurements of strangeness production and virtual photon emission in heavy-ion collisions. The latter observable has the advantage, that this radiation is emitted through out the collision and hence is very sensitive to the properties of the dense and hot system. The disadvantage however is its small branching ratio and the fact that the spectrometer integrates the radiation over time. Consequently, contributions from the late stage of the collision have to be identified and subtracted before conclusions about the radiation from the dense phase can be drawn. Hadrons carrying strangeness are similarly interesting as their production threshold is high compared to the available energy in an NN collision at these beam energies. Consequently, their production requires a certain degree of collectivity, like it is the case in multi-particle processes or in deep off-shell production.

A central part of the physics program of HADES are measurements of rare meson production in heavy-ion collisions and in respective elementary collisions. The focus of the latter are the decay of baryonic resonances into intermediate ρ mesons and into final states with open strangeness thus addressing the observables utilized for the study of dense matter. The program includes in particular the reconstruction of exclusive hadronic and semi-leptonic final states. The paper is organized in the following way: In the next Chapter, selected results of experiments addressing virtual photons are presented. The examples address the concept of a reference spectrum in comparison to which medium-effects are addressed. In Chapter 3 few results on strangeness are shown emphazising the connection to virtual photon produc-

tion and the role of baryonic resonance it. Chapter 4 gives a short status of the HADES campaign 2012–2014 and Chapter 5 provides an outlook on the upcoming physics program of HADES anticipated for the years 2018 to 2021 and the spectrometer upgrades planned for this campaign.

2. Dilepton Emission from Hadronic Systems

An important reference for the study of dilepton emission (here and in the following e^+e^- pairs) off strongly interacting matter is the production of dileptons in $p+p$ and $n+p$ collisions at energies below the threshold for η production. Expected contributions are then solely by conventional bremsstrahlung and due to Delta Dalitz-decay. HADES has observed a surprisingly large isospin dependence comparing $p+p$ with $n+p$ collisions at $T_{beam} = 1.25(\sqrt{s} = 2.4)$ GeV [2]. This strong deviation appears in the spectral distribution (dP/dM_{e+e-}) of the lepton pairs towards the kinematic limit. While conventional bremsstrahlung can not account for the effect, although there is a difference in $n+p$ and $p+p$ due to the absence of a electric dipole moment in the latter case, calculations including emission from the intrinsic charged pion line in an one-boson-exchange model for the $n+p$ case, and using a VDM form factor for the pion photon vertex, could reproduce the trend observed in the data. Charged pion transfer is only possible in $n+p$ reactions due to isospin restrictions. In a strict VDM picture such a process can be interpreted as the formation of a deep off-shell ρ-meson in the overlapping cloud of the by-passing baryons. To what degree such a production would rather proceed through an intermediate baryon resonance state, such as a $\Delta(1232)$ resonance, remains an open question. Indeed, calculations of the $\Delta(1232) \rightarrow Ne^+e^-$ electromagnetic transitiofrom factor in the kinematic region discussed above with the Spectator Quark Model [4] and a Two-component Model [5] show only little or moderate deviations from solutions assuming pure QED (point-like) transitions, respectively.

While at a proton beam energy of around 1 A GeV essentially $\Delta(1232)$ resonances are active in electron-pair production, the situation changes substantially at an energy of 3.5 A GeV . Fig. 2 shows the inclusive dilepton yield obtained by HADES in the channel $p+p \rightarrow e^+e^-X$ as a function of the dilepton invariant mass. The cocktail shown has been calculated with a microscopic transport model and represents only prompt dileptons while the data contains also contributions from Dalitz- and direct decays of long-lived mesons (dominantly π^0, η and ω). In the model, prompt dileptons stem solely from (off-shell) ρ meson production produced in baryonic resonance decays. The treatment of off-shell ρ–meson propagation leads to a modified mass distribution of the mesons governed by phase space constraints. The higher the resonance mass, the more prominently the ρ pole emerges, yet, the resulting spectral distribution of ρ mesons from baryonic resonance decays (all res.) significantly differs from a distribution obtained if prompt, non-resonant production is assumed (Phytia). The thin solid curve going through the data is the sum of mesonic and prompt dileptons. Although the model has a number of parameters which have to be adjusted, it illustrates how dilepton production might proceed through strict vector meson dominance and how important a detailed understanding of resonant ρ–nucleon coupling is for the theoretical description of dilepton production in heavy-ion collisions.

Indeed, the preparation of a reference spectrum based on elementary inclusive cross sections

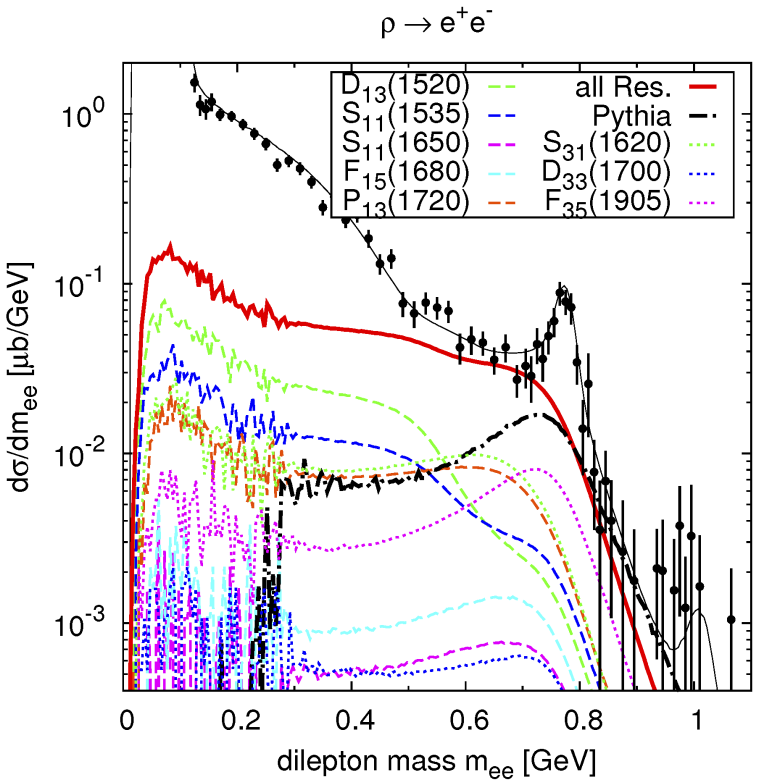

Figure 2: Dilepton invariant mass spectrum from $p + p$ collisions at 3.5 GeV (HADES data) compared to a calculation using a resonance model as implemented in microscopic transport codes. The cross sections for the excitation of the different baryonic resonances are obtained from a fit to data on meson production. All baryonic resonances, except the $\Delta(1232)$, produce lepton pairs via explicit decay to an intermediate ρ meson and subsequent annihilation into a pair of electrons. Figure taken from Ref. [3].

provided a conventional explanation for the inclusive electron pair spectra observed in $C+C$ collisions at 1 and 2 A GeV by HADES [6–8] and earlier by the DLS Collaboration [9], which could not be reproduced in microscopic model calculations at the time the DLS data was taken (DLS puzzle). It later turned out that within $\simeq 20\%$ uncertainty, $C + C$ collisions at these energies essentially appear as mere superposition of individual $N + N$ collisions, while a true excess radiation could only be observed in the heavier $Ar + KCl$ ($Ca + Ca$ in case of DLS) reactions at 1.76 A GeV .

A good description of this excess radiation can be obtained if emission out of thermalized system is assumed [10]. Under this assumption, the emissivity of matter at not too high temperatures is given by the thermal average of the in-medium ρ propagator for which ρ–baryon couplings are fundamentally important [11]. The spectra observed in experiments is then given as a four-volume integral over the emissivity, *weighted* with the time-dependent temperature and density profile of the hot and dense system. The latter can, e.g., be derived by coarse graining a microscopic transport code. Fig. 3 shows the dilepton excess radiation, obtained from the $Ar + KCl$ data by subtracting all known sources from long-lived

mesons decay, compared to a calculation assuming thermal emission and coarse graining UrQMD [12, 13]. The calculations agree well with data and the spectra show nearly exponential shapes, although the calculations are entirely based on VDM and hence dominated by large by off-shell ρ meson.

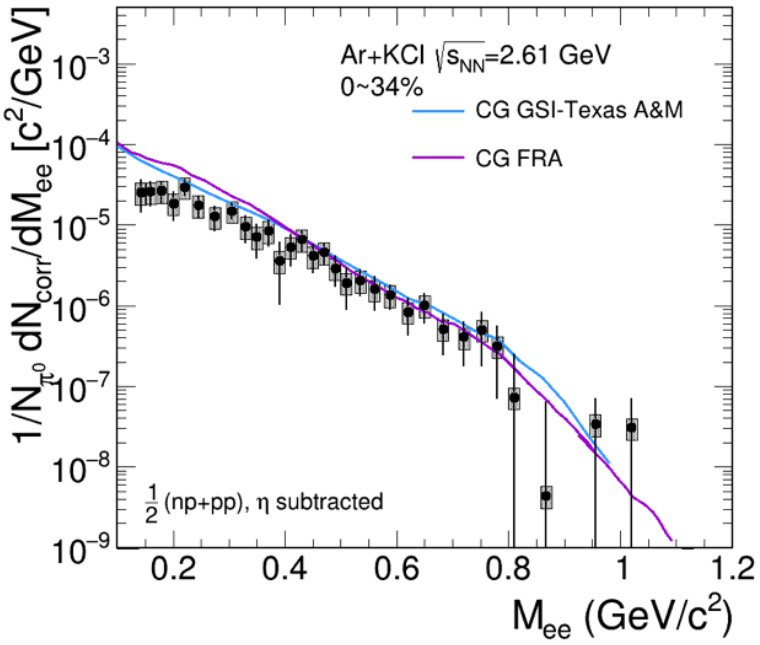

Figure 3: Dilepton excess radiation observed in $Ar + KCl$. Contributions from first chance NN collisions and late η–Dalitz decays have been subtracted from the data. The yield is normalized to the number of produced π^0 (to remove trivial A_{part} dependences). The colored lines show the results of two versions of corse grained UrQMD calculations using different concepts for obtaining the thermal parameters. The data has been analyzed for the 34% most central events.

3. Selected Results on Strangeness Production

Similarly important are baryonic resonances for the description of strangeness production in heavy-ion collisions, in particular at beam energies where the total energy in a single $N + N$ collision is not sufficient to produce a final state with strangeness. If instead binary collision occur, which include secondary (or even higher generation) baryonic resonance states, the kinematic constraints can be lifted beyond the effect of fermi motion. A theoretical description of secondary interactions beyond the low-density approximation is difficult but desirable as the collision frequencies are as high that asymptotic states are not easily reached between subsequent collisions.

A particular role in the production and propagation of strangeness is played by the $\Lambda(1405)$ resonance. The existence of this resonance influences the interaction of antikaons propagating through a baryonic medium since this resonance can be understood as a dynamically

produced antikaon-nucleon quasi-bound state [14]. Such a picture is also supported by lattice data if the strange magnetic form factor of the resonance is investigated [15]. The $\Lambda(1405)$ has been observed by HADES in $p+p$ collisions at 3.5 GeV collisions 4. The broad structure is attributed to the formation of the $\Lambda(1405)$ state which appears a little bit shifted, a hint that the state is a molecule and its appearance depending on the reaction dynamics.

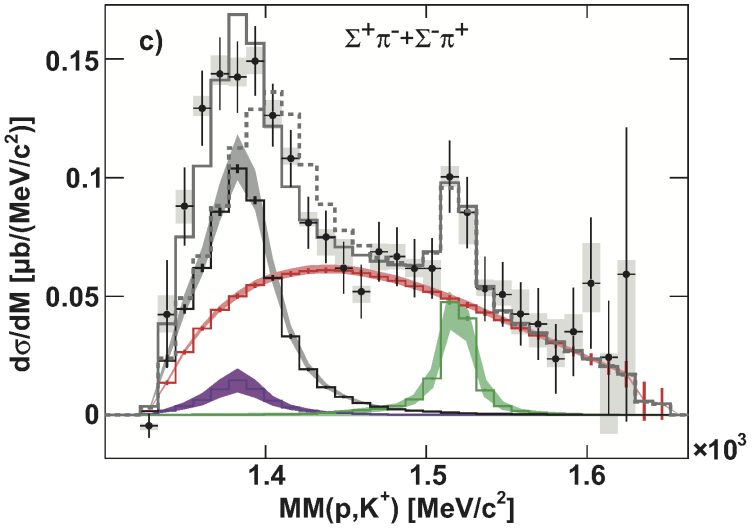

Figure 4: Missing mass distribution to the pK^+ subsystem of the exclusive final state $pK^+n\pi^+\pi^-$ reconstructed in $p+p$ reactions at 3.5 GeV. The distribution is interpreted in terms of contributions from $\Lambda(1405)$ and $\Lambda(1520)$, histograms shaded in grey and green, respectively, $\Sigma(1385)$ (purple) and channels not involving excited hyperons (red). The pole mass for the simulated $\Lambda(1405)$ contribution was fitted to the experimental distribution and favors a downward shift by 20 MeV/c^2
.

The resonant scattering, as well as the different NN thresholds for associated $(K\Lambda)$ and direct $(K\bar{K})$ kaon production, suggests a rather complex structure of kaon production in heavy-ion collisions at SIS18 (”threshold-”) energies. Yet, the yields observed in $Ar+KCl$ collisions at 1.76 A GeV shows a very simple behaviour. The multiplicities of all observed hadrons an be explained assuming a break-up (freeze-out) of a thermalized hadronic system if strangeness is treated canonically by implementing a *strangeness correlation radius* R_c. The latter leads to suppression of hadronic states with open strangeness but not for states with hidden strangeness like the ϕ. Fig. 5 shows the reconstructed hadron multiplicities in comparison with a fit using the THERMUS code. All multiplicities including states involving strange quarks are reproduced assuming a temperature of $\simeq 76$ MeV and a baryochemical potential of $\simeq 800$ MeV, except for the double strange baryon Ξ [16]. Note that ϕ is produced abundantly as expected by the statistical model and holds up for $\simeq 30\%$ of the produced antikaons [17].

These observations, as well as those in dilepton production are accordance with a picture describing the fireball as *strongly* interacting resonance gas. The observed hadron multiplicities resemble thermalization although, e.g., the ow pattern of protons does not. That raises the

question if the equilibration is driven by binary collisions of the (hadronic) constituents, as it is implied by the low-density approximation forming the basis of the model calculations used to describe heavy-ion collisions and medium-effects at these energies? Likely other mechanisms drive equilibration, like, e.g., a strong quantum mechanical entanglement [18]. To further scrutinize these observations, HADES focused on studying a heavy collision system at maximum SIS18 beam energy and on exploiting pion induced reactions.

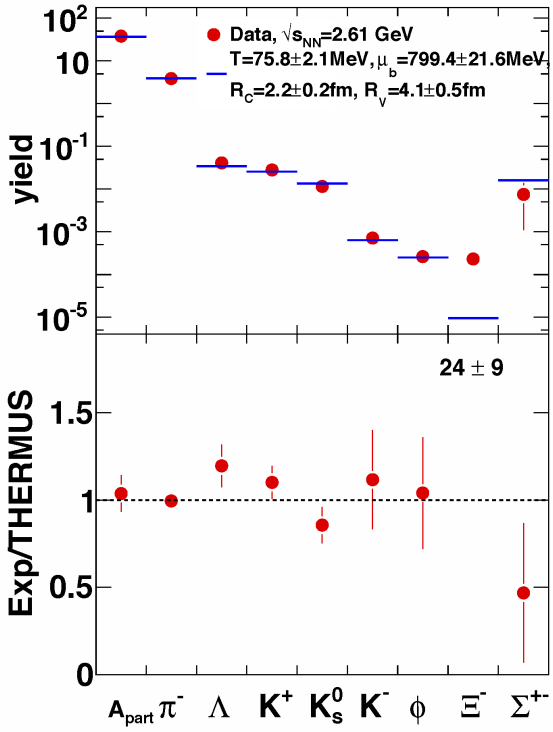

Figure 5: Hadron multiplicities in full phase space for 38% most central $Ar + KCl$ collisions at 1.76 A GeV. The data is compared to the expectation of a Statistical Hadronization Model (THERMUS). The extracted paramters for temperature and baryochemical potential fit weel in the systematics shown in Fig. 1.

4. The HADES campaign 2012–2014

During the first measurement campaign (2002-2007), HADES was operating with a 18-fold segmented inner time-of-flight detector system. This low granularity made runs with heavy collision systems impossible. In the shutdown period for SIS18, the HADES collaboration replaced this system by a RPC system with more than 1000 individual cells. Also replaced was the innermost layer of drift chambers.

In April 2012 HADES took 7.2×10^9 events during 30 days run for the collision system $Au + Au$ at 1.23 A GeV. For the first time, a nearly complete set of strange hadrons (ϕ, K^+, K^-, K^0) has been reconstructed at such low beam energies ($\sqrt{s}$ =2.4 A GeV). Again a large ϕ meson abundancy, which accounts for about 25% of the total K^- production, could

be observed - note that a NN collisions at this beam energy is $\simeq 500$ MeV below the $NN\phi$ threshold. Ongoing analysis work focuses on a further reduction of systematic errors and on a comprehensive comparison to results from transport calculations.

As expected already, the yield of dielectrons reconstructed in these collisions shows a strong excess above a reference spectrum. Two different analysis strategies have been implemented, one focusing on highest purity, the other on highest efficiency for electron positron reconstruction. The results nicely agree, though the one with higher statistics comes with the price of an higher uncertainty in the overall normalization. The spectrum again drops off nearly exponentially.

A first experiment with the GSI pion beam has been realized in 2014 with two weeks of beam on target in total. The first run was dedicated to strangeness production in cold matter in pion-induced reactions on light (12C) and heavy (74W) nuclei at a beam momentum of 1.7 GeV/c. The goal of the second run was to measure both double pion and dilepton production in π^-+p reactions around the pole of $N(1520)$ resonance using polyethylene and carbon targets. Data at four different pion beam momenta (0.656, 0.69, 0.748 and 0.8 GeV/c) were collected with the largest statistics in the case of 0.69 GeV/c momentum, aimed for dilepton production studies.

The two-pion production data samples have been included in the multichannel Partial Wave Analysis (PWA) developed by the Bonn-Gatchina group, which allows for the extraction of the various $2\pi N$ channels ($\Delta\pi, \rho N, \cdots$). The total (resonant+non-resonant) ρ is derived and converted into a e^+e^- contribution using the Vector Dominance Model (VDM) assumption. Adding to this ρ contribution a cocktail of point-like baryonic sources, the exclusive dilepton production can be described quite nicely. This demonstrates the consistency between the dilepton and double pion production channels and suggests that the involved time like baryonic electromagnetic transitions can be described by VDM. The ρN couplings of the $N(1520)$ are also of high interest due to the connection with the expected medium modification of the ρ meson spectral function. Most of the new results will be presented on the upcoming Quark Matter Conference in February 2017.

5. HADES at FAIR Phase–0

With the start of FAIR Phase 0 in 2018, most of the detector systems will reach an age of more than 15 years. Hence, we have started an upgrade program replacing the UV detector of the RICH by a detector based on MAPMTs. The development of this detector is a joint initiative between HADES and CBM, the same modules will later also be used in the CBM RICH. The pre-shower detector (polar angle coverage from 18 to 45 degree), which augmented electron/positron identification and also served as additional tracking detector in front of the low-granularity time-of-flight system during the first experimental campaign, will be replaced by an electromagnetic calorimeter (ECAL). This new detector is based on recycled lead glass crystal from the former OPAL calorimeter. For the first time, this will enable studies of radiative baryonic resonance decays with real photons. Moreover, the success of the experimental program addressing elementary reactions calls for an instrumentation of the acceptance region between polar angles of 2 to 8 degree in order to enlarge the phase space acceptance. This solid angle will be equipped with tracking stations and a new RPC-based time-of-flight wall. The tracking system will be based on developments for the

PANDA tracker which will be composed of by 5 mm straw tubes. Last but not least a moderate upgrade of the DAQ system will increase the band width such that interaction rates of up to 100 kHz are in reach for elementary reactions and around 20 kHz for heavy-ion reactions.

Further experiments on baryonic-resonance and cold-matter physics will be realized, taking advantage of foreseen improvement of the extraction and increase of the space charge limit. In addition, with the ECAL, the capacity of HADES to provide high precision data for PWA for baryonic resonances with masses up to 2 GeV/c^2 will be extended to exit channels with neutral mesons. HADES at the moment represents the only facility world-wide, which combines a pion beam with dilepton spectrometry and acts as a precursor in view of existing plans for meson beam facilities for baryon spectroscopy. Emphasis will be on the electromagnetic transition form factors of baryonic resonances, the coupling of vector mesons and kaons to baryons and medium effects in cold nuclear matter.

Measurements of hadron production off cold nuclear matter provide an important reference for understanding heavy-ion collisions. They also provide an ideal test bed for microscopic transport theory. HADES has already studied $p + Nb$ collisions at 3.5 GeV in 2007. Yet, many of the the interesting observation made suffer from statistical significance or call for multi-differential analysis. Moreover, particle identification in the 2007 run was limited since no fast start detector had been available at this time. Meanwhile, HADES has developed such detectors based on mono-crystal CVD diamond which combine high rate capability with excellent time resolution for minimum ionizing particles. A high statistics run would enable very important studies like, ϕ production and propagation both in the hadronic and leptonic final state, in-medium w-meson, multi-strange baryon production, short range correlation (SCA) and two particle correlation studies aiming at determining, e.g., the λp phase shifts.

The combined measurement of dielectrons and strangeness performed by HADES in $Ar + KCl$ and Au+Au collisions have provided new intriguing results which call for further systematic investigations. We propose an experiment which focuses on measuring a medium-heavy collision system at the maximum energy at SIS18, to increase the NN center-of-mass energy in favour of an enhanced strangeness production. Silver, e.g., can be stripped to charge state 45^+ behind the UNILAC and would then allow acceleration in SIS18 to 1.67 A GeV.

The main goals are to search for multi-strange baryons in connection to our finding in $p+Nb$ and $Ar+KCl$, and to extend the dielectron and strangeness excitation functions. Indeed, the unexpected high cascade yield is by now not explained theoretically and call for more data (see also above). In the dielectrons channel, we will focus on studies of properties of the low-mass excess as well as on vector meson (ρ, ω, ϕ) spectroscopy. The strangeness study will include ϕ meson production via the $K^+K^?$ decay channel, kaon production characteristics, $\Lambda(1115)$, $\Sigma(1385)$ and $\Xi(1321)$ strange baryon production, and HBT correlations.

The motivation for operating HADES as part of the Compressed Baryonic Matter program at SIS100 is two-fold: First, HADES can bridge the gap from the SIS18 energies to the SIS100 region were CBM acceptance is favourable. It enables the option to measure dilepton spectra in heavy-ion collisions with two different spectrometers to so minimize systematic uncertainties. Second, HADES can serve as ideal spectrometer to continue reference measurements

focusing on cold matter studies. As medium-effects show a strong momentum dependence, the relevant phase space for meson production and propagation is near to the target rapidity.

Finally, HADES can also be operated with a liquid hydrogen target, which is not possible in CBM. Any reference measurements, as well as a continuation of the physics program of HADES at SIS18 is possible at the new experimental site.

6. **Acknowledgments**

The HADES collaboration gratefully acknowledges the support by the grants LIP Coimbra, Coimbra (Portugal) PTDC/FIS/113339/2009, UJ Kraków (Poland) NCN 2013/10/M/ST2/00042, TU München, Garching (Germany) MLL München: DFG EClust 153, VH–NG–330 BMBF 06MT9156 TP5 GSI TMKrue 1012 NPI AS CR, Rez, Rez (Czech Republic) GACR 13–06759S, NPI AS CR, Rez, USC - S. de Compostela, Santiago de Compostela (Spain) CPAN: CSD2007-00042, Göthe University, Frankfurt (Germany): HA216/EMMI HIC for FAIR (LOEWE) BMBF:06FY9100I GSI F&E, IN2P3/CNRS (France).

References

[1] B. J. Schaefer and J. Wambach, Nucl. Phys. A **757**, 479 (2005); [nucl-th/0403039].

[2] G. Agakishiev *et al.* [HADES Collaboration], Phys. Rev. C **84**, 014902 (2011); [arXiv:1103.0876 [nucl-ex]].

[3] J. Weil, H. van Hees, and U. Mosel, Eur. Phys. J. A **48**, 111 (2012); Erratum: [Eur. Phys. J. A **48**, 150 (2012)]; [arXiv:1203.3557 [nucl-th]].

[4] G. Ramalho, M. T. Pena, J. Weil, H. van Hees, and U. Mosel, Phys. Rev. D **93**, 033004 (2016); [arXiv:1512.03764 [hep-ph]].

[5] Q. Wan and F. Iachello, Int. J. Mod. Phys. A **20**, 1846 (2005).

[6] G. Agakishiev *et al.* [HADES Collaboration], Phys. Lett. B **690**, 118 (2010); [arXiv:0910.5875 [nucl-ex]].

[7] G. Agakichiev *et al.* [HADES Collaboration], Phys. Rev. Lett. **98**, 052302 (2007); [nucl-ex/0608031].

[8] G. Agakishiev *et al.* [HADES Collaboration], Phys. Lett. B **663**, 43 (2008); [arXiv:0711.4281 [nucl-ex]].

[9] R. J. Porter *et al.* [DLS Collaboration], Phys. Rev. Lett. **79**, 1229 (1997); [nucl-ex/9703001].

[10] C. Gale and J. I. Kapusta, Phys. Rev. C **35**, 2107 (1987).

[11] R. Rapp, G. Chanfray, and J. Wambach, Nucl. Phys. A **617**, 472 (1997); [hep-ph/9702210].

[12] T. Galatyuk, P. M. Hohler, R. Rapp, F. Seck, and J. Stroth, Eur. Phys. J. A **52**, 131 (2016); [arXiv:1512.08688 [nucl-th]].

[13] S. Endres, H. van Hees, J. Weil, and M. Bleicher, Phys. Rev. C **92**, 014911 (2015); [arXiv:1505.06131 [nucl-th]].

[14] L. Tolos, A. Ramos, and E. Oset, Prog. Theor. Phys. Suppl. **168**, 635 (2007); [nucl-th/0702089 [NUCL-TH]].

[15] W. Kamleh, J. M. M. Hall, D. B. Leinweber, B. J. Menadue, B. J. Owen, A. W. Thomas, and R. D. Young, PoS CD **15**, 037 (2016).

[16] G. Agakishiev *et al.* [HADES Collaboration], Phys. Rev. Lett. **103**, 132301 (2009); [arXiv:0907.3582 [nucl-ex]].

[17] G. Agakishiev *et al.* [HADES Collaboration], Phys. Rev. C **80**, 025209 (2009); [arXiv:0902.3487 [nucl-ex]].

[18] J. Stroth [HADES Collaboration], Nucl. Phys. A **862-863**, 205 (2011).

2.11 Hadron Physics with High-Momentum Hadron Beams at J-PARC

Hiroyuki Noumi (for E50 Collaboration)
Research Center for Nuclear Physics (RCNP)
Osaka University
Osaka, 567-0047, Japan

Abstract

Baryon spectroscopy with heavy flavors provides unique opportunities to study internal motions of ingredients in baryons, from which we can learn the effective degrees of freedom to describe hadrons. We proposed an experiment on charmed baryon spectroscopy via the (π^-, D^{*-}) reaction at the J-PARC high-momentum beam line. Mass spectrum from the ground state to highly-excited states of the excitation energy up to more than 1 GeV will be observed by means of a missing mass technique. Production cross sections and decay branching ratios of these states will be measured. It is worthy to compare how nature of baryons with different flavors changes. In particular, double-strangeness baryons, Ξ, are of interest. A neutral kaon beam at J-Lab is unique to produce Ξ baryons. Hadron beams at J-PARC play complimentary roles to the neutral kaon beam at J-Lab.

1. Baryon Spectroscopy with Heavy Flavors

"How hadrons are formed from quarks?" is a fundamental question in hadron physics. We know that the quantum chromo-dynamics (QCD) is a fundamental theory to describe dynamics of quarks and gluons. However, it is still very hard to describe hadrons by solving the QCD equation in low energy because of its non-perturbative nature of the strong interaction, where the coupling constant becomes very large when the energy scale is close to the scale parameter $\Lambda_{\rm QCD}$. Quarks drastically change their nature below $\Lambda_{\rm QCD}$. Then, constituent quarks as effective degree of freedom to describe hadrons seem to work rather well. Actually, the constituent quark model well describes properties of hadrons in the ground state, such as masses, spin-flavor classifications, magnetic moment of octet baryons, and so no. However, it sometimes fails in excited states. In particular, not only recent reports on so-called exotic hadrons, such as X, Y, Z, and pentaquark states in heavy sector but also a long-standing puzzle in $\Lambda(1405)$ indicate that we need a new aspect in describing hadrons. Internal correlations among ingredients of hadrons such as diquarks and hadron clusters are expected to play an important role. Since they are confined in a hadron, hadron spectroscopy to look into more details of internal structure or motions of the composites in hadrons is necessary.

Since the color magnetic interaction between quarks is proportional to the inverse of the quark mass, spin-dependent interactions to a heavy quark vanish in the heavy quark mass limit. In the heavy quark mass limit, a heavy quark spin and the spin of the other system become good quantum numbers. This is the so-called heavy quark symmetry of QCD. Let us consider a baryon with a heavy quark. A relative motion between two light quarks (ρ mode) and a collective motion of the light quark pair (λ mode) are separated in excited states, as illustrated in Fig. 1. This is known as the so-called isotope shift. These states are further split due to spin-dependent interactions between quarks [1]. The spin-correlation between

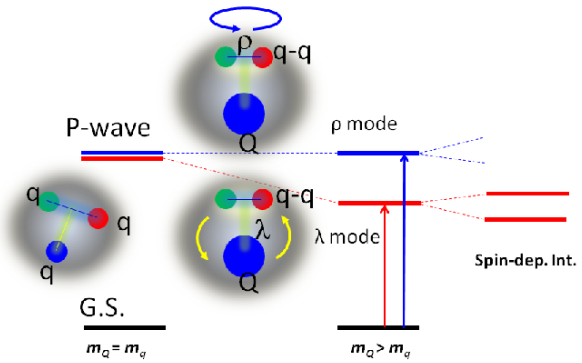

Figure 1: Schematic level structure of excited baryons with a heavy quark

light quarks becomes stronger than those to a light quark and a heavy quark due to the heavy quark spin symmetry. Internal structure of the baryon with a heavy quark is characterized by the two light-quark (diquark) correlation. Nature of these baryons is reflected in mass, decay width (branching ratio), and production rate.

Therefore, we proposed an experimental study of charmed baryons via the (π^-, D^{*-}) reaction on hydrogen [2] at the J-PARC high-momentum beam line. In the reaction, we reconstruct charmed baryons by means of missing mass technique. An excitation spectrum of charmed baryon states can be measured independent of their decay final states. We could also identify decay modes with detecting a decay particle together with scattered D^{*-} and identifying a daughter particle in a missing mass. A branching ratio (partial decay width) of the decay mode can be obtained rather easily. Branching ratios provide information on diquark motions of excited charmed baryons, as described later. This is an advantage of the missing mass method.

2. Beam Line

A new beam line, called high-momentum beam line, is being constructed in the Hadron Experimental Facility of the Japan Proton Accelerator Research Complex (J-PARC). It is branched from the slow extraction primary beam line in the switch yard. A small fraction of the primary beam is transported to the experimental area, located about 130 m downstream from the branch point, for the E16 experiment which aims at measuring spectral changes of vector mesons in nuclei [3].

The high-momentum beam line can deliver secondary beams if we install a production target at the branching point. The layout of the beam line magnets are arranged so as to transport secondary beams up to 20 GeV/c, as shown in Fig. 2. The beam line is carefully designed to realize a dispersive beam at the dispersive focal point, where a momentum and a horizontal position of the secondary particles are strongly correlated. Fig. 3-top demonstrates the correlation calculated by the DECAY TURTLE [4]. We place 3 sextupole magnets to reduce second order aberrations and to sharpen the correlation. The calculation tells that a momentum resolution of 0.12% is expected by measuring a beam position with a spatial resolution of 1 mm, as illustrated in Fig. 3-bottom. The momentum resolution is mostly determined by

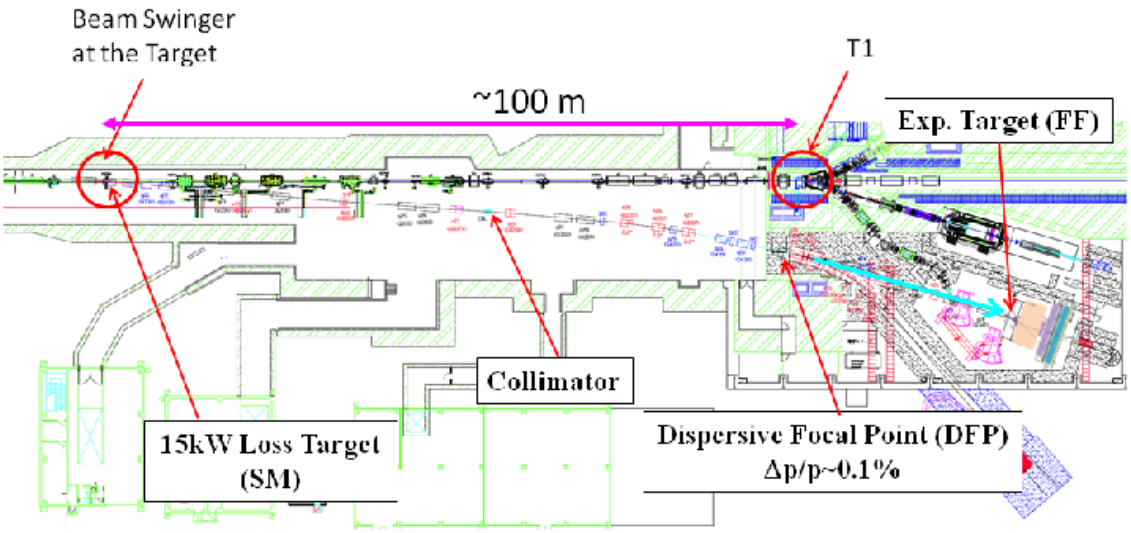

Figure 2: High-momentum beam line at the J-PARC Hadron Experimental Facility

a beam size at the production target (actually, its image at the dispersive focal point). We assume the beam size of 1 mm in σ in the horizontal direction at the production target.

The beam line length and acceptance are 133 m and 1.5 msr·%. We estimated intensities of secondary particles by the so-called Sanford-Wang formula [5], assuming that a 6-cm thick platinum target is irradiated by a 30-GeV proton beam of 30 kW (15-kW beam loss at the target), as shown in Fig. 4. Here, a production angle for negative and positive particles are assumed to be 0° and 3.9°. We expect that the negative pion beam intensity is more than 10^7 per second at 20 GeV/c.

3. Spectrometer

An incident pion momentum will be measured at a resolution as good as ∼0.1% in the high-momentum beam line. We designed a spectrometer system to reconstruct scattered D^{*-} from its decay chain of $D^{*-} \to \bar{D}^0\pi^-$, $\bar{D}^0 \to K^+\pi^-$, as shown in Fig. 5. The spectrometer is based on a single dipole magnet with a circular pole of 2.1 m in diameter and a gap of 1 m. A rigidity of the magnet is 2.3 Tm. A typical momentum resolution is expected to be ∼0.5% at 5 GeV/c. A liquid hydrogen target of 57 cm in length (4 g/cm^2 in thickness) will be placed close to the entrance face of the magnet. Fiber trackers with 1 mm scintillating fiber will be placed just after the target. A set of drift chambers will be placed surrounding the pole and after the magnet to detect scattered particles with lower and higher momenta, respectively. A ring image cherenkov counter (RICH) with dual radiators of aerogel with a reflection index of 1.04 and a C_4F_{10} gas with an index of 1.00137 will be used for identifying pion, kaon, and proton in a wide momentum range from 2 to 16 GeV/c. Time of flight counters will be placed to identify scattered particles with lower momenta. The spectrometer covers about 60% of solid angle for scattered D^{*-} and about 80% for decay pions from produced charmed baryons.

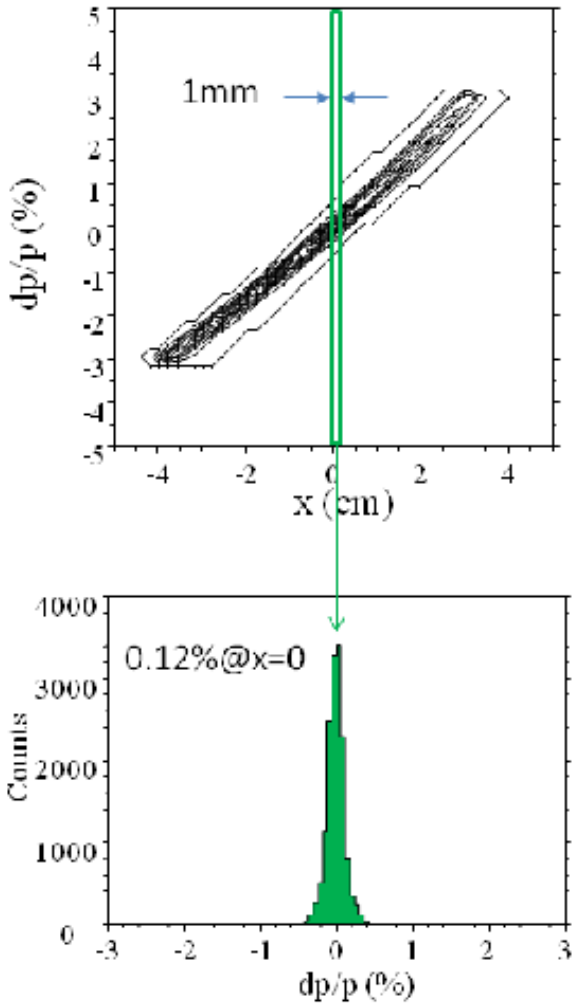

Figure 3: Left: correlation between beam momentum and position at the dispersive focal point. Right: momentum distribution within a 1-mm space in horizontal at the beam center.

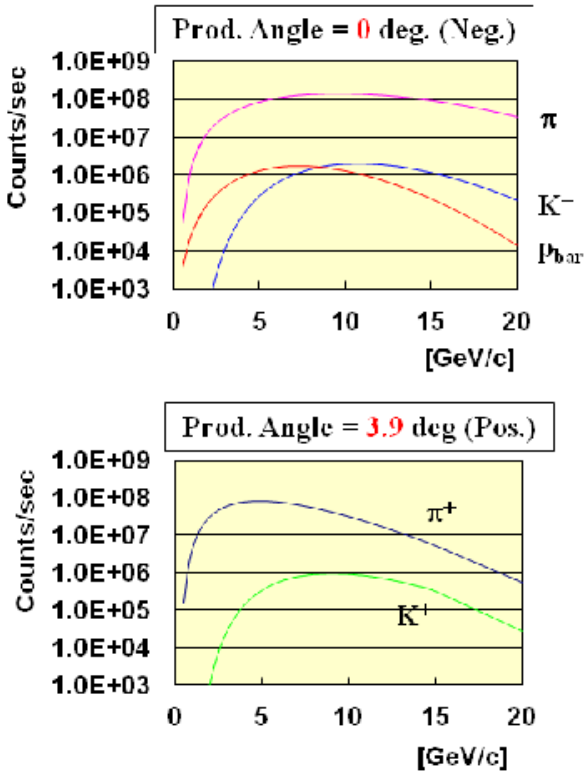

Figure 4: Intensities of secondary beams calculated by Sanform-Wang's formula [5]. See text for assumed conditions.

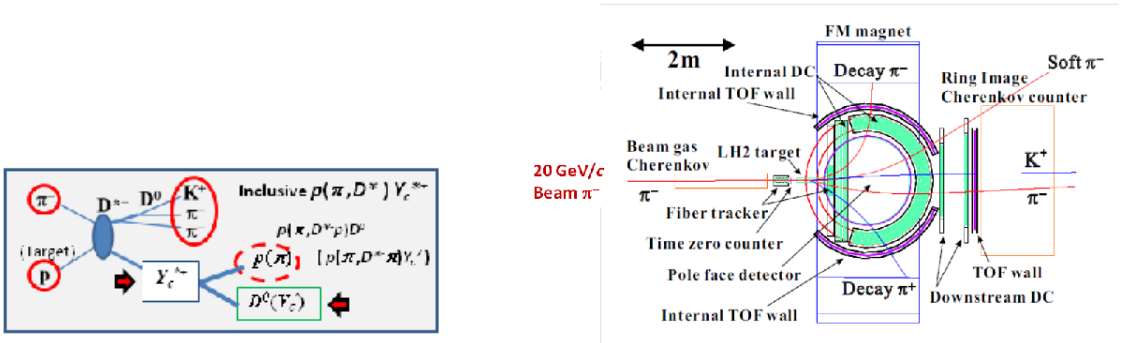

Figure 5: Top: reaction scheme to identify charmed baryons and their decays by means of a missing mass technique. Bottom:designed spectrometer layout

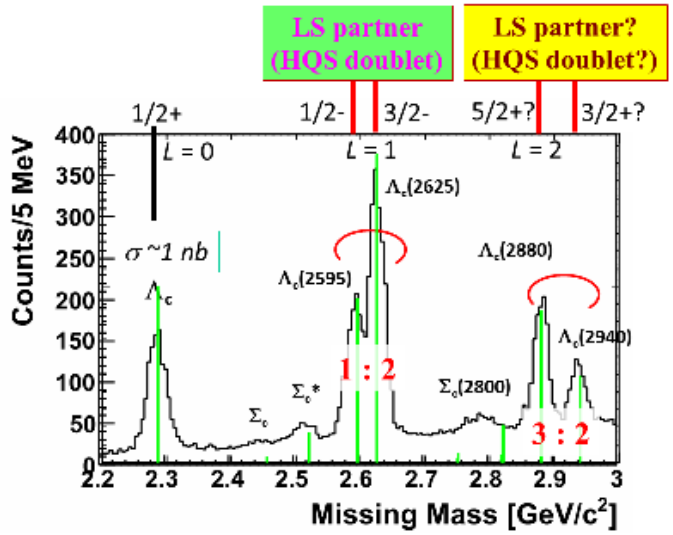

Figure 6: Expected missing mass spectrum in the (π^-, D^{*-}) reaction on hydrogen.

Identifying two charmed mesons from the decay final state, $K^+\pi^-\pi^-$, we could reduce huge background events of $K^+\pi^-\pi^-$ productions by a factor of $\sim 10^6$. Expected charmed baryon spectrum is demonstrated by a Monte Carlo simulation in Fig. 6. Here, the states reported by the Particle Data Group [6] are taken into account. One sees that a series of charmed baryons from the ground state to highly excited states with higher spins are clearly observed.

We found that the production cross sections of the excited states relative to that of the ground state do not go down. This is an important feature of the (π^-, D^{*-}) reaction. We estimated the production rates of the excited charmed baryons in the framework of a D^* exchange in the t-channel at a very forward scattering angle [7]. Employing harmonic oscillator wave functions of constituent quarks in the initial and final baryons, we estimate that the production rate, R, is expressed as

$$R \sim < \phi_f | \sqrt{2}\sigma_- \exp(i\mathbf{q_{eff}}\mathbf{r}) | \phi_i > \quad (1)$$

$$\sim (q_{eff}/A)^L \exp(-q_{eff}^2/2A^2), \quad (2)$$

where ϕ_i and ϕ_f represent initial and final states of baryons. An effective momentum transfer q_{eff}, taking a recoil effect of the residual ud diquark, is as large as 1.4 GeV/c in the $p(\pi^-, D^{*-})$ reaction at the pion beam momentum of 20 GeV/c. An oscillator parameter A is taken to be $\sim$0.4 GeV, which corresponds to the inverse of a typical baryon size. In this reaction, a u quark in a proton is converted to a c quark in the final charmed baryon in the reaction. The ud diquark behaves as a spectator. Thus, this reaction well populates λ-mode excited states, where an angular momentum L is introduced between a c quark and a diquark. Due to a large factor of (q_{eff}/A), an absolute value of the production cross section is reduced very much. On the other hand, the ratio of R for an excited state with L to that for the ground state ($L = 0$) is $\sim (q_{eff}/A)^L$, which does not go down even for $L > 0$. The (π^-, D^{*-}) reaction is suitable to populate higher spin states.

The λ-mode Λ_c baryons with $L > 0$ has two spin states coupled to $L \pm 1/2$. These states are LS partners. Therefore, we find that the production ratio of the two states should be L:L+1. Reversely, we can determine the spin-parity of the λ-mode Λ_c baryons by measuring the cross sections.

So far, a production cross section of Λ_c in the p(π^-, D^{*-}) reaction has not been measured. Only upper limit, 7 nb, was reported in 1985 [8]. We estimate the production cross section to be a few nano barn at incident pion momentum of 20 GeV/c [9] by employing a framework of reggeon exchange model, which describes binary peripheral reactions well at high energy. We expect to observe 1000 events of the ground state Λ_c production for 100 days.

Decay branching ratios carry information on internal structure of a baryon. The ratio of decay into a heavy meson and a light baryon to that into a light meson and a heavy baryon is of particular interesting. The former is expected to be dominant, if it is energetically allowed, in λ-mode excited baryon, which is an orbital excitation between a heavy quark and a light diquark. The situation is to be opposite in ρ-mode. One can find a suggestion in the case of $\Lambda(1520)$, which is a P-wave hyperon with spin-parity of $3/2^-$. In $\Lambda(1520)$ dominantly decays into a kaon and a nucleon, while a Q-value in the decay is smaller than that in the decay into a pion and a Σ hyperon. The $\Lambda(1520)$ hyperon can be classified as a λ-mode hyperon although ρ/λ mode classification has yet to be established in any baryon excited states. Systematic measurements of decay branching ratios for the excited charmed baryons are of particular importance.

4. **Baryon Spectroscopy with Different Flavors**

The above-mentioned discussion on internal structure of baryons with a single heavy quark can be extended to baryons with double heavy quarks. In the case of double heavy-quark baryons, the order of the excitation energy for λ and ρ modes interchanges. Here, the λ mode is a motion of the light quark to the heavy-quark pair, and the ρ mode is a relative motion between two heavy quarks. One expects that a λ mode excited state favors a decay into a light meson and a double heavy-quark baryon. A ρ mode state may dominantly decay into a single-heavy meson and a single-heavy baryon.

A several states of cascade hyperons Ξ are listed [6]. Little is known about their spin-parities and decay branching ratios. The $(\bar{K}, K^+)$ reaction is one of promising reactions to produce cascade hyperons. Since the $(\bar{K}, K^+)$ reaction has no single-meson exchange process in t channel, Ξ productions at backward angles are expected to play a principal role. ρ-mode Ξ hyperons may be populated well through u-channel process. It is quite worthy to measure production rates and decay branching ratios of Ξ hyperons.

5. **Concluding Remark**

- Masses, decay branching ratios, and production rates of baryons with heavy flavors provide information on internal motions of ingredients, such as diquark correlation.
- We proposed an experiment on charmed baryon spectroscopy via the (π^-, D^{*-}) reaction at the J-PARC high-momentum beam line. We will measure a mass spectrum of charmed baryons from the ground state to highly excited states in an excitation energy

range of more than 1 GeV by means of a missing mass technique. Production cross sections and decay branching ratios of produced charmed baryons will be measured.

- The present argument on baryon spectroscopy with a charm quark should be extended to those with different flavors. In particular, Ξ baryons are of interest as double-heavy quark system that can be accessible in experiment. Neutral kaon beam at Jlab is unique in hadron spectroscopy and plays a complimentary role to the J-PARC. Constructive collaboration to integrate efforts to realize hadron spectroscopy with hadron beams in JLab and J-PARC is desired.

References

[1] T. Yoshida, E. Hiyama, A. Hosaka, M. Oka, and K. Sadato, Phys. Rev. D **92**, 114029 (2015).

[2] H. Noumi $et\ al.$, "Charmed Baryon Spectroscopy via the (π^-, D^{*-}) reaction", J-PARC P50 Proposal, 2012:
`http://www.j-parc.jp/researcher/Hadron/en/Proposal_e.html#1301` .

[3] S. Yokkaichi $et\ al.$, "Electron pair spectrometer at the J-PARC 50-GeV PS to explore the chiral symmetry in QCD", J-PARC E16 Proposal, 2006:
`http://www.j-parc.jp/researcher/Hadron/en/Proposal_e.html\#0606` .

[4] Urs Rohrer, Compendium of Transport Enhancements,
http://aea.web.psi.ch/Urs_Rohrer/MyWeb/trancomp.htm .

[5] J. R. Sanford and C. L. Wang, BNL 11279 and BNL 11479, (1967); C. L. Wang, Phys. Rev. Lett. **25**, 1068 (1970).

[6] K. A. Olive *et al.* (Particle Data Group), Chin. Phys. C **38**, 090001 (2014).

[7] S. H. Kim, A. Hosaka, H. C. Kim, H. Noumi, and K. Shirotori, Prog. Theor. Exp. Phys. **103D01** (2014).

[8] J. H. Christensen, $et\ al.$, Phys. Rev. Lett. **55**, 154 (1985).

[9] S. H. Kim, A. Hosaka, H. C. Kim, and H. Noumi, Phys. Rev. D **92**, 094021 (2015).

2.12 $K^0\Lambda$ Photoproduction on the Neutron at $E_\gamma < 1.2$ GeV

Yusuke Tsuchikawa (for FOREST Collaboration)
Department of Physics
Nagoya University
Nagoya 464-8602, Japan

Abstract

Photoproduction of K^0 and Λ has been studied at the Research Center for Electron Photon Science (ELPH), Sendai, Japan. The $\gamma d \to K^0\Lambda p$ events are detected with the electromagnetic calorimeter FOREST near the threshold region. We present the first measurement of $K^0\Lambda$ photoproduction cross sections on the neutron.

1. Introduction

The simultaneous K^0 and Λ photoproduction is a good probe to study highly excited baryons which hardly couple to the well known channels (*e.g.,* πN and ηN). The $\gamma n \to K^0\Lambda$ reaction is expected to be sensitive to not only nucleon but also hyperon resonances. Because there is no charged K exchange as the t-channel contribution in the Born terms, it is expected there are relatively large contributions from the s- and u-channels in the $K^0\Lambda$ photoproduction on the neutron in comparison to the $K^+\Lambda$ photoproduction on the proton.

In addition, the prominent structure at $W \sim 1.67$ GeV which is seen in the η photoproduction cross section on the neutron as a narrow peak structure [1, 2] is one of the special interests in this study. While many experiments observed the structure, the origin of the structure is still an open question. The $K^0\Lambda$ system is similar to the ηn system from the following points; having 1/2-isospin, produced by the γn initial state, having an $s\bar{s}$ component. From the viewpoint, photoproduction of $K^0\Lambda$ may be a good channel to reveal the origin of the prominent structure.

Cross sections of the $\gamma d \to K^0\Lambda p$ reaction was reported by Tsukada *et al.* [3]. The differential cross sections were measured for $\cos\theta_K^{Lab} = [0.9, 1.0]$ and $E_\gamma = [0.9, 1.1]$ GeV, where $\cos\theta_K^{Lab}$ stands for the K^0 emission angle in the laboratory frame and E_γ stands for the incident photon energy.

This contribution presents the first measurement of K^0 angular distribution for the $\gamma d \to K^0\Lambda p$ reaction in the center-of-mass frame by using a 4π calorimeter named FOREST which is introduced in the next section.

2. Experiment

Meson photoproduction experiments are carried out at ELPH, Sendai. The bremsstrahlung photon beam [4] is generated by inserting a 11 μm thick carbon fiber to the circulating electrons in the 1.2 GeV synchrotron [5]. Liquid hydrogen or deuterium target [6] is bombarded with the 0.5–1.2 GeV tagged photons. A four pi calorimeter FOREST [7] detects the emitted particles produced by the photo-induced reactions. FOREST consists of three calorimeters made of 192 pure CsI crystals, 252 lead/scintillating fiber modules, and 62 lead glasses. The energy resolutions of the calorimeters are 3% [8], 7% [9, 10], and 5% [11] for 1 GeV

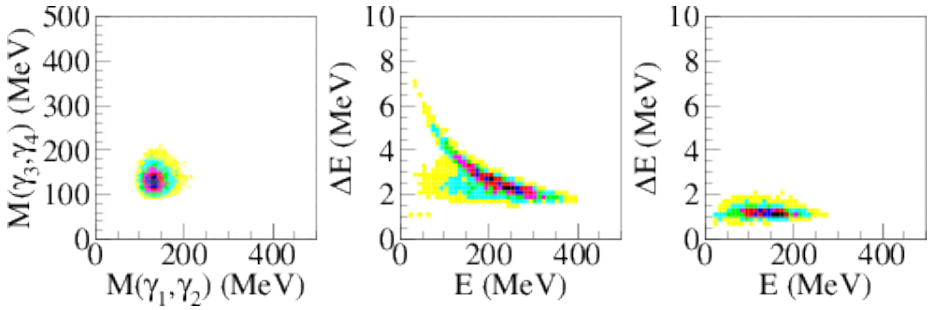

Figure 1: The $\gamma\gamma$ invariant masses (left), ΔE-E plots for proton (center) and charged pion (right).

photons, respectively. Three hodoscopes are situated in front of the calorimeters for charge identification. The hodoscopes are made of 72, 18, and 12 pieces of 5 mm thick plastic scintillators.

3. Analysis, Results, and Discussion

The $\gamma n \to K^0\Lambda$ reaction is identified by focussing on the reaction chains; $K^0 \to \pi^0\pi^0 \to \gamma\gamma\gamma\gamma$ and $\Lambda \to p\pi^-$. Event selection for the $K^0\Lambda$ photoproduction is performed by detecting all of the below particles by the calorimeters. Hence, four neutral and two charged particles are required to be detected as clusters in the calorimeters. Four neutral clusters within 2 ns in the FOREST detectors are required for four photons from K^0. Two charged particles detected at later timing from the four photons are required as p and π^-. The proton and charged pion are identified by using timing difference between the two charged particles. Measured energies, polar angles, and azimuthal angles of the six particles and incident photon energy are kinematically fitted to satisfy four constraints which is related the $\gamma n \to K^0\Lambda$ reaction kinematics with assuming the target neutron is at rest. Figure 1 shows $\gamma\gamma$ invariant masses of selected photons and ΔE-E plots of the selected proton and that of the charged pions.

It is clearly shown that the particle selection for four photons, proton, and charged pion works well. The four photon invariant mass distribution shows a clear peak structure around the K^0 rest mass (Fig. 2). The K^0 yield as a function of $\cos\theta_K^{CM}$ for different energy bins are estimated by fitting linear combination of the gaussian and background distribution to the measured distributions. The background shape is estimated by using GEANT4 with $\gamma n \to \pi^0\pi^0\pi^-p$ reaction. Figure 2 shows the simulated distributions well reproduce the measured background shapes for all energy bins.

Differential cross sections are derived from the estimated yields of K^0 signals. Figure 3 shows the differential cross sections as a function of $\cos\theta_K^{CM}$ for different incident photon energy E_γ where $\cos\theta_K^{CM}$ stands for the K^0 emission angle in the center-of-mass (CM) frame and E_γ stands for the incident photon energy.

The first measurement of angular distribution for the $K^0\Lambda$ photoproduction in the CM frame shows flat shapes near the reaction threshold but shows backward enhancement in the higher energy parts in this energy region. Comparisons with the theoretical curves given by the Kaon-MAID [12–14] and Saclay-Lyon A [15] models are performed. The measured shapes of the differential cross sections favor the latter one. It indicates that hyperon resonances

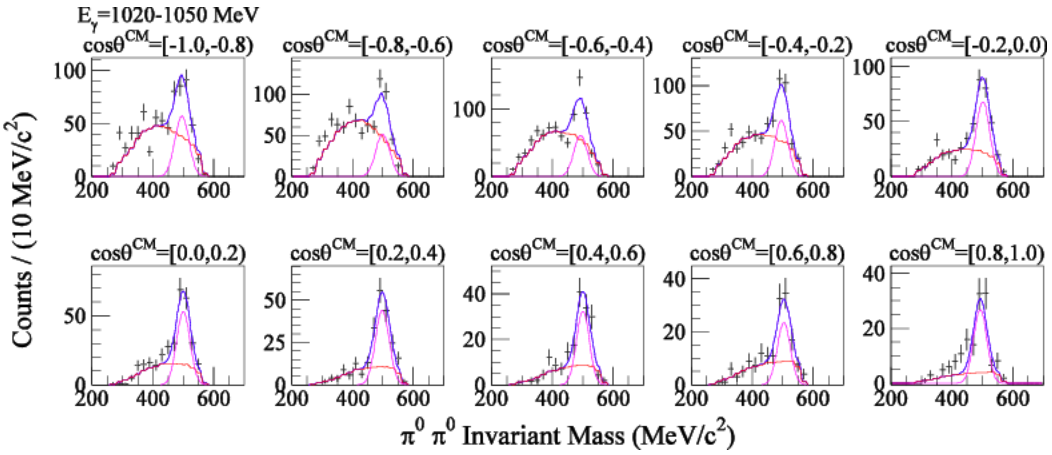

Figure 2: The four photon invariant mass distributions (black ponits) for different $\cos^{CM}_K$. The magenta line shows the fitted gaussian and red line shows simulated distribution. The blue line shows the combination of the above two functions.

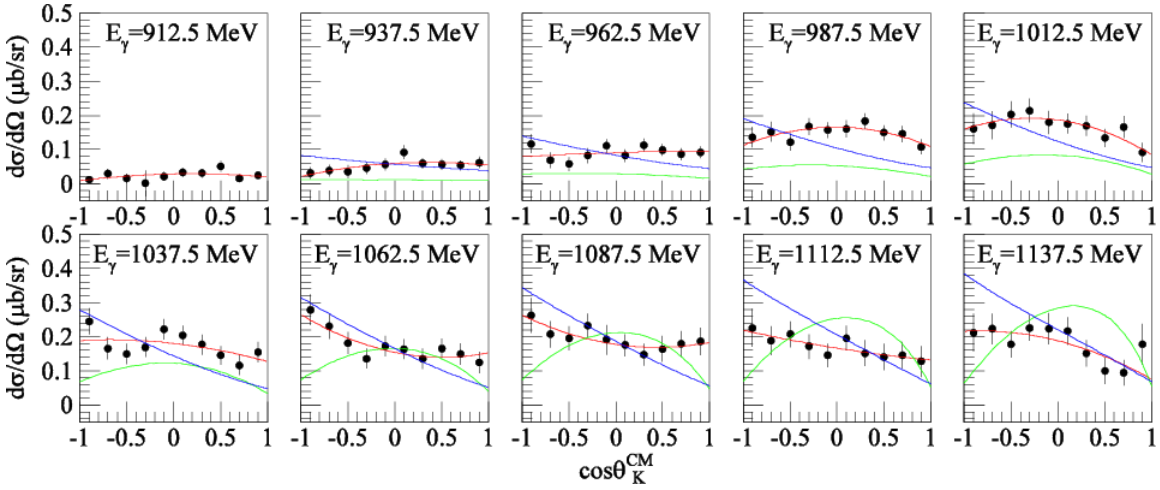

Figure 3: Differential cross sections of $\gamma n \rightarrow K^0\Lambda$ reaction as a function of K^0 emission angle in the CM frame $\cos\theta^{CM}_K$ for different incident photon energy E_γ (black points). The green (blue) line shows the theoretical curve given by Kaon-MAID [12–14] (Saclay-Lyon A [15]). The red line shows fitted Legendre polynomials.

play important roles in the K^0 Λ photoproduction since the difference between two models; the Kaon-MAID includes various nucleon resonances, while the Saclay-Lyon A includes various hyperon resonances.

4. **Summary**

The $K^0\Lambda$ photoproduction on the neutron is studied at ELPH with the 4π electromagnetic calorimeter FOREST via $K^0 \to \pi^0\pi^0 \to \gamma\gamma\gamma\gamma$ and $\Lambda \to p\pi^-$ decay modes. The K^0 signal is clearly observed in the four photon invariant mass distribution as a narrow peak. The first measurement of the differential cross section as a function of K^0 emission angle in the CM frame reveals the angular distribution of this reaction shows backward enhancement in higher energy region, while it shows flat distribution near the reaction threshold. By comparing the measured distributions with two theoretical curves given by Kaon-MAID and Saclay-Lyon A models, the measured distribution indicates that hyperon resonances play important roles in the $\gamma n \to K^0\Lambda$ reaction.

5. **Acknowledgments**

This work was supported in part by Grants-in-Aid for Scientific Research (B) (17340063), for Specially promoted Research (19002003), for Scientific Research (A) (24244022), and for Scientific Research (C) (26400287).

References

[1] T. Ishikawa *et al.*, PoS (Hadron2013), 95.

[2] D. Werthmuller *et al.*, Phys. Rev. C **90**, 015205 (2014).

[3] K. Tsukada *et al.*, Phys. Rev. C **78**, 014001 (2008).

[4] T. Ishikawa, Nucl. Instr. and Meth. A **622**, 1 (2010).

[5] F. Hinode, in: *Proceedings of 2005 Particle Accelerator Conference*, **41**, 2458 (2005).

[6] R. Hashimoto, Res. Rep. of LNS **41**, 31 (2008).

[7] T. Ishikawa *et al.*, Nucl. Instr. and Meth. A **832**, 108 (2016).

[8] T. Ishikawa *et al.*, Res. Rep. of LNS **40**, 6 (2007).

[9] H. Sugai, T. Ishikawa *et al.*, Res. Rep. of LNS **42&43**, 88 (2010).

[10] A. Nakamura, T. Ishikawa *et al.*, Res. Rep. of LNS **42&43**, 75 (2010).

[11] K. Mochizuki, T. Ishikawa *et al.*, Res. Rep. of LNS **40**, 15 (2007).

[12] T. Mart *et al.*, Phys. Rev. C **61**, 012201 (1999).

[13] T. Mart *et al.*, Phys. Rev. C **62**, 038201 (2000).

[14] F. X. Lee *et al.*, Nucl. Phys. A **695**, 237 (2001).

[15] T. Mizutani *et al.*, Phys. Rev. C **58**, 75 (1998).

2.13 Excited Hyperon Possibilities in Relativistic Heavy Ion Collisions

Rene Bellwied
Physics Department
University of Houston
617 SR1 Building
Houston, TX 77204, U.S.A.

Abstract

I will review the latest experimental measurements from RHIC and the LHC in the context of predictions by lattice QCD and statistical hadronization models with regard to ground state, resonance and exotic particle production in the strange quark sector. I will propose possible future measurements at YSTAR and the heavy ion experiments at RHIC and the LHC which might shed light on the question of hadronization in the non-perturbative regime and the production of, and interactions in, specic hadronic bound states.

1. Introduction

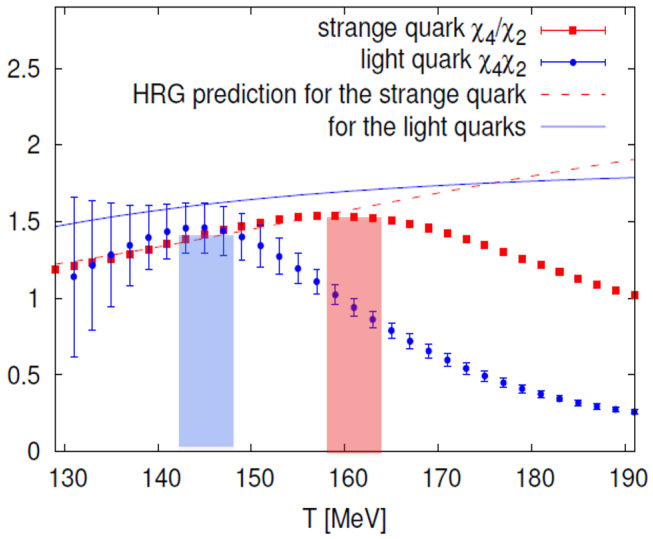

Figure 1: Continuum extrapolated lattice QCD results on the difference between light and strange quark susceptibility ratios, in this case χ_4/χ_2 [1].

Recent lattice QCD calculations in the QCD crossover transition region between a deconned phase of quark and gluons and a hadronic resonance gas have revealed a potentially interesting sub-structure related to the hadronization process. Studies of avor dependent susceptibilities, which can be equated to experimental measurements of conserved quantum number uctuations, seem to indicate a slight avor hierarchy in the three quark sector (u,d,s) in thermalized systems. Specically, the ratios of higher order susceptibilities in the strange sector show a higher transition temperature than in the light sector [1]. Both pseudo-critical temperatures are still within the error bars of the quoted transition temperature based on all

lattice QCD order parameters [2, 3] which is 154±9 MeV, but the difference of the specific susceptibilities is around 18 MeV and well outside their individual uncertainties, as shown in Fig. 1.

This difference might also be confirmed by statistical thermal model calculations that try to describe the yields of emitted hadrons from a QGP based on a common chemical freeze-out temperature. Although the yields measured by ALICE at the LHC in 2.76 TeV PbPb collisions can be described by a common temperature of 156±2 MeV, with a reasonable χ^2, the fit improves markedly if one allows the light quark baryons to have a lower temperature than the strange quark baryons, which is shown in Fig. 2 [4].

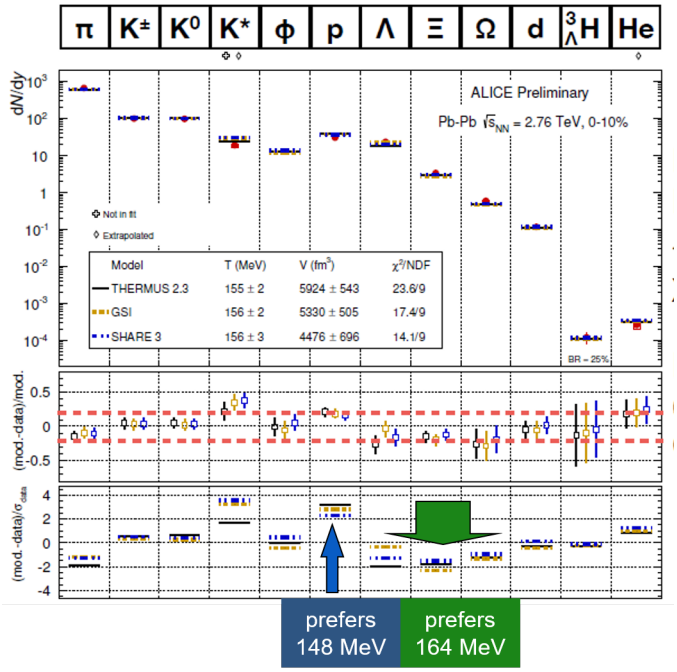

Figure 2: Statistical Hadronization Model fits to all measured particle yields in ALICE [4]. Although all three models converge on a common temperature, the main deviations seem to be flavor dependent.

A similar result has been found when the thermal fluctuations of particle yields as measured by STAR [5, 6], which can be related to the light quark dominated susceptibilities of the electric charge and the baryon number on the lattice, have been compared to statistical model calculations [7]. Fig. 3 shows that the deduced chemical freeze-out temperature is well below a common fit based on particle yields which takes into account all particle species, including strange particles.

2. **Possible Measurements in the Strange Sector**

If one assumes that strange and light quarks indeed prefer different freeze-out temperatures then the question arises how this could impact the hadronization mechanism and abundance

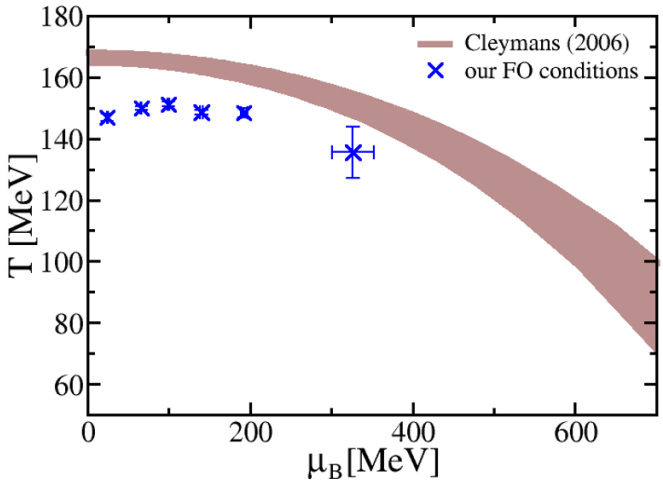

Figure 3: Chemical freeze-out temperature as a function of the baryo-chemical potential from a Hadron Resonance Gas model analysis of STAR net-proton and net-charge fluctuations, compared to a common freeze-out curve based on all measured particle yields [7].

of specific hadronic species. In other words, is the production of strange particles enhanced in a particular temperature range in the crossover region ?

This question is rather complex since most of the accessible species are quark mixtures of light and strange quarks, and the only pure strange baryon, the Ω, has a low cross section, even in relativistic heavy ion collisions. Furthermore besides the production of ground state baryons, one also has to account for the formation of resonant states and potentially even exotic strange multi-quark states and hypernuclei. Although hypernuclei are likely formed through coalescence at the very end of the evolution of the hadronic system, i.e., between chemical and kinetic freeze-out of the thermal hadronic system, studies comparing measured yields of molecular matter and anti-matter produced at the LHC with predictions from statistical hadronization models have shown that the actual yield of triton and helium states is well described with models assuming a chemical freeze-out near 156 MeV [8]. Although any state formed at these temperatures with a binding energy in the keV range will almost certainly dissolve, it seems its regeneration cross section is fixed by the chemical freeze-out from the deconfined state. This is likely due to the fact that the entropy to baryon ratio is frozen in at that time [9]. Therefore, with respect to determining a likely hypernucleus yield one can employ the SHM predictions as long as the assumed temperature is within the range determined by lattice QCD susceptibility calculations. Recent measurements performed at RHIC [10] and the LHC [11] reveal cross sections which are in agreement with thermal model predictions at a freeze-out temperature in between the two extremes of pure light and strange quark states, although the error bars are such that no strong conclusion can be drawn from these statistics limited measurements.

SHM predictions for exotic states, in particular the H-Dibaryon and the strange pentaquark, postulated early on based on measurements by NA49 at the CERN-SPS [12], have been compared to measurements in PbPb and pp collisions at the LHC, and no evidence for these

exotic states has been found, see Figs. 4 and 5 [13, 14] and Dr. Doenigus presentation at this workshop. At the same time Fig.5 shows that signals of hadronic resonant states, in this case the $\Xi(1530)$ are strong at LHC energies and can be well reconstructed through their hadronic decay channels.

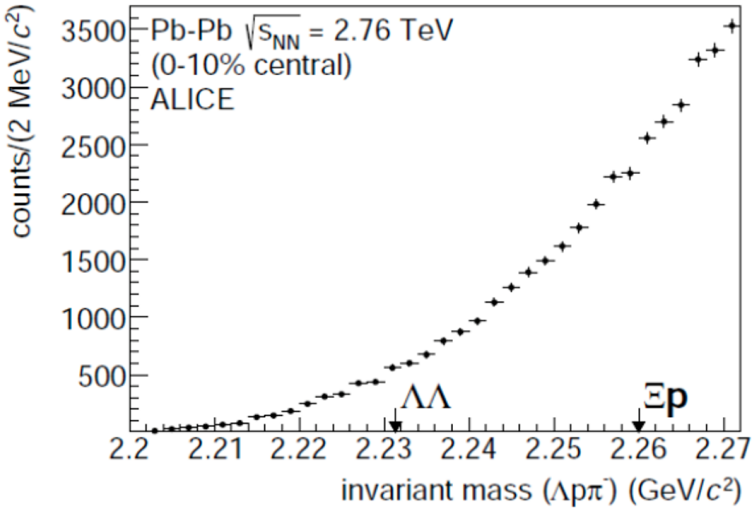

Figure 4: Results from searches for $\Lambda\Lambda$ and Ξp bound states in 2.76 TeV PbPb collisions in ALICE [13]. No evidence for Di-baryon states has been found at limits well below the thermal model predictions.

Since the evidence for exotic states in the strange sector is small and the hypernuclei seem to be not particularly enhanced, the emphasis of any future experimental program trying to understand hadron production should be shifting towards strange baryonic resonance production. Elementary collisions at RHIC and LHC energies might well provide the link between future measurements in the YSTAR experiment at JLab and the future analysis of strange resonance enhancements in heavy ion collisions at RHIC and the LHC. Both the $\Lambda(1405)$ and the $\Lambda(1520)$ have been determined in relativistic heavy ion experiments [15, 16], so has the $\Sigma(1385)$ [14]. Figs. 6 show the latest results in pPb collisions from ALICE for the Σ and Ξ resonant states.

3. **Input from Theoretical Calculations**

In addition to the experimental determination of potential enhancements of strange ground and resonant states, the topic can also be addressed by comparing lattice QCD calculations with model predictions based on a non-interacting hadronic resonance gas (HRG). I will here only briefly describe the basics, since the contribution by Prof. Ratti to these proceedings gives much more detail. The HRG model has shown to be very effective in describing the hadronic phase of lattice QCD thermodynamics very well up to the pseudo-critical temperature. The early model by Hagedorn, which effectively describes interactions of hadrons by simply increasing the number of possible resonant states exponentially as a function of temperature, captures the behavior of the hadronic gas very well as long as the temperature

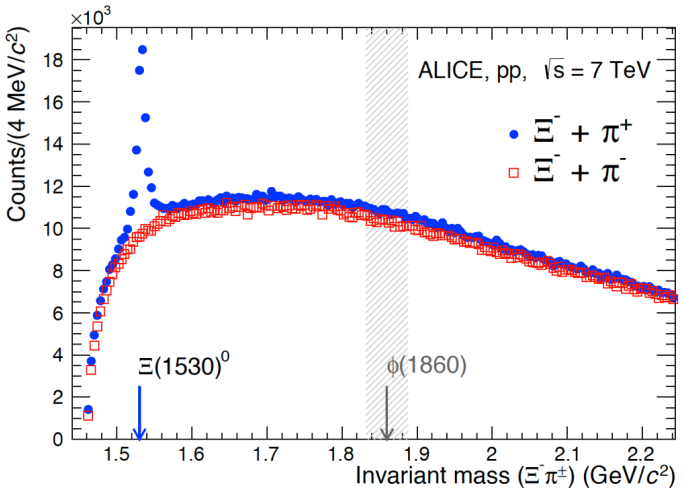

Figure 5: Results from searches for the $\Xi(1530)$ resonance and the $\phi(1860)$ pentaquark in 7 TeV pp collisions in ALICE [13]. No evidence for the strange pentaquark state has been found at limits well below the thermal model predictions.

is low enough [17]. In case of a flavor hierarchy in the transition region one would expect the number of strange resonances to higher temperature, than the number of light quark resonances. Such an approach has been proposed in the recent past [18], based on predictions which highlight the difference between strange resonances in the PDG 2008 listings [19] and the simplest non-relativistic Quark Model [20]. Indeed adding states to the PDG listing seemed to initially improve the agreement between HRG and lattice QCD below the transition temperature. More detailed studies have followed, which are presented in Prof. Ratti's ntribution. An interesting conclusion that arises out of these studies is that the improvement in the listing of strange resonances between PDG-2008 [19] and PDG-2014 [21] definitely brought the HRG calculations closer to the lattice QCD data. By looking at details in the remaining discrepancy it seems that the effect is more carried by singly strange resonances rather than multi-strange resonances. This is good news for the experiments since the Λ and Σ resonances below 2 GeV/c^2 are will within reach of both the JLab and the RHIC/LHC experiments.

4. Conclusion

It is my opinion that comparisons between quark model predictions and lattice QCD, in addition to future measurements in the strange baryonic resonance sector, will shed light on a multitude of interesting questions:

- Which quark model gives the best description of the experimental situation in a hadron gas near the QCD crossover? It seems the simple non-relativistic quark model considerably over-estimates the number of possible states, but models based on di-quark structures [22] or enhanced quark interactions in the baryon (hypercentral models [23]) give a better description of the thermal hadronic system calculated by lattice QCD.

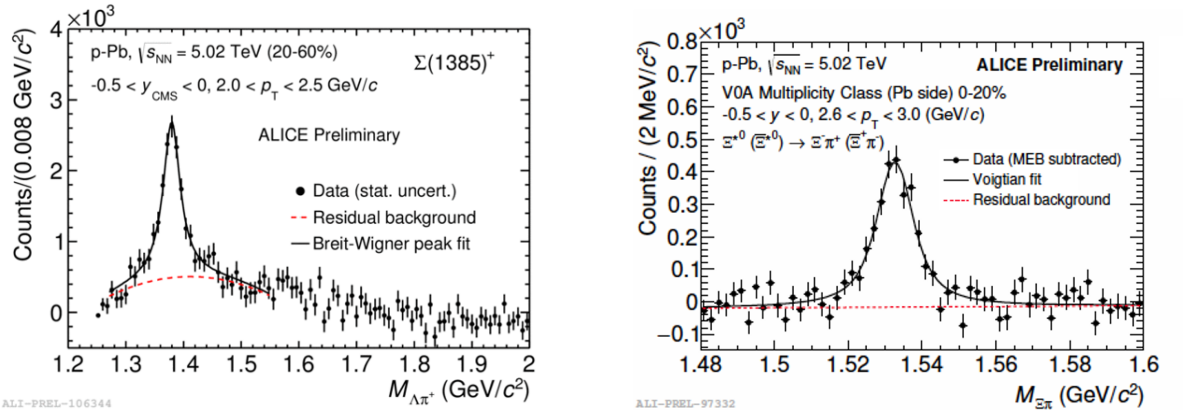

Figure 6: Preliminary results for $\Sigma(1385)$and $\Xi(1530)$ resonant states in 5.02 TeV pPb collisions in ALICE.

- Can one go as far as using model comparisons to postulate evidence or lack of evidence for di-quark structures? Can one specify the necessary interactions between quarks in the baryons?
- Do we understand the hadronization mechanism of light-strange quark baryons by focusing on potential yield enhancements of specific resonant states?
- Can we determine exotic state probabilities in the strange sector from measuring new strange resonances?
- Can we determine a flavor hierarchy in the QCD transition based on specific strange resonance yields?

There has been up to now relatively little interest in expanding the list of hyperon resonances in heavy ion erence in yield between pp and heavy ion reactions has been primarily used to determine the lifetime of the hadronic phase between chemical and kinetic freeze-out rather than determining potential enhancement patterns in specic channels. But the advent of the detailed lattice QCD studies, as well as the interest in an expanding YSTAR program at JLab in order to better understand the hadronization mechanism in the non-perturbative regime, denitely generates a bridge towards more detailed measurements of resonance production out of the deconned phase at RHIC and LHC. Together with the YSTAR program these measurements might well solve the mystery of hadron formation and the interactions of the contributing quarks and gluons.

References

[1] R. Bellwied, S. Borsanyi, Z. Fodor, S. D. Katz, and C. Ratti, Phys. Rev. Lett. **111**, 202302 (2013).

[2] S. Borsanyi *et al.* [Wuppertal-Budapest Collaboration], JHEP **1009**, 073 (2010).

[3] A. Bazavov *et al.* [HotQCD Collaboration], Phys. Rev. D **90**, 094503 (2014).

[4] M. Floris, Nucl. Phys. A **931**, 103 (2014).

[5] L. Adamczyk *et al.* [STAR Collaboration], Phys. Rev. Lett. **112**, 032302 (2014).

[6] L. Adamczyk *et al.* [STAR Collaboration], Phys. Rev. Lett. **113**, 092301 (2014).

[7] P. Alba, W. Alberico, R. Bellwied, M. Bluhm, V. Mantovani Sarti, M. Nahrgang, and C. Ratti, Phys. Lett. B **738**, 305 (2014).

[8] A. Andronic, P. Braun-Munzinger, J. Stachel, and H. Stocker, Phys. Lett. B **697**, 203 (2011).

[9] P. J. Siemens and J. I. Kapusta, Phys. Rev. Lett. **43**, 1486 (1979).

[10] B. I. Abelev *et al.* [STAR Collaboration], Science **328**, 58 (2010).

[11] J. Adam *et al.* [ALICE Collaboration], Phys. Lett. B **754**, 360 (2016).

[12] C. Alt *et al.* [NA49 Collaboration], Phys. Rev. Lett. **92**, 042003 (2004).

[13] J. Adam *et al.* [ALICE Collaboration], Phys. Lett. B **752**, 267 (2016).

[14] B. B. Abelev *et al.* [ALICE Collaboration], Eur. Phys. J. C **75**, 1 (2015).

[15] G. Agakishiev *et al.* [HADES Collaboration], Phys. Rev. C **87**, 025201 (2013).

[16] C. Markert [STAR Collaboration], J. Phys. G **28**, 1753 (2002).

[17] R. Hagedorn, Prog. Sci. Culture **1**, 395 (1976).

[18] A. Bazavov *et al.*, Phys. Rev. Lett. **113**, 072001 (2014).

[19] C. Amsler *et al.* [Particle Data Group], Phys. Lett. B **667**, 1 (2008).

[20] S. Capstick and N. Isgur, Phys. Rev. D **34**, 2809 (1986); [AIP Conf. Proc. **132**, 267 (1985)].

[21] K. A. Olive *et al.* [Particle Data Group], Chin. Phys. C **38**, 090001 (2014).

[22] E. Santopinto and J. Ferretti, Phys. Rev. C **92**, 025202 (2015).

[23] M. M. Giannini and E. Santopinto, Chin. J. Phys. **53**, 020301 (2015).

2.14 Light Flavour Hadron Production at the LHC: Equilibrium Thermodynamics at Work

Benjamin Dönigus
Institut für Kernphysik
Goethe-Universität Frankfurt
D-60438 Frankfurt am Main, Germany

Abstract

The measurement of the production of light flavoured hadrons in high-energy collisions can be used to determine the chemical freeze-out temperature by assuming a (statistical) thermal model. In particular, we focus here on the production of (multi-)strange hadrons, resonances, (hyper-)nuclei and the search for strange exotica with ALICE at the LHC in view of the equilibrium thermal model. Recent measurements of (multi-)strange hadrons and resonances performed in high-multiplicity proton-proton (pp) and proton-lead (p-Pb) collisions have shown features that are similar to those observed in lead-lead (Pb-Pb) collisions. The values of particle ratios of strange to non-strange hadrons in high-multiplicity pp and p–Pb collisions approach the ones in Pb–Pb. A similar trend is observed for light nuclei, namely the deuteron-to-proton ratio is rising in pp and p–Pb and reaches the thermal model expectation for Pb–Pb multiplicities. In addition, the thermal model can be used to predict particle yields of possible states and thus can be used to test the existence of these particles. This is shown exemplarily for a search for two exotic dibaryons whose upper limits on the production yields are significantly below the thermal model expectations whereas the known states are quite well described within an equilibrium thermal model approach.

1. Introduction

Ultra-relativistic heavy-ion collisions at the LHC offer a unique way to study QCD matter at very high temperatures. Lattice QCD calculations [1, 2] suggest that a transition from confined hadrons to a state of deconfined matter, the so-called quark-gluon plasma, is happening at temperatures above $T_c = (154 \pm 9)$ MeV and/or energy densities above $\epsilon_c = 0.34 \pm 0.16$ GeV/fm^3. These are clearly reached in these collisions as one can deduce for instance from the measurement of direct photon transverse momentum spectra. These lead to effective temperatures of $T_{eff} = (297 \pm 12(stat) \pm 41(syst))$ MeV averaged over the collision, extracted through the slope of the spectra [3]. Comparisons to models lead to initial temperatures of up to 740 MeV [4].

The evolution of the collisions themselves are imagined usually as a sequence of the following stages: two Lorentz contracted nuclei approach each other, they collide, and after a short time (less than 1 fm/c) a quark-gluon plasma is formed which eventually expands, cools down and hadronises. Finally the hadrons rescatter and freeze out. The temperature where the hadrons stop being produced is called chemical freeze-out temperature T_{ch} and the temperature when the hadrons stop scattering is denoted as kinetic freeze-out temperature T_{fo}.

If one uses an analogy between a light source and a particle source one can extract also a temperature from the measured multiplicities of the different particle species. This is

possible using an approach based on a grand canonical ensemble with the main ingredients: (chemical freeze-out) temperature T_{ch}, volume V and baryo-chemical potential μ_B. The latter is basically zero at the LHC, namely baryons and anti-baryons are produced with equal amounts [5]. This approach is called (statistical) thermal model and the measurement of the production yield of different particle species, such as π, K, p, etc. can be used to extract a temperature of about 156 MeV at the LHC [6]. If this is done for the different available energies at different laboratories one sees that there is an increase up to energies reached at the SPS at CERN and then the temperature stays constant. This is another hint that the quark-gluon plasma is formed around a temperature of 159 MeV, which is the average of the extracted temperatures in the aforementioned plateau (T_{lim}). This leads to the assumption $T_{lim} \approx T_{ch} \approx T_c$ [7].

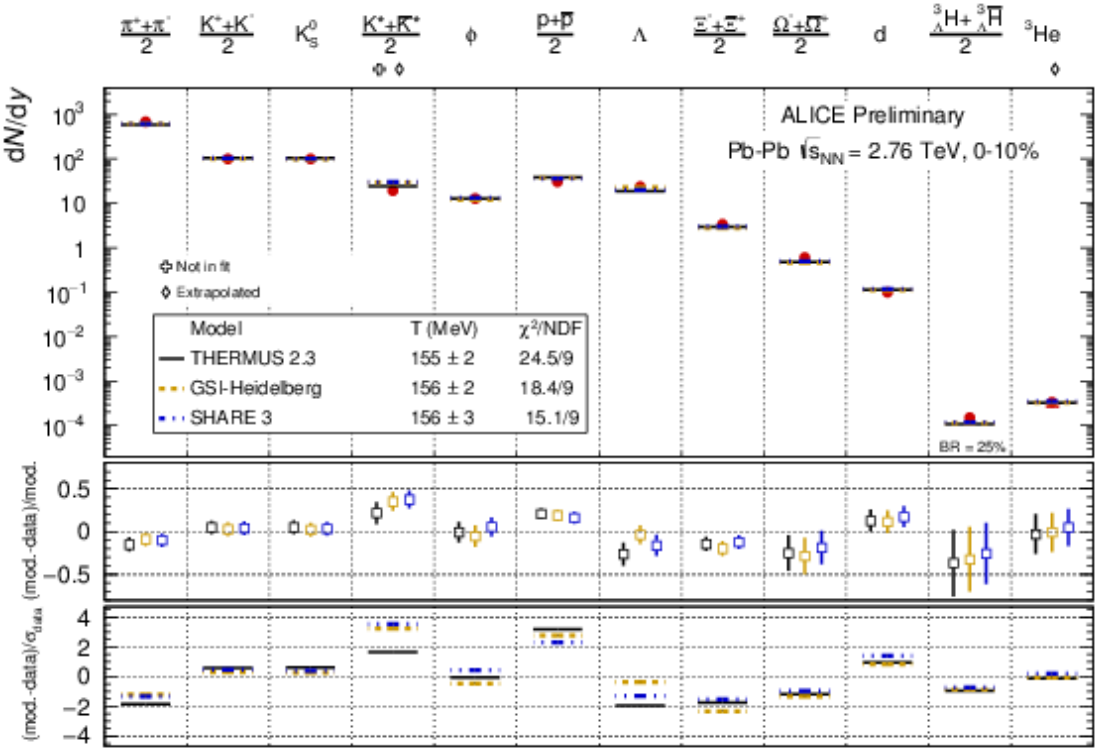

Figure 1: Comparison of three thermal model implementations, used to fit light flavoured hadron production yields measured in Pb–Pb collisions at $\sqrt{s_{\rm NN}} = 2.76$ TeV with the ALICE detector. The models THERMUS [8], GSI-Heidelberg [7] and SHARE [9] agree well, as visible in the lower two panels showing the difference between model and data once as ratio to the model and once as ratio to the experimental uncertaint. All model fits lead to a temperature of about $T_{ch} = 156$ MeV.

An example thermal model fit using production yield measurements of the ALICE Collaboration is shown in Fig. 1. The fit compares three different implementations of thermal models (THERMUS [8], GSI-Heidelberg [7] and SHARE [9]). The three different thermal model implementations agree well and result in a temperature of about $T_{ch} = 156$ MeV. The ther-

mal model can also be used to predict the production of particles as for instance described in [10].

2. **Strangeness**

Recently, pp and p–Pb collisions have received large attention from the heavy-ion community. Normally, these are only seen as baseline measurements compared to the quark-gluon plasma formed in Pb–Pb collisions, for instance quantified in the nuclear modification factor R_{AA}. Nowadays, studies have been carried out to compare these small systems more directly to heavy-ion collisions. To achieve this, measurements of the production yields of different particle species have been performed as a function of the charged particle multiplicity $\mathrm{d}N_{\mathrm{ch}}/\mathrm{d}\eta$.

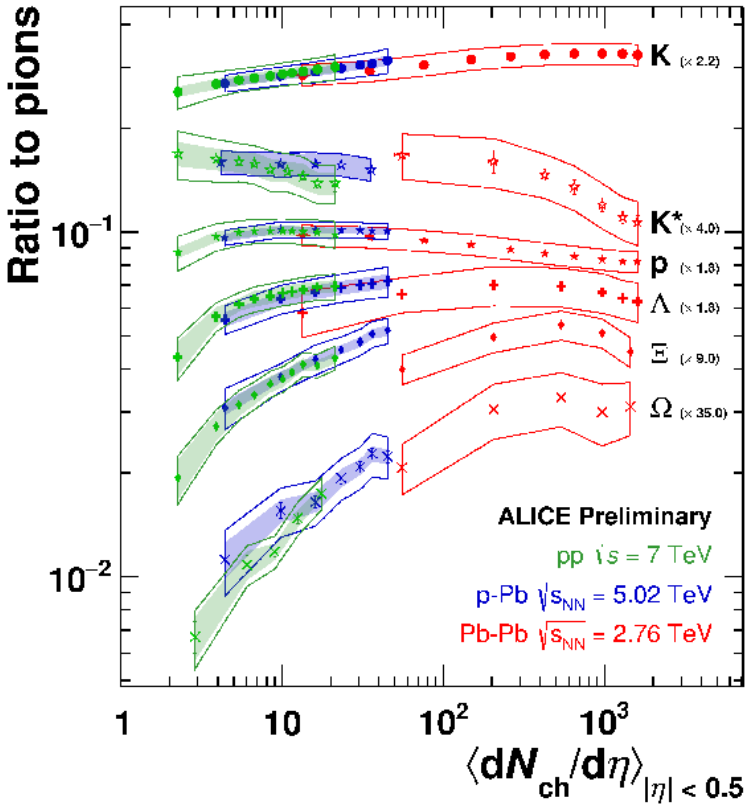

Figure 2: Ratios of the production yield to the yield of pions for K^-, $\mathrm{K}(892)^*$, p, Λ, Ξ^- and Ω^- as a function of the mean charged particle multiplicity $\langle \mathrm{d}N_{\mathrm{ch}}/\mathrm{d}\eta \rangle$ measured at mid-rapidity ($|\eta| < 0.5$).

The ratios of the production yield of K^-, $\mathrm{K}(892)^*$, p, Λ, Ξ^- and Ω^- compared to the yield of pions as a function of the mean charged particle multiplicity $\langle \mathrm{d}N_{\mathrm{ch}}/\mathrm{d}\eta \rangle$ measured at mid-rapidity ($|\eta| < 0.5$) are displayed in Fig. 2. One can see that the K/π and the p/π ratios are basically flat for all collision systems, wheras the $\mathrm{K}(892)^*/\pi$ ratio is nearly constant in pp and p–Pb collisions but starts to drop for increasing multiplicities in Pb–Pb collisions.

The hyperon-to-pion ratios, namely Λ/π, Ξ/π and Ω/π show a clear rise already at low multiplicities and seem to reach a saturation for Pb-Pb multiplicities, where the thermal model expectation value is reached. More details on the measurement can be found in [11, 12].

Before its observation, many signatures of the quark-gluon plasma have been proposed. One of the earliest ones was the possible enhancement of strangeness in ultra-relativistic heavy-ion collisions, relative to the production in elementary collisions [13, 14]. This was observed at the SPS [15] but is nowadays often interpreted in an opposite direction, as a lifting of the suppression when moving from elementary collisions such as pp to Pb–Pb for instance [16, 17]. This can be understood also as the necessity to treat strangeness canonically and not as introduced before in a grand canonical ensemble [18, 19].

3. Resonances

Resonances are of particular interest in the study of heavy-ion collisions, mainly because their lifetimes are typically shorter than the lifetime of the fireball, i.e., 10 fm/c. Therefore, resonances can decay inside the fireball and can either be lost or regenerated. As such, resonances can be used as probes for the lifetime of the hadronic phase, because of their different lifetimes. The suppression of K(892)* only visible in Pb–Pb collisions relative to pions as shown in Fig. 2 is clearly supporting this fact. The lifetime of the K(892)* is 4.2 fm/c and it is clearly stronger suppressed with increasing multiplicity of the collision. In contrary, the $\phi(1020)$ has a lifetime of 45 fm/c and seems to be unsuppressed [20, 21]. The suppression effect can be semi-quantitatively described by EPOS [22, 23] with an UrQMD [24, 25] afterburner for the hadronic phase [26].

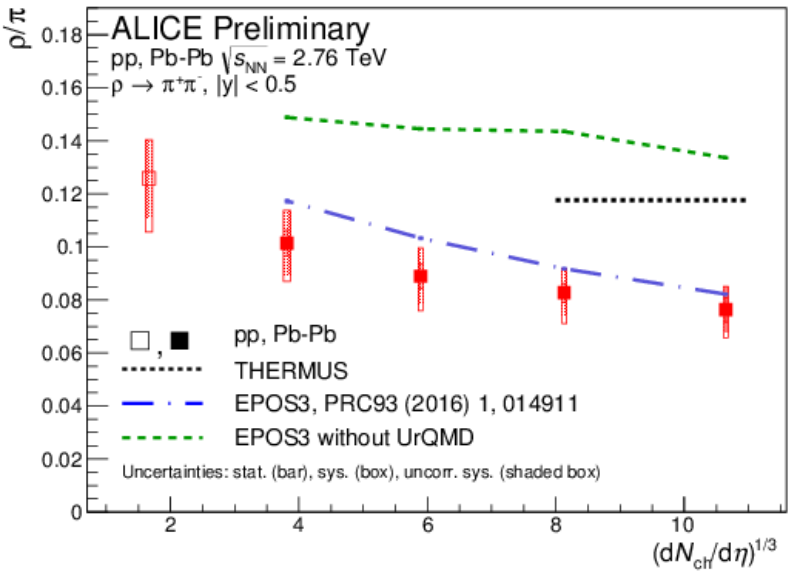

Figure 3: ρ/π ratio as a function of the scaled charged particle multiplicity ($\langle \mathrm{d}N_{\mathrm{ch}}/\mathrm{d}\eta \rangle^{1/3}$), measured in $|y| < 0.5$ in pp and Pb–Pb collisions. In addition, a thermal model prediction and two EPOS predictions are depicted. From Ref. [27].

Recently, the ALICE Collaboration has released new data including also the study of the $\rho(770)$ [27], with a lifetime of only 1.3 fm/c. Also this shows a clear suppression with increasing multiplicity as visible from Fig. 3. The figure shows in addition the comparison to a thermal model expectation and the trend expected from EPOS for two cases, once with and once without a UrQMD afterburner to simulate the hadronic phase. The trend of the data matches the case of EPOS with the afterburner.

Clearly, more data and especially the study of more resonances is needed to get a complete picture here.

4. **(Hyper-)Nuclei**

Another set of interesting results comes from the measurement of light (anti-)(hyper-)nuclei, which seem to contradict the observations discussed before. When one looks at the deuteron-to-proton ratio as a function of the charged particle multiplicity as visualised in Fig. 4 a similar trend is observed as for the hyperon-to-pion ratios discussed before, namely an increase in the small systems with increasing multiplicity which stops when the thermal model expectation is reached for the Pb–Pb values [28].

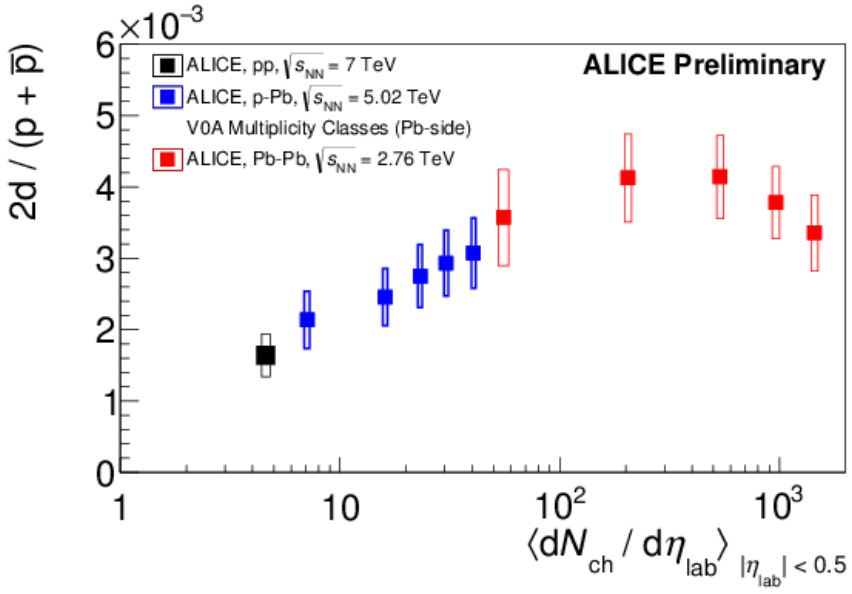

Figure 4: Deuteron-over-proton ratio as a function of the charged particle multiplicity for pp, p–Pb and Pb–Pb. Taken from Ref. [29].

The aforementioned contradiction comes from the comparison with the resonance results discussed before, where the existence of a hadronic phase is observed from the suppressed production yields of short lived resonances due to rescattering. A similar rescattering should also occur for light nuclei, especially because the nuclei are expected to be produced at the temperature of 156 MeV (as all other particles) which is 2-3 orders of magnitude above the binding energies of the nucleons in the (hyper-)nuclei. The most extreme example is the hypertriton, which has a separation energy of the Λ of only 130 keV but its production is very well described by the equilibrium thermal model [30].

5. Exotica

Since also the production of light (anti-)(hyper-)nuclei is well described by the thermal model it is expected that it can be used to make predictions for unobserved exotic states, as for instance strange baryons as ΛΛ and Λn bound states. A search was performed and is reported in [31]. The estimated upper limits of these states are well below the expectation of the thermal model, clearly depending on the lifetime and the branching ratio of these states. If reasonable values are picked for the lifetimes and the branching ratios of these states the upper limits are about 25 times below the thermal model expectation as shown in Fig. 5.

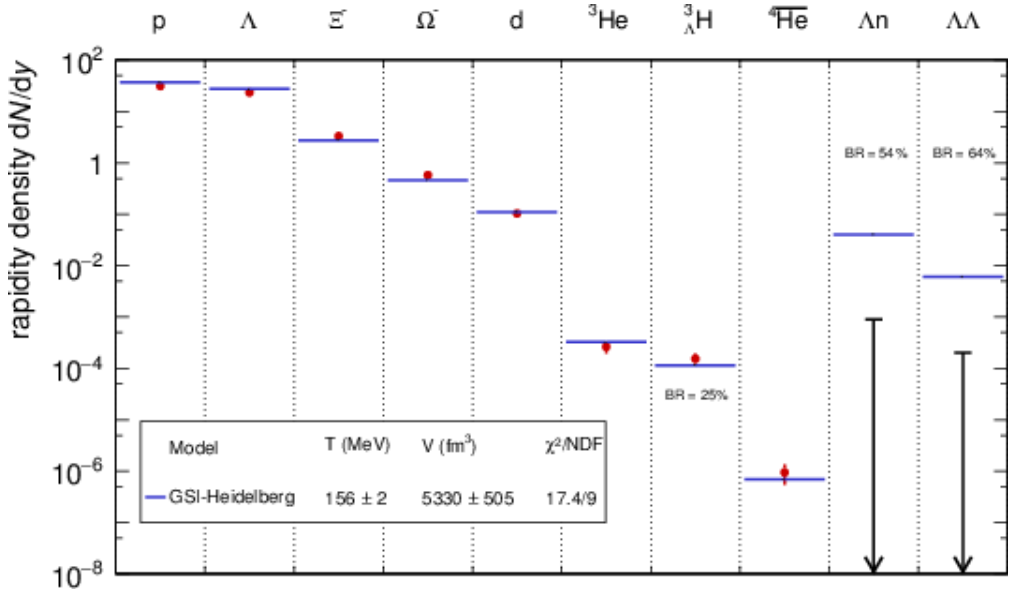

Figure 5: Comparison of data to thermal-model predictions. The production yields measured with ALICE are shown as red dots and the results of the calculations are shown as blue lines. The upper limits at 99% CL determined by ALICE are indicated as black arrows. Figure taken from Ref. [32].

6. Conclusion

Interesting physics has been observed in the strangeness sector in all collision systems at the LHC. The trend seen for the hyperon-to-pion ratio matching pp, p–Pb and Pb–Pb collisions can be understood as a lifting of the strangeness suppression in elementary collisions. Short lived resonances show a clear suppression with increasing multiplicity, which is due to the rescattering in the hadronic phase. Here new resonances could clearly help to map the lifetime of the hadronic phase further down. A copious production of loosely bound objects is measured by ALICE as predicted by the thermal model. This is creating a riddle, because the clearly observed hadronic phase and the rescattering for resonances is contradicting the measured yields of light (hyper-)nuclei which should also be destroyed and thus reduced in the hadronic phase. The estimated upper limits for the searched exotica are 25 times below the thermal model expectation which makes their existence questionable. More data and more studies are needed in order to establish a scenario which seamlessly describes

all observations. Therefore, the observation of new hyperon resonances can clearly help to complete the picture.

7. **Acknowledgments**

The author gratefully acknowledges the support from the German Bundesministerium fur Bildung, Wissenschaft, Forschung und Technologie (BMBF) though the project grant 05P2015 - ALICE at High Rate (BMBF-FSP202).

References

[1] A. Bazavov *et al.* (hotQCD Collaboration), Phys. Rev. D **90**, 094503 (2014).

[2] S. Borsanyi *et al.* (Budapest-Wuppertal group), JHEP **09**, 073 (2010).

[3] J. Adam *et al.* (ALICE Collaboration), Phys. Lett. B **754**, 235 (2015).

[4] R. Chatterjee *et al.*, Phys. Rev. C **88**, 034901 (2013).

[5] A. Andronic *et al.*, J. Phys. G **38**, 124081 (2013).

[6] M. Floris, Nucl. Phys. A **931**, 103 (2014).

[7] A. Andronic *et al.*, Phys. Lett. B **673**, 142 (2009), erratum ibid **678**, 516 (2009).

[8] S. Wheaton *et al.*, Comp. Phys. Comm. **180**, 84 (2009).

[9] G. Torrieri *et al.*, Comp. Phys. Comm. **167**, 229 (2005); **175**, 635 (2006); **185**, 2056 (2014).

[10] A. Andronic *et al.*, Phys. Lett. B **697**, 203 (2011).

[11] J. Adam *et al.* (ALICE Collaboration), Phys. Lett. B **758**, 389 (2016).

[12] J. Adam *et al.* (ALICE Collaboration), arXiv:1606.07424 (2016).

[13] J. Rafelski and B. Müller, Phys. Rev. Lett. **48**, 1066 (1982), erratum ibid **56**, 2334 (1986).

[14] B. Müller, P. Koch, and J. Rafelski, Phys. Rept. **142**, 167 (1986).

[15] F. Antinori *et al.*, J. Phys. G **32**, 427 (2006).

[16] C. Blume and C. Markert, Prog. Part. Nucl. Phys. **66**, 834 (2011).

[17] S. Hamieh, K. Redlich, and A. Tounsi, Phys. Lett. B **486**, 61 (2000).

[18] K. Redlich and A. Tounsi, Eur. Phys. J. C **24**, 589 (2002).

[19] A. Tounsi, A. Mischke, and K. Redlich, Nucl. Phys. A **715**, 565c (2003).

[20] B. Abelev *et al.* (ALICE Collaboration), Phys. Rev. C **91**, 024609 (2015).

[21] J. Adam *et al.* (ALICE Collaboration), Eur. Phys. J. C **76**, 245 (2016).

[22] H. J. Drescher, M. Hladik, S. Ostapchenko, T. Pierog, and K. Werner, Phys. Rep. **350**, 93 (2001).

[23] T. Pierog *et al.*, Phys. Rev. C **92**, 034906 (2015).

[24] S. A. Bass *et al.*, Prog. Part. Nucl. Phys. **41**, 255 (1998); **41**, 225 (1998).

[25] M. Bleicher *et al.*, J. Phys. G **25**, 1859 (1999).

[26] A. G. Knospe *et al.*, Phys. Rev. C **93**, 014911 (2016).

[27] A. G. Knospe (for the ALICE Collaboration), arXiv:1610.09529 (2016).

[28] J. Adam *et al.* (ALICE Collaboration), Phys. Rev. C **93**, 024917 (2016).

[29] N. Sharma (for the ALICE Collaboration), Nucl. Phys. A **956**, 461 (2016).

[30] J. Adam *et al.* (ALICE Collaboration), Phys. Lett. B **754**, 360 (2016).

[31] J. Adam *et al.* (ALICE Collaboration), Phys. Lett. B **752**, 267 (2016).

[32] P. Braun-Munzinger, B. Dönigus, and N. Löher, CERN Courier, September 2015.

2.15 Constraining the Hadronic Spectrum from Lattice QCD Thermodynamics

Paolo Alba
Frankfurt Institute for Advanced Studies
Goethe Universität Frankfurt
D-60438 Frankfurt am Main, Germany

Rene Bellwied
Physics Department
University of Houston
617 SR1 Building
Houston, TX 77204, U.S.A.

Szabolcs Borsanyi
Department of Physics
Wuppertal University
D-42119 Wuppertal, Germany

Zoltan Fodor
Department of Physics
Wuppertal University
D-42119 Wuppertal, Germany &
Inst. for Theoretical Physics
Eötvös University
H-1117 Budapest, Hungary &
Jülich Supercomputing Centre
Forschungszentrum Jülich
D-52425 Jülich, Germany

Jana Günther
Department of Physics
Wuppertal University
D-42119 Wuppertal, Germany

Sandor Katz
Inst. for Theoretical Physics
Eötvös University
H-1117 Budapest, Hungary &
TA-ELTE "Lendület" Lattice Gauge Theory Research Group
H-1117 Budapest, Hungary

Valentina Mantovani Sarti
Department of Physics
Torino University and INFN

10125 Torino, Italy

Jacquelyn Noronha-Hostler
Department of Physics
University of Houston
617 SR1 Building
Houston TX 77204, U.S.A.

Paolo Parotto
Physics Department
University of Houston
617 SR1 Building
Houston, TX 77204, U.S.A.

Attila Pasztor
Department of Physics
Wuppertal University
D-42119 Wuppertal, Germany

Israel Portillo Vazquez
Physics Department
University of Houston
617 SR1 Building
Houston, TX 77204, U.S.A.

Claudia Ratti
Department of Physics
University of Houston
617 SR1 Building
Houston TX 77204, U.S.A.

Abstract

We study the effect of not-yet-detected or poorly known hadronic states on several thermodynamic observables, which we calculate in the Hadron Resonance Gas (HRG) model and compare to lattice QCD results. Our analysis shows that the inclusion of such states is crucial to reproduce the lattice data.

1. Introduction

The precision reached by lattice QCD simulations in recent years allows unprecedented quantitative calculations of thermodynamic quantities. In particular, the transition temperature of QCD [1–4], the QCD equation of state at zero [5–8] and small chemical potential [9, 10] and fluctuations of quark flavors and/or conserved charges near the QCD transition [11–13] are now known with high accuracy. The latter are particularly useful because they carry information on the chemical composition of the system and can be used to extract information on the degrees of freedom which populate the system in the vicinity of the

phase transition [14–16]. Besides, they can be related to the experimental measurements of moments of net-charge distributions in order to extract the chemical freeze-out temperature and chemical potential of a heavy ion collision [17–22].

The Hadron Resonance Gas (HRG) model [23–27] yields a good description of most thermodynamic quantities in the hadronic phase. It is based on the idea that strongly interacting matter in the ground state can be described in terms of a non-interacting gas of hadrons and resonances. The only input of the model is the hadronic spectrum: usually it includes all well-known hadrons in the Particle Data Book, namely the ones rated with at least two stars. Recently, it has been noticed that some more differential observables present a discrepancy between lattice and HRG model results. The inclusion of not-yet-detected states, such as the ones predicted by the Quark Model (QM) [28, 29] has been proposed in order to improve the agreement [30, 31].

2. Approach and Results

The HRG model provides a satisfactory description of several thermodynamic quantities below the phase transition temperature. However, it was recently noticed that discrepancies are starting to appear when more differential observables are being calculated. These observables are often expressed in terms of fluctuations of conserved charges, defined as

$$\chi^{BQS}_{lmn} = \left(\frac{\partial^{l+m+n} P(T,\mu_B,\mu_Q,\mu_S)/T^4}{\partial(\mu_B/T)^l \partial(\mu_Q/T)^m \partial(\mu_S/T)^n} \right)_{\mu_i=0}. \tag{1}$$

Such quantities can be evaluated on the lattice, but also in the HRG model approach. The starting point for the model is the total pressure, written as a sum over all known baryons and mesons of the pressure of a non interacting bosonic and fermionic gas:

$$P_{tot}(T,\mu_k) = \sum_k P_k(T,\mu_k) = \sum_k (-1)^{B_k+1} \frac{d_k T}{(2\pi)^3} \int d^3\vec{p} \ln\left(1 + (-1)^{B_k+1} \exp\left[-\frac{(\sqrt{\vec{p}^2+m_k^2}-\mu_k)}{T}\right]\right). \tag{2}$$

Here the single particle chemical potential is defined with respect to the global conserved charges (baryonic B, electric Q and strangeness S) as $\mu_k = B_k\mu_B + Q_k\mu_Q + S_k\mu_S$. More details on the HRG model used here can be found in Ref. [32].

In principle, the chemical potentials for baryon number, electric charge and strangeness can be chosen independently. However, to match the experimental situation in a heavy-ion collision, a common choice is to fix them by imposing the following conditions:

$$\langle n_S \rangle = 0 \qquad \langle n_Q \rangle = \tfrac{Z}{A}\langle n_B \rangle \simeq \langle 0.4 n_B \rangle. \tag{3}$$

In lattice calculations to leading order in μ_B, the ratio μ_S/μ_B which satisfies the above conditions reads [18, 19]:

$$\left(\frac{\mu_S}{\mu_B}\right)_{LO} = -\frac{\chi^{BS}_{11}}{\chi^S_2} - \frac{\chi^{QS}_{11}}{\chi^S_2}\frac{\mu_Q}{\mu_B}; \tag{4}$$

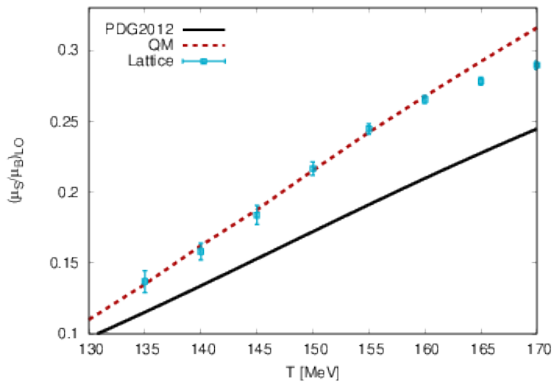

Figure 1: Ratio μ_S/μ_B at leading order as a function of the temperature. The two curves are the HRG model result obtained with the well-known states from the PDG2012 (full black line) and Quark Model (dotted red line).

The lattice results for this observable are shown in Fig. 1, in comparison to the HRG model results based on the well-established states from the PDG2012 (full, black line) and the Quark Model (dotted, red line). The improvement due to the inclusion of the QM states is evident. However, for other observables such as χ_4^S/χ_2^S and χ_{11}^{us}, the agreement between HRG model and lattice gets worse when the QM states are included (see the two panels of Fig. 2).

By observing these plots we can already try to understand what the issue could be. The ratio χ_4^S/χ_2^S is proportional to the average strangeness squared in the system. The fact that the QM overestimates the data means that it either predicts too many multi-strange states or not enough $S = 1$ states. Analogously, χ_{11}^{us} measures the correlation between u and s quarks: it is positive for baryons and negative for mesons. The fact that the QM overestimates the data means that it either predicts too many strange baryons or not enough strange mesons.

In order to solve this ambiguity, we decided to look at each particle family separately, dividing them according to their baryonic and strangeness content. In order to do so, we defined the partial pressures for each family in the hadronic phase, according to the following equations [15]:

$$\begin{aligned} P(\hat{\mu}_B, \hat{\mu}_S) &= P_{00} + P_{10}\cosh(\hat{\mu}_B) + P_{0|1|}\cosh(\hat{\mu}_S) \\ &+ P_{1|1|}\cosh(\hat{\mu}_B - \hat{\mu}_S) \\ &+ P_{1|2|}\cosh(\hat{\mu}_B - 2\hat{\mu}_S) \\ &+ P_{1|3|}\cosh(\hat{\mu}_B - 3\hat{\mu}_S)\ , \end{aligned} \tag{5}$$

where $\hat{\mu}_i = \mu_i/T$, and the indexes are $P_{B|S|}$.

Our results are shown in Fig. 3. The first five panels show the contributions of strange mesons, non-strange baryons and baryons with $|S| = 1, 2, 3$ respectively. All lattice results are continuum-extrapolated, with the exception of the strange mesons, for which the finite-N_t lattice data do not scale. The last panel shows the relative contribution of the single

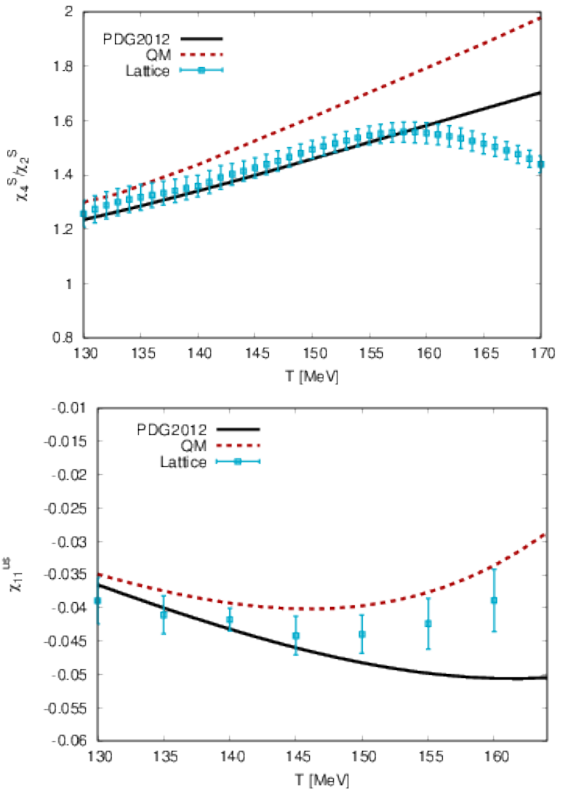

Figure 2: Upper panel: χ_4^S/χ_2^S as a function of the temperature. The lattice results from Ref. [16] are compared to the HRG model calculations based on the PDG2012 (black solid line) and the QM (red dashed line). Lower panel: comparison of up-strange correlator χ_{11}^{us} simulated on the lattice [13] and calculated in the HRG model using the PDG2012 (solid black line) and the QM (dashed red line) spectra.

families to the total pressure, from which it is evident that there are more than three orders of magnitude between the total pressure and the smallest contribution due to the $|S| = 3$ baryons. The method we used for this analysis, namely simulations at imaginary μ_B and μ_S, was crucial in order to extract a signal for the multi-strange baryons. From all panels except the non-strange baryons, it is evident that the HRG model based on the well-established states listed in the PDG2016 is not enough to reproduce the lattice results. The additional one-star states are the minimal choice which allows to reproduce most of the data. In some cases (strange mesons and $|S| = 3$ baryons), even more states are required to reproduce the data: for the $|S| = 3$ baryons a better agreement is obtained when including the Ω resonances predicted by the QM, while for the strange mesons, the continuum extrapolation (once available) will lie above all curves, even the ones including the QM states. Therefore, our analysis shows that additional states are needed in order to reproduce the lattice results, with respect to the the well-established ones listed in the most updated version of the PDG.

The minimal choice which reproduces almost all the observables is the PDG2016+. Besides reproducing most of the partial pressures, this choice also allows to correctly describe $(\mu_S/\mu_B)_{LO}$ and χ_4^S/χ_2^S, as shown in Fig. 4. Inclusion of additional states predicted by the

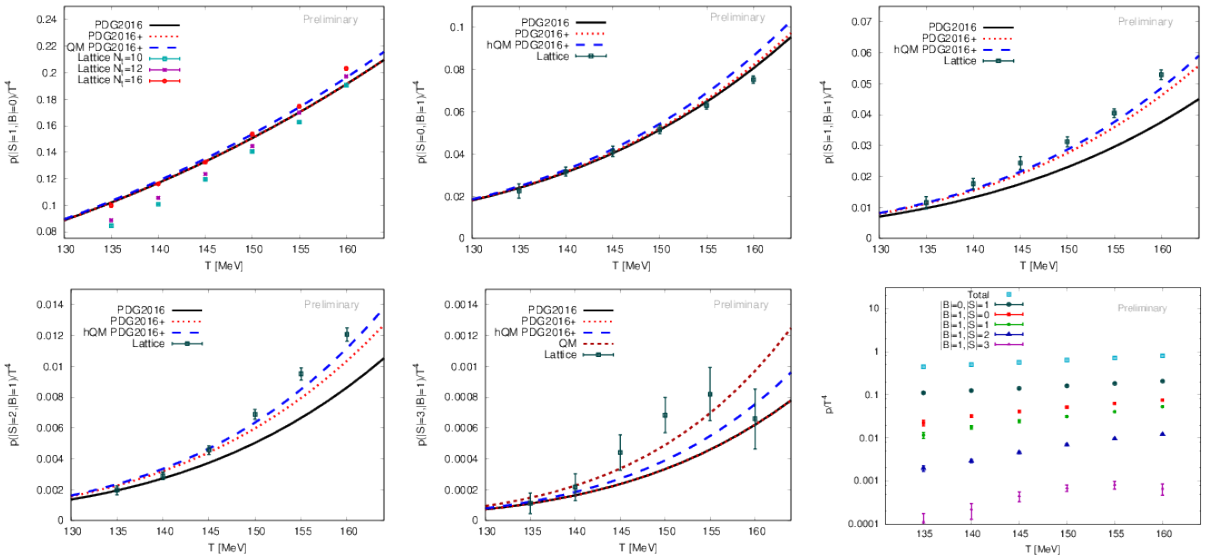

Figure 3: Partial pressures for the different hadronic families as functions of the temperature. The upper panels show the contributions due to strange mesons (left), non-strange baryons (center) and baryons with $|S| = 1$ (right). The lower panels show the contributions due to $|S| = 2$ baryons (left), $|S| = 3$ baryons (center) and the relative contributions of the single families with respect to the total (right). In the first five panels, the points are the lattice results, while the curves are PDG2016 (solid black), PDG2016+ (with inclusion of one star states, red dotted), PDG2016+ and additional states from the hQM (blue, dashed) [33–37]. In the lower center panel, the dark red short-dashed curve corresponds to the PDG2016+ with inclusion of the Ω resonances predicted by the QM [28, 29].

hQM pushes the agreement with the lattice to higher temperature for most observables.

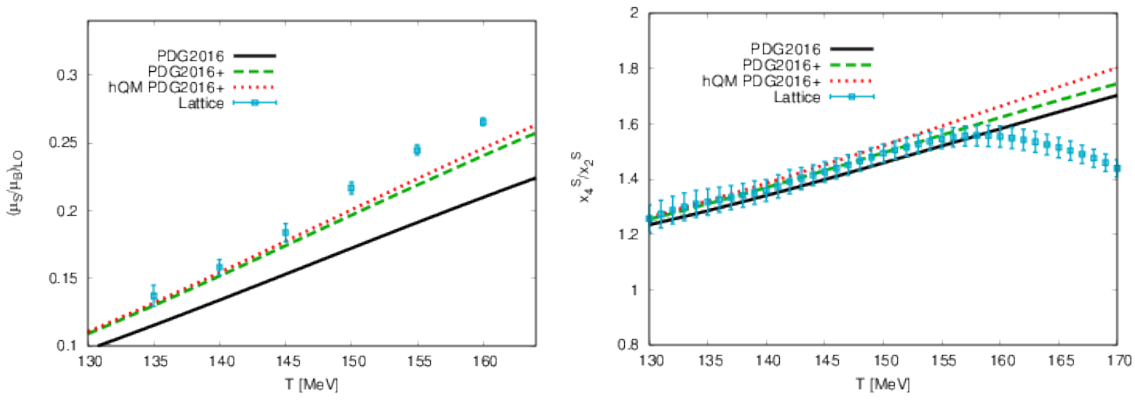

Figure 4: Left: $(\mu_S/\mu_B)_{LO}$ as a function of the temperature. Right: χ_4^S/χ_2^S as a function of the temperature. In both panels, the lattice data are shown in comparison to the HRG model curves based on the PDG 2016 (black, solid line), the PDG2016+ (green, dashed line) and the PDG2016+ with additional states from the hQM (red, dotted line).

3. Conclusions

We have calculated several thermodynamic quantities on the lattice and compared them to the predictions of the HRG model based on the PDG2016, PDG2016+ and PDG2016+ with the addition of states predicted by the hQM. Besides χ_4^S/χ_2^S and $(\mu_S/\mu_B)_{LO}$, we have extracted the contribution to the QCD pressure in the hadronic phase due to several hadronic families, grouped according to their baryon and strangeness content. Our analysis clearly shows that the well-established states listed in the most updated version of the PDG are not enough to correctly reproduce the lattice results. The minimal choice which reproduces most of the data is the PDG2016 with the inclusion of one-star states which are not well-established. In some cases, such as the strange mesons and $|S| = 3$ baryons, there is room to add even more states. These results will potentially affect all phenomenological applications of the HRG model, including thermal fits and other calculations relevant to heavy-ion physics.

4. Acknowledgments

We acknowledge fruitful discussions with Elena Santopinto, Igor Strakovsky, Moskov Amaryan and Mark Manley. This material is based upon work supported by the National Science Foundation under grant no. PHY–1513864 and by the U.S. Department of Energy, Office of Science, Office of Nuclear Physics, within the framework of the Beam Energy Scan Theory (BEST) Topical Collaboration. The work of R. Bellwied is supported through DOE grant DE–FG02–07ER41521. An award of computer time was provided by the INCITE program. This research used resources of the Argonne Leadership Computing Facility, which is a DOE Office of Science User Facility supported under Contract DE–AC02–06CH11357. The authors gratefully acknowledge the Gauss Centre for Supercomputing (GCS) for providing computing time for a GCS Large-Scale Project on the GCS share of the supercomputer JUQUEEN [38] at Jülich Supercomputing Centre (JSC). The authors gratefully acknowledge computing time on the Hazel Hen machine at HLRS.

References

[1] Y. Aoki, Z. Fodor, S. Katz, and K. Szabo, Phys. Lett. B **643**, 46 (2006); arXiv:hep–lat/0609068 [hep–lat].

[2] Y. Aoki, S. Borsanyi, S. Durr, Z. Fodor, S. D. Katz *et al.*, JHEP **0906**, 088 (2009); arXiv:0903.4155 [hep–lat].

[3] S. Borsanyi *et al.* (Wuppertal-Budapest Collaboration), JHEP **1009**, 073 (2010), arXiv:1005.3508 [hep–lat].

[4] A. Bazavov *et al.*, Phys. Rev. D **85**, 054503 (2012); arXiv:1111.1710 [hep–lat].

[5] S. Borsanyi, G. Endrodi, Z. Fodor, A. Jakovac, S. D. Katz *et al.*, JHEP **1011**, 077 (2010); arXiv:1007.2580 [hep–lat].

[6] S. Borsanyi, Z. Fodor, C. Hölbling, S. D. Katz, S. Krieg *et al.*, Phys. Lett. B **730**, 99 (2014); arXiv:1309.5258 [hep–lat].

[7] A. Bazavov *et al.* (HotQCD Collaboration), Phys. Rev. D **90**, 094503 (2014), arXiv:1407.6387 [hep–lat].

[8] S. Borsanyi *et al.*, Nature **539**, 69 (2016); arXiv:1606.07494 [hep–lat].

[9] S. Borsanyi, G. Endrodi, Z. Fodor, S. Katz, S. Krieg *et al.*, JHEP **1208**, 053 (2012); arXiv:1204.6710 [hep–lat].

[10] J. Gunther, R. Bellwied, S. Borsanyi, Z. Fodor, S. D. Katz, A. Pasztor, and C. Ratti, (2016), arXiv:1607.02493 [hep–lat].

[11] S. Borsanyi, Z. Fodor, S. D. Katz, S. Krieg, C. Ratti, *et al.*, JHEP **1201**, 138 (2012); arXiv:1112.4416 [hep–lat].

[12] A. Bazavov *et al.* (HotQCD Collaboration), Phys. Rev. D **86**, 034509 (2012); arXiv:1203.0784 [hep–lat].

[13] R. Bellwied, S. Borsanyi, Z. Fodor, S. D. Katz, A. Pasztor, C. Ratti, and K. K. Szabo, Phys. Rev. D **92**, 114505 (2015); arXiv:1507.04627 [hep–lat].

[14] V. Koch, A. Majumder, and J. Randrup, Phys. Rev. Lett. **95**, 182301 (2005), arXiv:nucl–th/0505052 [nucl–th].

[15] A. Bazavov, H. T. Ding, P. Hegde, O. Kaczmarek, F. Karsch *et al.*, Phys. Rev. Lett. **111**, 082301 (2013), arXiv:1304.7220 [hep–lat].

[16] R. Bellwied, S. Borsanyi, Z. Fodor, S. D. Katz, and C. Ratti, Phys. Rev. Lett. **111**, 202302 (2013), arXiv:1305.6297 [hep–lat].

[17] F. Karsch, Central Eur. J. Phys. **10**, 1234 (2012), arXiv:1202.4173 [hep–lat].

[18] A. Bazavov, H. Ding, P. Hegde, O. Kaczmarek, F. Karsch **et al.**, Phys. Rev. Lett. **109**, 192302 (2012); arXiv:1208.1220 [hep–lat].

[19] S. Borsanyi, Z. Fodor, S. Katz, S. Krieg, C. Ratti *et al.*, Phys. Rev. Lett. **111**, 062005 (2013); arXiv:1305.5161 [hep–lat].

[20] S. Borsanyi, Z. Fodor, S. Katz, S. Krieg, C. Ratti *et al.*, Phys. Rev. Lett. **113**, 052301 (2014); arXiv:1403.4576 [hep–lat].

[21] S. Mukherjee, P. Petreczky, and S. Sharma, Phys. Rev. D **93**, 014502 (2016), arXiv:1509.08887 [hep–lat].

[22] J. Noronha-Hostler, R. Bellwied, J. Gunther, P. Parotto, A. Pasztor, I. P. Vazquez, and C. Ratti, (2016); arXiv:1607.02527 [hep–ph].

[23] R. Dashen, S.-K. Ma, and H. J. Bernstein, Phys. Rev. **187**, 345 (1969).

[24] R. Venugopalan and M. Prakash, Nucl. Phys. A **546**, 718 (1992).

[25] F. Karsch, K. Redlich, and A. Tawk, Eur. Phys. J. C **29**, 549 (2003); arXiv:hep–ph/0303108 [hep–ph].

[26] F. Karsch, K. Redlich, and A. Tawk, Phys. Lett. B **571**, 67 (2003); arXiv:hep–ph/0306208 [hep–ph].

[27] A. Tawk, Phys. Rev. D **71**, 054502 (2005); arXiv:hep–ph/0412336 [hep–ph].

[28] S. Capstick and N. Isgur, Phys. Rev. D **34**, 2809 (1986).

[29] D. Ebert, R. Faustov, and V. Galkin, Phys. Rev. D **79**, 114029 (2009); arXiv:0903.5183 [hep–ph].

[30] A. Majumder and B. Muller, Phys. Rev. Lett. **105**, 252002 (2010); arXiv:1008.1747 [hep–ph].

[31] A. Bazavov, H. T. Ding, P. Hegde, O. Kaczmarek, F. Karsch *et al.*, Phys. Rev. Lett. **113**, 072001 (2014); arXiv:1404.6511 [hep–lat].

[32] P. Alba, W. Alberico, R. Bellwied, M. Bluhm, V. Mantovani Sarti *et al.*, Phys. Lett. B **738**, 305 (2014); arXiv:1403.4903 [hep–ph].

[33] M. Ferraris, M. M Giannini, M. Pizzo, E. Santopinto, and L. Tiator, Phys. Lett. B **364**, 231 (1995).

[34] M. M. Giannini, E. Santopinto, and A. Vassallo, Eur. Phys. J. A **12**, 447 (2001), arXiv:nucl-th/0111073 [nucl–th].

[35] M. M. Giannini, E. Santopinto, and A. Vassallo, Eur. Phys. J. A **25**, 241 (2005); arXiv:nucl–th/0506032 [nucl–th].

[36] J. Ferretti, R. Bijker, G. Galata, H. Garcia-Tecocoatzi, and E. Santopinto, Phys. Rev. D **94**, 074040 (2016); arXiv:1506.07469 [hep–ph].

[37] M. M. Giannini and E. Santopinto, Chin. J. Phys. **53**, 020301 (2015); arXiv:1501.03722 [nucl–th].

[38] JUQUEEN: IBM Blue Gene/Q Supercomputer System at the Jülich Supercomputing Centre, Tech. Rep. 1 A1 (Jülich Supercomputing Centre, http://dx.doi.org/10.17815/jlsrf-1-18 2015).

2.16 Strange Hadrons from the Lattice

Robert G. Edwards
Theory Center
Jefferson Lab
12000 Jefferson Ave.
Newport News, VA 23606, U.S.A.

Abstract

Lattice QCD has recently made signicant progress in determining the excited state spectrum of Quantum Chromodynamics. We describe in these proceedings a program for these calculations and indicate future directions.

1. The End of the Beginning

One of the enigmatic features of Quantum Chromodynamics (QCD) is its excited state spectrum. The presence of such states was inferred, at least initially, by their characteristic bumps in scattering cross sections. The plethora of such states drove the development of an explanation via effective models of the spectrum – such as the Quark Model composed of constituent particles called quarks . A feature of these models is that there is a global symmetry of the spectrum under global rotations of a "flavor" under the Lie group $SU(3)$. The three constituents particle are the up, down and strange. The Quark Model works reasonable well at describing the spectrum of baryon states, but there is a catch. By construction in the model, the overall wave function for baryons are symmetric which is clearly at odds with their fermionic nature. It was postulated that the quarks carry a new kind of "charge" that transformed under a local gauge symmetry called "color". With three kinds of color charge, baryon wave-functions can be antisymmetric as required by Fermi-Dirac statistics.

The existence of the Ω baryon provided strong support for the existence of color. Combined with insight gained from deep inelastic scattering experiments, we now believe that the underlying theory of the strong interactions is, in fact, QCD which is described in terms of the interactions of quarks and gluons. These "quarks", though, are thought to have a fairly small amount of mass. How do we reconcile this nice, simple, and elegant theory of quarks with the massive hadrons seen in experiments? What is the origin of spin? In particular, there are spin $\frac{5}{2}$ hadrons. How is that possible?

The existence of the Ω is only a small sample of the implications implied by the existence of three color charges. The color gauge fields themselves must carry color, thus implying the glue interacts with itself. One picture of the "constituent" quarks in the Quark Model is that they gain their mass through screening, or "dressing" of the "current" quarks by the glue as well as other virtual fluctuations from the vacuum. It seems a preferred pattern of these constituent quarks is groups of three to form a baryon, or in a quark and antiquark pair configuration to form a meson. But this is only an effective picture. Is it correct in any level of detail? Why only these simple quark configurations? There are new indications that tetraquark and even pentaquark configurations might exist. What about the glue itself – does the existence of three color charges have more implications?

Spectroscopy has been an active field of study over many years. The unexplained mysteries arising from experiment challenges our understanding of QCD. To address these fundamental questions we need theoretical guidance and predictions directly from QCD. Thus, we also need a new generation of experiments to find if there are yet even more unexpected configurations, and certainly unexplained, properties of hadrons as well as measuring the production amplitudes for these states. A burning question is what is the spectrum of QCD featuring strange quarks? The presence of these states might help explain properties of the QCD thermodynamic phase transition at finite temperature, and is a motivation for the Ystar program.

There has been significant theoretical progress towards answering some of these fundamental questions. Lattice QCD is the only known fully non-perturbative, systematically improvable method we have available to answer these questions. Recent progress is highly suggestive that there is a rich spectrum of hadrons beyond what is predicated by the Quark Model. What has been missing from these initial studies is the information on branching fractions of decays. There has been very recent progress in this area as well.

This proceedings summarizes some of the results from the Hadron Spectrum Collaboration pertaining to the calculation of the light and strange quark baryon spectrum of QCD.

2. Predictions from QCD

(a) Glimpse of the Baryon Spectrum

The fundamental theory of the strong interactions – QCD – is simple and elegant, but it is not amenable to perturbative methods to extract some observable, and it is precisely the strongly interacting properties of the three color charges that make it so complicated – and interesting! We must regulate the theory to make a calculation, and a finite-volume lattice is a straightforward method to do so. The basic quantity that we compute are correlation functions of quark and gluon fields. These functions in Euclidean space can be written as an infinite sum of exponentials decaying in time. The coefficients in the exponents is the discrete energy of the finite-volume versions of states, and the coefficient in front of the exponential is the matrix element of the overlap of the creation (or annihilation) operator with the states going into the vacuum. These overlap factors are thus a probe of the wave-function of the state. A large basis of operators thus provides multiple probes of the state, and also provides a powerful method to extract the towering of finite-volume energies.

The Hadron Spectrum collaboration, centered at Jefferson Lab, has been pursuing a campaign to compute the spectrum of QCD. In Figure 1 is shown the determination of the discrete energy of states in a finite-volume where the pion mass in this world, with two light and one strange dynamical set of quarks, is 524 MeV. Shown is the positive parity spectrum of the Nucleon and Delta. The horizontal bars show the magnitude of the overlap factor for a particular operator across each of the states. The counting of the levels and the structure of the operator constructions is consistent with the $SU(6) \times O(3)$ prediction of the non-relativistic quark model, but with the important addition of states that have a hybrid-like nature, and are indicated by a thick black border for the boxes denoting the mass.

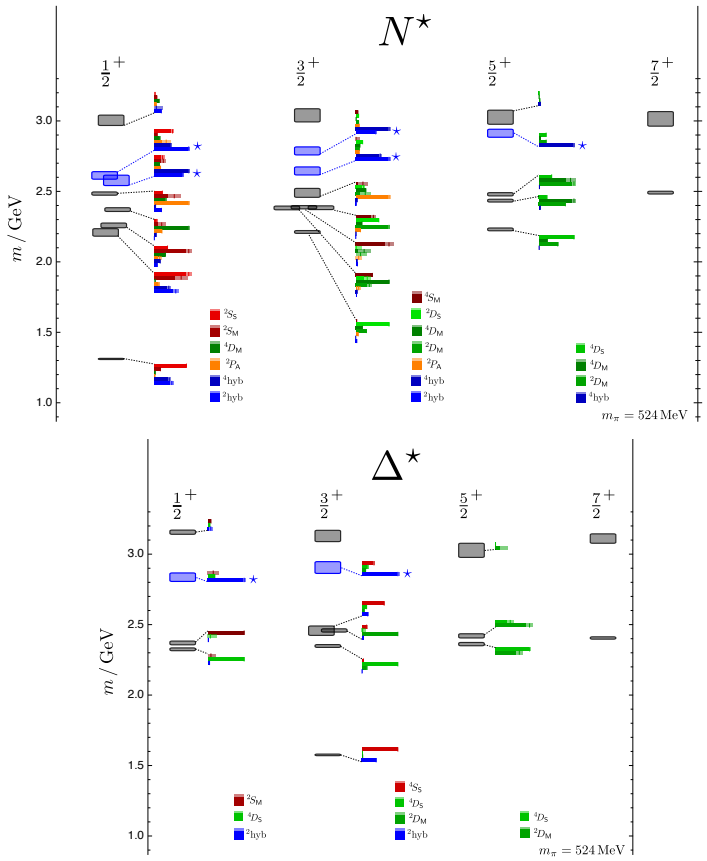

Figure 1: Results from Ref. [1]. Extracted spectrum of Nucleon and Delta states indicated by J^P at a pion mass of 524 MeV. Rectangle height indicates the statistical uncertainty in mass determination. Histograms indicate the relative size of matrix elements $\left\langle \mathfrak{n} \middle| \mathcal{O}_i^\dagger(0) \middle| 0 \right\rangle$ for a "non-relativistic" subset of the operators used with the lighter area at the head of each bar being the statistical uncertainty. Operator labeling follows a spectroscopic convention as described in [2] with $^{2S+1}L_\pi$ and π indicating the permutation structure of the quark fields. The operator constructions include those featuring only upper Dirac-spin components as well as lower components, and also hybrid-like constructions featuring chromomagnetic gluon fields. Asterisks indicate states having dominant overlap onto hybrid operators. The counting of the levels is consistent with the $SU(6) \times O(3)$ predictions of the non-relativistic quark model, but with the important addition of states that are hybrid-like.

In the left panel of Figure 2 is shown the positive and negative parity spectrum in the flavor symmetric limit of QCD, where the u, d and s quarks are degenerate. In this limit, there is an exact $SU(3)_F$ symmetry. The overlap factors and energies suggest again a pattern of states consistent with $SU(6) \times O(3)$ with the number of states determined by the flavor representation.

As we decrease the light-quark masses, the $SU(3)$ flavor structure is broken suggesting there should be mixing of flavor representations within a fixed isospin and total flavor

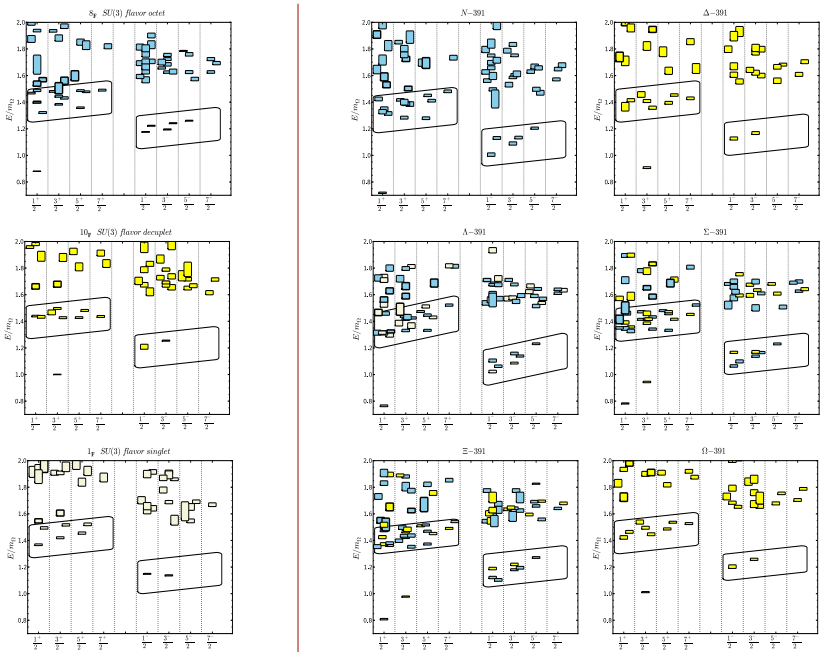

Figure 2: Results from Ref. [3]. Left panel: baryon excited states in flavor irreps $\mathbf{8_F}$, $\mathbf{10_F}$ and $\mathbf{1_F}$ obtained using the flavor-symmetric point, with m_π = 702 MeV are shown versus J^P. Right panel: results for baryon excited states using the ensemble with m_π = 391 MeV are shown versus J^P. Colors are used to display the flavor symmetry of dominant operators as follows: blue for $\mathbf{8_F}$; beige for $\mathbf{1_F}$; yellow for $\mathbf{10_F}$. Symbols with thick border lines indicate states with strong hybrid content. The lowest bands of positive- and negative-parity states are highlighted within slanted boxes.

number. Shown in the right panel of Figure 2 is the spectrum with a pion mass of 391 MeV. The color of the boxes denotes the flavor structure of the dominant overlap factors for the states. As the light quark mass is not appreciably smaller than the strange quark mass, we expect the mixing to be small, and indeed, all the states could be cleanly separated into fixed flavor representations. In this quark mass limit, the isospin=0 with strangeness=-1 components of the 1_F and 8_F operator constructions are allowed to mix, and as seen in the panel for the Λ in the figure, we see a pattern of both $\mathbf{8_F}$ and $\mathbf{1_F}$ states superimposed on each other, but with negligible flavor mixing. A similar observation is found for mixing of the Σ and Ξ states in $\mathbf{8_F}$ and $\mathbf{10_F}$. We expect that is the quark mass is decreased that there should be more mixing among the appropriate flavor representations.

The operators are constructed with flavor and spin transforming according to the appropriate flavor representation and spin construction. This operator flavor and spin part is multiplied by a spatial part that has some number of units of spatial gauge covariant

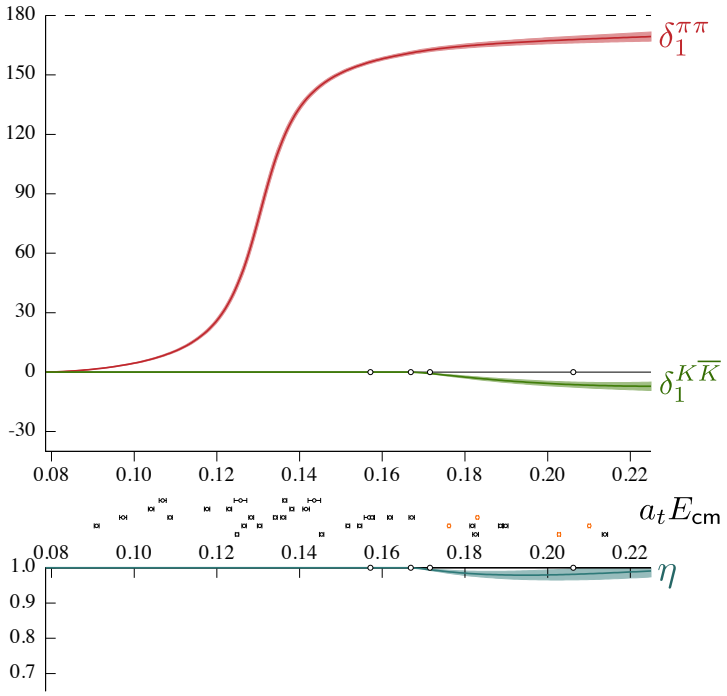

Figure 3: Results from Ref. [4] with a pion mass of 236 MeV. Shown are the coupled P-wave $\pi\pi$ and $K\overline{K}$ isospin-1 phase shifts δ and inelasticity η from a single K-matrix fit. Statistical uncertainty shown by the shaded band. The central points show the energy levels constraining the amplitude extraction with those dominated by $\pi\pi$-like and $\overline{q}q$-like operators shown in black and those with significant $K\overline{K}$ contributions shown in orange. On axis circles show the opening of the 4π, $\bar{K}K$, $\eta\pi\pi$ and $\pi\bar{K}K$ thresholds.

derivatives which resemble orbital angular momentum. In the spectroscopic notation, we group operators according to the number of units of orbital angular momentum. The bands around the states indicate their grouping according to their dominant spectral overlaps which we find to be consistent with this grouping of orbital angular momentum.

That the grouping follows such a pattern moving up in energy has a plausible explanation. Each unit of orbital angular momentum flips the parity of the state. In analogy to the Bohr model, each unit of orbital angular momentum brings in some unit of energy, roughly on the scale of Λ_{QCD}. Thus, we might expect a band of states alternating as we go up in energy. Of course, the states become more numerous as we go up in units of orbital angular momentum, so this simple picture will not be so neat and clean.

This pattern of states also happens to be a prediction of the Quark Model. It should be emphasized that the Quark Model are not baked into the lattice calculations. Rather, the operator constructions happen to be all that are allowed by continuum symmetries. They are easily classified according to the spectroscopic notation which happens to be the preferred way of constructing the Quark Model. That the two happen to agree in

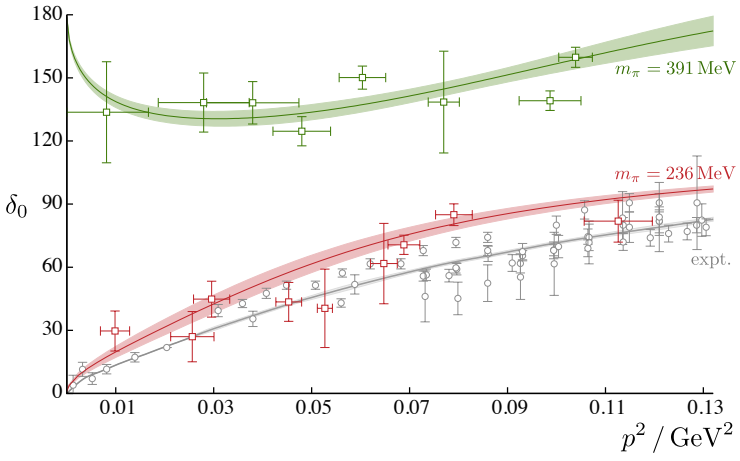

Figure 4: Results from Ref. [5]. Isoscalar S-wave $\pi\pi$ elastic scattering phase-shift, δ_0, plotted against the scattering momentum, $p^2 = (E_{\mathsf{cm}}/2)^2 - m_\pi^2$, computed at a pion mass of 391 and 236 MeV. The colored curves are the result of a K-matrix "pole plus constant" with Chew-Mandelstam phase-space parameterization. The gray points show experimental data [6–9] and the gray curve shows the constrained dispersive description of these data presented in Ref. [10].

overall structure (but certainly not in detail) is suggestive that their are some effective degrees of freedom at play that are captured in the Quark Model.

However, the addition of the hybrid states is something new again. The overall picture so far from the lattice calculations suggest the spectrum roughly resembles a collection of constituent quarks and a constituent glue, with the quarks transforming as $S = \frac{1}{2}$ and $\mathbf{3_C}$ in color, and the glue transforming according to $J_{PC} = 1^{+-}$ in an $\mathbf{8_C}$ in color. The overall state must be a singlet in color. The pattern of energies suggest that the constituent glue has an effective mass of roughly 1.3 GeV.

The lattice results so far did not attempt to classify resonances according to their structure. The calculations shown have been at pion masses at 391 MeV and above. If these states are indeed resonances, they must decay. That the lattice results so far appear so clean and consistent is possibly that the pion mass is large and the phase space for decays is small. To make this picture more rigorous requires extending the calculations to allow for decays, and that program is described next.

(b) **Resonances and Decays**

What is observably measurable are scattering amplitudes as a function of energy. A resonance could appear as a bump in these amplitudes, but more generally, we ascertain a resonance as a pole in the scattering amplitude when continued into the complex plane of energy. Of course, very few resonances are expected to be a pole in a purely elastic decay into a single channel two particles. More generally, we expect decays of a resonance into many channels. Using a partial wave picture, a pole can appear in many partial waves. It is thus critical that the lattice methods be extended to provide such decay information.

Exploiting the finite-volume nature of the lattice calculations, an elegant formalism

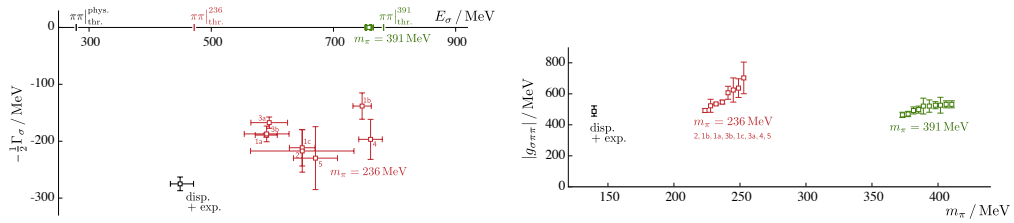

Figure 5: Results from Ref. [5] for isoscalar elastic $\pi\pi$ scattering. Left panel: t-matrix pole positions for a variety of parameterizations [K-matrix "pole plus polynomial" forms with (1a − c) and without Chew-Mandelstam phase-space (2) and/or Adler zero [11](3a, b), relativistic Breit-Wigner(4) and effective range expansion(5)]. Red points: resonant pole (unphysical sheet) at $m_\pi = 236$ MeV. Black point: Resonant pole from dispersive analysis of experimental data (conservative average presented in Ref. [12]). Right panel: Coupling $g_{\sigma\pi\pi}$ from t-matrix residue at the pole - points from various parameterizations are shifted horizontally for clarity. The phenomenological determinations of the experimental results employ Roy-Steiner constraints on the scattering amplitudes while the lattice results do not (yet). Nevertheless, there is consistency of the extracted coupling to the $\pi\pi$ channel across between the phenomenological and lattice results.

has been developed, generically called the Lüscher formalism, that relates the infinite-volume Minkowski scattering amplitude to the discrete energy spectrum encoded within a set of known, finite-volume functions. These Lüscher functions are also functions of the lattice cubic representation and total momenta of the system. The discrete spectrum of energies changes significantly according to the total momenta and cubic group representation. Thus, we can map out scattering amplitudes by determining the energy spectrum in different moving frames. The finite-volume formalism has also been extended to coupled channel systems of two particles.

To illustrate the method, shown in Figure 3 is the first calculation of the P-wave scattering amplitude(s) for the simplest resonance in QCD – the ρ meson. The sets of dots between the upper and lower panel show the discrete energies measured in different frames. Solving the relation for the energies, the form of the amplitude, including any parameters within it, must be adjusted to agree with the "measured" lattice energies. As the lattice energies can be determined in many moving frames, there are many constraints on the details of the amplitude. In the ρ system, one can see that as the CM energy of the system is increased, the amplitude opens at the threshold for the $\bar{K}K$ channel and the amplitude (here encoded as a phase shift) for that decay mode becomes small, but non-zero. This is the first demonstration from a lattice calculation of such behavior, and opens the door to the calculation of amplitudes in more complicated systems.

One such system that has been a mystery for decades is the existence of the σ meson in isospin=0 $\pi\pi$ scattering. In Figure 4 is the first such calculation of the elastic S-wave isoscalar scattering amplitude, as a function of the pion mass. We see that the form of the amplitude channels significantly as the phase space for the decay becomes more open, and it approaches the phenomenologically determined amplitude. Shown in Figure 5 are the pole locations and the decay couplings determined from the residue

of the pole in the complex energy plance of the scattering amplitude. While the pole location changes significantly as the pion mass decreases, we see the coupling appears to be fairly consistent with a constant.

These results suggest that it is possible to determine scattering amplitude and resonance properties directly from QCD. Determining amplitudes for mesons is technically simpler for lattice QCD, but it is possible to extend these calculations to the baryon sectors. First results have appeared from other groups.

3. **Outlook**

The Hadron Spectrum Collaboration has embarked on a ambitious program to determine resonance decays for mesons with an emphasis on exotic mesons – relevant for the GlueX program – and also the baryon spectrum relevant for both GlueX and CLAS12, as well as other facilities around the world. There is a great deal of work to do, but the results to date are encouraging. It is possible to determine scattering amplitudes and extract resonance properties directly from QCD. As the pion mass in the calculations is decreased, the phase space for decays can become large, thus the scattering formalism will be essential to extract resonance properties, reliably, in complicated channels.

The lattice QCD efforts do not exist in a vacuum (sorry, bad pun), but go hand in hand with the experimental analysis efforts. The scattering amplitudes determined from the lattice must agree with those from experiment. The formalism for scattering amplitudes in complicated channels can be complicated mathematically. Thus a close interaction between the communities is needed for a successful spectroscopy program.

References

[1] J. J. Dudek and R. G. Edwards, Phys. Rev. D **85**, 054016 (2012); [arXiv:1201.2349 [hep-ph]].

[2] R. G. Edwards, J. J. Dudek, D. G. Richards, and S. J. Wallace, Phys. Rev. D **84**, 074508 (2011); [arXiv:1104.5152 [hep-ph]].

[3] R. G. Edwards *et al.* [Hadron Spectrum Collaboration], Phys. Rev. D **87**, 054506 (2013); [arXiv:1212.5236 [hep-ph]].

[4] D. J. Wilson, R. A. Briceno, J. J. Dudek, R. G. Edwards, and C. E. Thomas, Phys. Rev. D **92**, 094502 (2015); [arXiv:1507.02599 [hep-ph]].

[5] R. A. Briceno, J. J. Dudek, R. G. Edwards, and D. J. Wilson, Phys. Rev. Lett. **118**, 022002 (2017); [arXiv:1607.05900 [hep-ph]].

[6] S. D. Protopopescu *et al.*, Phys. Rev. D **7**, 1279 (1973).

[7] B. Hyams *et al.*, Nucl. Phys. B **64**, 134 (1973).

[8] G. Grayer *et al.*, Nucl. Phys. B **75**, 189 (1974).

[9] P. Estabrooks and A. D. Martin, Nucl. Phys. B **79**, 301 (1974).

[10] R. Garcia-Martin, R. Kaminski, J. R. Pelaez, and J. Ruiz de Elvira, Phys. Rev. Lett. **107**, 072001 (2011); [arXiv:1107.1635 [hep-ph]].

[11] S. L. Adler, Phys. Rev. **137**, B1022 (1965).

[12] J. R. Pelaez, Phys. Rept. **658**, 1 (2016); [arXiv:1510.00653 [hep-ph]].

2.17 Implications of Missing Resonances in Heavy Ions Collisions

Jacquelyn Noronha-Hostler
Department of Physics
University of Houston
617 SR1 Building
Houston TX 77204, U.S.A.

Abstract

Between 2004 until today many new resonances in the QCD spectrum have been added by the Particle Data Group. However, it is still possible that there are further states that have yet to be measured, as predicted by Lattice QCD calculations and Quark Models. In this paper, I review how these missing states would influence the field of heavy-ion collisions. Additionally, the quantum numbers that characterize these missing states are also discussed.

1. Introduction

Efforts at Jefferson Laboratory have resulted in a significant increase in the number of known QCD resonances since 2004, which are now listed in the Particle Data Group (PDG). Furthermore, various theory groups have predicted even further states using Lattice QCD [1] and quark models [2, 3], giving marginal support to an exponentially increasing mass spectrum [4] up to a given value of mass. Even amongst the resonances listed within the PDG some are more confidentially measured than others. Thus, a star system rating was developed where states with the highest confidence level are listed as **** states and those with the least are $*$ states.

It is natural to wonder how many more states are still missing and what is the top possible maximum mass of these resonances. The implications of these missing resonances have been studied extensively over the last 15 years in the field of heavy-ion collisions. Results that have garnered the most attention include the effect of missing resonances on the transport coefficients in the hadron gas phase [5] as well as the possibility that there are missing strange baryons found using Lattice QCD [6]. This proceedings reviews some of the main findings in the field of heavy-ion collisions and also discusses the mass range and the quantum numbers within which further missing states may be measured.

2. Comparisons with Lattice QCD

At the transition region between the hadron gas phase into the Quark Gluon Plasma, Lattice Quantum Chromodynamics (QCD) has been enormously successful in calculating thermodynamic quantities. In the early 2000's the hadron resonance gas model (where it is assumed that an interacting gas of hadrons can be described by a gas of non-interacting hadrons and their resonances) was used to calculate thermodynamic quantities. For instance, the pressure of the hadron resonance gas model is

$$p/T^4 = \sum_i^{PDG} \frac{d_i}{2\pi^2}\left(\frac{m_i}{T}\right)^2 \sum_{k=1}^{\infty} \frac{(\pm 1)^{k+1}}{k^2} K_2\left(\frac{km_i}{T}\right) \cosh\left[\frac{k\left(B_i\mu_B + S_i\mu_S + Q_i\mu_Q\right)}{T}\right] \quad (1)$$

where d_i is the degeneracy, m_i is the mass, B_i is the baryon number, S_i is the strangeness, and Q_i is the electric charge of each individual hadron taken into account. Thus, the only real variable in this model is the total number of resonances as dictated by the PDG.

Due to having fewer experimentally measured resonances in the early 2000's, the hadron gas model was unable to match Lattice QCD calculations of the pressure, energy density and entropy [7] (an unphysical pion mass was also an issue on the lattice side but that has now been resolved). Using the PDG lists from 2004 predictions were made that missing states would improve the fits to Lattice QCD results [5, 8, 9], which were later confirmed [10] when the PDG's 2014 list [11] was released. However, more massive resonances should not contribute strongly to the total pressure and, thus, if further missing states are measured it is very unlikely that they would affect the comparisons with Lattice QCD thermodynamic quantities. Additionally, such comparisons make it very difficult to determine the quantum numbers of missing resonances and, thus, more differential observables from Lattice QCD are currently being introduced. As a final note, it has also been postulated that missing states can assist in understanding phase changes from hadronic to deconfined matter and the order of the phase transition [12–17].

3. **Searching for Missing Resonances Assuming an Exponential Mass Spectrum**

In the 1960's Hagedorn [4] suggested that QCD resonances followed an exponentially increasing mass spectrum. In his picture, there was a limiting temperature T_H above which as one adds in more energy to the system the temperature would not increase but rather it would open up new degrees of freedom.

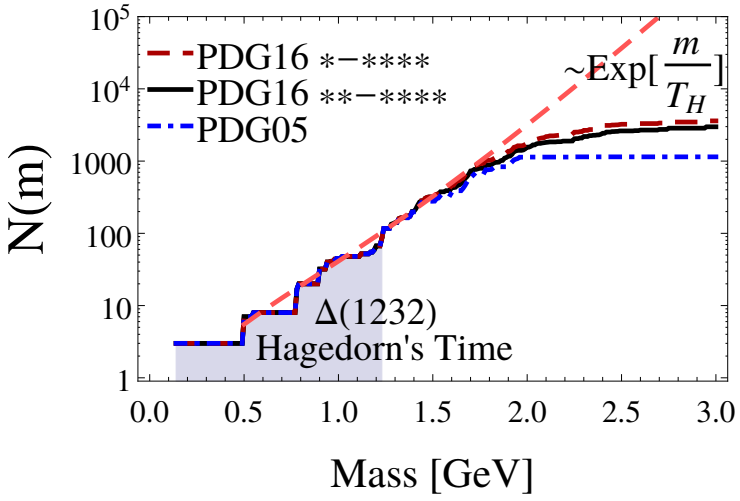

Figure 1: Mass spectrum of all known (light and strange) hadrons as listed in the PDG from 2004 [18] and 2016 [19] either for more well-measured states (**-****) or all possibly measured states (*-****).

In Hagedorn's time resonances were only measured up to $\Delta(1232)$. However, in the most recent release from the Particle Data Group (PDG) [19] (light and strange) hadrons were

measured up to $m \sim 2.5$ GeV. One can see in Fig. 1 that the mass range that demonstrates an exponentially increasing mass spectrum has expanded significantly from the 1960's and, in fact, even between 2004 to 2016 many new states have been measured (although reservations regarding an exponential mass spectrum were also discussed here [20]).

Returning to Fig. 1, the mass spectrum of all light and strange hadrons are plotted versus their mass such that:

$$N(m) = \sum_i d_i \Theta(m - m_i) \tag{2}$$

where d_i is their degeneracy and m_i is the mass of the i^{th} resonance. The exponential fit made in Fig. 1 is based upon Hagedorn's Ansatz for the degeneracy of "Hagedorn States" (i.e., the massive states missing from the exponentially increase mass spectrum):

$$\rho(M) = \int_{M_0}^{M} \frac{A}{[m^2 + (m_0)^2]^a} e^{\frac{m}{T_H}} dm \tag{3}$$

where m_0 is the mass of the lowest stable particle of the spectrum, $T_H = 165$ MeV is the Hagedorn temperature such that $T_c \leq T_H$ (a discussion on the choice of T_H follows below), M_0 is the minimum mass where Hagedorn states begin, and A is a free parameter. The power of a has a non-trivial affect such that when $a = 3/2$ Hagedorn states are more likely to decay into two body decays and when $a = 5/4$ multi-body decays are more likely [21]. I assume that multi-body decays are more likely with heavier resonances (and a brief glance through the PDG booklet confirms this assumption) so $a = 5/4$ is taken.

In Refs. [22–24], the known hadrons were separated by families (light mesons, strange mesons etc.) in order to extract their individual mass spectra. Here I return to this approach to determine:

- if all families see an exponentially increasing mass spectrum,
- if there are any gaps in the mass spectrum that could possibly be filled with missing states,
- if there are variations in the needed Hagedorn temperature by species (following the idea in [25, 26]).

In Fig. 2, the mass spectra of the light mesons and baryons are shown where both are fitted to a temperature of $T_H = 155$ MeV, which is almost exactly what one would expect from Lattice QCD. Light mesons begin to deviate from an exponential mass spectrum at around $M \sim 1.5$ GeV whereas light baryons deviate around $M \sim 2$ GeV. In both cases a visible improvement was seen going from the PDG 2004 to 2016. For light hadrons the difference between *-**** states and **-**** states are negligible.

In Fig. 3, the strange mesons and baryons are shown by their strangeness content. Unlike for the light hadrons, a higher Hagedorn temperature of $T_H = 175$ MeV is needed in order to fit the mass spectra (the one exception being Omega baryons), which is in-line with the possibility that strange particles have a higher transition temperature than light ones. While $|S| = 1$ and $|S| = 2$ baryons work well with an exponential mass spectrum up to $M \sim 2$ GeV and $M \sim 1.7$ GeV, respectively, the strange mesons and Omega baryons do not fit well to

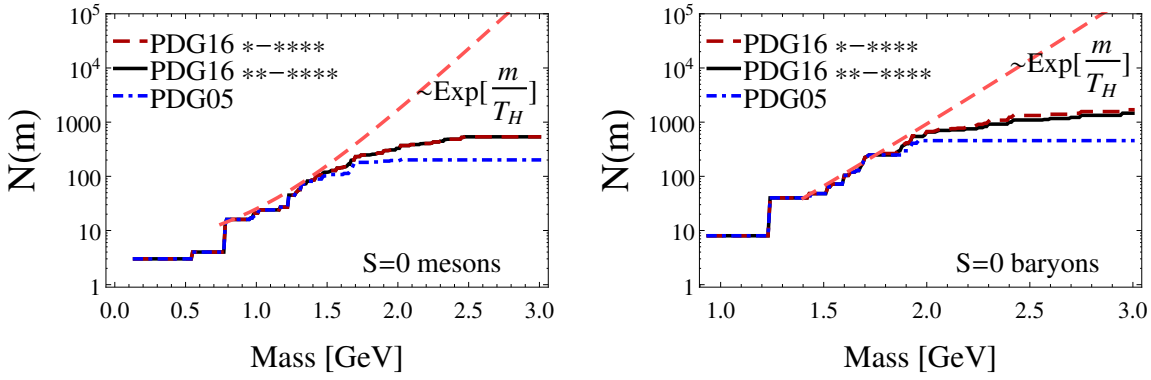

Figure 2: Mass spectrum of all known light mesons (left) and light baryons (right) as listed in the PDG from 2004 [18] and 2016 [19] either for more well-measured states (**-****) or all possibly measured states (*-****).

exponential mass spectra. In the case of strange mesons, it appears that there is a large gap in the $M = 1 - 1.5$ GeV region. For Omega baryons there are so few states that the only possibility is to fit the spectrum with a $T_H = 300$ MeV because the $T_H = 175$ MeV was significantly too stiff, which is well above the expected values. Thus, looking for mid-mass strange mesons and $|S| = 3$ baryons are likely candidates for missing states. Additionally, $|S| = 1$ and $|S| = 2$ may have missing states but most likely only in the more massive region $M \gtrsim 2$ GeV.

4. **Freeze-out Parameters and Chemical Equilibration Time**

In heavy-ion collisions, the system size is extremely small and is constantly expanding (at almost the speed of light) and cooling down. Thus, due to dynamical effects, hadrons may not manage to reach chemical equilibrium on such short time scales. However, due to the success of thermal fits [27], many believe that even on such short time scales chemical equilibrium can be reached. Studies found that $2 \leftrightarrow 2$ body reactions were not able to reach chemical equilibrium on such short time scales, especially at SPS energies and higher. It was then suggested that multi-mesonic reactions could speed up chemical equilibration times [28, 29] to explain SPS energies, however, with the known resonances it was still not enough to explain RHIC data [30]. To describe RHIC energies extra, massive resonances were needed that had large decay widths and could act as a catalyst to speed up hadronic reactions [31–38].

In Fig. 4, the description of these missing states from [34, 35] is shown within a cooling, expanding fireball compared to experimental data from RHIC. Because all reactions are dynamical, there is not a set “freeze-out temperature" but each species is allowed to reach chemical equilibrium on its own, which varies according to the description of the Hagedorn Spectrum, branching ratios, and initial conditions. A summary of the final particle ratios is shown in Fig. 5 compared to LHC experimental particle ratios.

Further studies have investigated if these missing resonances could affect the freeze-out temperature of hadrons [6, 39], i.e., at what temperature hadrons reach chemical equilibrium. However, it is unlikely that additional states beyond the PDG 2004/2016 will strongly af-

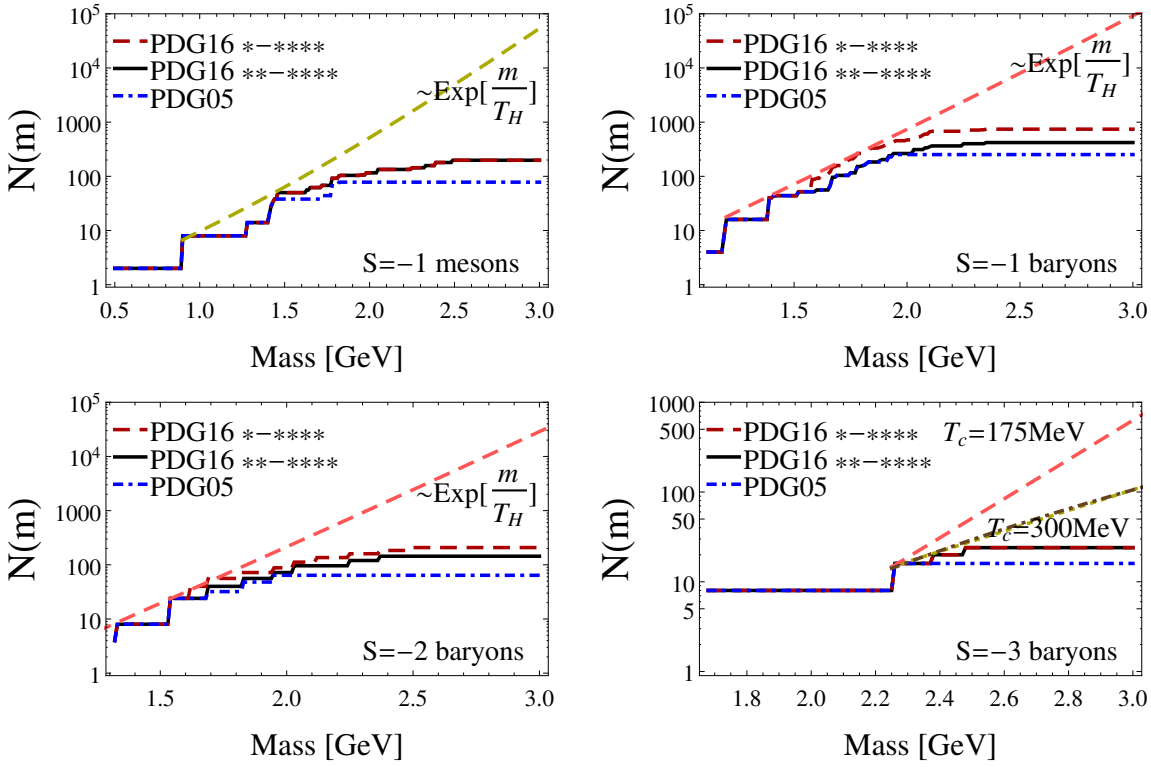

Figure 3: Mass spectrum of all known strange hadrons (mesons and baryons $|S| = 1 - 3$) as listed in the PDG from 2004 [18] and 2016 [19] either for more well-measured states (**-****) or all possibly measured states (*-****).

fect the freeze-out temperature [40]. Additionally, they were proposed as a solution for the tension between strange and light particles yields in theoretical models [6, 41, 42] though another likely solution may be a difference between the light and strange freeze-out temperatures [25, 26].

5. Transport Coefficients and Hydrodynamics

One of the most significant findings in heavy-ion collisions is that the Quark Gluon Plasma is a nearly perfect fluid (extremely small viscous effects), which can be well described by relativistic viscous hydrodynamics (for a review, see [43]). Adding in missing resonances helped to explain the extremely low shear viscosity to entropy density ratio expected at the phase transition between the hadron gas phase and the Quark Gluon Plasma [5, 9] as shown on the left in Fig. 6. This calculation also gave support to the presence of a peak in the bulk viscosity [44] at the phase transition region, as shown on the right in Fig. 6.

The major signature of perfect fluidity in heavy-ion collisions is known as elliptical flow, v_2. Elliptical flow is the second Fourier coefficient of the particle spectra and indicates that there is a strong (spatial) elliptical shape in the initial conditions, which is turned into an elliptical shape in momentum space due to the Quark Gluon Plasma's nearly perfect fluid-like nature. If the Quark Gluon Plasma did not act as a fluid or if it was very viscous than $v_2 \sim 0$.

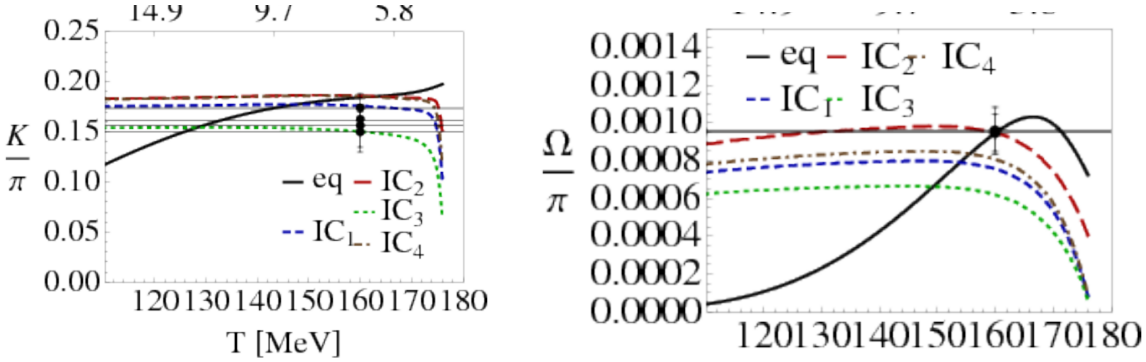

Figure 4: K/π ratio and Ω/π ratio in a cooling, expanding fireball where the reactions are driven by Hagedorn states [34, 35] compared to RHIC data.

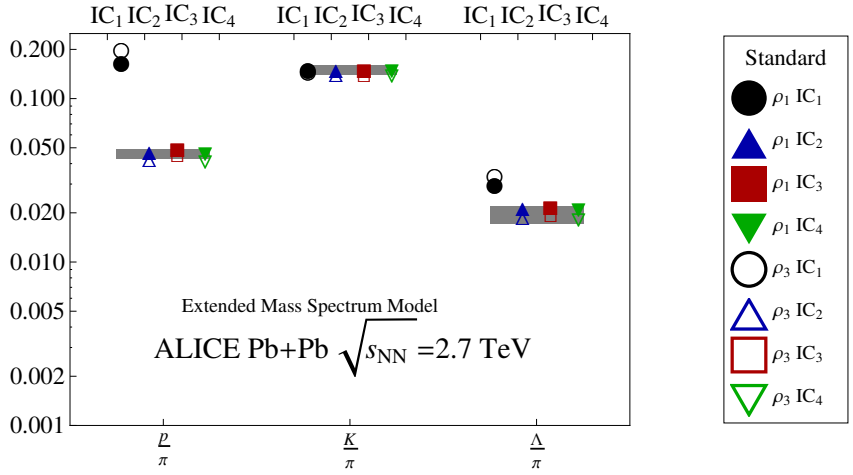

Figure 5: Particle ratios calculated within a dynamical multi-body interaction model using Hagedorn states [34, 35] compared to ALICE data.

In Ref. [45], the effects of adding in missing states were studied on v_2. For high momenta and higher freeze-out temperatures extra resonances suppressed elliptical flow. Thus, missing states not included in hydrodynamical models introduce a systematic error in comparisons of v_2 to experimental data. Recently, the hadron gas phase was shown to play a significant role in photon production [46] though theoretical calculations still underpredict experimental photon yields. It would be interesting to see if effects from missing resonances play a role in solving the photon "puzzle".

6. Conclusions

In conclusion, missing resonances can affect various aspects of heavy-ion collisions. The dynamics of the hadron gas phase plays a crucial role in comparisons between theoretical models and experimental data. If there are missing resonances, they contribute as a source of systematic error in all theoretical calculations. Using an exponential mass spectra, there

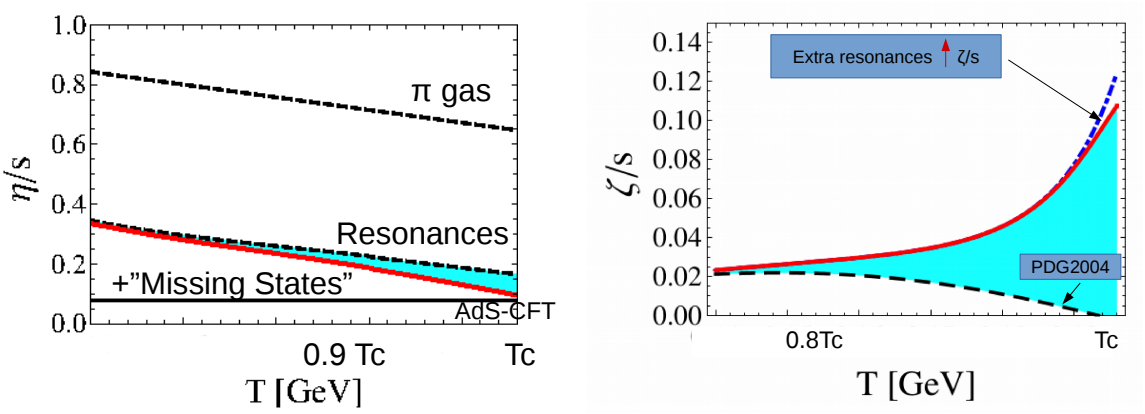

Figure 6: The effect of adding in missing resonances to the shear viscosity to entropy density ratio (left) and bulk viscosity to entropy density ratio (right) within the hadron gas phase [5].

may be a gap in the strange mesons between $m = 1 - 1.5$ GeV, which is a potential region to search for new resonances. Therefore, strange hadron observables may be especially sensitive to missing states.

Due to the sensitivity of heavy-ion collisions to missing resonances, a strong collaboration between the fields of hadron spectroscopy and heavy-ion collisions could be extremely fruitful. For instance, the creation of a database that included all the known PDG resonances (and eventually also states predicted by Lattice QCD or Quark Models) with all their characteristic information (degeneracy, mass, quantum numbers, decay channels, etc) sorted by their star rating in a format that is compatible with heavy-ion codes, would significantly speed up comparisons between the fields and allow for systematic checks on which resonances influence heavy-ion observables the most.

7. **Acknowledgments**

This work is supported by the National Science Foundation under grant no. PHY-1513864.

References

[1] J. J. Dudek *et al.*, Phys. Rev. Lett. **103**, 262001 (2009); arXiv:0909.0200 [hep-ph].

[2] S. Capstick and N. Isgur, Phys. Rev. D **34**, 2809 (1986), AIP Conf. Proc. **132**, 267 (1985).

[3] D. Ebert, R. N. Faustov, and V. O. Galkin, Phys. Rev. D **79**, 114029 (2009); arXiv:0903.5183 [hep-ph].

[4] R. Hagedorn, Nuovo Cim. Suppl. **3**, 147 (1965).

[5] J. Noronha-Hostler, J. Noronha, and C. Greiner, Phys. Rev. Lett. **103**, 172302 (2009); arXiv:0811.1571 [nucl-th].

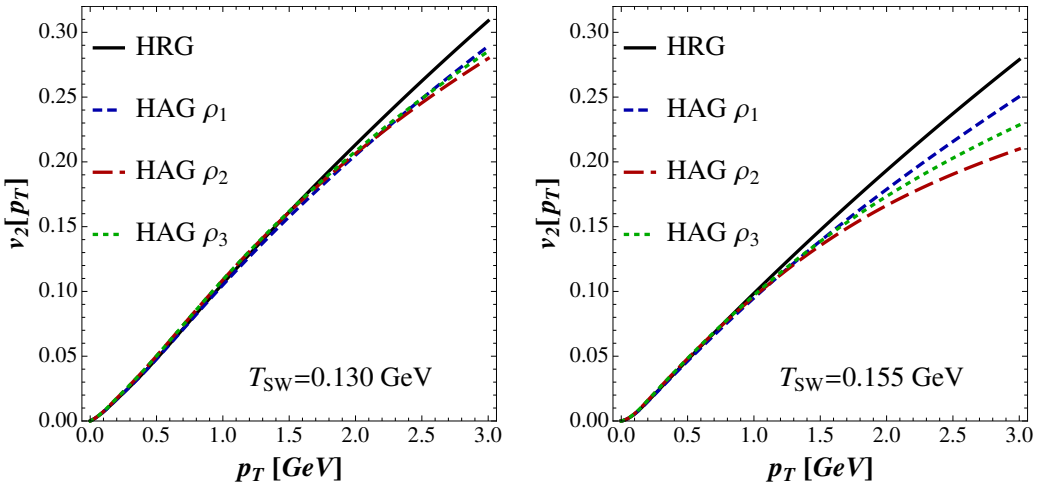

Figure 7: Effect of different descriptions of Hagedorn states on the elliptical flow at $T_{SW} = 130$ MeV (left) and $T_{SW} = 155$ MeV (right) from [45]. Solid line includes all PDG2014 resonances.

[6] A. Bazavov *et al.*, Phys. Rev. Lett. **113**, 072001 (2014); arXiv:1404.6511 [hep-lat].

[7] F. Karsch, K. Redlich, and A. Tawk, Eur. Phys. J. C **29**, 549 (2003), arXiv:hep-ph/0303108 [hep-ph].

[8] A. Majumder and B. Muller, Phys. Rev. Lett. **105**, 252002 (2010); arXiv:1008.1747 [hep-ph].

[9] J. Noronha-Hostler, J. Noronha, and C. Greiner, Phys. Rev. C **86**, 024913 (2012); arXiv:1206.5138 [nucl-th].

[10] S. Borsanyi *et al.*, Phys. Lett. B **730**, 99 (2014); arXiv:1309.5258 [hep-lat].

[11] K. A. Olive *et al.* (Particle Data Group), Chin. Phys. C **38**, 090001 (2014).

[12] L. G. Moretto, K. A. Bugaev, J. B. Elliott, and L. Phair, Europhys. Lett. **76**, 402 (2006); arXiv:nucl-th/0504010 [nucl-th].

[13] V. V. Begun, M. I. Gorenstein, and W. Greiner, J. Phys. G **36**, 095005 (2009); arXiv:0906.3205 [nucl-th].

[14] I. Zakout, C. Greiner, and J. Schaffner-Bielich, Nucl. Phys. A **781**, 150 (2007); arXiv:nucl-th/0605052 [nucl-th].

[15] L. Ferroni and V. Koch, Phys. Rev. C **79**, 034905 (2009); arXiv:0812.1044 [nucl-th].

[16] K. A. Bugaev, V. K. Petrov, and G. M. Zinovjev, Phys. Rev. C **79**, 054913 (2009); arXiv:0807.2391 [hep-ph].

[17] A. I. Ivanytskyi, K. A. Bugaev, A. S. Sorin, and G. M. Zinovjev, Phys. Rev. E **86**, 061107 (2012); arXiv:1211.3815 [nucl-th].

[18] S. Eidelman *et al*. (Particle Data Group), Phys. Lett. B **592**, 1 (2004).

[19] C. Patrignani **et al**. (Particle Data Group), Chin. Phys. C **40**, 100001 (2016).

[20] T. D. Cohen and V. Krejcirik, J. Phys. G **39**, 055001 (2012); arXiv:1107.2130 [hep-ph].

[21] S. C. Frautschi, Phys. Rev. D **3**, 2821 (1971).

[22] W. Broniowski, W. Florkowski, and L. Ya. Glozman, Phys. Rev. D **70**, 117503 (2004); arXiv:hep-ph/0407290 [hep-ph].

[23] S. Chatterjee, R. M. Godbole, and S. Gupta, Phys. Rev. C **81**, 044907 (2010); arXiv:0906.2523 [hep-ph].

[24] P. M. Lo, M. Marczenko, K. Redlich, and C. Sasaki, Phys. Rev. C **92**, 055206 (2015); arXiv:1507.06398 [nucl-th].

[25] R. Bellwied *et al.*, Phys. Rev. Lett. **111**, 202302 (2013); arXiv:1305.6297 [hep-lat].

[26] J. Noronha-Hostler *et al.*, (2016), arXiv:1607.02527 [hep-ph].

[27] A. Andronic, P. Braun-Munzinger, and J. Stachel, Nucl. Phys. A **772**, 167 (2006); arXiv:nucl-th/0511071 [nucl-th].

[28] R. Rapp and E. V. Shuryak, Phys. Rev. Lett. **86**, 2980 (2001); arXiv:hep-ph/0008326 [hep-ph].

[29] J. I. Kapusta and I. Shovkovy, Phys. Rev. C **68**, 014901 (2003); arXiv:nucl-th/0209075 [nucl-th].

[30] U. Heinz and G. Kestin, PoS **CPOD2006**, 038 (2006); arXiv:nucl-th/0612105 [nucl-th].

[31] C. Greiner *et al.*, J. Phys. G **31**, S725 (2005); arXiv:hep-ph/0412095 [hep-ph].

[32] S. Pal and P. Danielewicz, Phys. Lett. B **627**, 55 (2005); arXiv:nucl-th/0505049 [nucl-th].

[33] J. Noronha-Hostler, C. Greiner, and I. A. Shovkovy (2007), arXiv:nucl-th/0703079 [nucl-th].

[34] J. Noronha-Hostler, C. Greiner, and I. A. Shovkovy, Phys. Rev. Lett. **100**, 252301 (2008); arXiv:0711.0930 [nucl-th].

[35] J. Noronha-Hostler, M. Beitel, C. Greiner, and I. Shovkovy, Phys. Rev. C **81**, 054909 (2010); arXiv:0909.2908 [nucl-th].

[36] S. Pal and W. Greiner, Phys. Rev. C **87**, 054905 (2013).

[37] M. Beitel, K. Gallmeister, and C. Greiner, Phys. Rev. C **90**, 045203 (2014); arXiv:1402.1458 [hep-ph].

[38] M. Beitel, C. Greiner, and H. Stoecker, Phys. Rev. C **94**, 021902 (2016); arXiv:1601.02474 [hep-ph].

[39] J. Noronha-Hostler, H. Ahmad, J. Noronha, and C. Greiner, Phys. Rev. C **82**, 024913 (2010); arXiv:0906.3960 [nucl-th].

[40] J. Noronha-Hostler *et al.* (2016), arXiv:1610.00221 [nucl-th].

[41] J. Noronha-Hostler and C. Greiner, (2014), arXiv:1405.7298 [nucl-th].

[42] J. Noronha-Hostler and C. Greiner, Nucl. Phys. A **931**, 1108 (2014); arXiv:1408.0761 [nucl-th].

[43] U. Heinz and R. Snellings, Ann. Rev. Nucl. Part. Sci. **63**, 123 (2013); arXiv:1301.2826 [nucl-th].

[44] F. Karsch, D. Kharzeev, and K. Tuchin, Phys. Lett. B **663**, 217 (2008); arXiv:0711.0914 [hep-ph].

[45] J. Noronha-Hostler *et al.*, Phys. Rev. C **89**, 054904 (2014); arXiv:1302.7038 [nucl-th].

[46] J.-F. Paquet *et al.*, Phys. Rev. C **93**, 044906 (2016); arXiv:1509.06738 [hep-ph].

2.18 Thermal Shifts, Fluctuations, and Missing States

Enrique Ruiz Arriola
Departamento de Física Atómica, Molecular y Nuclear and
Instituto Carlos I de Física Teórica y Computacional
Universidad de Granada
E-18071 Granada, Spain

Wojciech Broniowski
Institute of Physics, Jan Kochanowski University
25-406 Kielce, Poland &
The H. Niewodniczański Institute of Nuclear Physics
Polish Academy of Sciences
PL-31342 Cracow, Poland

Eugenio Megías
Max-Planck-Institut für Physik (Werner-Heisenberg-Institut)
D-80805 Munich, Germany &
Departamento de Física Teórica
Universidad del País Vasco UPV/EHU, Apartado 644
48080 Bilbao, Spain

Lorenzo L. Salcedo
Departamento de Física Atómica, Molecular y Nuclear and
Instituto Carlos I de Física Teórica y Computacional
Universidad de Granada
E-18071 Granada, Spain

Abstract

Thermal shifts and fluctuations at finite temperature below the deconfinement crossover from hadronic matter to the quark-gluon plasma provide a viable way to search for missing states with given quantum numbers in the hadronic spectrum. We analyze three realizations of the hadron resonance gas model in the light quark (uds) sector: the states from the Particle Data Group tables with or without width and from the Relativized Quark Model. We elaborate on the meaning of hadronic completeness and thermodynamical equivalence on the light of lattice QCD trace anomaly, heavy quark entropy shift and baryon,charge and strangeness susceptibilities.

1. Introduction

The concept of missing states in QCD is intimately related to the completeness of the hadronic spectrum. The issue was anticipated by Hagedorn in the mid 60's [1] when analyzing the mass-level density $\rho(M)$ and *predicting* the bulk of states at higher masses, which later on were experimentally confirmed. This also implies that the states may be *counted* one

by one (and hence ordered) by, say, the cumulative number of states function,

$$N(M) = \sum_n g_n \theta(M - M_n)\,, \tag{1}$$

with g_n the total degeneracy and $\rho(M) = dN(M)/dM$. Updated analyses of the Hagedorn hypothesis may be found in [2, 3]. The function $N(M)$ assumes integer values, and the best mass resolution is $\Delta M = \min_n(M_{n+1} - M_n)$. For bound states, where the spectrum is discrete, this is a well defined procedure. In the continuum, this can only be done by putting the system in a box with finite but sufficiently large volume which acts as an infrared cut-off $V^{1/3}\Delta M \gg 1$. The ultraviolet cut-off is the maximum mass $M_{\rm max}$ in Eq. (1).

The commonly accepted reference for hadronic states is the Particle Data Group (PDG) table [4], a compilation reflecting a consensus in the particle physics community and which grades states *,**,***, and ****, according to the growing confidence in their existence, respectively. Global features of the hadronic spectrum may depend on whether we decide to promote or demote their significance, according to some theoretical prejudice. Of course, we expect the PDG hadronic states to have a one-to-one correspondence with colour neutral eigenstates of the QCD Hamiltonian; indeed, ground and some excited states have been determined on the lattice [5]. For hadronic states with only light (uds) quarks the maximum mass, $M_{\rm max}$, recorded by PDG is around 2.5 GeV for mesons and baryons, hence currently $N(M_{\rm max}) \sim 2.5 \times 10^3$. So far, the states listed by PDG echo the standard quark model classification for mesons ($\bar{q}q$) and baryons (qqq). Because of this feature, it will be pertinent to consider also the Relativized Quark Model (RQM) for mesons [6] and Baryons [7], as first done for $N(M)$ in [8] (Fig. 9). The remarkable coincidence $N_{\rm PDG}(M) \sim N_{\rm RQM}(M)$ up to $M_{\rm max}$ for *bot* mesons and baryons has been shown in Ref. [9]. The so-called "further states" may or may not be confirmed or expected and have not been clearly regarded by the PDG as identified, although they could be exotic tetraquarks, $\bar{q}q\bar{q}q$, pentaquarks, $\bar{q}qqqq$, glueballs gg, ggg or hybrids $\bar{q}qg$ [10].

In this contribution we analyze thermodynamic measures (various susceptibilities) which are sensitive to missing states. The setup corresponds to heating up the vacuum without dissolving its constituent hadrons into quarks and gluons and testing quark-hadron duality at temperatures below $T_c \sim 150$ MeV. Obviously, such a framework is inefficient for individual states, but becomes competitive if globally a relatively large number of states are missing. As reported in [11, 12] the Hagedorn conjectured behaviour of $N(M) \sim Ae^{M/T_H}$ for $M > M_{\rm max}$ may influence the results close to T_c, at temperatures above $T > 140$ MeV. According to [12], there is not much room for such states in the one-body observables, where they would spoil the agreement with the lattice data, unless suitable repulsion between states is simultaneously incorporated. Here will make no attempt to complete the spectrum beyond $M_{\rm max}$.

2. Prehistory of Missing States

The use of thermodynamical arguments to characterize the existence of missing states is a rather old subject which goes back to the early beginnings of the kinetic theory of gases and the equipartition theorem. In its most general form it states that every degree of freedom

contributes to the mean energy with $\frac{1}{2}k_BT$.[1]. Therefore $\bar{E} = N\nu k_BT/2$, where ν is the total number of degrees of freedom. Generally, $\nu = \nu_{\rm translation} + \nu_{\rm vibration} + \nu_{\rm rotation}$ and the molar specific heat is $c_V/R = \nu/2$. A major obstacle at the time was pointed out by J. C. Maxwell in 1860 in connection to the specific heat of the diatomic gas such as, e.g., H_2, where a priori the total number of degrees of freedom is $\nu = 3_{\rm trans} + 2_{\rm vib} + 2_{\rm rot} = 7$. This would imply $c_V/R = 7/2$, whereas experimentally at room temperature one has $c_V/R \approx 5/2$. This is because the vibrational degrees of freedom are not active due to high excitation energy, and become visible only as the dissociation temperature of ~ 3200 K is approached. Likewise, as T is decreased, the rotational degrees of freedom are also frozen and below ~ 70 K, $c_V/R = 3/2$, as for the monoatomic molecules.

In modern terms the "freezing" of degrees of freedom is related to the quantization of energy levels for the Hamiltonian $H\Psi_n = E_n\Psi_n$ with energy eigenvalues above the temperature, $E_n > T$, contributing negligibly to the partition function

$$Z = {\rm Tr}e^{-H/T} = \sum_n e^{-E_n/T}. \tag{2}$$

In QCD, the quantized energy levels are the masses of the existing hadronic states and, like in the Maxwell argument, the states which are not activated when $M_n > T$ do not contribute.

3. Completeness of the Hadron Spectrum

Completeness of the listed PDG states [4] is a subtle issue. On the one hand they are mapped into the $\bar{q}q$ and qqq quark model states. On the other hand, most reported states are not stable particles but resonances produced as intermediate steps in a scattering process.

With a finite lifetime τ_R, they are characterized by a mass distribution $\rho_R(M)$, with a central value M_R and a width $\Gamma_R \sim \hbar/\tau_R$. From a rigorous point of view resonances are poles of the *exact* amplitude in the second Riemann sheet in the complex s plane at $s = M^2 - iM\Gamma$. For multichannel scattering with N channels one has 2^N Riemann sheets, depending on which cuts have been crossed (see, e.g., [15, 16] for discussions in the meson-baryon $S = 0, -1$ sectors). Despite the rigor of these definitions, complex energies are not directly measured. An analytic continuation of a phenomenological and approximate scattering amplitude, taking into account a process dependent background, is needed and the arbitrariness grows with the width of the resonance [17] (see, e.g., for the specific 0^{++} case [18]). On average, most of the resonances listed by PDG [4] can be regarded as narrow, since one finds $\langle\Gamma_R/M_R\rangle = 0.12(8)$ ***both*** for mesons and baryons [19, 20], a fact numerically consistent

[1]The story around this principle illustrates many of the issues under discussion, including the contribution of an anonymous referee [13] D. Bernoulli [14] was the first who found in 1738 that the Boyle-Mariotte, Gay-Lussac, and Charles equations could be unified and understood by means of Newton's equations and in statistical terms. His work was forgotten, and only in 1845 J. J. Waterston submitted a paper to the Philosophical Transactions of the Royal Society (PTRS) which was rejected with a remark "The paper is nothing but nonsense, unfit even for reading before the Society". Hence this work was also ignored. Maxwell, in 1859, managed to publish the case of rigid molecules, and Boltzmann generalized it in 1868 to its modern form including rotational and vibrational degrees of freedom. Lord Rayleigh in 1895, found by chance Waterston's paper in the archives and decided to publish it in PTRS twelve years after Waterston's death with a commentary: "had he put forward his investigation as a development of Bernoulli a referee migh have hesitated to call it nonsense. It is probable that Waterston was unaquainted with his work.".

with the large N_c theoretical expectation $\Gamma_R/M_R = \mathcal{O}(N_c^{-1})$ [21]. In the Hamiltonian picture, resonances are identified as the so-called Gamow states and are not normalizable in the usual Hilbert space, as they are not conventional irreducible representations of the Poincarè group [22]. The completeness relation involves bound states and the continuum, which can be rewritten as a discrete sum of the Gamow states and a remainder [23].

The meaning of completeness is fairly clear within a given Hilbert space $\mathcal{H}$ with specified degrees of freedom when only bound states are possible. For instance, if we restrict ourselves to the meson $(\bar{q}q)$ or baryon (qqq) sectors, such as in RQM [6, 7], we can diagonalize the $\bar{q}q$ and qqq Hamiltonians with confining potentials in a given already complete basis, which is truncated but large enough that states with $M_n \leq M_{\max}$ converge. Thus we write

$$\mathcal{H}_{\rm RQM} = \mathcal{H}_{\bar{q}q} \oplus \mathcal{H}_{qqq} \oplus \mathcal{H}_{\bar{q}\bar{q}\bar{q}} \tag{3}$$

Within this framework, hadrons are stable, extended, and composite particles. This is explicitly illustrated by the virial relations in the massless quark limit [9] $M_{\bar{q}q} = 2\sigma\langle r\rangle_{\bar{q}q}$ and $M_{qqq} = N_c\sigma\langle r\rangle_{qq}$, which shows that hadrons are larger the heavier they become. Many of these states may decay by strong processes, such as $\rho \to 2\pi$ or $\Delta \to N\pi$, where a coupling to the continuum is needed by incorporating the $\mathcal{H}_{\bar{q}q\bar{q}q}$ and $\mathcal{H}_{\bar{q}qqqq}$ Fock state. As a result, the pole mass is shifted into the complex plane $M \to M + \Delta M - i\Gamma/2$. The mass-shift $\Delta M \sim \Gamma$ depends parametrically on the coupling to the continuum $\Delta M \sim \Gamma$ so that in the large N_c limit, $\Delta M/M = \mathcal{O}(N_c^{-1})$ [24].

On the lattice, hadrons are constructed as interpolating fields in a finite-volume box. Completeness proceeds along similar lines, with the important modification that resonances are characterized by volume-independent and real mass shifts. The connection to physical resonances in the complex energy plane requires also analytical extrapolation (for a review see, e.g., [25]).

4. Thermodynamic Equivalence

Be it the PDG [4], RQM [6, 7], or the lattice excited QCD [5], the partition function can be constructed from the (complete) energy localized colour neutral eigenstates, Eq. (2). The lattice at finite temperatures, or the ultrarelativistic heavy ions collisions, generate global colour neutral configurations which along the crossover are expected to delocalize. Most of the emerging physical quark-hadron duality picture has to do with the thermodynamical equivalence of different approaches.

According to the quantum virial expansion [26] one can compute the partition function from the knowledge of the S-matrix in the complete Hilbert space, i.e., involving all possible processes with any number of elementary particles in both the initial and final states, $n \to m$. In practice, hadrons have been taken as the building blocks in this approach, which for obvious practical reasons has never been taken beyond the $2 \to 2$ reactions, where the corresponding phase shifts are involved. In the case of narrow resonances one can replace the total contribution entering in terms of phase shifts by the resonance itself [27], whereby the resonance can be assumed to be elementary and point-like [28]. The result conforms to the Hadron Resonance Gas (HRG) as initially proposed by Hagedorn [1]. This provides the formal basis for modern HRG calculations using the PDG compilation. As mentioned

above, most states entering the HRG are resonances with a given width, Γ. Therefore we will also consider the effect of smearing the mass distribution according to the replacement

$$\sum_R F(m_R^2) \to \int d\mu^2 F(\mu^2) \Delta_\Gamma(\mu^2 - m_R^2) \tag{4}$$

for an observable $F(\mu^2)$. [2]

However, the elementary constituents are both quarks and gluons. A different derivation proceeds along chiral quark-gluon models with a quantum and local Polyakov loop [33, 34]. [3] The action corresponds to creating, e.g., a quark at location $\vec{x}$ and momentum $\vec{p}$ in the medium

$$e^{-E(\vec{p})/T} \Omega(\vec{x})^\dagger, \tag{5}$$

where in the static gauge $\Omega(\vec{x}) = e^{igA_4(\vec{x})/T}$. Consequently, the total action can be separated into different quark and gluon sectors according to the low temperature partonic expansion around the vacuum [9, 37]

$$Z = Z_0 + Z_{\bar{q}q} + Z_{qqq} + Z_{\bar{q}\bar{q}\bar{q}} + \cdots \sim Z_{\rm RQM}. \tag{6}$$

Subsequent hadronization of $\bar{q}q$ and qqq states uses the cluster properties of the Polyakov loop correlator and group properties of the Haar measure, as well as the quantum, composite and extended nature of hadronic states. One appealing feature of this "microscopic" derivation of the HRG is the counting of states according to the quark model for the lowest Fock state components, but ambiguities arise when a given colour neutral multiquark state admits a separation into colour neutral irreducible subsystems [9, 38]. We take this result as our justification to use RQM. [4]

The fact that we use thermodynamic quantities to make a quantitative comparison does not sidestep the problem of discriminating different spectra. The best example is provided by a direct comparison of HRG using either PDG or RQM [6, 7] in terms of the trace anomaly, $\mathcal{A}(T) \equiv (\epsilon - 3P)/T^4$ which are hardly indistinguishable within the lattice QCD uncertainties from the WB [39] and HotQCD [40] collaborations (see Fig. 1 of Ref. [9]). As already mentioned the states with $M > M_{\rm max}$ with an exponential Hagedorn distribution are relevant below T_c [12] only at $T > 140$ MeV, and their contribution may be overcome with repulsive effects. Actually, the volume effects are expected to play a significant role; the excluded volume exceeds the total volume around $T \lesssim T_c$ (see Fig. 9 of Ref. [9]).

[2] Ideally the profile function should be determined from the scattering phase-shift [27], which displays cancellations [29, 30] and irrelevance of some weakly bound states [31] but it is not always available. Here we take a simple normalized Gaussian profile distribution. A Breit-Wigner representation works well around the resonance, but it has very long tails which do not faithfully represent the background. An upper bound for the error is to use the half-width rule [19, 32] according to which PDG masses are varied within half the width, i.e., taking $M_R \pm \Gamma_R/2$. We do not use this large N_c motivated prescription here as we feel that it largely overestimates the uncertainties for *all resonances* in the $N_c = 3$ world.

[3] This is unlike the more popular PNJL model [35, 36], where the quantum and local nature of $\Omega(\vec{x})$ is ignored, thus introducing an undesirable group coordinates dependence. In addition, in PNJL the Polyakov loop in the adjoint representation is not quenched, contradicting lattice calculations.

[4] Bound state masses are shifted when coupled to the continuum, so if we take a simple average estimate $\langle \Delta M/M \rangle_{\rm RQM} \sim \langle \Gamma/M \rangle_{\rm PDG} \sim 0.12(8)$. This roughly corresponds to take $5\% - 20\%$ uncertainty in T.

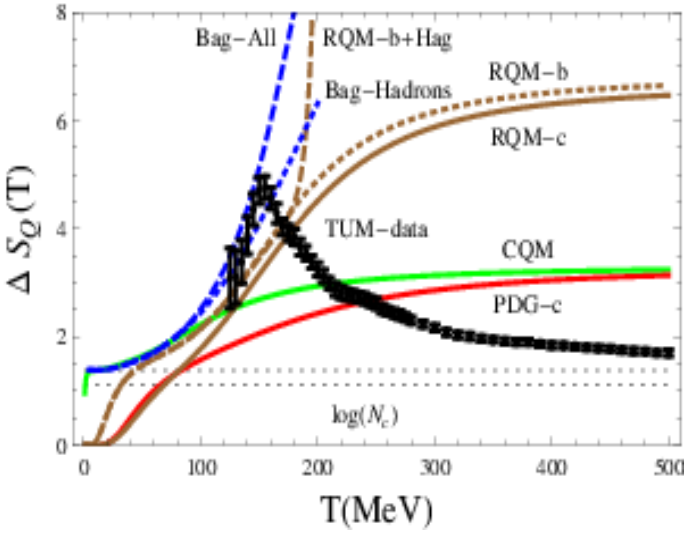

Figure 1: The entropy as a function of the temperature. We show results from various hadronic models: the bag model including all ($Q\bar{q}$, Qqq and $Q\bar{q}g$) states and just hadrons, the RQM with one c- or b-quark and the PDG states with one c-quark. The Hagedorn extrapolation of the b-spectrum is also displayed. We also plot the CQM with uds quarks and constituent mass $M = 300\ MeV$ and the bare $m_u = 2.5\ MeV$, $m_d = 5\ MeV$, $m_s = 95\ MeV$ masses. Horizontal lines mark $\Delta S_Q(0) = \log 2N_f$, with $N_f = 2$ the number of light degenerate flavours, and $\Delta S_Q(\infty) = \log(N_c)$. Lattice data for 2+1 flavours are taken from Ref. [46].

5. Thermal Shifts

The idea of thermal shifts is to study the change of thermodynamic quantities under the presence of local external sources. This looks very much like adding an impurity to a macroscopic system or adding a grain of salt to a bunch of snow. By looking a these thermal shift we may also assess a possible existence of missing states. An interesting hadronic example is provided by the free energy shift caused by a heavy quark placed in a hot medium with vacuum quantum numbers, which corresponds to a ratio of partition functions which can be identified with the Polyakov loop expectation value. This free energy shift is ambiguous and hence it is better to deal with the corresponding entropy shift and the specific heat, which are directly measurable quantities. A hadronic representation of Polyakov loop and its entropy has been analyzed [41, 42]. The implications of thermal shifts due to a heavy source or a heavy $Q\bar{Q}$ pair located at a fixed distance r at the hadronic level has recently been considered in [43–45].

Fig. 1 from Ref. [43] makes a good case for different categories of missing charm or bottom states. On the one hand the PDG is clearly insufficient to describe the entropy shift. So, we clearly miss higher mass states. Guided by the thermodynamic equivalence of PDG and RQM in the uds sector [9], we may complete the PDG spectrum using the RQM in the c- or b- sectors. As we see there is a big improvement and, moreover, the change when going from c to b is sufficiently small. Nonetheless, we have still missing states, a feature that is not mended when extending the spectrum a la Hagedorn. When a Bag model with the heavy

source located at the center is considered for singly heavy hadrons $Q\bar{q}$, Qqq, and a hybrid $Q\bar{q}g$ the TUM lattice data are well reproduced.

6. Fluctuations

The connection between fluctuations and the abundance of hadronic resonances was pointed out by Jeon and Koch [47], who later [48] proposed it as a signal for the Quark-Gluon Plasma formation from the partition function (for pedagogical reviews see, e.g., [49, 50]). Implications for heavy ion collisions are reviewed in [51]. In Ref. [52], the event-by-event statistical analysis of ultrarelativistic heavy ions-collisions was compared to the HRG with a given chemical potential. Of course, any mismatch in this kind of analyses suggests missing resonances. Here we are concerned with the simplest vacuum zero density case. Actually, some authors have understood the significance of fluctuations as a possible hint of missing states [53].

Fluctuations of conserved charges, i.e., fulfilling $[Q_A, H] = 0$, are a way of selecting given quantum numbers [50] and become particularly simple in terms of the grand-canonical partition function which is given by

$$Z = \mathrm{Tr} e^{-(H-\sum_A \mu_A Q_A)/T} \qquad \Omega = -T \log Z. \tag{7}$$

with Ω the corresponding potential. One then gets

$$-\frac{\partial \Omega}{\partial \mu_A} = \langle Q_A \rangle_T, \quad -T \frac{\partial^2 \Omega}{\partial \mu_A \partial \mu_B} = \langle \Delta Q_A \Delta Q_B \rangle_T, \tag{8}$$

where $\Delta Q_A = Q_A - \langle Q_A \rangle_T$. In the uds sector the only conserved charges are the electric charge Q, the baryon charge B and the strangeness S, which is equivalent to the number of u, d, and s quarks. We consider the hot vacuum (no chemical potential) $\langle B \rangle_T = \langle Q \rangle_T = \langle S \rangle_T = 0$.

For $N_f = 2 + 1$, fluctuations have been computed on the lattice by the WB [54] and HotQCD [55] collaborations with the high temperature asymptotic limits

$$\chi_{BB}(T) = V^{-1} \langle B^2 \rangle_T \to \frac{1}{N_c} \tag{9}$$

$$\chi_{QQ}(T) = V^{-1} \langle Q^2 \rangle_T \to \sum_{i=1}^{N_f} q_i^2 \tag{10}$$

$$\chi_{SS}(T) = V^{-1} \langle S^2 \rangle_T \to 1, \tag{11}$$

where $(q_u, q_d, q_s, \dots) = (2/3, -1/3, -1/3, \dots)$. Higher order cumulants, such as skewness and kurtosis originally analyzed in Ref. [56], have also recently been computed more accurately [57], but we do not discuss them here.

In the hadron resonance model, the charges are carried by various species of hadrons, $Q_A = \sum_i q_A^{(i)} N_i$, where N_i is the number of hadrons of type i, hence

$$\langle \Delta Q_A \Delta Q_B \rangle_T = \sum_{i,j} q_A^{(i)} q_B^{(j)} \langle \Delta N_i \Delta N_j \rangle_T. \tag{12}$$

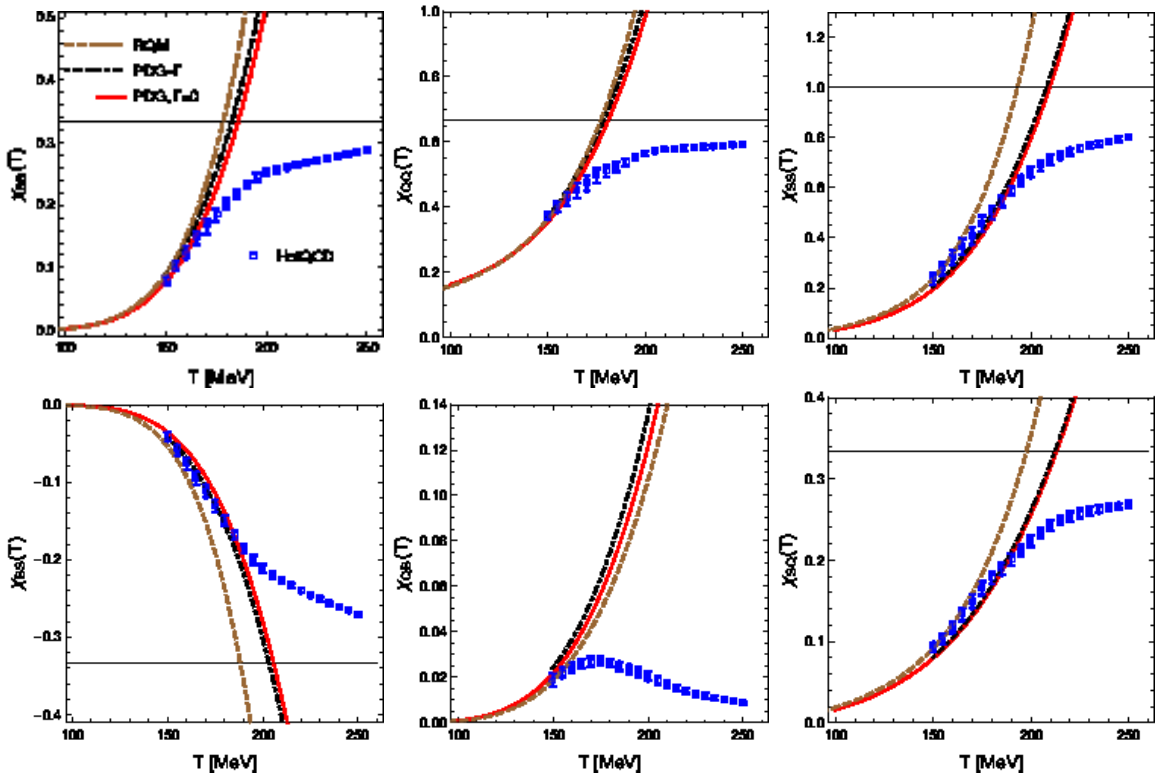

Figure 2: Baryon, charge and strangeness susceptibilities from HRG with the PDG, PDG(Γ) and RQM spectra, compared to the lattice HotQCD [55] data. WB data [54] are compatible with them so they are not plotted.

The average number of hadrons is

$$\langle N_i\rangle_T = V\int\frac{d^3k}{(2\pi)^3}\frac{g_i}{e^{E_{k,i}/T}+\eta_i} = \frac{VT^3}{2\pi^2}\sum_{n=1}^{\infty} g_i\frac{(-\eta_i)^{n+1}}{n}\left(\frac{M_i}{T}\right)^2 K_2(nM_i/T)$$

where $E_{k,i} = \sqrt{M_i^2+k^2}$, g_i is the degeneracy and $\eta_i = \mp 1$ for bosons/fermions respectively. In practice the Boltzmann approximation (i.e., just keeping $n = 1$) is sufficient. Regarding the fluctuations, since the different species are uncorrelated $\langle\Delta n_\alpha\Delta n_\beta\rangle_T = \delta_{\alpha\beta}\langle n_\alpha\rangle_T(1-\eta_\alpha\langle n_\alpha\rangle_T)$, for the occupation numbers. Since $\langle n_\alpha\rangle_T \ll 1$,

$$\langle\Delta Q_A\Delta Q_B\rangle_T \approx \sum_i q_A^{(i)}q_B^{(i)}\langle N_i\rangle_T. \tag{13}$$

Our results for the susceptibilities are depicted in Fig. 2 where we show the HotQCD lattice data [55] (the earlier WB data [54] are compatible with them so they are not included in the figure to avoid cluttering.). We compare with the standard HRG model, denoted as PDG, the HRG including a Gaussian width profile, which we denote as PDG (Γ), and the RQM.

Our scheme here is to include *all* states from PDG, which as mentioned are mapped into the standard quark model classification of mesons as $\bar{q}q$ and baryons as qqq as the only hadronic states. This choice of states provides a visible effect in the SB correlator bringing it closer to the lattice data as compared to [53] where only $****$ PDG states are considered. The inclusion of width effects is also generally quite sizeable and cannot be ignored, as it has routinely been done in many HRG comparisons in the past (see however [12, 32]). Nevertheless, there are other ways to include the width profile which will somehow blur the PDG(Γ) result, and a more systematic study, perhaps including also volume effects, would be most helpful.

The remarkable good agreement of the trace anomaly found between PDG and RQM [9] or the PDG(Γ) [12] compared with lattice QCD results from WB [39] and HotQCD [40] collaborations gets a bit spoiled in terms of the considered fluctuations, where these spectra may feature missing or exceeding states. For instance, a look at the BB correlation in Fig. 2 suggests that the RQM has too many baryonic states but not too many charged states. Therefore, the thermodynamic equivalence will depend on the quantum numbers, enhancing the relevance of a fluctuation analysis, as done here, in the discussion of quark-hadron duality.

7. Conclusions

In the present contribution we have revised the thermodynamical equivalence between the PDG, RQM, and lattice QCD for temperatures below the hadron-gas—quark-gluon-plasma crossover for the case of an entropy shift due to a heavy quark and fluctuations via Baryon, Charge and Strangeness susceptibilities as diagnostic tools for missing states.

The analysis of the entropy shift due to a heavy quark suggests that there are conventional (high mass) missing states in single charm, or bottom hadrons ($Q\bar{q}$ and Qqq) and it looks likely that a large number of hybrids ($Q\bar{q}g$) is also missing.

In the pure light uds sector, our perception on the missing states may change when finite width effects are placed into the calculation. This effectively corresponds to redistribute the mass spectrum weighted with an asymmetric Boltzmann factor. From that point of view the missing states effect could also be regarded as a missing mass effect. At this level the highest temperature of agreement for the trace anomaly seems to be $T \lesssim 150$ MeV between either the HRG based on PDG, PDG (Γ) or RQM spectra and current QCD finite temperature calculations. However, the separate analysis in terms of B, Q, S fluctuations reveals a less obvious pattern regarding the verification of quark-hadron duality. While the HRG has arbitrated the lattice QCD discrepancies for the trace anomaly in the past, in the case of fluctuations we are now confronted with the opposite situation. Lattice data agree but are not universally reproduced by any of the three HRG realizations considered here. This may offer a unique opportunity to refine these models including other effects and which deserves further studies.

8. Acknowledgments

We thank Pok Man Lo and Michal Marczenko for useful communications. This work is supported by Spanish Ministerio de Economía y Competitividad and European FEDER funds under contracts FIS2014-59386-P and FPA2015-64041-C2-1-P, Junta de Andalucía grant FQM-225, and Spanish Consolider Ingenio 2010 Programme CPAN (CSD2007-00042).

W.B. is supported by the Polish National Science Center grant 2015/19/B/ST2/00937. The research of E.M. is supported by the European Union under a Marie Curie Intra-European fellowship (FP7-PEOPLE-2013-IEF) with project number PIEF-GA-2013-623006, and by the Universidad del País Vasco UPV/EHU, Bilbao, Spain, as a Visiting Professor.

References

[1] R. Hagedorn, Nuovo Cim. Suppl. **3**, 147 (1965).

[2] W. Broniowski and W. Florkowski, Phys. Lett. B **490**, 223 (2000); hep-ph/0004104.

[3] W. Broniowski, W. Florkowski, and L.Ya. Glozman, Phys. Rev. D **70**, 117503 (2004); hep-ph/0407290.

[4] C. Patrignani (Particle Data Group) *et al.*, Chin. Phys. C **40**, 100001 (2016).

[5] R. G. Edwards *et al.*, Phys. Rev. D **87**, 054506 (2013); hep-ph/1212.5236.

[6] S. Godfrey and N. Isgur, Phys. Rev. D **32**, 189 (1985).

[7] S. Capstick and N. Isgur, Phys. Rev. D **34**, 2809 (1986); AIP Conf. Proc. **132**, 267 (1985).

[8] W. Broniowski, Few-quark problems. Proceedings, Mini-Workshop, Bled, Slovenia, July 8-15, 2000, p. 3, 2000, hep-ph/0008112.

[9] E. Ruiz Arriola, L. L. Salcedo, and E. Megias, Acta Phys. Polon. B **45**, 2407 (2014); hep-ph/1410.3869.

[10] R. A. Briceño *et al.*, Chin. Phys. C **40**, 042001 (2016); hep-ph/1511.06779.

[11] A. Majumder and B. Muller, Phys. Rev. Lett. **105**, 252002 (2010); hep-ph/1008.1747.

[12] W. Broniowski, Mini-Workshop Bled 2016: Quarks, Hadrons, Matter Bled, Slovenia, July 3-10, 2016, 2016, hep-ph/1610.09676.

[13] S. G. Brush, Archive for History of Exact Sciences **4**, 145 (1967).

[14] D. Bernoulli, Hydrodynamica sive de viribus et motibus fluidorum commentarii (Johann Reinhold Dulsecker, 1738).

[15] J. Nieves and E. Ruiz Arriola, Phys. Rev. D **64**, 116008 (2001); hep-ph/0104307.

[16] C. Garcia-Recio *et al.*, Phys. Rev. D **67**, 076009 (2003); hep-ph/0210311.

[17] S. Ciulli, C. Pomponiu, and I. Sabba Stefanescu, Phys. Repts. (1975); Acta Phys. Austriaca Suppl. **14**, 469 (1975).

[18] I. Caprini *et al.*, Phys. Rev. D **93**, 076004 (2016); hep-ph/1602.02062.

[19] E. Ruiz Arriola and W. Broniowski, Proceedings, Mini-Workshop on Understanding hadronic spectra: Bled, Slovenia, July 3-10, 2011, pp. 7–17, 2011; hep-ph/1110.2863.

[20] P. Masjuan, E. Ruiz Arriola, and W. Broniowski, Phys. Rev. D **85**, 094006 (2012); hep-ph/1203.4782.

[21] E. Witten, Nucl. Phys. B **160**, 57 (1979).

[22] A. R. Bohm and Y. Sato, Phys. Rev. D **71**, 085018 (2005).

[23] T. Berggren, Nucl. Phys. A **109**, 265 (1968).

[24] P. Masjuan, E. Ruiz Arriola, and W. Broniowski, Phys. Rev. D **87**, 014005 (2013); hep-ph/1210.0760.

[25] R. A. Briceño, Z. Davoudi, and T. C. Luu, J. Phys. G **42**, 023101 (2015); hep-ph/1406.5673.

[26] R. Dashen, S. K. Ma, and H. J. Bernstein, Phys. Rev. **187**, 345 (1969).

[27] R. F. Dashen and R. Rajaraman, Phys. Rev. D **10**, 694 (1974).

[28] R. F. Dashen and R. Rajaraman, Phys. Rev. D **10**, 708 (1974).

[29] R. Venugopalan and M. Prakash, Nucl. Phys. A **546**, 718 (1992).

[30] W. Broniowski, F. Giacosa, and V. Begun, Phys. Rev. C **92**, 034905 (2015); hep-ph/1506.01260.

[31] E. Ruiz Arriola, L. L. Salcedo, and E. Megias, Acta Phys. Polon. Supp. **8**, 439 (2015); hep-ph/1505.02922.

[32] E. Ruiz Arriola, W. Broniowski, and P. Masjuan, Acta Phys. Polon. Supp. **6**, 95 (2013); hep-ph/1210.7153.

[33] E. Megias, E. Ruiz Arriola and L. L. Salcedo, Phys. Rev. D **74**, 065005 (2006); hep-ph/0412308.

[34] E. Megias, E. Ruiz Arriola, and L. L. Salcedo, Phys. Rev. D **74**, 114014 (2006); hep-ph/0607338.

[35] K. Fukushima, Phys. Lett. B **591**, 277 (2004); hep-ph/0310121.

[36] C. Ratti, M. A. Thaler, and W. Weise, Phys. Rev. D **73**, 014019 (2006); hep-ph/0506234.

[37] E. Ruiz Arriola, E. Megias, and L. L. Salcedo, AIP Conf. Proc. **1520**, 185 (2013); hep-ph/1207.4875.

[38] E. Megias, E. Ruiz Arriola, and L. L. Salcedo, Phys. Rev. D **89**, 076006 (2014); hep-ph/1311.2814.

[39] S. Borsanyi *et al.*, Phys. Lett. B **730**, 99 (2014); hep-ph/1309.5258.

[40] A. Bazavov (HotQCD Collaboration) *et al.*, Phys. Rev. D **90**, 094503 (2014); hep-ph/1407.6387.

[41] E. Megias, E. Ruiz Arriola, and L. L. Salcedo, Phys. Rev. Lett. **109**, 151601 (2012); hep-ph/1204.2424.

[42] E. Megias, E. Ruiz Arriola, and L. L. Salcedo, Nucl. Phys. Proc. Suppl. **234**, 313 (2013); hep-ph/1207.7287.

[43] E. Megias, E. Ruiz Arriola, and L. L. Salcedo, Acta Phys. Polon. Supp. **9**, 401 (2016); hep-ph/1605.04453.

[44] E. Ruiz Arriola, L. L. Salcedo, and E. Megias, 12th Conference on Quark Confinement and the Hadron Spectrum (Confinement XII) Thessaloniki, Greece, August 28-September **2**, 2016, 2016; hep-ph/1611.03255.

[45] E. Megias, E. Ruiz Arriola, and L. L. Salcedo, Phys. Rev. D **94**, 096010 (2016); hep-ph/1603.04642.

[46] A. Bazavov *et al.*, Phys. Rev. D **93**, 114502 (2016); hep-ph/1603.06637.

[47] S. Jeon and V. Koch, Phys. Rev. Lett. **83**, 5435 (1999); nucl-th/9906074.

[48] S. Jeon and V. Koch, Phys. Rev. Lett. **85**, 2076 (2000); hep-ph/0003168.

[49] V. Koch, Hadronic Fluctuations and Correlations, Chapter of the book Relativistic Heavy Ion Physics, R. Stock (Ed.), Springer, Heidelberg, 2010, p. 626-652.

[50] M. Asakawa and M. Kitazawa, Prog. Part. Nucl. Phys. **90**, 299 (2016); hep-ph/1512.05038.

[51] P. Braun-Munzinger *et al.*, Phys. Rept. **621**, 76 (2016); hep-ph/1510.00442.

[52] A. Bazavov *et al.*, Phys. Rev. Lett. **113**, 072001 (2014); hep-ph/1404.6511.

[53] P. Man Lo *et al.*, Eur. Phys. J. A **52**, 235 (2016).

[54] S. Borsanyi *et al.*, JHEP **01**, 138 (2012); hep-ph/1112.4416.

[55] A. Bazavov (HotQCD Collaboration) *et al.*, Phys. Rev. D **86**, 034509 (2012); hep-ph/1203.0784.

[56] S. Ejiri, F. Karsch, and K. Redlich, Phys. Lett. B **633**, 275 (2006); hep-ph/0509051.

[57] R. Bellwied *et al.*, Phys. Rev. D **92**, 114505 (2015); hep-ph/1507.04627.

2.19 Interplay of Repulsive Interactions and Extra Strange Resonances

Paolo Alba
Frankfurt Institute for Advanced Studies
Goethe Universität Frankfurt
D-60438 Frankfurt am Main, Germany

Abstract

From simulations on lattice it is suggested that there exist missing states in the strange sector of the hadronic spectrum. Since those predictions mainly rely on the Hadron-Resonance Gas model assumption, it is important to check the influence of all the known possible implementation of such a model, in particular the effect of repulsive forces among hadrons. I explore the interplay between the inclusion of extra states predicted by the Quark Model, which I expect to be in line with possible future discoveries, and the corresponding repulsive forces parametrized trough the Excluded Volume. I find that the inclusion of Quark Model states improves the description of some observables, but in order to have an overall improvement for most of the available observables, repulsive interactions are needed. I check experimental measured yields and results from lattice simulations as well. I find that there is a better description of the data when including both effects, within a reasonable temperature range.

1. Introduction

In recent years the HIC program was very successful in providing results on strong interactions. Among these it is remarkable the success of the statistical hadronization model, which assumes that immediately after the collision the system thermalizes into a fireball from which hadrons are emitted. This result has been furtherly tested against hadron production [1], and with hydrodynamical simulations [2]. However it is worth to mention that other options exist, e.g., a microscopical description through transport models, from which it is possible to access directly the partonic nature of those interactions.

Lattice simulations provided excellent results, and in recent years it was possible to improve the accuracy and precision of those, in order to be able to analyze experimental data [3], and being able to do important step forward in the understanding of the QCD transition; this is extremely important because allows to directly connect the experiment with first principle calculations. From these, we know that the confinement transition is a crossover [4], i.e., does not allow to clearly asses when there is the passage between the two phases, but only to estimate a (pseudo-)critical temperature of about 150 MeV [5]. This has important consequences, e.g., the fact that the crossover acts differently for different constituent, hinting for a flavor hierarchy in the critical temperature [6].

Fluctuations of conserved charges have been proposed to be able to test these assumptions, and have been proven to be very sensitive observables from lattice simulations [6], and from experimental measurements [7, 8].

One important tool used to overcome the inner differences between experimental measurements and lattice is the Hadron-Resonance Gas (HRG) model, which has proven to be successful in the description of particle yields [9], and shows a good agreement with lattice simulations [10] and experimental measurements for the fluctuations of conserved charges [11].

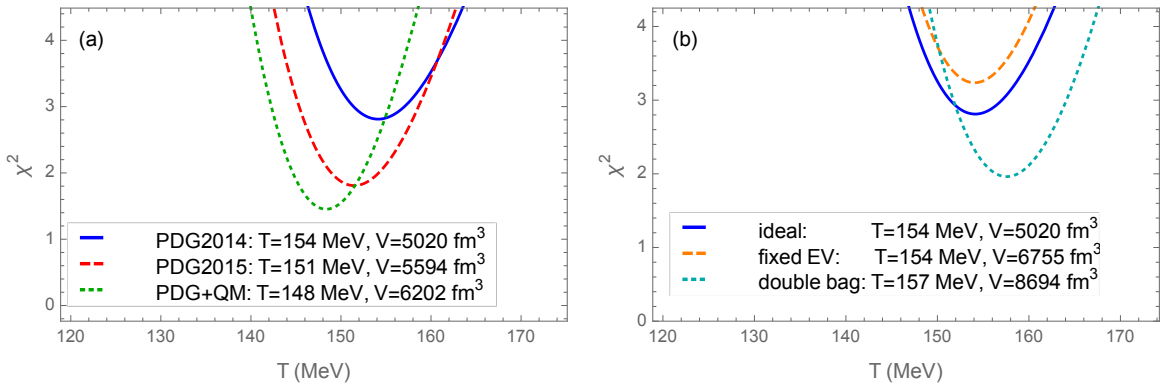

Figure 1: χ^2 profile with temperature from the fit to particle yields measured by the ALICE collaboration for PbPb collision at 2.76 TeV [14–16]. For every temperature the volume is minimized, but the baryon chemical potential is fixed to zero. On panel (a) is showed the effect of the inclusion of higher-mass states, while on panel (b) is showed the effect of EV effects.

2. Quark Model

From the discrepancy between lattice calculations and HRG predictions for a specific observable, it has been proposed that the actual measured hadronic spectrum is lacking in some states in the strange sector [12], and that Quark-Model (QM) predictions could fill the gap restoring the agreement between the two frameworks. However it is easy to check that the wild inclusion of all those states can ruin the agreement with other observables, due in particular to multi-strange baryons.

Indeed, this is connected with the uncertainty coming from the particle list used as an input in the HRG model, which relies essentially on the measured experimental states listed by the Particle Data Group [13].

In order to check the reliability of those states, I show in Fig. 1, panel (a), the χ^2 profile in temperature for the fit to particle yields from PbPb collisions at 2.76 TeV measured by the ALICE collaboration [14–16] (see [17] for more details), with χ^2 given by:

$$\chi^2 = \frac{1}{N_{\rm dof}} \sum_{h=1}^{N} \frac{\left(\langle N_h^{\rm exp}\rangle - \langle N_h\rangle\right)^2}{\sigma_h^2} \,. \tag{1}$$

It comes out that the updates from the PDG improve the description of the data (see also Table 1); extracting the informations on the branching ratios from the PDG 2015 and applying them to the QM states, the χ^2 is further decreased, leaving the freeze-out parameters almost unaffected.

By the way there are different options available for QM calculations with respect to the one employed here, which are essentially the most crude and most abundant.

A similar improvement can be achieved accounting for repulsive interactions (see Fig. 1 panel (b)), as will be explained in the following section.

Table 1: Freeze-out parameters, and corresponding χ^2 from the fit to particle yields measured by the ALICE collaboration for PbPb collision at 2.76 TeV [14–16] for different particle lists and EV parameterizations. In the last column is shown the χ^2 for observables calculated on the lattice for temperatures below 164 MeV; the parameters are the ones obtained from the fit to particle yields.

list	EV	χ^2_{yields}	T (MeV)	V (fm^3)	$\chi^2_{lattice}$
PDG2014	id	22.49/8 $\cong$ 2.81	154.19 $\pm$ 2.29	5047 $\pm$ 663	9.49
PDG2015	id	14.47/8 $\cong$ 1.8	151.53 $\pm$ 2.12	5620 $\pm$ 705	8.65
QM	id	11.62/8 $\cong$ 1.45	148.39 $\pm$ 1.18	6227 $\pm$ 722	15.905
PDG2014	fix	22.65/7 $\cong$ 3.23	154.11 $\pm$ 2.28	5934 $\pm$ 701	10.95
QM	fix	11.74/7 $\cong$ 1.67	148.33 $\pm$ 1.18	7131 $\pm$ 760	6.98
PDG2014	2b	11.77/6 $\cong$ 1.96	157.64 $\pm$ 2.46	5734 $\pm$ 620	14.07
QM	2b	13.47/6 $\cong$ 2.24	149.27 $\pm$ 1.8	7483 $\pm$ 704	1.705

3. Repulsive Forces

The inclusion of resonance formation mediates the attractive interactions among hadrons, neglecting the repulsive ones which however are present in the experimental scattering measurements. The last can be implemented within the HRG model with the so called Excluded Volume (EV) [18]; hadrons are considered as hard spheres, and are assumed to repel each other when their effective radii r_i overlap. In this picture hadrons posses an eigenvolume given by $v_i = \frac{16}{3}\pi r_i^3$, which must be subtracted to the total volume of the system. This implies a transcendental equation for the system pressure p with a shifted single particle chemical potential $\bar{\mu}_i = \mu_i - v_i p$. The others thermodynamical quantities are obtained from usual relations, e.g., the particle densities are:

$$n_i(T,\mu_B) \;=\; \frac{n_i^{\rm id}(T,\mu_i^*)}{1+\sum_j\, v_j\, n_j^{\rm id}(T,\mu_j^*)}\,, \tag{2}$$

where it is clear the double fold suppression, coming from the shifted chemical potential and the overall denominator.

It has been pointed out that the proper inclusion of repulsive forces is relevant for resonances like the σ and the κ [19, 20], and in general can influence other resonances.

Since data are not available for all the hadronic species present in our lists, I employ different parameterizations for the particle eigenvolumes: fixed for all species, directly proportional to the particle mass (as one could expect for radial excitations from QM calculations), and inversely proportional. The last case, even if may look counterintuitive, has been explored theoretically [21], and can derive from the assumption of diquarks as constituents building blocks together with quarks. It has been pointed out how this assumption can improve the description of particle yields [17], and of lattice simulations in the pure gauge sector [22].

It is worth to note that for a fixed radius the relative densities stay constant (see Eq.2), essentially leaving unaffected results based on particle yields. The situation is different when looking at higher order cumulants, as can be seen in Fig. 2.

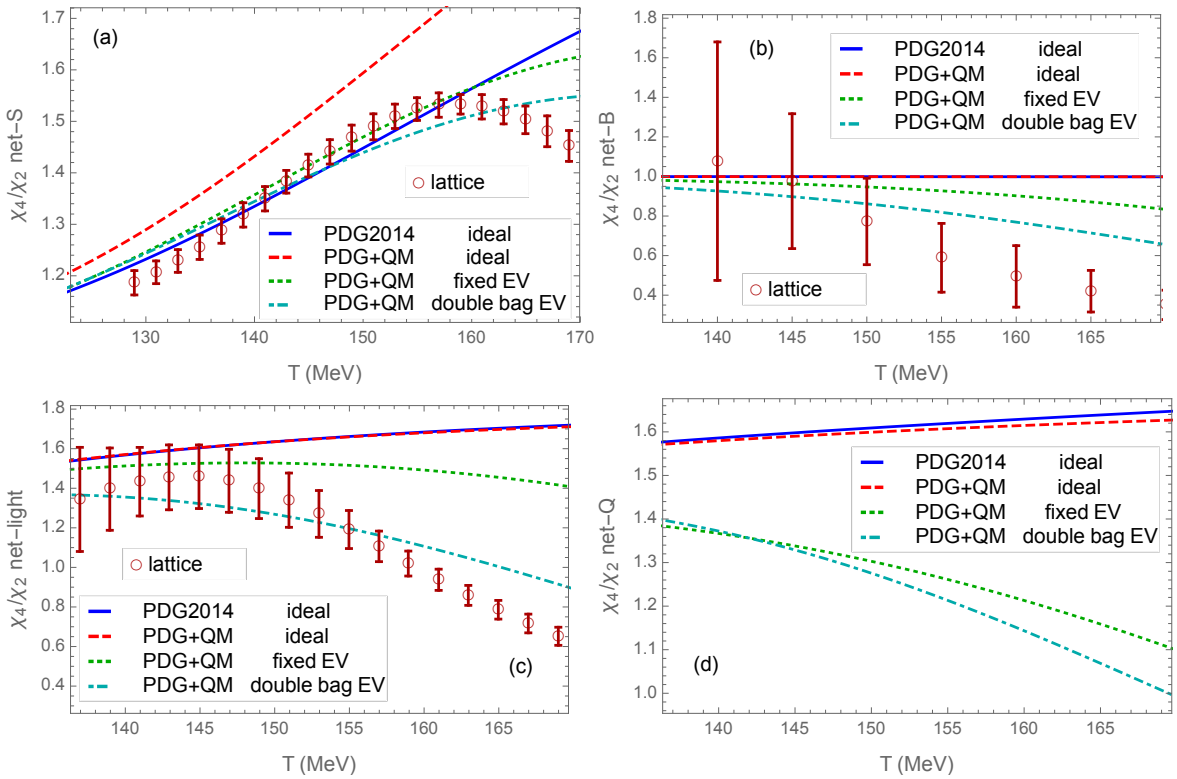

Figure 2: Comparison between lattice data [6, 24] and HRG calculations with different particle lists and particle eigenvolumes, for χ_4/χ_2 observables for different quantum numbers. Currently there are no lattice data available for net-electric charge.

4. **Comparison with Lattice**

In Table 1, I list the results from the fit to particle yields using the standard HRG (id), an EV with fixed radii (fix) and with radii proportional to the particle mass with proportionality constant dependent on the flavor (2b). The same EV parameters are applied for PDG2014, PDG2015 and QM lists. Here I also calculate the χ^2 for the different HRG options against the lattice data for pressure, interaction measure, χ_{11}^{us}, χ_{11}^{ud}, χ_2^s, $\mu_S/\mu_B|_{LO}$, $\chi_4/\chi_2|_{net-B}$, $\chi_4/\chi_2|_{net-S}$ and $\chi_4/\chi_2|_{net-light}$ for temperatures below 164 MeV [3, 23, 24], which should be a reasonable range of temperatures near the crossover. I show that with the inclusion of QM states and with a 2b EV with $r_p = 0.36$ fm and $r_\Lambda = 0.27$ fm (it is convenient to parametrize the r_i with the ground state hadrons in order to have an immediate comparison), I can systematically improve the description of both experimental and lattice data, with hints from both sectors for smaller strange hadrons with respect to the light ones with the same mass.

In Fig. 2, I show a comparison between lattice and HRG predictions for the χ_4/χ_2 for net-light, net-B and net-S quantum numbers; the improvement due to the EV could be understood in terms of the statistical suppression due to the finite sizes of resonances; in particular in the strange sector the EV suppression balances the effect of the inclusion of multi-strange baryons (leaving unaffected the results for the $\mu_S\mu_B|_{LO}$). There are no data for the net-electric charge, and here I show my prediction for this quantity.

It is worth to note at this point that the EV parameters employed are solely obtained from a fit to particle yields, which result in freeze-out parameters compatible with the id case.

5. **Conclusion**

In conclusion, I studied the balance between attractive and repulsive forces within the HRG framework. I find that the simultaneous inclusion of higher-mass states and EV interactions improves the description of a large set of observables both from experimental measurements and lattice simulations, hinting in particular to a flavor dependent size. This could depend on the QM calculations employed, and can be critical the inclusion of exotic resonances like the $\kappa(800)$, which need still to be confirmed but which would have a large influence on observables related to strangeness.

A systematic study of all the different versions of the Quark Model against repulsive interactions is mandatory.

6. **Acknowledgments**

This work was supported by HIC for FAIR within the LOEWE program of the State of Hesse. I acknowledge the University of Houston for hosting me during the period in which this work was completed.

References

[1] P. Braun-Munzinger, J. Stachel, J. P. Wessels, and N. Xu, Phys. Lett. B **344**, 43 (1995); [nucl-th/9410026].

[2] E. Schnedermann, J. Sollfrank, and U. W. Heinz, Phys. Rev. C **48**, 2462 (1993); [nucl-th/9307020].

[3] S. Borsanyi, Z. Fodor, S. D. Katz, S. Krieg, C. Ratti, and K. K. Szabo, Phys. Rev. Lett. **111**, 062005 (2013); [arXiv:1305.5161 [hep-lat]].

[4] Y. Aoki, G. Endrodi, Z. Fodor, S. D. Katz and K. K. Szabo, Nature **443**, 675 (2006); [hep-lat/0611014].

[5] S. Borsanyi *et al.* [Wuppertal-Budapest Collaboration], JHEP **1009**, 073 (2010); [arXiv:1005.3508 [hep-lat]].

[6] R. Bellwied, S. Borsanyi, Z. Fodor, S. D. Katz, and C. Ratti, Phys. Rev. Lett. **111**, 202302 (2013); [arXiv:1305.6297 [hep-lat]].

[7] L. Adamczyk *et al.* [STAR Collaboration], Phys. Rev. Lett. **112**, 032302 (2014); [arXiv:1309.5681 [nucl-ex]].

[8] P. Alba, R. Bellwied, M. Bluhm, V. Mantovani Sarti, M. Nahrgang, and C. Ratti, Phys. Rev. C **92**, 064910 (2015); [arXiv:1504.03262 [hep-ph]].

[9] A. Andronic, P. Braun-Munzinger, and J. Stachel, Phys. Lett. B **673**, 142 (2009); Erratum: [Phys. Lett. B **678**, 516 (2009)]; [arXiv:0812.1186 [nucl-th]].

[10] S. Borsanyi, Z. Fodor, S. D. Katz, S. Krieg, C. Ratti, and K. Szabo, JHEP **1201**, 138 (2012); [arXiv:1112.4416 [hep-lat]].

[11] P. Alba, W. Alberico, R. Bellwied, M. Bluhm, V. Mantovani Sarti, M. Nahrgang, and C. Ratti, Phys. Lett. B **738**, 305 (2014); [arXiv:1403.4903 [hep-ph]].

[12] A. Bazavov *et al.*, Phys. Rev. Lett. **113**, 072001 (2014); [arXiv:1404.6511 [hep-lat]].

[13] C. Patrignani *et al.* [Particle Data Group], Chin. Phys. C **40**, 100001 (2016).

[14] B. Abelev *et al.* [ALICE Collaboration], Phys. Rev. C **88**, 044910 (2013); [arXiv:1303.0737 [hep-ex]].

[15] B. B. Abelev *et al.* [ALICE Collaboration], Phys. Rev. Lett. **111**, 222301 (2013); [arXiv:1307.5530 [nucl-ex]].

[16] B. B. Abelev *et al.* [ALICE Collaboration], Phys. Lett. B **728**, 216 (2014); Corrigendum: [Phys. Lett. B **734**, 409 (2014)]; [arXiv:1307.5543 [nucl-ex]].

[17] P. Alba, V. Vovchenko, M. I. Gorenstein, and H. Stoecker, arXiv:1606.06542 [hep-ph].

[18] D. H. Rischke, M. I. Gorenstein, H. Stoecker, and W. Greiner, Z. Phys. C **51**, 485 (1991).

[19] W. Broniowski, F. Giacosa, and V. Begun, Phys. Rev. C **92**, 034905 (2015); [arXiv:1506.01260 [nucl-th]].

[20] B. Friman, P. M. Lo, M. Marczenko, K. Redlich, and C. Sasaki, Phys. Rev. D **92**, 074003 (2015); [arXiv:1507.04183 [hep-ph]].

[21] T. Friedmann, Eur. Phys. J. C **73**, 2299 (2013); [arXiv:0910.2231 [hep-ph]].

[22] P. Alba, W. M. Alberico, A. Nada, M. Panero, and H. Stcker, arXiv:1611.05872 [hep-lat].

[23] S. Borsanyi, Z. Fodor, C. Hoelbling, S. D. Katz, S. Krieg, and K. K. Szabo, Phys. Lett. B **730**, 99 (2014); [arXiv:1309.5258 [hep-lat]].

[24] R. Bellwied, S. Borsanyi, Z. Fodor, S. D. Katz, A. Pasztor, C. Ratti, and K. K. Szabo, Phys. Rev. D **92**, 114505 (2015); [arXiv:1507.04627 [hep-lat]].

2.20 Missing Resonance Decays in Thermal Models

Viktor V. Begun
Faculty of Physics
Warsaw University of Technology
00-662 Warsaw, Poland

Volodymyr Yu. Vovchenko
Institute für Theoretishe Physik
Goethe Universität Frankfurt
D-60438 Frankfurt am Main, Germany &
Frankfurt Institute for Advanced Studies
Goethe Universität Frankfurt
D-60438 Frankfurt am Main, Germany &
Department of Physics
Taras Shevchenko National University of Kiev
03022 Kiev, Ukraine

Mark I. Gorenstein
Frankfurt Institute for Advanced Studies
Goethe Universität Frankfurt
D-60438 Frankfurt am Main, Germany &
Bogolyubov Institute for Theoretical Physics
03680 Kiev, Ukraine

Abstract

Detailed information on decay channel probabilities is absent for many high mass resonances, which are typically included in thermal models. In these cases, the sum over all known decay branching probabilities is smaller than 1. Due to this systematic uncertainty of the model, the exact charge conservation may appear to be violated. We estimate the corresponding number of missing charge states in the canonical ensemble formulation of the hadron resonance gas for p+p reactions at the SPS energy $E_{\rm lab} = 158$ GeV: $\Delta B \simeq 0.16$ for baryon charge, $\Delta Q \simeq 0.12$ for electric charge, and $\Delta S = -0.01$ for strangeness. The value of the considered effect is 5-8%, which seems to be important enough to include it as a systematic error in the calculations within a hadron gas.

1. The hadron-resonance gas model (HRG) allows to obtain particle multiplicities at different collision energies with a relatively good accuracy. In a simplest HRG hadrons and resonances are assumed to be non-interacting, and full chemical equilibrium is imposed. This model has just two free parameters - the temperature, T, and the baryon chemical potential, μ_B, which follow a simple analytic dependence as the function of collision energy [1, 2]. The HRG model works well for nucleus-nucleus (A+A) collisions, and even for elementary particle reactions $p + p$, $p + \bar{p}$ and $e^+ + e^-$ [3, 4] An analytic assumption about the form of the fireball hypersurface at freeze-out allows further to obtain the p_T spectra of measured particles for the cost of just one more parameter - the ratio of the freeze-out radius and time [5–7].

Many modifications to the standard HRG exist, which improve agreement with experimental data, in particular, the one at the LHC. These include sequential freeze-out [8], a mechanism of proton suppression due to re-scattering during the freeze-out [9], introducing different proper volumes for different particles [10], or considering the possibility of pion condensation [6, 11].

A list of stable particles and resonances is a key ingredient of a HRG model. Taking into account more/missing hadron resonances helped with data description at the SPS [12] and the LHC [13]. The problem is that the list of resonances and their properties is known well only up to $m \sim 1.5$ GeV. In particular, many decay channels for measured heavy resonances are unknown. Therefore, the amount of charge that is calculated in a HRG after including only the known decays of these resonances listed in Particle Data Tables [14] is different from the one before the decays [1]. The size of the latter effect can be estimated. For the case of a proton-proton reaction the charge of the system is known exactly, $B = Q = 2$, $S = 0$. If several total 4π multiplicities are available experimentally, then their fit in the HRG within the canonical ensemble gives the thermal parameters: temperature T, system volume V, and strangeness undersaturation parameter γ_S (see Ref. [2] for details). The resulting missing charge for the p+p reactions at laboratory momentum 158 GeV/c is $\Delta B/B \simeq 8\%$ for the baryon charge, $\Delta Q/Q \simeq 6\%$ for the electric charge, and $\Delta S = -0.01$ for strangeness [2]. These numbers reflect a strongest effect of the missing decay channels probabilities for heavy positively charged baryons.

There are alternative ways to deal with the problem of missing branching ratios. One option is to additionally normalize all the branching ratios to 100% [16, 17]. However, such a normalization produces some error: it artificially enhances the known channels, and, therefore, suppresses yet undiscovered channels. Another option is to assign same/similar branching ratios based on analogies to the nearest states with the same quantum numbers and known branching ratios [18].

Therefore, the value of the considered effect is 5-8%, which seems to be important enough to include it as a systematic error in the calculations within a HRG.

2. **Acknowledgments**

We thank H. Stroebele for a fruitful discussion. V. Y. V. acknowledges the support from HGS-HIRe for FAIR. The work of M. I. G. was supported by the Program of Fundamental Research of the Department of Physics and Astronomy of National Academy of Sciences of Ukraine.

References

[1] J. Cleymans, H. Oeschler, K. Redlich, and S. Wheaton, Phys. Rev. C **73**, 034905 (2006); hep-ph/0511094.

[1] Another aspects of missing charges in p+p reactions were recently reported in [15].

[2] V. Vovchenko, V. V. Begun, and M. I. Gorenstein, Phys. Rev. C **93**, 064906 (2016); 1512.08025.

[3] F. Becattini, Z. Phys. C69, 485 (1996).

[4] F. Becattini and U. W. Heinz, Z. Phys. C **76**, 269 (1997); hep-ph/9702274; [Erratum: Z. Phys. C **76**, 578 (1997)].

[5] W. Broniowski and W. Florkowski, Phys. Rev. Lett. **87**, 272302 (2001); nucl-th/0106050.

[6] V. Begun, W. Florkowski, and M. Rybczynski, Phys. Rev. C **90**, 014906 (2014); 1312.1487.

[7] V. Begun, W. Florkowski, and M. Rybczynski, Phys. Rev. C **90**, 054912 (2014); 1405.7252.

[8] S. Chatterjee, R. M. Godbole, and S. Gupta, Phys. Lett. B **727**, 554 (2013); 1306.2006.

[9] F. Becattini *et al.*, Phys. Rev. Lett. **111**, 082302 (2013); 1212.2431.

[10] P. Alba, V. Vovchenko, M. I. Gorenstein, and H. Stoecker, (2016), 1606.06542.

[11] V. Begun and W. Florkowski, Phys. Rev. C **91**, 054909 (2015); 1503.04040.

[12] E. Schnedermann, J. Sollfrank, and U. W. Heinz, Phys. Rev. C **48**, 2462 (1993); nucl-th/9307020.

[13] J. Noronha-Hostler and C. Greiner, Nucl. Phys. A **931**, 1108 (2014); 1408.0761.

[14] K. A. Olive *et al.* (Particle Data Group), Chin. Phys. C **38**, 090001 (2014).

[15] H. Stroebele, (2016), 1611.00615.

[16] G. Torrieri *et al.*, Comput. Phys. Commun. **167**, 229 (2005); nucl-th/0404083.

[17] S. Wheaton, J. Cleymans, and M. Hauer, Comput. Phys. Commun. **180**, 84 (2009); hep-ph/0407174.

[18] A. Andronic, P. Braun-Munzinger, and J. Stachel, Phys. Lett. B **673**, 142 (2009); 0812.1186; [Erratum: Phys. Lett. B **678** ,516 (2009)].

2.21 Discussion and Summary

Jose Goity
Department of Physics
Hampton University
Hampton, VA 23668, U.S.A. &
Thomas Jefferson National Accelerator Facility
Newport News, VA 23606, U.S.A.

Pasi Huovinen
Institute of Theoretical Physics
University of Wroclaw
PL-50204 Wroclaw, Poland

James Ritman
Institut fr Kernphysik
Forschungszentrum Jülich
D-52424, Jülich, Germany

Aihong Tang
Brookhaven National Laboratory
Upton, NY 11973, U.S.A.

After the scientific presentations were complete, and directly before the summary and concluding remarks, a session was held to discuss the common issues presented by multiple talks, in particular those items that are particularly relevant to the physics motivation and for a K0Long facility and what needs to be done to realize this facility. The very intense and lively discussions had a wide range of participants. This discussion was structured into several themes as presented below:

1. **What are the Synergies between Heavy Ion Collision Physics and the K0Long Facility?**

   Hadron production yields have been analyzed in heavy ion collisions with incident beam energies ranging from several GeV per nucleon up to Pb+Pb interactions at LHC energies. Statistical model calculations using specific parameters such as thermal and chemical freeze-out temperatures, baryon-, strangeness- and charm- chemical potentials, give surprisingly accurate descriptions of the measured results over many orders of magnitude of yield. These models give a very important baseline, upon which one can gauge, to which extent other observations are "simple" many-body effects, or can be attributed to, e.g., consequences of the deconfined phase.

   Despite the tremendous success of these calculations, some specific aspects require dedicated attention. In particular the calculation of yields for many longer lived resonances require knowledge of the higher lying states, that feed down to the lower lying states, which are finally observed by the detectors. The importance for Charmonium and Bottomonium states is very apparent. In the baryon sector the calculations take into account the resonances listed

in the Particle Data Book. For light quark states this approach seems to work well. For the hyperon sector, the quality of the results depends strongly upon which hyperon states are included in the calculation. The calculations are far off the data if only well-established resonances are included. If however those states with low confidence ("zero-star" or "1-star" resonances) are also included, then the level of agreement between the calculations and the data improves. Although the heavy ion data can not be used to prove the exact parameters of specific narrow resonances, they do however imply that a large number of narrow hyperon states, in a narrow mass interval must exist.

Therefore, it is evident that the spectroscopic results from a K0Long facility will greatly improve the reliability of the thermal model predictions in the baryon/hyperon sector. Concurrently, the heavy ion results provide a strong indication of how many narrow hyperon states are to be expected with masses up to roughly $2\ GeV/c^2$.

2. **Should these Experiments Rather Measure PP ?**

   The K0L facility is based on using a tertiary beam (electrons, photons, K0Long), with the corresponding reduction of rate at each step of the beam generation process. In contrast, proton-proton interactions can be operated at many orders of magnitude higher luminosity. Consequently, excited hyperons are produced at higher rates in the primary proton-proton collisions. These resonances however need to be cleanly identified in these high flux environments. Kinematic constraints that exploit exclusive event reconstruction tend to favor beam energies close to the production threshold, where the signal cross section drops rapidly compared to the total reaction cross section. Additional complications arise since either projectile or target (or both) can be excited. Thus, the multi-baryon final state has a large, irreducible physics background.

   The yield of exotics in proton-proton collisions and/or heavy ion collisions might be enhanced due to the high temperature and high density environment, however, due to the background mentioned above, attempts of search in those collisions would be better viewed as opportunistic play.

3. **How to go beyond "Bump-Hunting"?**

   In the relevant kinematic range it is expected that there are many overlapping resonances of various spin-parity quantum numbers. As clearly shown in, e.g., photon, pion and kaon induced reactions, it is essential to apply partial wave analyses to the data to reliably extract resonance information from the ensemble of final states. This is well understood in the community, and powerful techniques are being further developed. This development and the use of these programs requires continued, very close interaction between theory and experiment, as for instance already practiced at JPAC.

4. **From Theory: How Many Y^* States do we need to Measure?**

   Of course this general formulation of the question begs the answer "as many as possible". Instead it is more quantitative to ask how many states are needed for a specific purpose. For instance, how many states are needed to improve the statistical model calculations for heavy ion collisions to a given level of precision? Similarly, one could ask how many states are

needed to corroborate/confirm Lattice QCD predictions for this sector? In either case we are talking about on the order of 10 to tens of states.

5. **From Experiment: How Many States are Practically Feasible?**

   The experimental effort connected to measuring on the order of 10 states indicates that a dedicated measurement program is needed, and not just a single measurement. This is very important, since it means that the success of the K0L facility does not depend upon the existence or measurability of any single state.

   In order to achieve these stated scientific goals, the scope of the program will comprise the instrumental setup, and will require several months of beamtime. Specific details on the effort involved to setup the K0L facility as well as the amount of required beamtime have been presented during this workshop and will be included in the proposal for the facility.

6. **Which Decays Should be Measured?**

   An integral part of the K0L facility is the GlueX spectrometer, which will surround the hyperon production target. This provides excellent charged particle tracking capability for particles from both the primary and also delayed vertices. Furthermore, the calorimeters are well suited to measure photons from neutral pion decays.

   Kinematic over-constraints do allow events to be reconstructed if one particle is unmeasured. However, the resolution of the beam momentum worsens significantly for systems with increasing hyperon masses. Consequently, final states where the daughters are charged hadrons, or include at most one neutral pion, are ideal. This explicitly includes delayed decays of neutral particles, such as Lambda into proton π^-. The use of Cherenkov detectors in the GlueX spectrometer will significantly enhance the selectivity to charged kaons in the final state, which is vital for the S=-2 and S=-3 studies.

7. **Rates at JLab – Comparison to Other Facilities?**

   In the useful momentum range of 0.3 to 10 GeV/c there will be up to 10^4 K0L per second incident on the target inside GlueX. This flux will result in about 2×10^5 excited cascades and 4×10^3 excited Omegas per month.

   A similar program for KN scattering is under development at J-PARC with charged kaon beams. The current maximum momentum of secondary beamline of 2 GeV/c is available at the K1.8 beamline. This is however not sufficient to produce the first excited cascade states within the quark model. However, there are plans to create a high energy beamline in the momentum range 5 – 15 GeV/c to be used with the spectrometer commonly used with the J-PARC P50 experiment. The statistical power of proposed experiment with a K0L beam at JLab will be of the same order as that in J-PARC with a charged kaon beam. In BES-III and Belle, the hyperons are produced in charmonium or bottomium decays. The branching ratios of heavy quarkonia into multi-strange baryon-antibaryon states are however not very large. In LHCb, inclusive strange hyperons are produced in abundance, but PWA requires a well-defined initial state, which makes only hyperons from known states (e.g., bottomium) suitable. The production rates of hyperons from such decays are low. PANDA can access the full double- and triple-strange hyperon spectrum even with relatively low luminosities,

and the hyperons and the antihyperons can be measured exclusively. Those measurements are however on a longer time scale compared to when the K0L facility can be realized.

8. **Which Other Physics Potential is there with a K0L Beam?**

   A very interesting further opportunity for the K0L facility is to investigate K0L reactions on complex nuclei. By selecting events with the appropriate beam momentum together with a fast forward going pion, events can be identified, in which a hyperon is produced at low relative momentum to the target nucleus or into a bound state. Baryons with strangeness embedded in the nuclear environment, hypernuclei or hyperatoms, are the only available tool to approach the many-body aspect of the three-flavor strong interaction.

   Further potential exists to search for - or exclude - possible exotic baryonic states that can not easily be described by the usual 3 valence quark structure. Recent results from LHCb provide tantalizing hints for the existence of so-called pentaquarks that include a charm valence quark, however the interpretation of those results is under discussion. In contrast, elastic scattering of K0L with a hydrogen target gives unambiguous information on the potential existence of such states. With the given flux of K0L at the proposed facility, a clear proof of existence or proof of absence will be obtained within the integrated luminosity required for the excited hyperon spectroscopy program that forms the basis of this proposal.

3 List of Participants of YSTAR2016 Workshop

- Paolo Alba, Frankfurt Inst. for Advanced Studies <alba@fias.uni-frankfurt.de>
- Hisham Albataineh, Texas A&M U.-Kingsville <hisham@jlab.org>
- Moskov Amaryan, ODU <mamaryan@odu.edu>
- Mikhail Bashkanov, Edinburgh U. <mikhail.bashkanov@ed.ac.uk>
- Viktor Begun, Jan Kochanowski U. <viktor.begun@gmail.com>
- Rene Bellwied, Houston U. <bellwied@uh.edu>
- Jay Benesch, JLab <benesch@jlab.org>
- William J. Briscoe, GWU <briscoe@gwu.edu>
- Dilini Bulumulla, ODU <dilinib@jlab.org>
- Simon Capstick, FSU <capstick@fsu.edu>
- Eugene Chudakov, JLab <gen@jlab.org>
- Volker Crede, FSU <crede@fsu.edu>
- Pavel Degtyarenko, JLab <pavel@jlab.org>
- Benjamin Dönigus, <b.doenigus@gsi.de>
- Robert G. Edwards, JLab <edwards@jlab.org>
- Hovanes Egiyan, JLab <hovanes@jlab.org>
- Mathieu Ehrhart, <mehrh002@odu.edu>
- Ashley Ernst, FSU <ace15f@my.fsu.edu>
- Paul Eugenio, FSU <peugenio@fsu.edu>
- Ishara Fernando, Hampton U./JLab <ishara@jlab.org>
- Igor Filikhin, NCCU <ifilikhin@nccu.edu>
- Humberto Garcilazo, IPN, Mexico <humberto@esfm.ipn.mx>
- José L. Goity, Hampton U./JLab <goity@jlab.org>
- Helmut Haberzettl, GWU <helmut@gwu.edu>
- Avetik Hayrapetyan, JLU Giessen <Avetik.Hayrapetyan@uni-giessen.de>
- Pasi Huovinen, Wroclaw U. <huovinen@ift.uni.wroc.pl>

- Charles Hyde, ODU <chyde@odu.edu>
- David Jenkins, Virginia Tech <jenkins@jlab.org>
- Kanchan Khemchandani, Rio de Janeiro U. <kanchan.khemchandani@uerj.br>
- Chan Kim, GWU <kimchanwook@gwu.edu>
- Franz Klein, GWU <fklein@jlab.org>
- Valery Kubarovsky, JLab <vpk@jlab.org>
- Victoria Lagerquist, ODU <vlage001@odu.edu>
- Ilya Larin, Umass, Amherst <ilarin@jlab.org>
- Ziwei Lin, East Carolina U. <linz@ecu.edu>
- Maxim Mai, GWU <maximmai@gwu.edu>
- Mark Manley, KSU <manley@kent.edu>
- Valentina Mantovani Sarti, Torino U.-INFN <mantovan@to.infn.it>
- Alberto Martinez Torres, San Paulo U. <amartine@if.usp.br>
- Georgie Mbianda Njencheu, ODU <gmbia001@odu.edu>
- Eric Moffat, ODU <emoffat1@hotmail.com>
- Wayne Morris, ODU <morris3wh@gmail.com>
- Hugh Montgomery, JLab <mont@jlab.org>
- Fred Myhrer, USC <myhrer@sc.edu>
- James Napolitano, Temple U. <tuf43817@temple.edu>
- Joseph Newton, ODU <jnewt018@odu.edu>
- Jacquelyn Noronha-Hostler, Houston U. <jakinoronhahostler@gmail.com>
- Hiroyuki Noumi, RCNP, Osaka U. <noumi@rcnp.osaka-u.ac.jp>
- Hiroaki Ohnishi, RIKEN/RCNP Osaka U. <h-ohnishi@riken.jp>
- Gabriel Palacios Serrano, ODU <gpala001@odu.edu>
- Kijun Park, JLab <parkkj@jlab.org>
- Eugene Pasyuk, JLab <pasyuk@jlab.org>
- David Payette, ODU <payette@jlab.org>

- William Phelps, FIU <wphelps@jlab.org>
- Jiwan Poudel, ODU <jpoud001@odu.edu>
- Jianwei Qiu , JLab <gxiaofeng2001@yahoo.com>
- Claudia Ratti, Houston U. <cratti@uh.edu>
- James Ritman, FZJ <j.ritman@fz-juelich.de>
- Torri Roark, ODU <troar001@odu.edu>
- Enrique Ruiz Arriola, Granada U. Spain <earriola@ugr.es>
- Daniel Sadasivan, GWU <dansadasivan@gmail.com>
- Sergey Kuleshov, Federico Santa Maria U. <sergey.kuleshov@usm.cl>
- Igor Strakovsky, GWU <igor@gwu.edu>
- Joachim Stroth, Goethe U./ GSI <j.stroth@gsi.de>
- Aihong Tang, BNL <aihong@bnl.gov>
- Simon Taylor, JLab <staylor@jlab.org>
- Yusuke Tsuchikawa, Nagoya U. <tsuchikawa@phi.phys.nagoya-u.ac.jp>
- Daniel Watts, Edinburgh U. <dwatts1@ph.ed.ac.uk>
- Nilanga Wickramaarachchi, ODU <nwick001@odu.edu>
- Nicholas Zachariou, Edinburgh U. <nicholas@jlab.org>